VALIDATION OF NUMERICAL MODEL OF THE FLOW BEHAVIOUR
THROUGH SMOOTH AND STEPPED SPILLWAYS
USING LARGE-SCALE PHYSICAL MODEL

MISS DUANGRUDEE KOSITGITTIWONG

A DISSERTATION SUBMITTED IN PARTIAL FULFILLMENT
OF THE REQUIREMENTS FOR
THE DEGREE OF DOCTOR OF PHILOSOPHY (CIVIL ENGINEERING)
FACULTY OF ENGINEERING
KING MONGKUT'S UNIVERSITY OF TECHNOLOGY THONBURI
2012

Validation of Numerical Model of the Flow Behaviour through Smooth
and Stepped Spillways using Large-scale Physical Model

Ms. Duangrudee Kositgittiwong B.Eng. (Civil Engineering)

A Dissertation Submitted in Partial Fulfillment of the Requirements for
the Degree of Doctor of Philosophy (Civil Engineering)
Faculty of Engineering
King Mongkut's University of Technology Thonburi
2012

Dissertation Committee

……………………………………………   Chairman of Dissertation Committee
       (Prof. Somchai Wongwises, Dr.-Ing.)

……………………………………………   Member and Dissertation Advisor
       (Prof. Chaiyuth Chinnarasri, D.Eng.)

……………………………………………   Member
(Assoc. Prof. Suwatana Chittaladakorn, Ph.D.)

……………………………………………   Member
       (Lect. Chaiwat Ekkawatpanit, Ph.D.)

Dissertation Title	Validation of Numerical Model of the Flow Behaviour through Smooth and Stepped Spillways using Large-scale Physical Model
Dissertation Credits	48
Candidate	Miss Duangrudee Kositgittiwong
Dissertation Advisor	Prof. Dr. Chaiyuth Chinnarasri
Program	Doctor of Philosophy
Field of Study	Civil Engineering
Department	Civil Engineering
Faculty	Engineering
B.E.	2555

Abstract

This study was aimed to use a numerical model to validate the simulation of flow over three types of spillway which are: (i) smooth spillway, (ii) 25-step spillway, and (iii) 50-step spillway. The flow behaviour in the study is a high turbulence free surface two-phase flow; thus, the flow can be divided into two parts, a free surface two-phase flow and a high turbulence flow. The multiphase flow model and the turbulence model were used to simulate a free surface two-phase flow and a high turbulence flow, respectively.

The multiphase flow models used were the Volume of Fluid Model (VOF) and the Mixture Multiphase Flow Model (MMF). The linear-type turbulence models based on (1) the turbulent kinetic energy equation k and (2) the turbulent eddy dissipation ν, or the turbulent frequency $\check{S}$, were (i) Standard k-ν, (ii) Realisable k-ν, (iii) Renormalisation group k-ν, (iv) Standard k-$\check{S}$ and (v) Shear stress transport k-$\check{S}$ models. The simulation results were compared with the test results from the physical model which was larger and closer to the size of the prototype than the ones used in previous research. The discharge was varied with the Reynolds number (Re) in the range of 1.68×10^6 to 7.21×10^6.

The flow behaviour, the flow characteristics on a step, the velocity profiles, and the energy dissipation at the outlet of spillway of the simulation were verified with the physical model test data. This verification consisted of: (i) comparison of a multiphase flow model, (ii) comparison among various turbulence models, (iii) grid independence study, (iv) flow characteristics along stepped spillways, (v) flow characteristics on the step, (vi) velocity profiles, (vii) turbulence intensity, (viii) energy dissipation, (ix) pressure profiles on the step, and (x) the proposed coefficients for turbulence model. The results from the numerical model simulations showed a good agreement with the physical model test results. Based on this fact, this numerical model was further used to develop equations and charts for the preliminary design of spillways for any discharge.

Keywords : Flow Behaviour / Numerical Model / Physical Model / Smooth Spillway / Stepped Spillway / Turbulence Model

หัวข้อวิทยานิพนธ์	การยืนยันผลการใช้แบบจำลองเชิงตัวเลขในการจำลองพฤติกรรมการไหลในทางระบายน้ำล้นแบบราบเรียบและแบบขั้นบันไดโดยเปรียบเทียบกับแบบจำลองเชิงกายภาพ
หน่วยกิตของวิทยานิพนธ์	48
ผู้เขียน	นางสาวดวงฤดี โฆษิตกิตติวงศ์
อาจารย์ที่ปรึกษา	ศ.ดร.ชัยยุทธ ชินณะราศรี
หลักสูตร	ปรัชญาดุษฎีบัณฑิต
สาขาวิชา	วิศวกรรมโยธา
ภาควิชา	วิศวกรรมโยธา
คณะ	วิศวกรรมศาสตร์
พ.ศ.	2555

บทคัดย่อ

การศึกษาครั้งนี้มีวัตถุประสงค์เพื่อใช้แบบจำลองเชิงตัวเลขตรวจสอบและยืนยันการจำลองการไหลผ่านรางระบายน้ำล้นแบบต่างๆ ได้แก่ รางระบายน้ำล้นแบบราบเรียบ และรางระบายน้ำล้นแบบขั้นบันได 25 ขั้น และ 50 ขั้น การจำลองรูปแบบการไหลเพื่อศึกษาลักษณะคุณสมบัติต่างๆ จะต้องทำการเปรียบเทียบเพื่อหาแบบจำลองการไหลที่เหมาะสม เนื่องจากการไหลผ่านทางระบายน้ำล้นเป็นการไหลแบบสองสถานะที่มีความปั่นป่วนสูง พฤติกรรมการไหลจึงสามารถแบ่งออกได้เป็นสองส่วนคือ ส่วนที่เป็นการไหลแบบผิวอิสระที่มีการผสมกันของของไหลสองสถานะได้แก่น้ำและอากาศ และส่วนที่เป็นการไหลแบบปั่นป่วน

การศึกษาครั้งนี้ใช้แบบจำลอง Volume of Fluid (VOF) และแบบจำลอง Mixture multiphase flow (MMF) สำหรับจำลองส่วนที่เป็นการไหลสองสถานะแบบผิวอิสระ จากนั้นส่วนที่เป็นการไหลแบบปั่นป่วน จะใช้แบบจำลองการไหลแบบปั่นป่วนชนิดสองสมการซึ่งประกอบด้วย (1) สมการพลังงานจลน์ของความปั่นป่วน (k) และ (2) สมการอัตราการแพร่ของพลังงานจลน์ของความปั่นป่วน (ε) หรือสมการความถี่ของความปั่นป่วน (ω) แบบจำลองการไหลแบบปั่นป่วนที่นำมาใช้ ได้แก่ แบบจำลอง Standard k-ε แบบจำลอง Realisable k-ε แบบจำลอง Renormalisation group k-ε แบบจำลอง Standard k-ω และ แบบจำลอง Shear stress transport k-ω แบบจำลองเชิงกายภาพที่นำมาใช้เปรียบเทียบเหล่านี้มีลักษณะพิเศษคือเป็นแบบจำลองขนาดใหญ่ใกล้เคียงกับรางระบายน้ำที่ใช้งานจริง ซึ่งสามารถลดปัญหาการเกิดผลกระทบจากการย่อส่วนแบบจำลอง แบบจำลองทั้งหมดมีค่าเรย์โนลด์นัมเบอร์อยู่ระหว่าง 1.68×10^6 ถึง 7.21×10^6

การปรับเทียบและยืนยันแบบจำลอง จะใช้ข้อมูลต่างๆ ประกอบด้วยรูปแบบการไหล ลักษณะการไหลบนขั้นบันได โพรไฟล์ความเร็วการไหล และการสลายพลังงาน เป็นต้น ผลการศึกษา ประกอบด้วยการเปรียบเทียบแบบจำลองการไหลสองสถานะแบบผิวอิสระที่เหมาะสม และการเปรียบเทียบแบบจำลองการไหลแบบปั่นป่วนที่เหมาะสม ซึ่งสามารถนำไปใช้หาขนาดกริดที่เหมาะสม รวมถึงแสดงให้เห็นรูปแบบการไหลตามแนวยาวของรางระบายน้ำล้น รูปแบบการไหลปั่นป่วนบนขั้นบันได โพรไฟล์ความเร็วการไหล ความเข้มของความปั่นป่วน การสลายพลังงาน ความดันบนขั้นบันได และสัมประสิทธ์ของสมการที่เหมาะสม ผลการศึกษาพบว่าแบบจำลองเชิงตัวเลขสามารถใช้จำลองรูปแบบการไหลในทางระบายน้ำล้นได้ดีเมื่อเปรียบเทียบกับแบบจำลองเชิงกายภาพ นอกจากนี้สมการต่างๆ และแผนภาพที่ได้จากการศึกษาสามารถนำไปใช้ในการออกแบบรางระบายน้ำล้นเบื้องต้นที่มีอัตราการไหลออกแบบอยู่ในช่วงที่ศึกษาได้

คำสำคัญ : แบบจำลองเชิงตัวเลข / แบบจำลองเชิงกายภาพ / แบบจำลองการไหลแบบปั่นป่วน / พฤติกรรมการไหล / รางระบายน้ำล้นแบบขั้นบันได / รางระบายน้ำล้นแบบราบเรียบ

ACKNOWLEDGEMENTS

CONTENTS

LIST OF TABLES

LIST OF FIGURES

LIST OF ABBREVIATIONS

C_1	=	$\text{Max}\left[0.43, y/(y+5)\right], y = Sk/v$
C_2	=	Constant of 1.9
C_{1v}	=	Constant of 1.44
C_{3v}	=	Relation of flow velocity in x and y-direction, $C_{3v} = \tanh|v/u|$.
D	=	Constants of distribution of turbulence intensity
e_a^{ij}	=	Approximate relative error, %
e_{ext}^{ij}	=	Extrapolated relative error, %
E_0	=	Energy at the inlet section,
	=	Elevation head+1.5y_c, m
E_i	=	Energy at the point-of-interest section,
	=	flow depth measured in vertical direction + velocity head, m
E_L	=	Energy loss,
	=	E_0 - E_i, m
f_{ij}	=	Value of numerical solution,
	=	f_i - f_j
f_{ext}^{ij}	=	Extrapolated numerical solution
F_s	=	Safety factor
G_b	=	Generation of k due to buoyancy, kg/m-s^3
G_k	=	Generation of k due to the fluid shear,
	=	$\sim_t S^2$, kg/m-s^3
h	=	Step height, m
H	=	Flow depth normal to the slope, m
i	=	Index of step number
I	=	Turbulence intensity,
	=	u'/V
k	=	Turbulent kinetic energy, m^2/s^2
K_s	=	Roughness height,
	=	$h\cos_{\textit{v}}$, m
l	=	Step length, m
L	=	Spillway length in streamwise direction from upstream of spillway, m
L_I	=	Length of inception point from the first step
L_S	=	Length in streamwise direction from upstream of spillway to the point of interest, m
L_{SU}	=	Length of starting point of uniform flow
n	=	Exponent number of power law
n_d	=	Decay exponent
N	=	Total number of steps along the spillway
N_t	=	Total number of cells
P	=	Pressure, N/m^2
p	=	Apparent order for Grid Convergence Index
r_{ij}	=	Grid refinement ratio,
	=	h_{gi}/h_{gj}, i and j mean coarse and fine grids, respectively
Re	=	Reynolds number
s	=	Relative horizontal distance
	=	$il/L\cos_{\textit{v}}$

S	$=$	Modulus of the mean rate of strain tensor,
	$=$	$\sqrt{2S_{ij}S_{ij}}$, 1/s
S_k	$=$	Source terms of kinetic energy, kg/m-s^3
S_v	$=$	Source terms of dissipation rate, kg/m-s^4
t	$=$	Time, s
u_i	$=$	Velocity in x_i-direction, m/s
u_j	$=$	Velocity in x_j –direction, m/s
u_*	$=$	Friction velocity, m/s
u'	$=$	Fluctuating velocity, m/s
V	$=$	Velocity at point of interest, m/s
V_{90}	$=$	Velocity at the depth of 90% air concentration, m/s
y	$=$	Depth at point of interest normal to the slope, m
y_c	$=$	Critical depth, m
Y_M	$=$	Effect of compressibility on turbulence, kg/m-s^3
Γ_a	$=$	Volume fraction of air, %
Γ_w	$=$	Volume fraction of water, %
v	$=$	Turbulent dissipation rate, m^2/s^3
$\}$	$=$	Exponent number of distribution of turbulence intensity
$\sim$	$=$	Molecular dynamic viscosity, kg/m-s
$\sim_t$	$=$	Turbulent dynamic viscosity, kg/m-s
$\in$	$=$	Kinematic viscosity, m^2/s
$''$	$=$	Spillway slope, degree
$...$	$=$	Cell density, kg/m^3
$..._a$	$=$	Air density, kg/m^3
$..._w$	$=$	Water density, kg/m^3
$\dagger_k$	$=$	Turbulent Prandtl number for k,
	$=$	1.0
$\dagger_v$	$=$	Turbulent Prandtl number for v,
	$=$	1.2

CHAPTER 1 INTRODUCTION

This chapter presents the introduction, which consists of backgrounds, statement of problems, objectives, scope of the study, and details of this dissertation. The details are as follows:

1.1 Backgrounds

For recent years, there has been an increase in the frequency of large floods causing high inflows into reservoirs. Dam spillways must be designed to release the floodwaters in excess of the reservoir capacity. To prevent dam overtopping and the potential risk of failure, the appropriate design of spillways remains very important. To be safe, the spillway must be capable of passing high flow without jeopardizing the dam. Such in case when the large design flow is required; a specific spillway is needed to be designed to pass a larger flow. Due to the high flow over the spillway, the design should be very complicated and faces with cavitations and high flow kinetic energy problems. Some forms of structure, for example the stilling basin, located at the foot of the spillway have been used for energy dissipation. The stilling basin is a kind of energy dissipaters designed for the dissipation of energy from upstream flow. The good design for energy dissipater should reduce the flow velocity without any destruction of other hydraulic structures. The theory of using energy dissipater is; for example, change the flow type by constructing a hydraulic jump, change of channel or spillway roughness, add more air into the flow, etc. (Vischer and Hager, 1995).

A stepped spillway has a profile made up of steps and consisting of an open-channel with a series of drops. Construction of stepped spillways has recently become popular in many countries. They have become increasingly popular in view of their increased ability to dissipate energy on each step, rather than the traditional, smooth-surface spillways that require energy dissipation structures at their downstream end. The spillway steps serve as a macro roughness elements causing high flow resistance. Each step significantly dissipates kinetic energy. The rate of energy dissipation on each step is greatly increased. Ultimately, the large energy dissipaters at the toe of the spillways are not necessary (Boes and Hager, 2003a; Felder and Chanson, 2009). The aerated flow on the stepped spillway also reduces the cavitation problem that always occurs on the spillways (Chamani and Rajaratnam, 1999b).

The flow regime on a stepped spillway is very complex. It can be classified into three types: nappe flow, transition and skimming flow (Chanson, 1996; Chamani and Rajaratnam, 1999a; Chanson et al., 2002). Nappe flow is usually found on stepped spillway with large steps or at low discharges. A free-falling jet impacts from step to step with a fully aerated nappe cavity (Chanson, 2002). The transition flow occurs at discharges higher than the maximum required for nappe flow but lower than for the onset of skimming flow. The flow on each step generates a large horizontal vortex that recirculates water with or without air entrainment, whilst the water surface is wavy. Skimming flow occurs on stepped spillway with small steps or at high discharges (Chanson, 1996; Boes and Hager, 2003a). The air pocket along the vertical face of each step disappears in skimming flows. For practical engineering purposes, skimming flows are more relevant than nappe flows.

Scaled-down physical models of spillways were used as a tool to investigate the flow over stepped spillways. Many studies of various sizes of stepped spillways were investigated experimentally (Essery and Horner, 1978; Rajaratnam, 1990; Frizell, 1992; Peyras et al., 1992; Christodoulou, G.C., 1993; Ohtsu and Yasuda, 1997; Yasuda and Ohtsu, 1999; Ohtsu et al., 2000; Chen et al., 2002; Chanson and Toombes, 2002; Boes and Hager, 2003a, 2003b; Ohtsu et al., 2004; Amador, 2006). In highly air-entrained flows as two-phase flow through a spillway, the viscous forces and surface tension play a very important role in air entrainment. If these two secondary forces are ignored because of the scaled-down models, the scale effect, which is a term of critical problem used to describe slight distortions, can be occurred. Then, the data can be misinterpreted. Also, such modelling investigations are still quite expensive and time consuming due to the complexity of the flow.

Numerical modelling of spillways has become attractive due to the increase of computer performance and advances in Computational Fluid Dynamics (CFD). It can be used to investigate flow over spillways using reasonable sources, time and expense. A significant advantage of numerical simulations over laboratory experiments can be found in lower cost and shorter time requirements. However the challenge remains on the accuracy and the reliability of numerical models in face of the large air entrainment, high velocities and natural complexities of non-aerated and aerated portions of the flow on stepped spillways.

1.2   Statement of problems

The problem of using stepped spillway is the unknown of complex flow on each step. Even the flow through stepped spillway can dissipate a lot of energy and can decrease the cavitation problem, there is still no clarity of its processes. The physical model can not describe these processes clearly and completely. Therefore, if the numerical model can describe flow pattern and flow characteristics correctly, it would be the advantage for the design of stepped spillway.

Moreover, the numerical model with the equations and appropriate coefficients under the analytical solution can better show the flow process. Then, it would be better to have the specific coefficients and equations for simulation of the stepped spillways. It is also better if there are some equations that can be used to preliminary design of stepped spillway. At least, these equations can be an initial step to consider whether it is good or not to design the appropriate stepped spillway to release high flow.

One of the main questions in modelling stepped spillways is whether the physical and numerical models calibrated on small-scale physical models, can properly replicate the flow properties on large stepped spillways at the near-prototype scale. Table 1.1 lists a summary of the geometries of the various model-scale studies and corresponding turbulence models. Most of previous studies have normally investigated the flow through laboratory experiments on downscaled spillway models. The flow complexity along stepped spillways has caused definite uncertainties in extrapolating experimental results to prototype scales. Then, the scale effects is one of an important problems on the studies on the physical models.

The scale effect is a term of critical importance, used to describe slight distortions when viscosity and surface tension in highly air-entrained flows are ignored (Hunt and Kadavy, 2010). In two-phase flow through a spillway, viscosity and surface tension play an important role in air entrainment. This scale effect is attributed to high air-entrainment in flow over stepped spillway. The physical modelling of stepped spillways based upon a Froude similitude maybe sensitive to scale effects (Gonzalez and Chanson, 2004). If a Froude similitude is applied, the air bubbles are too large and cause too high detrainment rate. Moreover, flow recirculation on the step causes a momentum exchange with the main flow and suggests the need for a Reynolds similitude. Then, the guidances on modelling techniques for reducing scale effects was suggested (Boes, 2000a, 2003a, 2003b; Chanson, 1994a; Takahashi et al., 2006). The Reynolds number of at least 10^5 is proposed to minimize viscous effects (Boes, 2000a; Boes and Hager, 2003). A scale of 10:1 or larger is suggested for reducing the scale effects in modelling stepped spillways (Chanson, 2002). A minimum Weber number of 100 is recommended for surface tension effects to be negligible (Gonzalez and Chanson, 2004; Boes and Hager, 2003). Most of the previous studies focused on small scale stepped spillways and low discharge, the scale effect and possible advantages of numerical model deserve further consideration.

However, even if the numerical solution agrees well with the data from physical model, there is the uncertainty arising from the discretisation errors. The discretisation error is a potential deficiency in any phase of the modelling process due to lack of knowledge. Therefore, grid independence study has recently become important to determine whether the grid size is refined enough to produce good results with less discretisation error.

Table 1.1 Geometry of previous studies of numerical models on stepped spillways

Reference	Physical model from	Flow rate Q (m³/s)	Geometry			Maximum roughness $K_s = h\cos_{"}$ (m)	Number of steps N
			Slope " (degree)	Spillway height H (m)	Step height h (m)		
Chen et al.(2002)	Chen et al. (2002)	0.0200	53.1	0.79	0.02–0.06	0.04	13
Cheng et al.(2006)	Chen et al. (2002)	0.0300	53.1	0.83	0.02–0.06	0.04	13
Qian et al. (2009)	Amador (2006)	0.0800	51.3	2.00	0.0500	0.03	40
Tongkratoke et al. (2009)	Boes and Hager (2003b)	0.0233	30.0	2.85	0.0231	0.02	N/A
		0.0660	30.0	2.85	0.0462	0.04	N/A
		0.1866	30.0	2.85	0.0924	0.08	N/A
		0.0328	50.0	4.36	0.0311	0.02	N/A
		0.1705	50.0	4.36	0.0933	0.06	N/A
	Chanson and Toombes (2002)	0.0580	21.8	1.00	0.1000	0.10	9
		0.1140	21.8	1.00	0.1000	0.10	9

Remark: N/A = Not available

1.3   Objectives

1. To model the complex flow pattern of two-phase turbulence flow in spillways by the numerical model.

2. To establish which turbulence model and multiphase flow model are appropriate for the simulation of skimming flow over stepped spillways and to predict the flow

velocity with smallest deviation. The appropriate grid size for the simulation is also suggested based on Grid Convergence Index (GCI)

3. To expand the simulation results from numerical models to large scale physical models to ensure proper simulation of flow in complex multiphase flows.

4. To present the energy dissipation from flow over stepped spillway which is the most important advantages of using stepped spillways.

5. To develop the equations and charts for the preliminary design of spillways for any cases of possible discharges.

1.4   Scope of the study

The present study is to model the complex flow pattern of two-phase turbulence flow in spillways by using the numerical model. The appropriate turbulence model and multiphase flow model for the simulation of skimming flow over stepped spillways and prediction of the flow velocity with smallest deviation are established. The appropriate grid size for the simulation is also suggested based on Grid Convergence Index (GCI) in order to minimize the discretisation error. The numerical model is suggested to expand the simulation results from numerical models to large scale physical models to ensure proper simulation of flow in complex multiphase flows. The analytical solution and also the results from the numerical models are used to develop the equations and charts for the preliminary design of spillways for extreme events. One of the most important advantages of stepped spillway is the energy dissipation. Then, the equations of energy dissipation from using of stepped spillway are proposed.

The assumption of the complex turbulence flow in spillways is the flow would be two-phase free surface flow without any large or observable suspended sediment that can affect the flow pattern.

The simulation results from numerical models are compared to the large scale physical models to ensure proper simulation of flow in complex multiphase flows. Some parameters from the results will be compared with some previous studies. The physical models used to calibrate and verify the numerical models are from the study of Ward (2002). They were carried out at Colorado State University with the largest step height. The flow discharge up to 3.3 m^3/s corresponds to Reynolds numbers ranging from $1.68\times10^6 \leq \mathrm{Re} \leq 7.21\times10^6$. The physical model used in the present study is thus, the largest in size or near-prototype size, ever simulated by a numerical model. The flow velocity data is used to establish which turbulence model and multiphase flow model are appropriate for the simulation of skimming flow over stepped spillways.

The appropriate grid size for the simulation is suggested based on Grid Convergence Index (GCI). The smallest grid size is designed based upon the capability of the Dell Precision workstation with Intel Xeon CPU X3330 at 2.66 GHz, 2.67 GHz, and 8.0 GB of RAM and OS of Microsoft Server HPC Edition. The results from the numerical models are used to develop the equations and charts for the preliminary design of

spillways. The analytical solution is used to propose some coefficients of the equations used in the numerical models.

The energy dissipation from flow over stepped spillway is studied from the starting point of spillway to the end of last step of spillways.

1.5 Details of the dissertation

This dissertation consists of six chapters. The first chapter presents the introduction of the present study. The backgrounds, the statement of problem, the objectives, and the scope of study are also presented in this chapter. The literature review is shown in Chapter 2. Then, Chapter 3 shows the related theory. In Chapter 4, the methodology is shown. The results are presented and discussed in Chapter 5. Conclusions and recommendations from the study are presented in Chapter 6. Finally, references and appendices are also presented.

CHAPTER 2 LITERATURE REVIEW

This chapter presents the literature review of the study on spillways, stepped spillway, flow regimes, pressure distribution, energy dissipation, numerical model, multiphase flow model, turbulence model, grid convergence index. The recommendations from literatures are also presented. All literatures of each topic are summarised as follows;

2.1 Spillways

Dam and reservoirs are being used in many countries in various sizes. They can be constructed by many kinds of materials e.g.; earth fill, rock fill, concrete masonry, roller compacted concrete (RCC), etc. depending on availability of materials, cost, and mass stability. They can be overflowed and cause the overtopping problem if their capacities are less than the difference between inflow and outflow. The most sensitive structures are earth-fill dams, which can be destroyed by a small overtopping (Khatsuria, 2005). Even the dam that made of other kinds of materials can withstand the overtopping; overflow jet would be more concern about the immediate flow downstream, indirectly. It can cause other damages to the nearby structures and cause failure to them.

All dams, then, should be constructed with the high safety device to prevent the overtopping. As a result of dam safety policies, the spillway design flood are among the most conservative dam safety policies. The spillway should be designed to pass probable maximum flood (PMF) (Dubler and Grigg, 1996). It is also designed to surplus the excess water or flood. Takasu and Yamaguchi (1988) discussed about seven more functions on the spillway. They are; (i) maintain water in river, (ii) discharge water for utilization, (iii) maintain water level for flood control system, (iv) control floods, (v) control additional flood from upstream, (vi) release surplus water, and (vii) lower water level. Spillways have been classified, according to the most prominent feature by Khatsuria (2005), as shown in Figure 2.1.

A. Ogee spillway	B. Chute spillway
C. Side channel spillway	D. Shaft spillway
E. Siphon spillway	F. Straight drop or overfall spillway
G. Tunnel spillway/Culvert spillway	H. Labyrinth spillway
I. Stepped spillway	
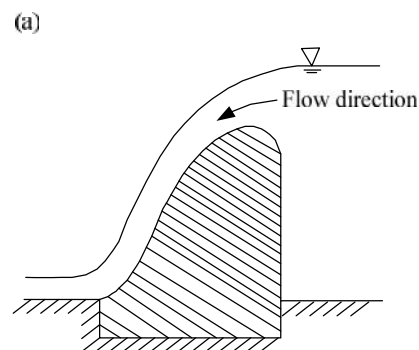
Source: Chanson (2002)

(a) Ogee spillway

Figure 2.1 Types of spillways

(b)

Flow direction

Flow direction

Source: Mccabe (2012)

(c)

Flow direction

Dam Crest

Flow direction

Source: Water Affairs (2012)

(d)

Flow direction

Outlet

Flow direction

Source: Water Affairs (2012)

(e)

Flow direction

Dam Crest

Flow direction

Outlet

(b) Chute spillway
(d) Shaft spillway

(c) Side channel spillway
(e) Siphon spillway

Figure 2.1 (Cont.) Types of spillways

(f)

Flow direction

Flow direction

Source: James (2012)

(g)

Dam Crest

Outlet

Flow direction

Flow direction

Source: Ross (2012)

(h)

Dam Crest

Flow direction

Flow direction

Source: Walsh Construction (2012)

(i)

Flow direction

Flow direction

Source: Takahashi et al. (2006)

(f) Straight drop or overfall spillway   (g) Tunnel spillway/Culvert spillway
(h) Labyrinth spillway   (i) Stepped spillway

Figure 2.1 (Cont.) Types of spillways

2.2   Stepped spillways

A stepped spillway having a profile made up of steps and consisting of an open-channel with a series of drops is becoming popular for high efficiency controlled release of overflow into a downstream river. The step faces of the spillway can dissipate the energy of the overflow and reduce the size of the energy dissipater needed at downstream of the spillway. Stepped spillway, which is also called stepped-channel spillways, staircase waste waterways, stepped spillways, and stepped chutes have been used for more than 3,000 years (Chanson, 2000,2002). There is some evidences showing that during the 19th century and early 20th century, dams were built with overflow stepped spillways. After the progresses and techniques in hydraulic jump stilling basins, stepped spillways had been neglected and expertise about them had been lost for a while (Chanson, 2001). In the early 1980's, the first RCC dam was constructed and then spread out the world. A number of previous studies mentioned the associated spillways are being constructed with a step-wise profile in about 34% of the 145 existing dams (Hollingworth and Druyts, 1986; Dunstan, 1994; Chanson and Toombes, 2002b). They have become popular due to the low-cost and the speed of construction (Logie, 1985; Parker, 1992)

The energy that can be dissipated downstream of the stepped spillway can eliminate or reduce the need for a large energy dissipater or stilling basins at the toe of the spillway. Then, the need for improved knowledge on the evaluation of energy dissipation at the downstream of the stepped spillway is getting higher with the increased size of the dams. The previous studies have been developed for the flow patterns or characteristics on stepped spillways, flow in aerated and non-aerated zones, air entrainment or air concentration distribution, flow depths, flow velocity, energy dissipation, pressure fluctuations, and cavitation erosion (Sorensen, 1985; Rajaratnam, 1990; Stephenson, 1991; Peyras et al., 1992; Ru et al., 1994; Gaston, 1995; Rice and Kadavy, 1996; Chamani and Rajaratnam, 1999; Pegram et al., 1999; Matos, 2000; Chanson and Toombes, 2001; Chanson, 2002; Boes and Hager, 2003a,b; Ohtsu et al., 2004; Andre, 2004; Andre et al., 2004; Gonzalez, 2005)

2.3   Flow regimes

The flow regime on a stepped spillway is classified into three types: nappe flow, transition and skimming flow (Chanson, 1996; Chamani and Rajaratnam, 1999; Chanson et al., 2002). Nappe flow is usually found on large steps or at low discharges appeared as a free-falling jet impacts from step to step with a fully aerated nappe cavity (Chanson, 2002). Skimming flows occur on small steps or at high discharges (Boes and Hager, 2003a; Chanson, 1996). The air pocket along the vertical face of each step disappears in skimming flows. The transition occurs at discharges higher than the maximum required for nappe flow but lower than for the onset of skimming flow. The flow on each step generates a large horizontal vortex that recirculates water with or without air entrainment, whilst the water surface is wavy. For practical engineering purposes, skimming flows are more relevant than nappe flows.

At the upstream end of skimming flows over stepped spillways, the water surface is rather smooth without air entrainment. The boundary layer thickness is less than the

flow depth and this zone is called the "non-aerated zone". The boundary layer develops and reaches the flow depth after a few steps at a location called the inception point. At the downstream of the inception point, flow is rapidly aerated. The free surface becomes wavy with significant air entrainment in this zone, called the "aerated zone" (Boes and Hager, 2003b; Ohtsu et al., 2004; Cheng et al., 2006). There is a line, called "pseudo-bottom", created over the external edges connected from tip to tip of the steps.

At each section of the aerated zone, the flow depth can be distinguished into at least two regions from using the pseudo-bottom; upper and lower regions (Chamani and Rajaratnam, 1999a, 1999b). The lower region beneath the pseudo-bottom consists of water containing individual air bubbles distributed throughout the flow and exchanged with the upper region. There was the development of the recirculation on each step. Most of the energy was dissipated to maintain recirculation in the lower region. It was maintained by turbulent stress between the main flow and the recirculating underneath (Matos et al., 1999; Sanchez-Juny et al., 2000; De Marinis et al., 2001; Khatsuria, 2005). The upper region, above the pseudo-bottom, contains a wavy water surface in which air is trapped by waves (Chanson and Toombes, 2002; Boes and Hager, 2003a, 2003b; Amador, 2006).

Many scaled-down physical model studies investigating flow over stepped spillways have been carried out in the past to study the flow characteristics and patterns. Some studies tested before year 2000 were collected in the study by Ward (2002). They are shown in Table 2.1. However, such modelling investigations are still quite expensive and time consuming due to the complexity of the flow. There are also the studies about the pressure field in skimming flow (Ohtsu and Yasuda, 1997; Matos et al., 1999; Sanchez-Juny et al., 2000; Andre et al., 2001; Amador et al., 2004; Tabbara et al., 2005).

Table 2.1 Previous studies on physical models (Modified from Frizell (2006) and Ward (2002))

Reference	Slope, $_,,$ (degree)	Slope, H:V	Model scale	Number of steps	Step height, h (m)	Discharge, Q (m³/s)	Unit discharge, q (m³/s/m)
Essery and Horner (1978)	11.31	5:1	-	12	0.16	-	-
	21.80	2.5:1		20	0.03		
	22.83	2.38:1		30, 20, 10, 8	0.09, 0.17, 0.33, 1.48		
	27.74	1.9:1		30, 10	0.12, 0.42		
	32.25	1.58:1		10	0.5		
	36.35	1.36:1		30, 10	0.16, 0.58		
	40.10	1.19:1		30, 10	0.19, 0.67		
	45.00	1:1		20	0.03		
Stephenson (1979)	18.4	3:1	-	1 to 4	0.49	-	-
	45.0	1:1					
Sorensen (1985)	52.0	0.78:1	(i) 1/10	(i) 15	0.200	(i) 0.052 to 2.49	(i) 0.05 to 2.54
			(ii) 1/25	(ii) 59		(ii) 0.063 to 1.16	(ii) 0.06 to 1.18
Stephenson (1991)	54.5	0.7:1	-	-	-	-	-

Table 2.1(Cont.) Previous studies on physical models (Modified from Frizell (2006) and Ward (2002))

Reference	Slope, θ (degree)	Slope, H:V	Model scale	Number of steps	Step height, h (m)	Discharge, Q (m³/s)	Unit discharge, q (m³/s/m)
Frizell (1992)	26.6	2:1	-	-	0.16	6 to 17.6	0.4 to 1.17
Peyras et al. (1992)	18.4 26.6 45.0	3:1 2:1 1:1	1/5	3 4 5	0.66 0.66 0.66	7.5 to 30.1	0.43 to 2.70
Christodoulou (1993)	55	0.7:1	-	15	0.082	0.35 to 1.59	0.215 to 0.97
Chamani and Rajaratnem (1994, 1999)	59 51.3	0.6:1 0.8:1	1/4.87, 1/10, 1/20	-	0.41, 0.2, 0.1	0.74 to 2.2	0.74 to 2.2
Gaston (1995)	26.6	2:1	-		0.21	16.6 to 160.9	3.33 to 30.03
Rice and Kadavy (1996)	21.8	2.5:1	1/20	27	0.10	1.74 to 4.34	0.70 to 1.74
Pegram et al. (1999)	59	0.6:1	(i) 1/10 (ii) 1/20	(i) 120 (ii) 240	0.082 to 0.66	(i) 2.6 (ii) 5.2	(i) 1.3 (ii) 2.6
Pinheiro and Fael (2000)	26.6 11.3	2:1 5:1	-	10	0.164	1.41	0.614
Chanson (2002)	21.8	2.5:1	-	9	0.328	1.41 to 6.36	0.43 to 1.94
Chen et al. (2002)	53.1	0.75:1	-	13	0.02 to 0.06	0.02 to 0.03	0.067 to 0.10
Ward (2002)	26.6	2:1	-	25, 50	2.0, 1.0	7.1 to 116	1.17 to 2.97
Andre (2004)	18.5 30	3:1 1.73:1	1/5 to 1/10	67	0.197	4.92	< 3.0
Gonzalez and Chanson (2004)	15.9	3.5:1	1/2	9	0.328, 0.164	5.28, 2.12 to 2.82	1.61, 0.646 to 0.86
Gonzalez and Chanson (2004b)	3.4	16.83:1	1/2	18	0.469, 0.2346	1.31 to 3.89, 0.35 to 1.41	0.8 to 2.37, 0.215 to 0.86
Sanchez-Juny and Dolz (2005)	51.3	0.8:1	-	40	0.10	0.20	0.33
Amador (2006)	51.3	0.8:1	-	40	0.05	0.08	0.03 to 0.11
Pfister et al. (2006)	50	0.84:1	1/12.9 1/3.2	25	1.20 0.30	0.45	0.90
Gonzalez and Chanson (2007)	-	0.84:1, 0.60:1	-	-	0.017 to 0.125	-	0.0006 to 0.58
Hunt et al. (2008)	14.04	4:1	1/8	40	0.038	0.198, 0.36, 0.50, 0.756, 1.116, 1.476	0.11, 0.20, 0.28, 0.42, 0.62, 0.82
Meireles and Matos (2009)	26.6	2:1	-	20, 10	0.025, 0.05	0.021 to 0.056	0.03 to 0.08
Roshan et al. (2010)	10.87	5.17:1	1/20	12, 23	6.5, 3.25	1.69 to 11.77	0.026 to 0.181
Bombardelli et al. (2011)	53	0.75:1	-	-	0.04	-	0.08 to 0.18
Felder and Chanson (2011)	26.6	2:1	-	10, 20	0.10, 0.05	0.02 to 0:237	0.057 to 0.237 and 0.021 to 0.218
Meireles et al. (2012)	53	0.75:1	-	10	0.02, 0.04, 0.08	0.05-0.20	0.05 to 0.20

2.3.1 Nappe flow

The nappe flow regime, as shown in Figure 2.2, can be defined as a succession of free-falling nappes (Chanson, 1996). In the nappe flow, the steps act as a series of overfalls from one step to another (Frizell, 2006). The flow leaves the step as a free-falling jet and impinges on the tread of the next step as a series of small free falls (Chanson, 1996; Ward, 2002). Generally, for small discharge, a free-falling nappe is found at the brink of the step while a hydraulic jump is observed on the step face (Chinnarasri and Wongwises (2006). In the nappe flow regime, three kinds of sub-regimes have been distinguished: (i) nappe regime with subcritical flow, (ii) nappe regime with mixed flow, and (iii) nappe regime with supercritical flow (Fratino, 2004).
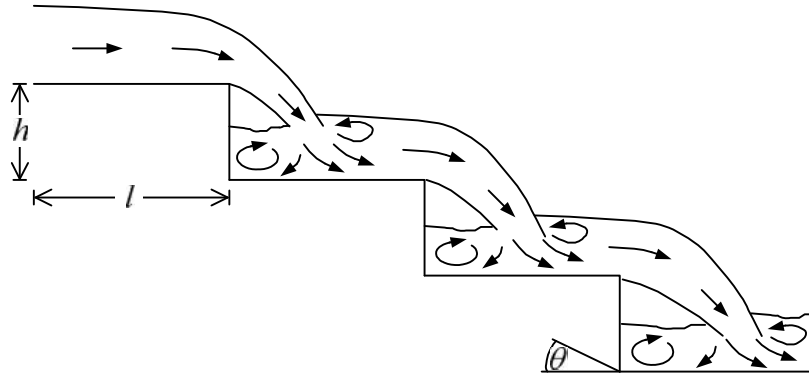
Figure 2.2 Nappe flow regime

Chanson (1994) proposed the equation for the occurrence of nappe flow with the fully developed hydraulic jump as follows;

$$\frac{y_c}{h} \leq 0.0.916\left(\frac{h}{l}\right)^{1.276} \tag{2.1}$$

for $0.2 \leq h/l \leq 0.6$.

Chanson (2001) proposed the upper limit of a nappe flow regime as follows;

$$\frac{y_c}{h} = 0.89 - 0.4\left(\frac{h}{l}\right) \tag{2.2}$$

for $0.05 \leq h/l \leq 1.7$.

Yasuda et al. (2001) proposed the lower limit of the step height for the nappe flow as follows;

$$\frac{h}{y_c} = 0.57\left(\frac{h}{l}\right)^3 + 1.3 \tag{2.3}$$

for $0.1 \leq h/l \leq 1.43$ and $0 < h/y_c \leq 1.37$.

Chinnarasri (2002) also proposed the upper limit of nappe flow as follows;

$$\frac{y_c}{h} = 0.98(0.55)^{h/l} \tag{2.4}$$

Chinnarasri and Wongwises (2004) proposed the maximum discharge for the nappe flow regime as follows;

$$\frac{y_c}{h} = 0.927 - 0.005_n - 0.388\left(\frac{h}{l}\right) \tag{2.5}$$

for $0.1 \le h/l \le 1.73$.

Roshan et al. (2010) found that the nappe and transition flow regimes occur at low discharge while skimming flow regime at high discharge. They showed experimentally that in case of 12-steps spillways, nappe or transition flow occur at discharge per unit width lower than 0.138 m^2/s.

The energy loss in nappe flow is greater for fewer steps for the same spillway height and discharge. It also decreases as the number of steps increases for the same spillway height and discharge (Chanson, 1994b; Matos and Quintela, 1995). Then, for the low dams with large steps, nappe flow can dissipate more energy than skimming flow (Andre, 2004). On the other hand, a spillway designed for a nappe flow would require large steps and flat slopes which means the construction cost would be very high (Frizell, 1992). Chamani and Rajaratnam (1994) presented the equation for the energy dissipation as shown in equation (2.6). It is summarised and confirmed again that this equation provided the best agreement among proposed equations by the others (Pinheiro and Fael, 2000).

$$\frac{E_L}{E_i} = \frac{\left\{(1-A)^N\left[1+1.5\left(\frac{y_c}{h}\right)\right] + \sum_{i=1}^{N-1}(1-A)^i\right\}}{N+1.5\left(\frac{y_c}{h}\right)} \tag{2.6}$$

where E_L = energy loss, $E_L = E_0 - E_i$

E_0 = energy at the inlet section, E_0 = (Elevation head+1.5y_c)

E_i = energy at the point-of-interest section,

   = (flow depth measured in vertical direction +velocity head)

$A = \left[0.30 - 0.35\left(\frac{h}{l}\right)\right] - \left[0.54 - 0.27\left(\frac{h}{l}\right)\right]\log\left(\frac{y_c}{h}\right)$

N = Number of steps

2.3.2 Transition flow

Ohtsu and Yasuda (1997) firstly introduced the transition flow region. The earlier studies about flow regime never mentioned about transition flow before. Then, all the studies were developed for the onset of skimming flow. For the transition flow, as shown in Figure 2.3, it appears chaotic with strong splashing and many droplet ejections just downstream the section where the air entrainment process takes place (Chanson and Toombes, 2004). The aeration process generally begins when the first deflected nappe occurs and develops in four different regions (Fratino, 2004). The free surface presents an undular profile characterised by wave length similar to the stepped invert profile and the air cavities under the falling nappes show an alternating trend in size when the flow passes from one step to another (Ohtsu et al., 2001; Chanson and Toombes, 2004).
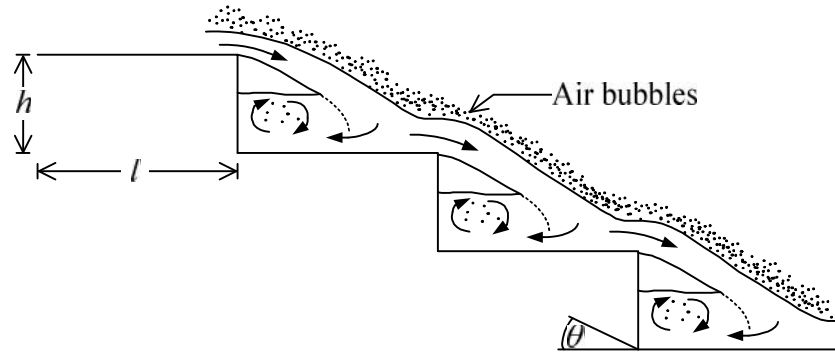
Figure 2.3 Transition flow regime

From the study of Ohtsu and Yasuda (1997), two empirical equations able to evaluate the upper limit for the nappe flow regime and the lower limit for the skimming flow regime were defined, respectively, as follows (Yasuda et al., 2001; Fratino, 2004);

$$\frac{y_c}{h} = \left[0.57\left(\frac{h}{l}\right)^3 + 1.3 \right]^{-1} \tag{2.7}$$

$$\frac{y_c}{h} = 0.862\left(\frac{h}{l}\right)^{-0.165} \tag{2.8}$$

where the spillway slope should be lower than 55°.

Chanson and Toombes (2004) defined two equations for the lower and upper limit of transition flows, respectively, as follow;

$$\frac{y_c}{h} > 0.9174 - 0.381\frac{h}{l} \tag{2.9}$$

$$\frac{k}{h} > \frac{0.9821}{\left(\frac{h}{l} + 0.388\right)^{0.384}} \tag{2.10}$$

where equations (2.9) and (2.10) are valid for the spillway slope between 0° - 60° and 0° - 56°, respectively.

2.3.3 Skimming flow

The skimming flow regime, as shown in Figure 2.4, were conducted corresponding to the largest discharges per unit width. The waters flow down a stepped channel as a coherent stream skimming over the pseudo-bottom formed by step edges (Rajaratnam 1990). Beneath the flow, cavity vortices are developed and recirculation is maintained through the transmission of shear stress from the main stream. Skimming flows are characterised by very significant form losses and momentum transfer from the main stream to the recirculation zones. There is an obvious analogy with skimming flows past large roughness elements and cavities (Gonzalez and Chanson, 2004b).
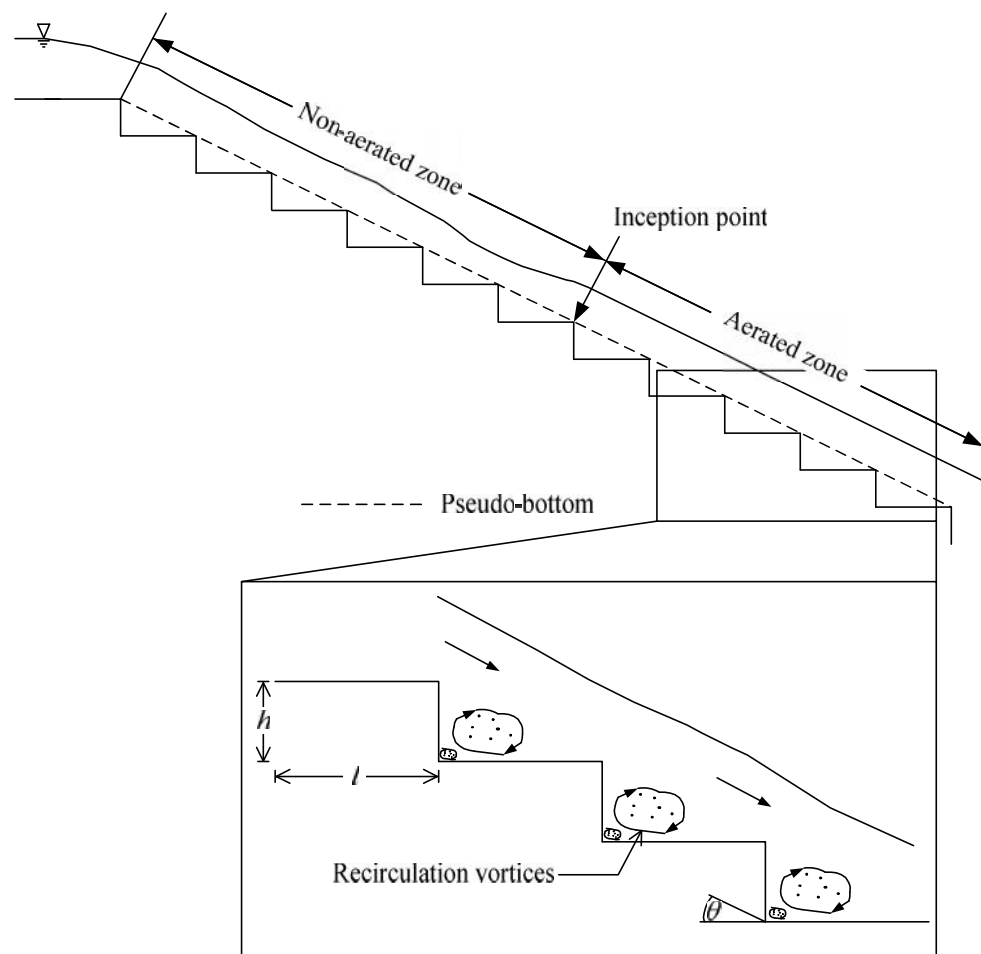
Figure 2.4 Skimming flow regime

The skimming flow looked similar to some self-aerated flow down smooth chutes. At the upstream end, the flow was smooth and transparent. This zone can be called the "non-aerated zone". When the outer edge of the developing bottom boundary layer reached the free surface, turbulence induced strong aeration. This point can be called as an inception point. Downstream of the point of inception of free-surface aeration, the air–water flow became fully developed and strong exchanges of air–water and momentum occurred between the main stream and the atmosphere. This zone can be

called the "aerated zone". An intense cavity recirculation was observed below the pseudo-bottom formed by the step edges. The air–water flow mixture consisted of a bubbly region (Void fraction < 30%), a spray region (Void fraction > 70%) and an intermediate zone in between (Gonzalez and Chanson, 2008).

Rajaratnam (1990) presents the equation for skimming flow, which includes transition flow at that time, as follows;

$$\frac{y_c}{h} > 0.8 \tag{2.11}$$

for $0.4 \le h/l \le 0.9$.

Chanson (1994) proposed the equation for the onset of skimming flow for spillway slopes range from 11.3 to 38.7 as follows;

$$\frac{y_c}{h} > 1.057 - 0.465\frac{h}{l} \tag{2.12}$$

Mondardo and Fabiani (1995) presents the equation for skimming flow, which include transition flow at that time, as follows;

$$\frac{y_c}{h} > 1.1974 - 0.59501\frac{h}{l} \tag{2.13}$$

Ohtsu et al. (2001) found that the limit of the relative critical depth for the skimming flows depends on the channel slope as follows;

$$\frac{y_c}{h} = \frac{6}{7}\left(\tan_{\theta}\right)^{-1/6} \tag{2.14}$$

where the spillway slope is $5.7^{0} \le \theta \le 55^{0}$.

Boes (2000a) presents the equation for skimming flow, which include transition flow at that time, as follows;

$$\frac{y_c}{h} = 0.91 - 0.14\left(\frac{h}{l}\right) \tag{2.15}$$

for $0.47 \le h/l \le 1.43$.

Chinnarasri and Wongwises (2004) proposed the minimum discharge required for the onset of skimming flow on horizontal and inclined steps as follows;

$$\frac{y_c}{h} = \left(0.844 + 0.003_{\theta}\right)\left(\frac{h}{l}\right)^{-0.153 + 0.004_{\theta}} \tag{2.16}$$

for $0.1 \leq h/l \leq 1.73$.

2.4 Pressure distribution on steps

In the skimming flow, the lower region on the step contains recirculating with high turbulence. The pressure field is expected to exhibit intense pressure fluctuations. Then, it is important to know whether pressure fluctuation can cause cavitation (Khatsuria, 2005). The pressures distribution mainly located in the upstream zone of the stepped spillway depends on the discharge different flow regions of the skimming flow; developing flow, rapidly varied flow or gradually varied flow regions.

Sanchez-Juny et al. (2000) and Sanchez-Juny and Dolz (2003) studied pressures distribution along the stepped spillway with a pressure transducer and flow visualizing technique. It was found that mean pressures are positive all along the spillway whereas both maximum and minimum pressures are located upstream of the inception point. The pressure at upstream is greater varied than downstream. Similar behaviour has already been presented by Othsu and Yasuda (1997). For the pressure profiles on the horizontal face of a step, the flow hits the downstream half of the horizontal face. At the upstream half of the horizontal face, the largest discharge and the lowest pressures were found because this zone is characterised by a boundary separation of the flow. Similar behaviours were already shown by Frizell (1992). For the pressure profiles on the vertical face of a step, the mean pressures can be negative. It can be less negative for the greater discharge because the region near the outer edge of the step is characterised by a boundary separation of the vortices. The area near the continuous horizontal face receives the impact of the recirculating flow. Therefore, the mean pressures will be positive though lower than those observed on the impact zone of the horizontal face. The study by Xun (1994) is also in the same trend and confirm the study of Sanchez-Juny et al. (2000).

Chinnarasri (2002) also experimentally studied the pressure on the horizontal step face. The pressure in his study was the time averaged pressure. It was found that the maximum time averaged pressure, $P_{\max}$, on the horizontal step face is located at the H_i below the crest as

$$\frac{P\max}{\text{x}H_i} = 1.28\left(\frac{q^2}{gH_i^3}\right)^{0.31} \tag{2.17}$$

Amador et al. (2004) found that the pressure profiles show the flows impacts in the downstream half of the horizontal face because the mean pressures are larger than in the upstream half. The pressures are governed by the cavity flow. The high variances of the pressures were also found on the downstream half. The negative pressures at the inner region of the step can be found because the mean pressures are smaller at the upstream half. For the vertical face near the outer edge, there is a separation flow region and negative pressures were found. It means that the pressures over the vertical faces are affected by the separation of the shear layer and the recirculation zone in the cavity.

Amador et al. (2009) investigated the dynamic pressures along the spillways. The difference of the dynamic pressure between non-aerated and aerated zone was found. For the aerated zone, it was found that the largest dynamic pressures on the horizontal faces near the step edge where pressures are governed by the impact of the overlying flow. The zone near the outer step corner on the vertical faces is identified as critical zone of cavitation risk. Then, the pressures are affected by flow separation and the relative mean values are close to zero although significant pressure fluctuations are observed. The region near the outer step edge of the horizontal face is characterised by a positively skewed distribution. On the other hand, the outer step corner of the vertical face, a negatively skewed function is observed.

For the transition flow, Fratino et al. (2003) found that the pressure values at the upstream are much greater than the pressure at the downstream. It means that there might be a cavitation risk at the upstream and more investigations are further needed. At the downstream, aeration surface and steady wavy flow may affect the fewer pressure.

In the nappe flow regime, Sanchez-Juny and Dolz (2005) found that the tread of the step can be divided into two zones, which are different from the skimming flow. The downstream quarter of the horizontal face is characterized by the impact of the upper flow. The maximum pressures in the outer end of the steps show values of around three times the step height. The upstream three quarters of the horizontal face are characterized by a hydrostatic behavior. In this zone, the lower discharge can cause the lower pressure fluctuations. The transition flow was also studied. It was found that the pressures begin to show the hydrostatic pattern because they were governed by the eddy trapped under the skimming flow.

2.5   Energy dissipation

The energy dissipation can be observed and calculated from the energy between the inlet section at the approach channel of spillway, E_0, and any section of interesting step, E_i, as shown in Figure 2.5.

The energy E_0 consists of elevation head from datum to the inlet, H_0, flow depth, y_c, and velocity head, $V_0^2/2g$,

$$E_0 = H_0 + y_c + \frac{V_0^2}{2g} \tag{2.18}$$

where the datum is located on the interesting step. The term of velocity head can be changed to be in terms of flow as

$$y_c^3 = \frac{q^2}{g} \tag{2.19}$$
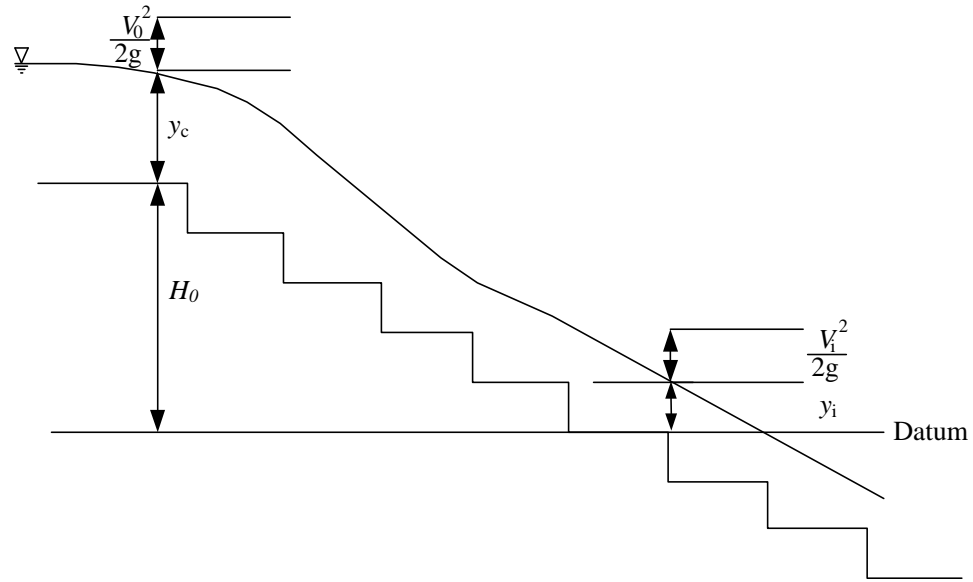
Figure 2.5 Parameters of the calculation of energy dissipation

The term of velocity head, then, can be written as

$$\frac{V_0^2}{2g} = \frac{Q^2}{2gA^2} = \frac{q^2 B^2}{2gy_c^2 B^2} = \frac{q^2}{2gy_c^2} \tag{2.20}$$

Substitute q^2 from equation (2.3) into (2.4),

$$\frac{V_0^2}{2g} = \frac{gy_c^3}{2gy_c^2} = \frac{y_c}{2} \tag{2.21}$$

Then, equation (2.2) becomes

$$E_0 = H_0 + y_c + \frac{y_c}{2} = H_0 + 1.5y_c \tag{2.22}$$

The section of interesting step is also superimposed with the datum. Then, the energy E_i consists of flow depth measured, vertically, from the datum, y_i, and velocity head, $V_i^2/2g$,

$$E_i = y_i + \frac{V_i^2}{2g} \tag{2.23}$$

The energy loss, E_L, is the difference between energy at the inlet section, E_0, and the energy at the section of interesting step, E_i.

$$E_L = E_0 - E_i \tag{2.24}$$

The energy dissipation, E_L/E_0, is one of the dimensionless parameter which is widely used to study the energy dissipation characteristics.

Several previous studies have been performed on physical models of stepped spillway. However, the results were valid only for that case and could only be used as a guide for other similar cases (Chatila and Jurdi, 2004). For the skimming flow through the stepped spillway, it is the high level of free-surface aeration (Rajaratnam, 1990; Matos, 2000). The free surface air is trapped and released, and the resulting two-phase mixture interacts with the flow turbulence. It yield some intricate air-water structure associated with complicated energy dissipation mechanisms (Chanson and Toombes, 2002; Gonzalez and Chanson, 2004b; Carosi and Chanson, 2008).

Young (1982) studied the feasibility of a stepped spillway for the Upper Stillwater Dam and found a 75% energy reduction. Sorensen (1985) studied the design of steps and their spacing on the spillway face in order to optimise the energy dissipation. It was found that adding a few steps to the face of the spillway eliminated the deflecting water jet. Peyras et al. (1992) and Israngkura and Chinnarasri (1994) found the relative energy loss is influenced by the drop number, where the drop number, q^2/gH_T^3, is the function consists of q = flow discharge per channel width, g = gravitational acceleration, and H_T = total drop height. Moreover, the relative energy loss also depends on the spillway slope. Chinnarasri and Wongwises (2006) presented the relative energy loss, E_L/E_0 decreases as the relative critical flow depth increases. In the nappe flow, the characteristic height does not much affect the relative energy loss because most energy loss is due to the occurrence of the hydraulic jump and impact of the jet on the step face. In transition flow, the characteristic height has higher influence on the relative energy loss than in nappe flow. As the characteristic height increases, the relative energy loss increases. In skimming flow, the effect of characteristic height is clearly observed.

Christodoulou (1993) found that energy loss due to the steps depends on the ratio of the critical depth to the step height, as well as on the number of steps. Shvainshtein (1999) concluded that spillway is an effective energy dissipater and can greatly reduce the size of energy dissipater downstream. The total energy losses can be taken into account by means of the velocity coefficient, which is used for determining the conjugate depth at the toe of the spillway and ultimately for calculating devices for transition of the pool.

Chanson (1995), Boes (1999), Matos (2000), Chatila and Jurdi (2004), Hunt and Kadavy (2010) found that the energy dissipation rate will then decrease with increasing discharge as it reaches a stage where the effect of the steps is very small and a stepped spillway acts similar to a smooth one. For the largest flow rates, the discharge was not fully developed at the downstream end of the spillway and the residual energy might be overestimated (Chanson, 2002; Meireles and Matos, 2009)

As the number of steps increases, the energy dissipated is increased. As same as the conclusion from the study by Chamani and Rajaratnam (1994), Boes (1999), Andre et al. (2004), Chanson and Gonzalez (2004), Chatila and Jurdi (2004) found that the

number of steps is more important than the size of the steps. This is due to the fact that steps act as macro-roughness that increase friction and then change the kinetic energy into heat or thermal energy. Felder and Chanson (2011) indicated that the rate of energy dissipation was about the same for uniform and non-uniform stepped configurations. The non-uniform stepped configurations might induce some flow instabilities for smaller flow rates. Chanson (2002) suggests that greater energy dissipation occurs in stepped spillways under nappe flow regime, which most occurs in stepped spillways with large step heights on relatively flat slopes. However, the maximum design flow in these particular spillways is rarely nappe flow.

2.6   Numerical model

Computational Fluid Dynamics (CFD) is a type of numerical model that can be used to solve problems involving fluid flow. A CFD can provide a significant amount of computation time and more economical solution than a physical model. The fundamental principles for all numerical models are similar. Problems can be described, physically, by a set of partial differential equations. Then, a numerical method is used to formulate a set of algebraic equations that represent the partial differential equations. An approximate solution of a set of algebraic equations is obtained through some form of either an iterative or matrix solution. The solutions from the numerical model are mostly calibrated and verified through comparisons to field observations or physical model experiments (Chanel, 2008)

The two well established and widely used numerical methods are the Finite Difference and Finite Element Methods, FDM and FEM, respectively. Tabbara et al. (2005) used the FEM to predict stepped flows for small scale experiments. In the upper part of the flume as well as in the bottom part steps were introduced along the chute such that the envelope of their tips followed the smooth spillway chute profile. Although their results were encouraging, physical or laboratory measurements are still crucial for providing reference data. Benmamar et al. (2003) developed a numerical model based on the implicit FDM for the development of a two-dimensional boundary layer over a steep stepped spillway. The finite volume method, which has been extensively used to model a wide range of fluid-flow problems, was originally developed as a special FDM. One of the CFD model studies in the spillway is from Kim et al. (2010). The FLOW-3d model was used with the initial design plan of the Karian dam in Indonesia. The results showed that the flow in the approach channel was unstable. A revised plan was formulated and the appropriate amended design was examined using numerical modelling. Carvalho and Amador (2008) also simulated the flow in the non-aerated region by using the FLOW-3d with the FDM. Their numerical results were compared with the physical data and found a good agreement in the non-aerated region.

Another numerical method that is widely used in the simulation of flow in different forms is the Finite Volume Method, FVM. It is similar to both FDM and FEM in which their values are calculated at discrete places on mesh geometry. Its name refers the structure of its geometry which means the small volume surrounding each node point on a mesh. The surface integrals in a partial differential equation that contain a divergence term are converted to volume integrals, using the divergence theorem. These terms are then evaluated as fluxes at the surfaces of each finite volume. The FEM and FVM are

compared by the comparisons on free surface flow equations including air entrainment and applied to calculation of the flow in a spillway. The FVM requires less computational effort than the FEM (Unami et al., 1999). A successful use of Fluent which is the FVM to model the spillway was found since 2006 (Dargahi, 2006; Sartaj et al., 2006).

Turan et al. (2006) studied the tailrace flow on Brownlee Dam on the Snake River. The 1/48 physical model was built. The FVM was used to simulated with two kinds of turbulence models, Reynolds Stress Model, RSM, and standard k-ε model. Predicted results of the model will contribute to the understanding of the physics of this entrainment. Khan et al. (2008) studied a model of the forebay of The Dalles Dam to investigate the effects of blocking the upper 12.3 m of the turbine intakes. The study demonstrates that commercial available CFD software packages can be a valuable tool for investigating forebay hydraulics and designing passage facilities at hydropower plants. Fu et al. (2008) investigated a flow field around a removable spillway weir structure at Little Goose Dam by using FVM. It is also used to predict the discharge for a given forebay elevation. The model can be used to evaluate the possible reduction of the spillway capacity during a Probably Maximum Flood (PMF) event.

Tadayon and Ramamurthy (2009) investigated three different turbulence models which are; Reynolds Stress Model, RSM, Renormalised k-ε model, RNG k-ε, and standard k-ε model, to analyse the flow over circular spillways. The FVM was also used for the numerical simulation. Dastgheib et al. (2012) carried out, with uses the FVM to simulate the free surface location and predict flow features such as velocity, pressures and complex free surface in different regimes including nappe, transition and skimming flow. A 1:20 physical model was constructed within the Hydraulics Laboratory with the stepped spillways of 12 steps. The results were satisfactorily validated using experimental datasets.

Although some literature shows successful comparisons between CFD and physical model as a cost-effective and reliable tool, it still cannot be considered as a complete replacement of physical model for all hydraulic engineering projects (Li et al., 2011). It still have some limitations in accurate simulation of the formation of free surface and vortices. Hence, more study would provide the confidence to use numerical model for different design purposes. Also, with the use of the finite volume method to simulate the complexity of flow, different kinds of multiphase flow and turbulence algorithms in the numerical method can be used to simulate the flow over stepped spillways.

A multiphase flow can be defined as a mixture of flow which consists of more than two phases. For the flow over stepped spillway, free surface flow with high turbulence of air is of interests. Both air and water cannot be ignored from the model because of their influence on the fluid dynamic behaviour. Then, in the numerical model, the multiphase flow model should be used in simulation. Two types of the multiphase flow model are used in the present study; (i) Volume of Fluid model (VOF), and (ii) Mixture multiphase flow model (MMF).

The Volume of Fluid model, VOF, with an unstructured grid was used by Chen et al. (2002) and Cheng et al. (2006) for the as multiphase flow simulation of stepped spillways. The simulated pressure profiles on the horizontal step surface were quite similar to the physical model measurements. However, the pressure profiles on the vertical faces of each step were slightly different between the numerical and physical models. Dong and Lee (2006) studied the numerical simulation of skimming flow over a mild stepped channel. Their channel consisted of 40 steps at a channel slope of $=10^{o}$ and 20°. All air boundaries were defined as pressure boundaries with zero pressure specified. Smooth channel flow was also simulated to compare the hydraulic characteristics with the stepped spillway overflow.

Qian et al. (2009) used a mixture multiphase flow model, MMF, to simulate flows over a stepped spillway with various kinds of turbulence models: (1) the realisable k-ν model; (2) the shear stress transport SST k-Š model; (3) the v^2-f model; and (4) the large eddy simulation LES model. The realisable k-ν model showed good performance for the simulation of flows involving rotation, boundary layer and recirculation. In their study, only one unit discharge, $q = 0.11\text{m}^2$/s, was used. Cheng et al. (2006) used a physical spillway model with 13-steps at various step height (2, 2.4, 3, 4, 5, and 6 cm) for validation of the MMF numerical model with a Renormalisation Group Theory k-ε algorithm (RNG). The only tested discharge was 0.03 m^3/s. However, the Reynolds numbers for some cases in their study were relatively out of proportion with the need to meet prototype conditions. Some limitations with Froude similitude at low Reynolds number therefore emphasised that numerical results should be validated with large scale models.

The turbulence model is also used in order to simulate the turbulence flow between two phases of fluid. Among the linear turbulence models, the widely used two-equation model is based on: (1) the turbulent kinetic energy equation k and (2) the turbulent eddy dissipation ν, or the turbulent frequency Š. Five different turbulence models were chosen in the present study to simulate the flow over stepped spillways: the Standard k-ν, the Realisable k-ν, the Renormalisation group k-ν , the Standard k-Š and the Shear stress transport k-Š model.

Chen et al. (2002) used a standard k-ν model to simulate the flow. The first five step heights were 0.02, 0.024, 0.03, 0.04 and 0.05 m. Downstream were eight more steps with a uniform step height of 0.06 m. The overall height of spillway was 0.789 m and the number of steps was only 13 which were too short to attain the aerated zone. The trends of velocity and pressure profiles from numerical and physical models were similar but the error at some points was more than 20%. The results proved to be consistent with the flow characteristics and measured surface profiles. Cheng et al. (2006) used a mixture model to reproduce the flow over a stepped spillway, including also the interaction between entrained air and cavity recirculation in the flow, velocity distribution and the pressure profiles on the step surface. The Renormalisation group k-ε model (RNG k-ε) was chosen and their numerical results successfully reproduced the flow over the stepped spillway of the physical model. The results were helpful for understanding the rates of energy dissipation. Tongkratoke et al. (2009) used other turbulence models: a linear, the LES and the non-linear model of Craft et al. (1996).

They modified the non-linear model to simulate the stepped spillways from Chanson and Toombes (2002) and Boes and Hager (2003b). The Rl k-ν showed the most satisfactory results amongst the linear turbulence models. The modified non-linear model also showed higher accuracy than other non-linear models.

2.7 Grid convergence index

In order to perform a grid convergence study, Roache et al. (1986) suggested a grid convergence index, GCI, to provide a consistent manner in reporting the results of grid convergence studies and estimate a discretisation error on the grid convergence of the solution. The GCI is a measure of the percentage the computed value is away from the numerical value. It is based upon a grid refinement error estimator derived from the theory of generalised Richardson Extrapolation (Roache et al., 1986). The methodology consists of five steps (Roache, 1997; Celik et al., 2008).

First, define the representative grid sizes, then, select three different grid resolutions with a grid refinement ratio, r_{ij}, of higher than 1.3 to obtain good results of using GCI (Roache et al., 1998), where $r_{ij} = h_{gi}/h_{gj}$, h_g define a representative grid size = $[(1/N)\Sigma(\Delta A_k)]^{1/2}$, N means the total number of cells and ΔA_k is the area of the kth cell. Subscript i means coarser grid while subscript j means finer grid.

Then, the apparent order, p, is calculated from the equations as (Schwer, 2008)

$$p = \frac{\left|\ln\left|\frac{f_{32}}{f_{21}}\right| + q(p)\right|}{\ln r_{21}}$$

(2.25)

$$q(p) = \ln\left(\frac{r_{21}^p - s}{r_{32}^p - s}\right)$$

(2.26)

$$s = sign\left(\frac{f_{32}}{f_{21}}\right)$$

(2.27)

where $f_{ij} = f_i - f_j$, f means a value of numerical solution. GCI is given by

$$GCI_{ij} = F_s \frac{e_a^{ij}}{r_{ij}^p - 1}$$

(2.28)

where F_s is a safety factor which is recommended to be 1.25 for comparison over three or more grids (Roache et al., 1998), e_a^{ij} is the approximate relative error, $e_a^{ij} = |(f_i - f_j) / f_j|$. Next step is a calculation of the extrapolated solution, f_{ext}^{ij}, and the extrapolated relative error, e_{ext}^{ij}, from equations (2.38) and (2.39), respectively. Both terms can be used to show the extrapolated results.

$$f_{ext}{}^{ij} = \frac{r_{ij}^{p} f_j - f_i}{r_{ij}^{p} - 1} \tag{2.29}$$

$$e_{ext}{}^{ij} = \left| \frac{f_{ext}{}^{ij} - f_j}{f_{ext}{}^{ij}} \right| \tag{2.30}$$

Finally, the calculation of approximate relative error and GCI are given by

$$e_a{}^{ij} = \left| \frac{f_i - f_j}{f_j} \right| \tag{2.31}$$

$$\text{GCI}_{ij} = F_s \frac{e_a{}^{ij}}{r_{ij}^{p} - 1} \tag{2.32}$$

2.8   Recommendations from literature

Flow in stepped spillway is two phases flow which is very complex especially on each step. There is none of any previous study that can define the flow on each step in any flow regime although the flow on each step can describe the physical characteristics of other related parameters, for example; flow velocity, energy dissipation. The instrument on the physical model cannot be used to collect the data at some points, for example; the location near the spillway floor, because of the effect of the floor. The physical model data at the middle zone, which is far enough from the effect of the floor, then, can be used to calibrate and verify the numerical model. Then, the numerical model can be used to predict the data near the floor or near the surface. However, the appropriate size of physical model should be used to calibrate and verify the model to eliminate the scale effect problem. Most of the previous studies were done on the small scale models and then, the simulation were calibrated and verified on the small scale physical models.

The equations and charts for the preliminary design of spillways for any cases of possible discharges and also the properties of parameters related to the energy dissipation which are from the simulation of large scale model have never been mentioned in any previous studies.

The turbulence model and multiphase flow model should be suggested in order to simulate the complex flow through the stepped spillway with smallest deviation. The appropriate grid size for the simulation has never been suggested though it can save cost and time for simulation. The Grid Convergence Index (GCI) was suggested to simulate some kinds of flow but it never been used with flow through the stepped spillway. Then, the appropriate turbulence and multiphase flow models should be suggested under the study of GCI to get the good results on simulation of flow through the stepped spillway.

CHAPTER 3 THEORY

This chapter presents the basic theory of the study. It consists of the equations of conservation; Mass conservation equation, Momentum conservation equation, and the Finite Volume Method (FVM) for numerical study.

Generally, a CFD model study consists of the following steps: i) obtaining the data of the physical model for grid development; ii) selecting or developing appropriate model method; iii) define the boundary conditions based on available field information; iv) develop the computational grids; v) calibrate and verify the model; and vi) analyse various parameters or scenarios.

3.1 Equations of conservation

In the time of development of the computational fluid dynamics, CFD, it has been one of the best tools for the prediction of flow. However, complex flow through stepped spillway still needs more studies and researches to be understood. The description of the physical processes of flow involves a variety of computational methodologies to predict the quantities of the components and its behavior (Franz and Melching, 1997).

The related conservation principles are; (i) the mass conservation, and (ii) the momentum conservation.

3.1.1 Mass conservation equation

Mass conservation equation or continuity equation states that the mass of a closed system of substances will remain constant, regardless of the processes acting inside the system. Matter cannot be created nor destroyed, although it may be changed in form. Consider the flow model shown in Figure 3.1, an infinitesimally small fluid element moving with the flow.
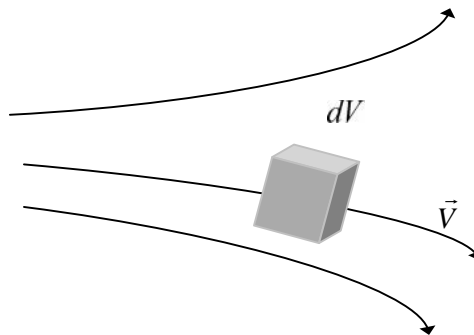
Figure 3.1 Definition sketch for flow model

Fluid element has a fixed mass, but its shape and volume change as it moves. Define *dm* and *dV* as the fixed and variable volume, respectively. Then we get equation (3.1).

$$dm = ... dV \tag{3.1}$$

Since mass is conserved, the rate of change of mass of fluid element is zero as the element moves along the flow. The substantial derivative, $D(dm)/Dt$, define the time rate of change of mass of moving fluid element was used for define physical meaning. Then we get equation (3.2)

$$\frac{D(dm)}{Dt} = 0 \qquad (3.2)$$

Substituting equation (3.1) into equation (3.2), we get equation (3.3)

$$\frac{D(\ldots dV)}{Dt} = dV\frac{D\ldots}{Dt} + \ldots\frac{D(dV)}{Dt} = 0 \qquad (3.3)$$

Rearranging equation (3.3) to be equation (3.4)

$$\frac{D\ldots}{Dt} + \ldots\left[\frac{1}{dV}\frac{D(dV)}{Dt}\right] = 0 \qquad (3.4)$$

From the divergence of the velocity and its physical meaning, then equation (3.4) becomes equation (3.5).

$$\frac{D\ldots}{Dt} + \ldots\nabla\cdot\vec{V} = 0 \qquad (3.5)$$

From the substantial derivative, $\frac{D}{Dt} = \frac{\partial}{\partial t} + \vec{V}\cdot\nabla\ldots$, we get equation (3.6)

$$\frac{\partial\ldots}{\partial t} + \nabla\cdot\left(\ldots\vec{V}\right) = 0 \qquad (3.6)$$

Equation (3.6) is mass conservation equation or continuity equation used to be the governing equation.

3.1.2 Momentum conservation equation

The momentum equation is a statement of Newton's Second Law and relates the sum of the forces acting on an element of fluid to its acceleration or rate of change of momentum. Newton's Second Law can be written as The Rate of change of momentum of a body is equal to the resultant force acting on the body, and takes place in the direction of the force. We can write it as equation (3.7). The moving fluid element model is sketched in more detail in Figure 3.2.

$$F = ma \qquad (3.7)$$

$$\left(\tau_{yx} + \frac{\partial \tau_{yx}}{\partial y}dy\right)dxdz$$

$$\tau_{zx}dxdy$$

$$\left(p + \frac{\partial p}{\partial x}dx\right)dydz$$

$$pdydz$$

$$\tau_{xx}dydz$$

$$\left(\tau_{xx} + \frac{\partial \tau_{xx}}{\partial x}dx\right)dydz$$

$$\tau_{yx}dxdz$$

$$\left(\tau_{zx} + \frac{\partial \tau_{zx}}{\partial z}dz\right)dxdy$$
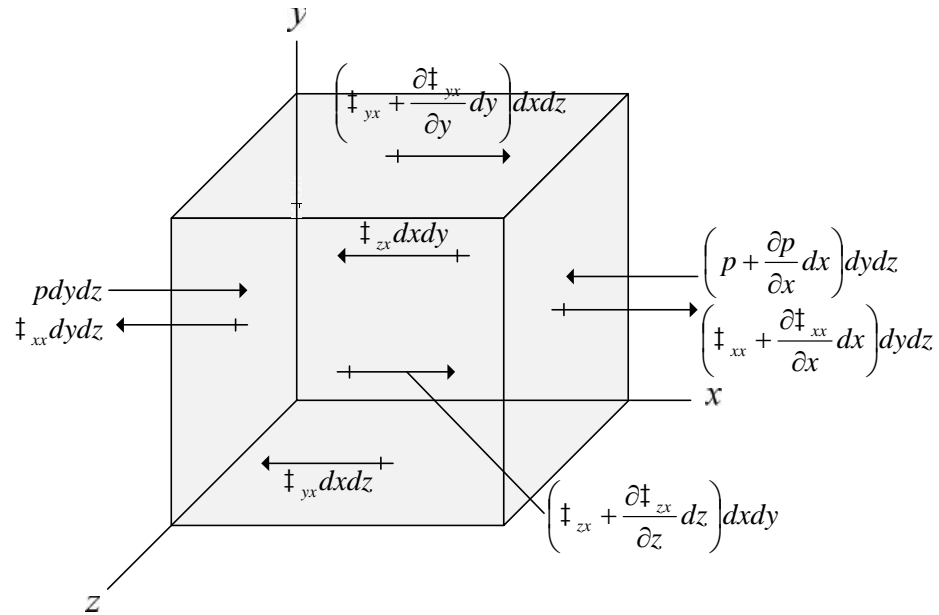
Figure 3.2 Moving fluid element model for the *x* component

The sources of the forces are classified into 2 groups; body forces and surface forces. Body forces act directly on the volumetric mass of the fluid element, hence, the body force on fluid element acting in *x* direction is shown in equation (3.8). Surface forces act directly on the surface of fluid element, hence, net surface force on fluid element acting in *x* direction is shown in equation (3.9).

Body force on fluid element acting in *x* direction $= \rho f_x (dxdydz)$ (3.8)

where f_x is the body force on *x*-direction. Finally, only f_y can be applied in the equation as a gravitational acceleration, *g*.

Net surface force in *x* direction $=$
$$\begin{aligned}
&\left[p - \left(p + \frac{\partial p}{\partial x}dx\right)\right]dydz \\
&+ \left[\left(\tau_{xx} + \frac{\partial \tau_{xx}}{\partial x}dx\right) - \tau_{xx}\right]dydz \\
&+ \left[\left(\tau_{yx} + \frac{\partial \tau_{yx}}{\partial y}dy\right) - \tau_{yx}\right]dxdz \\
&+ \left[\left(\tau_{zx} + \frac{\partial \tau_{zx}}{\partial z}dz\right) - \tau_{xx}\right]dxdy
\end{aligned}$$
      (3.9)

The total force in the *x* direction F_x is the sum of equations (3.8) and (3.9) and it is shown in equation (3.10).

$$F_x = \left[-\frac{\partial p}{\partial x} + \frac{\partial \tau_{xx}}{\partial x} + \frac{\partial \tau_{yx}}{\partial y} + \frac{\partial \tau_{zx}}{\partial z} \right] dxdydz + \rho f_x \, dxdydz \qquad (3.10)$$

Consider the mass of the fluid element, $m = \rho(dxdydz)$ and the component of acceleration in the x direction, $a_x = \dfrac{Du}{Dt}$, equation (3.7) in the x direction can be written as equation (3.11).

$$F_x = \rho(dxdydz)\frac{Du}{Dt} \qquad (3.11)$$

Equation (3.12) is the rearranged form of the equality of equations (3.10) and (3.11)

$$\rho\frac{Du}{Dt} = -\frac{\partial p}{\partial x} + \frac{\partial \tau_{xx}}{\partial x} + \frac{\partial \tau_{yx}}{\partial y} + \frac{\partial \tau_{zx}}{\partial z} + \rho f_x \qquad (3.12)$$

From the substantial derivative as mentioned above, we get equation (3.13)

$$\rho\frac{Du}{Dt} = \rho\frac{\partial u}{\partial t} + \rho\vec{V}\cdot\nabla u \qquad (3.13)$$

From the derivative, $\dfrac{\partial(\rho u)}{\partial t} = \rho\dfrac{\partial u}{\partial t} + u\dfrac{\partial \rho}{\partial t}$, and the vector identity for the divergence of the product of a scalar times a vector, $\nabla\cdot(\rho u\vec{V}) = u\nabla\cdot(\rho\vec{V}) + (\rho\vec{V})\cdot\nabla u$, then we get equation (3.14)

$$\rho\frac{Du}{Dt} = \frac{\partial(\rho u)}{\partial t} - u\left[\frac{\partial \rho}{\partial t} + \nabla\cdot(\rho\vec{V})\right] + \nabla\cdot(\rho u\vec{V}) \qquad (3.14)$$

The terms in the bracket are the form of mass conservation equation that equal to zero. Thus equation (3.14) is reduced to equation (3.15).

$$\rho\frac{Du}{Dt} = \frac{\partial(\rho u)}{\partial t} + \nabla\cdot(\rho u\vec{V}) \qquad (3.15)$$

Substitute equation (3.15) into equation (3.12), then it becomes equation (3.16)

$$\frac{\partial(\rho u)}{\partial t} + \nabla\cdot(\rho u\vec{V}) = -\frac{\partial p}{\partial x} + \frac{\partial \tau_{xx}}{\partial x} + \frac{\partial \tau_{yx}}{\partial y} + \frac{\partial \tau_{zx}}{\partial z} + \rho f_x \qquad (3.16a)$$

Similarly, the y and z components can be obtained as

$$\frac{\partial(\rho v)}{\partial t} + \nabla\cdot(\rho v\vec{V}) = -\frac{\partial p}{\partial y} + \frac{\partial \tau_{xy}}{\partial x} + \frac{\partial \tau_{yy}}{\partial y} + \frac{\partial \tau_{zy}}{\partial z} + \rho f_y \qquad (3.16b)$$

$$\frac{\partial(\rho w)}{\partial t}+\nabla\cdot\left(\rho w\vec{V}\right)=-\frac{\partial p}{\partial z}+\frac{\partial\tau_{xz}}{\partial x}+\frac{\partial\tau_{yz}}{\partial y}+\frac{\partial\tau_{zz}}{\partial z}+\rho f_z \tag{3.16c}$$

For such fluids, Stokes in 1845 obtained equations (3.17*a*) to (3.17*f*)

$$\tau_{xx}=-\frac{2}{3}\mu\left(\nabla\cdot\vec{V}\right)+2\mu\frac{\partial u}{\partial x} \tag{3.17a}$$

$$\tau_{yy}=-\frac{2}{3}\mu\left(\nabla\cdot\vec{V}\right)+2\mu\frac{\partial v}{\partial y} \tag{3.17b}$$

$$\tau_{zz}=-\frac{2}{3}\mu\left(\nabla\cdot\vec{V}\right)+2\mu\frac{\partial w}{\partial z} \tag{3.17c}$$

$$\tau_{xy}=\tau_{yx}=\mu\left[\frac{\partial v}{\partial x}+\frac{\partial u}{\partial y}\right] \tag{3.17d}$$

$$\tau_{xz}=\tau_{zx}=\mu\left[\frac{\partial u}{\partial z}+\frac{\partial w}{\partial x}\right] \tag{3.17e}$$

$$\tau_{yz}=\tau_{zy}=\mu\left[\frac{\partial w}{\partial y}+\frac{\partial v}{\partial z}\right] \tag{3.17f}$$

where μ is the molecular viscosity coefficient. Equations (3.16a) to (3.16c) are the Navier-Stokes equations and they can be written as one equation as shown in equation (3.18).

$$\frac{\partial}{\partial t}\left(\rho\vec{V}\right)+\nabla\cdot\left(\rho\vec{V}\vec{V}\right)=-\nabla p+\nabla\cdot\left(\tau\right)+\rho\vec{f} \tag{3.18}$$

3.2   Finite Volume Method

The Finite Volume Method, FVM, is a method for representing and evaluating partial differential equations as algebraic equations. It is one of the most versatile discretisation techniques used in CFD. The advantage of the finite volume method is that it is easily formulated to allow for unstructured meshes. Finite volume refers to the small volume surrounding each node point on a mesh. In this method, volume integrals in a partial differential equation that contain a divergence term are converted to surface integrals, using the divergence theorem. These terms are then evaluated as fluxes at the surfaces of each finite volume. Based on the control volume formulation of analytical fluid dynamics, the first step in the FVM is to divide the domain into a number of control volumes where the variable of interest is located at the centroid of the control volume as shown in Figure 3.3. The next step is to integrate the differential form of the governing equations over each control volume. Interpolation profiles are then assumed in order to describe the variation of the concerned variable between cell centroids.
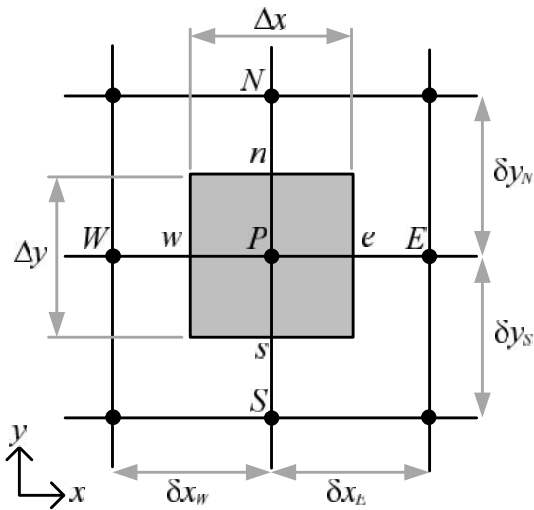
Figure 3.3 Grid cells

For each computational loop, volume is adjusted from the last value of previous grid cell as shown in Figure 3.4. The Q_i^n at the i_{th} grid and the t_n time is estimated from equation (3.19).
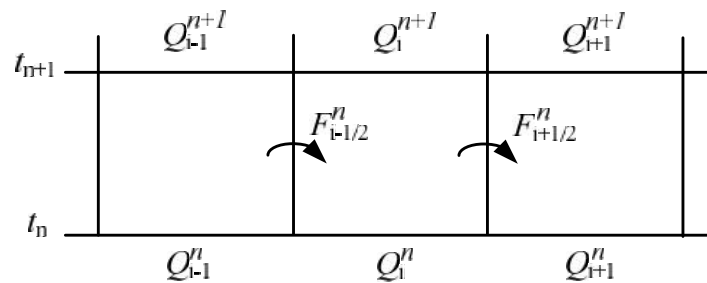
Figure 3.4 Computational directions

$$Q_i^n \approx \frac{1}{\Delta x} \int_{x_{i-1/2}}^{x_{i+1/2}} q(x,t_n)dx \equiv \frac{1}{\Delta x} \int_{c_i} q(x,t_n)dx \qquad (3.19)$$

where $\Delta x = x_{i+1/2} - x_{i-1/2}$ is grid cell length

For Finite volume method, there are many schemes for appropriate solving, they are;
    - First-Order Upwind Scheme: this method assign that properties at skin of object are equal to at center of object. It is appropriate used for grid parallel flow.
    - Second-Order Upwind Scheme: this method assign that properties at skin of object is averaged from two-side cells. It is appropriate used with triangle and hexagon grid cells that flow is not parallel with grid.
    - QUICK Scheme: this method assign that properties of cells depend on weight of important. It is more accurate than two above-mentioned methods if it is used for cubic or hexagon meshes eddy computation.

- Power-Law Scheme: this method uses the interpolation from other grids and its accuracy is equal to First-Order Upwind Scheme.

- A modified HRIC Scheme: this method is appropriate for VOF method. It is available for implicit and explicit computations.

3.3   Multiphase flow model

A multiphase flow can be defined as a mixture of flow which consists of more than two phases. For the flow over stepped spillway, free surface flow with high turbulence of air is of interests. Both air and water cannot be ignored from the model because of their influence on the fluid dynamic behaviour. Then, in the numerical model, the multiphase flow model should be used in simulation. Two types of the multiphase flow model are used in the present study; (i) Volume of Fluid model (VOF), and (ii) Mixture multiphase flow model (MMF).

3.3.1   Volume of fluid model (VOF)

Volume of fluid model, VOF, which was completely reported in Hirt and Nichols (1981), is based on a concept of a fractional volume and the fact that the phases are not interpenetrating. It is an interface capturing scheme for the free surface flow with the interface of each fluid is the point of focus (Nikseresht et al., 2008). Each control volume can be filled with either a single fluid phase or combination phases. The volume fractions of all phases in each control volume sum to unity. In this study, there were 2 phases; air and water flow along the spillway. Due to the volume fraction of each phase in each control volume, the fields for velocity, pressure, and temperature are shared to be the same. The variables for pure water, air, or even mixture can be represented. If r_w and r_a are assumed to be the volume fraction of water and air, respectively, the cell density can be computed by

$$\dots = r_w \dots_w + r_a \dots_a = r_w \dots_w + (1 - r_w) \dots_a \tag{3.20}$$

where $\dots_w$ is water density, and $\dots_a$ is air density. The other variables can be computed, instead of density, by the same volume fraction of equation (3.20).

Two schemes of interface tracking are used; the standard interpolation and the geometric reconstruction schemes. The standard interpolation is used to interpolate the properties of a cell when it is completely filled with one phase. The geometric reconstruction scheme is used near the interface between phases to represent the interface between air and water. The equation for tracking the surface between two phase is

$$\frac{Ðr_w}{Ðt} + u_i \frac{Ðr_w}{Ðx_i} = 0 \tag{3.21}$$

where t is time and u_i is the velocity in x_i-direction.

Firstly, the position of the linear interface relative to the centre of each partially-filled cell is calculated. Then, the advecting amount of fluid through each face is calculated

using the computed linear interface representation and information about the normal and tangential velocity distribution on the face. Finally, the balances of fluxes, from the calculation during the previous step, are used to calculate the volume fraction.

The continuity equation for water, as shown in equation (3.22), is used.

$$\frac{\partial \rho}{\partial t} + \frac{\partial \rho u_i}{\partial x_i} = 0 \tag{3.22}$$

The momentum equation, equation (3.23), in the x_i-direction is dependent on the volume fractions of all phases through the density, ρ , and molecular viscosity, μ.

$$\frac{\partial \rho u_i}{\partial t} + \frac{\partial \rho u_i u_j}{\partial x_j} = -\frac{\partial p}{\partial x_i} + \frac{\partial}{\partial x_j}(\mu + \mu_t)\left(\frac{\partial u_i}{\partial x_j} + \frac{\partial u_j}{\partial x_i}\right) \tag{3.23}$$

where u_j is the velocity in x_j -direction, μ_t is the turbulence viscosity, which can be calculated by the turbulent kinetic energy, k, and turbulent dissipation rate, ε, in the turbulence model.

3.3.2 Mixture multiphase flow model (MMF)

Mixture multiphase flow model, MMF, used in this study, was proposed by Johansen et al. (1990). It is a simplified multiphase model that can be used where the phases move at different velocities. It can model n phases by the continuity and momentum equations for the mixture, and the volume fraction equation for the secondary phases. The continuity equation for the mixture is

$$\frac{\partial \rho_m}{\partial t} + \frac{\partial \rho_m u_{mi}}{\partial x_i} = 0 \tag{3.24}$$

where u_{mi} and ρ_m are the mixture velocity in x_i-direction and mixture density, respectively. Both u_{mi} and ρ_m can be defined as

$$u_{mi} = \frac{\sum_{k=1}^{n} \Gamma_k \rho_k u_{ki}}{\rho_m} \tag{3.25}$$

$$\rho_m = \sum_{k=1}^{n} \Gamma_k \rho_k \tag{3.26}$$

where Γ_k , ρ_k , and u_{ki} are volume fraction, density of kth-phase, and the velocity of kth-phase in x_i-direction, respectively.

The momentum equation for the mixture can be obtained by summing the individual momentum equations for all phases, as shown in equation (3.27)

$$\frac{\partial}{\partial t}\left(\cdots_m u_{mi}\right)+\frac{\partial\left(\cdots_m u_{mi} u_{mj}\right)}{\partial x_j}$$

$$=-\frac{\partial p_{mi}}{\partial x_i}+\frac{\partial\left[\sum_{k=1}^{n}\Gamma_k \ddagger_k - \sum_{k=1}^{n}\Gamma_k \cdots_{lk}\overline{u_{Fki} u_{Fkj}}\right]}{\partial x_j}-\frac{\partial\left(\sum_{k=1}^{n}\Gamma_k \cdots_k u_{Mki} u_{Mkj}\right)}{\partial x_j}+\cdots_m g + M_m \qquad (3.27)$$

The first term on the right hand side is the mixture pressure which can be assumed that it equals to the pressure of the kth-phase pressure. The second term, $\sum_{k=1}^{n}\Gamma_k \ddagger_k$ shows the average viscous stress which $\ddagger_k$ means the kth-phase stress. Next, the turbulent stress is $\sum_{k=1}^{n}\Gamma_k \cdots_{lk}\overline{u_{Fki} u_{Fkj}}$, which $\cdots_{lk}$ is local velocity of kth-phase, and u_{Fki} and u_{Fkj} are the fluctuating velocity components of kth-phase in x_i and x_j-direction, respectively. The $\sum_{k=1}^{n}\Gamma_k \cdots_k u_{Mki} u_{Mkj}$ term means the diffusion stress. The terms u_{Mki} and u_{Mkj} are the diffusion velocities which mean the difference between k^{th}-phase velocity and velocity at the centre of mixture mass in x_i and x_j-direction, respectively, $u_{Mk}=u_k-u_m$. The last term, M_m, shows the momentum of mixture that is the effect from surface tension force. It can be computed by the sum of momentum in each phase.

The VOF and MMF models were used to deal with the multiphase fluids. The same main limitations for using both VOF and MMF are;
- Both models cannot be used with the density-based solvers. Only the pressure-based solver is allowed.
- Only one phase can be defined as a compressible gas.
- Streamwise periodic flow with specified mass flow rate cannot be modeled.
However, there are 2 main differences between these models as the manner in which they handle phase interpenetration and the phase velocities.

1. Phase interpenetration
The phases are not interpenetrating in VOF while MMF allows the phases to be interpenetrating. In each control volume for VOF, the volume fractions of all phases sum to unity. Assume the volume fraction of the ath fluid is $_a$, then $_a$ can be;
- 0 if there is no the ath fluid in the control volume,
- 1 if there is only the ath fluid in the control volume, and
- $0 < _a < 1$ if there is the interface between the ath fluid and other fluid in the control volume. The equation for interphase tracking is used.

In MMF, the volume fractions for each phase in a control volume depend on the space of their phases. They can be equal to value between 0 to 1.

2. Phase velocities
For VOF, which the volume fraction of each phase is known, the variables and properties are shared and represent volume-averaged values. Therefore, depending on

the volume fraction, the variables and properties in a control volume can either represent only one of the phase or a mixture of all phases. The VOF solves a single set of continuity and momentum equations and tracking the volume fraction of each phase by tracking equation. In MMF, under the concept of slip velocities, each phase in a control volume can be allowed to move in different velocities. Also, other variables and properties can be different in each control volume. However, if any control volume is assumed to move at the same velocity, then MMF can be reduced to be a homogeneous multiphase model. The MMF solves the continuity and momentum equations for the mixture, and the volume fraction equation for the secondary phases, as well as algebraic expressions for the velocities if the phases are moving at different velocities.

With these two differences, the initial boundary condition was set differently. The air velocity in MMF can be set at zero and then reduced to homogeneous multiphase model while the air velocity in VOF is the same as water velocity.

3.4 Turbulence model

Among the linear turbulence models, the widely used two-equation model is based on: (1) the turbulent kinetic energy equation k and (2) the turbulent eddy dissipation ε, or the turbulent frequency ω. Five different turbulence models were chosen in the present study to simulate the flow over stepped spillways: the Standard k-ε, the Realisable k-ε, the Renormalisation group k-ε , the Standard k-ω and the Shear stress transport k-ω model.

3.4.1 Standard k-ε model (St k-ε)

Launder and Spalding (1974) developed the St k-ε model. The assumption is that the flow is fully turbulent and the effects of molecular viscosity are negligible. Therefore, the standard k-ε model is valid only for fully turbulent flows. The default values of the model constants have been determined from experiments with air and water for fundamental turbulent shear flows, including homogeneous shear flows and decaying isotropic grid turbulence. They have been found to work fairly well for a wide range of wall-bounded and free shear flows. It is a semi-empirical model based on the transport equations for k and ε, equations (3.28) and (3.29), respectively

$$\frac{\partial}{\partial t}(\rho k) + \frac{\partial}{\partial x_j}(\rho k u_j) = \frac{\partial}{\partial x_j}\left[\left(\mu + \frac{\mu_t}{\sigma_k}\right)\frac{\partial k}{\partial x_j}\right] + G_k + G_b - \rho\varepsilon - Y_M + S_k \tag{3.28}$$

$$\frac{\partial}{\partial t}(\rho \varepsilon) + \frac{\partial}{\partial x_i}(\rho \varepsilon u_i)$$
$$= \frac{\partial}{\partial x_j}\left[\left(\mu + \frac{\mu_t}{\sigma_\varepsilon}\right)\frac{\partial \varepsilon}{\partial x_j}\right] + C_{1\varepsilon}\frac{\varepsilon}{k}(G_k + C_{3\varepsilon}G_b) - C_{2\varepsilon}\rho\frac{\varepsilon^2}{k} + S_\varepsilon \tag{3.29}$$

where: σ_k = Prandtl numbers for k = 1.0, G_k = generation of turbulent kinetic energy due to mean velocity gradients, G_b = generation of turbulent kinetic energy due to buoyancy, Y_M = contribution of the fluctuating dilatation in turbulence, σ_ε = Prandtl numbers for ε = 1.3, $C_{1\varepsilon}$ = 1.44, $C_{2\varepsilon}$ = 1.92, $C_{3\varepsilon}$ = 1.0, and S_k, S_ε are user-defined source terms.

The equation for k is derived from the exact equation, whilst the equation for v is obtained using physical reasoning and bears little resemblance to its mathematically exact counterpart.

3.4.2 Realisable k-v model (Rl k-v)

Shih et al. (1995) developed the most-used Rl k-v model. It was first developed based on the "realisability" constraints; the positivity of normal Reynolds stresses and the Schwarz inequality for turbulent shear stresses. It was then found that the following flow types could be examined: (1) rotating homogeneous shear flows, (2) boundary-free shear flows including a mixing layer, planar and round jets, (3) channel flow and flat plate boundary layers with and without a pressure gradient and (4) backward facing step separated flows. The turbulent kinetic energy equation for k is equation (3.28) whereas a new equation for v, equation (3.30), has been derived from an exact equation for the transport of the mean-square vorticity fluctuation

$$\frac{\partial}{\partial t}(...v)+\frac{\partial}{\partial x_j}(...vu_j)$$
$$=\frac{\partial}{\partial x_j}\left[\left(\sim+\frac{\tilde{}_t}{\dagger_v}\right)\frac{\partial v}{\partial x_j}\right]+...C_1 S_v -...C_2\frac{v^2}{k+\sqrt{\hat{}\,v}}+C_{1v}\frac{v}{k}C_{3v}G_b+S_v \qquad (3.30)$$

where all parameters are the same as in the St k-v model except for $\hat{}$ = kinematic viscosity, $C_2 = 1.9$, $\dagger_v = 1.2$, $C_1 = $ max [0.43, $y/(y+5)$], $y = Sk/v$, $S \equiv (2S_{ij}S_{ij})^{0.5}$, $S_{ij} = (\partial u_i/\partial x_j)+(\partial u_j/\partial x_i)$. The term of G_k is removed from the equation for v, whilst the term of viscosity has been added because of the high effect from the Reynolds number in the flow.

3.4.3 Renormalisation group k-v model (RNG k-v)

Yakhot and Orszag (1986) derived the RNG k-v turbulence model from the Navier-Stokes equations using a technique of renormalisation group (RNG) methods. It significantly improved the accuracy for rapid flows. Because of the additional term in the v equation R_v the turbulence dissipation and mean shear can be better simulated at the interaction of phases. The effect of swirl on turbulence is included to enhance the accuracy for swirling flows. Due to a greater degree of non-linearity, computations with the RNG k-v model tend to take 10-15% more CPU time than the St k-v model. The equations for k and v in the RNG k-v turbulence are

$$\frac{\partial}{\partial t}(...k)+\frac{\partial}{\partial x_i}(...ku_i)=\frac{\partial}{\partial x_j}\left[\Gamma_k\tilde{}_{eff}\frac{\partial k}{\partial x_j}\right]+G_k+G_b-...v-Y_M+S_k \qquad (3.31)$$

$$\frac{\partial}{\partial t}(...v)+\frac{\partial}{\partial x_i}(...vu_i)$$
$$=\frac{\partial}{\partial x_j}\left[\Gamma_v\tilde{}_{eff}\frac{\partial v}{\partial x_j}\right]+C_{1v}\frac{v}{k}(G_k+C_{3v}G_b)-C_{2v}...\frac{v^2}{k}-R_v+S_v \qquad (3.32)$$

where: Γ_k, Γ_v = inverse effective Prandtl numbers for k and v, $\tilde{\mu}_{eff}$ = effective viscosity $= \tilde{\mu} + \tilde{\mu}_t$, $C_{1v} = 1.42$, $C_{2v} = 1.68$, $C_{3v} = 1.0$. The term $R_v = C_{\mu} \tilde{\rho} \eta^3 (1 - \eta / \eta_0) v^2 / k (1 + \varsigma \eta^3)$ where $C_{\mu} = 0.0845$, $\eta_0 = 4.38$, $\varsigma = 0.012$.

3.4.4 Standard k-$\check{S}$ model (St k-$\check{S}$)

The St k-$\check{S}$ model is based on the Wilcox k-$\check{S}$ model (Wilcox, 1988). It was developed for working with the compressibility and shear flow spreading. It can predict free shear flow spreading rates that are in well agreement with measurements for wakes, mixing layers and plane, round and radial jets and is thus, applicable to wall-bounded flows and free shear flows. It is an empirical model based on the equations for k and $\check{S}$, which can be the ratio of v to k. They are

$$\frac{\partial}{\partial t}(\rho k) + \frac{\partial}{\partial x_i}(\rho k u_i) = \frac{\partial}{\partial x_j}\left[\Gamma_k \frac{\partial k}{\partial x_j}\right] + G_k - Y_k + S_k \tag{3.33}$$

$$\frac{\partial}{\partial t}(\rho \check{S}) + \frac{\partial}{\partial x_i}(\rho \check{S} u_i) = \frac{\partial}{\partial x_j}\left[\Gamma_{\check{S}} \frac{\partial \check{S}}{\partial x_j}\right] + G_{\check{S}} - Y_{\check{S}} + S_{\check{S}} \tag{3.34}$$

where: $G_{\check{S}}$ = generation of $\check{S}$. Γ_k, $\Gamma_{\check{S}}$ = effective diffusivity of k and $\check{S}$, Y_k = dissipation of k, $Y_{\check{S}}$ = dissipation of $\check{S}$ due to turbulence, $S_{\check{S}}$ = user-defined source term.

3.4.5 Shear stress transport k-$\check{S}$ model (SST k-$\check{S}$)

Menter (1993) developed the SST k-$\check{S}$ model to blend effectively the robust and accurate formulation of the k-$\check{S}$ model in the near-wall region with the free-stream independence of the k-$\check{S}$ model in the far field. The differences between the SST k-$\check{S}$ model and the standard model are: (1) the gradual change from the standard k-$\check{S}$ model in the inner region of the boundary layer, to a high-Reynolds-number version of the k-v model in the outer part of the boundary layer and (2) the modified turbulent viscosity formulation to account for the transport effects of the principal turbulent shear stress. The equation for k is the same as in the St k-$\check{S}$ model, equation (3.33), while the $\check{S}$ model can be shown as

$$\frac{\partial}{\partial t}(\rho \check{S}) + \frac{\partial}{\partial x_i}(\rho \check{S} u_i) = \frac{\partial}{\partial x_j}\left[\Gamma_{\check{S}} \frac{\partial \check{S}}{\partial x_j}\right] + G_{\check{S}} - Y_{\check{S}} + D_{\check{S}} + S_{\check{S}} \tag{3.35}$$

where $D_{\check{S}}$ represents the cross-diffusion term.

3.5   Root mean square error (RMSE)

The operational evaluation process for the model comparison includes the calculation and analysis of statistical measures to characterise the performance of the models. The Root Mean Square Error, RMSE, or the Root Mean Square Deviation, RMSD, is one of the commonly used error index statistics (Chu and Shirmohammadi, 2004; Singh et al.,

2004; Vasquez-Amábile and Engel, 2005). It is the square root of the variance of the residuals or it means a measure of the difference between values predicted by a numerical model and the values actually observed from the physical model. The RMSE of a numerical model prediction with respect to the estimated variable X_{numer} is defined as the square root of the mean squared error;

$$RMSE = \sqrt{\frac{\sum_{i=1}^{n}\left(X_{phy,i} - X_{numer,i}\right)^2}{n}}$$ (3.36)

where X_{phy} is observed values from the physical model and X_{numer} is the modelled values from the numerical model at time/place i, n is the number of set of data.

The RMSE values can be used to distinguish model performance in a calibration period with that of a validation period as well as to compare the individual model performance to that of other predictive models. The value of the RMSE is highly sensitive to large errors and low RMSE values reflect a high accuracy in the numerical prediction. Singh et al. (2004) stated that RMSE values less than half the standard deviation of the data from physical model may be considered low and that either is appropriate for model evaluation.

CHAPTER 4 METHODOLOGY

This chapter presents the methodology of the study. It concludes the study of the physical model and the numerical model. The physical model part is the review of the previous study whereas the numerical model part is the methodology and setup of the simulation.

4.1　Physical model used in the present study

The physical model, tested by Ward (2002), was located at the outdoor of Engineering Research Center, Colorado State University, Fort Collins, USA. It is the same physical model that is used in the Hydraulic Laboratory Report HL-2005-06 which is one of the reports in the Hydraulic Laboratory Report series produced by the Bureau of Reclamation's Water Resources Research Laboratory in the United States (Frizell, 2006). It was the large scale model so the water was supplied from nearby Horsetooth Reservoir. The testing facilities of spillway system consist of water supply pipeline, baffled head box, entrance, concrete chute, stilling basin, and outlet works. The concrete chute is approximately 34.14 m long, 1.22 m wide, and 1.52 m deep on a 2H:1V slope and has a total height of 15.24 m. Plexiglass windows with the size of 1.22 m by 1.22 m were installed at five locations in the divided wall to provide observation of flow in the chute. A sonic flow meter in the supply pipeline to the facility headbox was used to monitor flow in the system. The schematic diagram and physical model are shown in Figure 4.1.

Figure 4.1 Physical model of the stepped spillway (Ward, 2002)

Data collected, included: flow pattern, flow characteristics, and velocity profiles, were measured and observed. The measurement locations on all spillways are shown in appendix A. Air concentration and velocity instrumentation were mounted on a point gage and carriage system. The manually operated carriage system allowed for two degrees of freedom with movement along the length of spillway parallel to the floor, and lateral movement within the width of the spillway. The remote operated, motorised point gage allowed for vertical movement of the instrumentation perpendicular to the floor of the spillway to obtain data profiles within the flow. All profiles were taken along the centerline of the flume (0.61 m lateral distance from the wall) normal to the spillway floor. Each profile consisted of anywhere from 3 to 30 data points depending upon the depth of flow and reading interval chosen. The lowest points were taken at approximately 0.015 m from the tip of the step. The highest points were taken where both instruments measured data that was near the dry-air readings and visually appeared almost out of the flow.

Videotape recording and photographs were used to collect the flow pattern at the overtopping crest and along the spillway. Flow condition in the present study may be described as high-velocity, turbulent, two-phase flow. Therefore, a probe to measure velocity was required that would withstand high impact forces and be able to accommodate a non-homogeneous fluid of varying density. The probe is sturdy and provides a means of continuous back flushing to ensure a single density fluid within the Pitot tube. Velocity from the back-flushing Pitot tube is determined by the difference in pressures at the kinetic and static ports while continuously back flushing to prevent air bubbles from entering the instrument. Therefore, a balance between ensuring that air does not enter the Pitot tube and the sensitivity of the pressure difference must be found. Based on the laboratory tests, back flushing pressures of between 2.5 and 8.0 psi were selected. The Pitot tube was patented in 1969 and manufactured by Rosemount, Inc. It was originally intended for mounting on the fuselage of an aircraft for the measurement of air velocity. Hence, a surplus Pitot tube was cut in a half to determine the internal flow path of the static and kinetic ports. The dynamic port is essentially a tube centered within the concentric outer shell with an exit at the tip of the instrument. The static ports penetrate the outer shell into the annulus surrounding the center tube.

The differential pressure between the static and kinetic ports is recorded using a calibrated differential pressure cell. The voltage output from the pressure cells is fed into a Sensotec Inc., model GM Conditioner-Indicator where voltage span and zero adjustments can be made using potentiometers provided on the unit. Back flushing pressure and flow through the pressure cell are both adjusted in air without flowing water such that the Sensotec unit displays zero voltage, corresponding to zero differential pressure and zero velocity. The signal from the Sensotec unit is sent to the Dataq data acquistion system and recorded on the computer with the WINDAQ/200 software. A sampling frequency of 120 Hz for a duration of 20 seconds was selected for recording the Pitot tube waveform. An average voltage obtained from the Pitot tube waveform can be converted to pressure head.

The air concentration probe was used to determine the percentage of air contained in flow. The principle for air concentration measuring is based on the difference in

electrical resistivity between air and water. The probe act as a bubble detector by passing a current through two conductors spaced a small distance apart and measuring the change in conductivity that occurs when a bubble impinges on the probe tip. The interruption of the current when a bubble passes is a step change from a relatively high conductivity with the probe in water, to nearly zero conductivity when a bubble breaks the conducting path (Ward, 2002).

The air probe used in the study by Ward (2002) was developed from the earlier probe which had a problem on the electroplating of the conductors, degradation of the probe's brass encasement, water entering and shorting the conductors, and streamlining of the supportive mechanism. The new one consists of two platinum wires as conductors, separated by 2.0 mm. The wires are encased in a non-conducting acrylic tip and fit into a 6.35 mm stainless supporting tube. With the air probe in water and no air present, a constant high voltage is conducted across the probe tip. When the air void is detected by the probe, the voltage drops to approximately zero volt. Inverters in the electronics package invert the output voltages resulting in a low voltage for clear water and a high voltage when air is detected. The ratio of air to water is approximately given by a ratio of time that a high voltage pulse is detected to the time that a low voltage pulse is detected during the measurement period.

The digital signal from the air probe was fed to a Dataq Instruments Inc., model number DI-220, portable data acquisition system attached to the IBM compatible personal computer. The DI-220 system receives the isolated digital signal from the electronics package, processes it as an analog waveform and outputs the waveform to the computer. The software provided with the acquisition system, WINDAQ/200, allows the real time display and record the waveform. The system provides the capability of sampling the signal at variable frequencies and durations. For the air probe, a frequency of 15,000 Hz for a duration of 5 seconds was selected based on a laboratory test and sensitivity analysis of sampling frequency.

In the present study, the air concentration in each section was collected to find the depth at which the air concentration is equal to 90%. It was found that the depth at 90% air concentration point can be considered as the depth of aerated flow on stepped spillways (Chamani and Rajaratnam, 1999).

Three types of spillways are detailed as follows;

i) The smooth spillway, flow discharges of 0.57, 1.13, 1.70, and 2.27 m^3/s were used. The data on the five locations were measured in the direction of normal to the spillway floor. They were at L_s/L=0.09, 0.28, 0.44, 0.60, and 0.76 where L_s is length in streamwise direction from upstream of spillway to the interesting point and L is the overall length of spillway.

ii) For the 25-step spillway, with $h = 0.61$ m and $l = 1.22$ m, y_c/h of 0.46, 0.73, 0.96, 1.16, 1.35, and 1.48 were used and they are labelled as $T_{0.46}$, $T_{0.73}$, $T_{0.96}$, $T_{1.16}$, $T_{1.35}$ and $T_{1.48}$, respectively. The corresponded discharges are 0.57, 1.13, 1.70, 2.27, 2.83 and 3.28 m^3/s, respectively.

iii) For the 50-step spillway, with $h = 0.31$ m and $l = 0.61$ m, y_c/h of 0.96, 1.48, 1.91, 2.32 and 2.69 were used. These cases are labelled as $F_{0.96}$, $F_{1.48}$, $F_{1.91}$, $F_{2.32}$ and $F_{2.69}$, respectively. The corresponded discharges are 0.60, 1.16, 1.70, 2.27 and 2.83 m^3/s, respectively.

The overall data can be summarised in Table 4.1

Table 4.1 Summarised data for physical model

Spillway	Discharge, Q (m^3/s)	Unit discharge, q (m^3/s/m)	Relative critical depth, y_c/h	Label	Measurement locations
Smooth	0.57	0.47	-	-	L_s/L=0.09, 0.28, 0.44, 0.60, and 0.76
	1.13	0.92	-	-	
	1.70	1.38	-	-	
	2.27	1.87	-	-	
25-step	0.57	0.47	0.46	$T_{0.46}$	$il/L\cos_{_n}$ = 0.16, 0.31, 0.47, 0.63, and 0.79
	1.13	0.92	0.73	$T_{0.73}$	
	1.70	1.38	0.96	$T_{0.96}$	
	2.27	1.87	1.16	$T_{1.16}$	
	2.83	2.33	1.34	$T_{1.35}$	
	3.28	2.69	1.48	$T_{1.48}$	
50-step	0.60	0.50	0.96	$F_{0.96}$	$il/L\cos_{_n}$ = 0.16, 0.31, 0.47, 0.63, and 0.79
	1.16	0.95	1.48	$F_{1.48}$	
	1.70	1.38	1.91	$F_{1.91}$	
	2.27	1.87	2.32	$F_{2.32}$	
	2.83	2.33	2.69	$F_{2.69}$	

4.2   Numerical model

The simulation is performed by a Dell Precision workstation with Intel Xeon CPU X3330 at 2.66 GHz, 2.67 GHz, and 8.0 GB of RAM and OS of Microsoft Server HPC Edition.

The FLUENT model is used as a tool for a numerical model study. Fluent is the provider of commercial computational fluid dynamics (CFD) software and services (Fluent Inc., 2005). It is a program for modelling fluid flow and heat transfer in complex geometries. The step of simulation on the numerical model can be shown in Figure 4.2. The domains of spillways are simulated in the same size of prototype in

physical models. Then, the uniformly-sized, structured grid sizes are chosen. The boundary conditions for each zone are specified to the domain. After that, the time step sizes are defined. The Courant number is used as a criterion of model stability. The equation is

$$\frac{\Delta t}{\Delta s} \leq 1 \tag{4-1}$$

where Δt = time step size (seconds) and Δs = grid size (m). The pressure-based segregated solver was used because it is multiphase flow with 2 materials, water and air, flow with different velocities. To start the initial calculation, the uniform velocity of water and the atmospheric pressure are specified at the water inlet and free surface zone, respectively. The momentum equation is then used to calculate by the VOF and MMF models in this step. Then, the values of parameters will transfer to solve the continuity equation. After that, the values of pressure and velocity are updated and put into the turbulence models. The converged criteria are checked at the difference of 0.0001 in order to assure that the results from the simulation is very close to the data from physical model. If they are already converged, the simulation will be stopped but if it is not converged, the under relaxation factors will be used to computed new values of parameters. They will be put again into the momentum equation and the processes will be repeated.
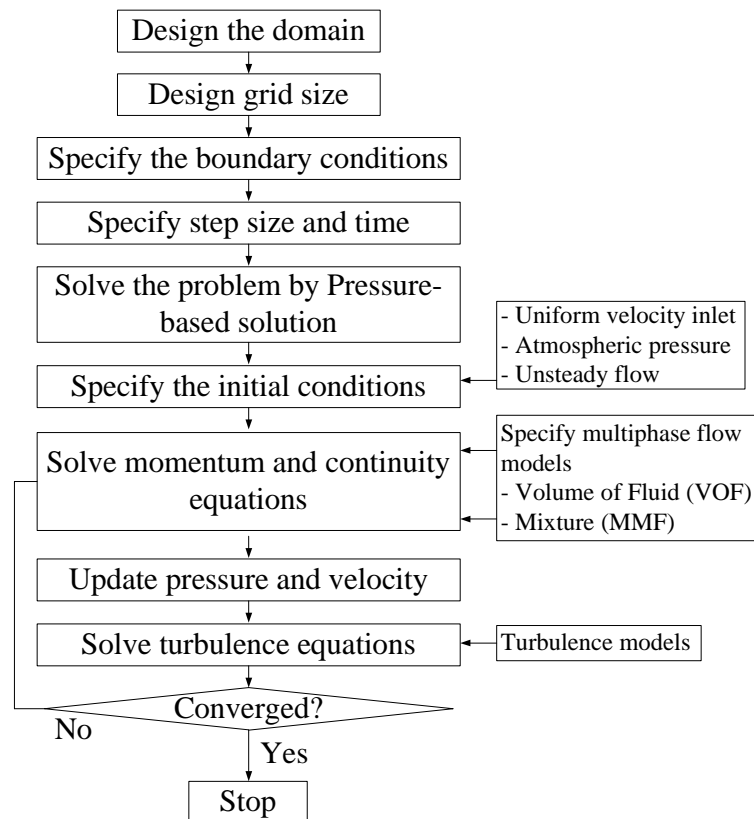
Figure 4.2 Schematic diagram for simulation

4.2.1 Domain and mesh generation

The whole meshed domain represents as a 2D grid as shown in Figure 4.3. The 2D grid was used because the results from the physical model were collected only at the centreline. Also, the use of 2D grid takes much less time than 3D grid. The calculation domain was discretised into structured grid with various sizes of 0.035×0.035, 0.05×0.05 and 0.10×0.10 m^2 quadrilateral cells.

4.2.2 Boundary conditions

The inlet section is at the upstream of the spillway which consists of the inlet of water at bottom and the inlet of air at top. The inlet water velocity was the initial condition and was set uniformly at the water inlet and flow through the spillway which was initially full of air. The air boundaries were defined as an inlet pressure with the atmospheric pressure. The outlet of the spillways at the downstream was defined as an outlet pressure so the water can flow out freely. The simulated time in the model is 300 seconds which the flow has already became the steady state in the physical model. The time for the computation for a typical case is about 60 hours.
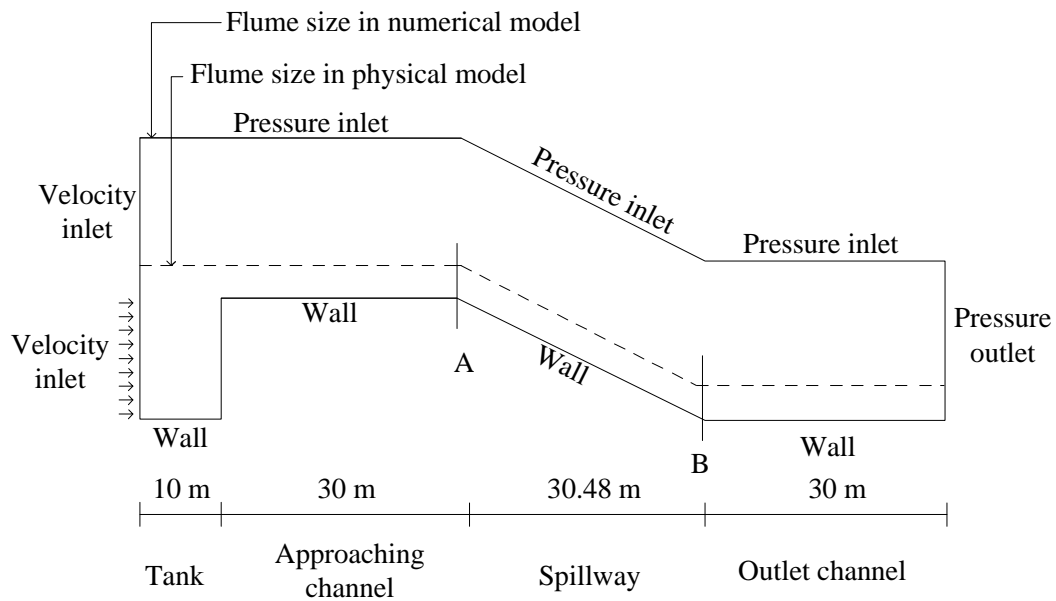
Figure 4.3 Schematic diagram for domain

4.2.3 Discretisation

For Finite volume method, there are many schemes for appropriate solving, they are
- First-Order Upwind Scheme: this method assigns that properties at skin of object are equal to at centre of object. It is appropriate used for grid parallel flow.
- Second-Order Upwind Scheme: this method assigns that properties at skin of object is averaged from two-side cells. It is appropriate used with triangle and hexagon grid cells that flow is not parallel with grid.

    - QUICK Scheme: this method assigns that properties of cells depend on weight of important. It is more accurate than two methods above if it is used for cubic or hexagon meshes eddy computation.
    - Power-Law Scheme: this method uses the interpolation from other grid and it accuracy is equal to First-Order Upwind Scheme.
    - A modified HRIC Scheme: this method is appropriate for VOF method. It is available for implicit and explicit computations.

The implicit equation can be solved iteratively at each time level before moving to the next time step. The advantage of the fully implicit scheme is that it is unconditionally stable with respect to time step size. The under-relaxation of equations, also known as implicit relaxation, is used in the pressure-based solver to stabilise the convergence behaviour of the outer nonlinear iterations by introducing selective amounts of interesting variable, w, in the system of discretised equations.

The under-relaxation factors, r, ranging between 0 and 1 was assigned to stabilise the computation. An under-relaxation value near 0 represents a solution which does not change significantly from the previous iteration while an under-relaxation value near 1 means the iteration moves forward very quickly. The following values were used in this study: $r = 0.2$ for continuity and momentum equations; 0.8 for turbulence equations; and 0.2 for water fraction equation. These factors were different from the default values of the numerical model because of the high level for turbulence and flow complexity which takes much more time than other flow cases.

In a simple form, the new value of the variable w within a cell depends upon the value from the previous step, w_{pre}, and the under-relaxation factor, r, can be calculated from

$$w = w_{pre} + r\left(\Delta w\right) \tag{4-2}$$

where Δw = the difference between the new and previous values of the variable w.

CHAPTER 5 RESULTS AND DISCUSSION

This chapter presents the results and discussion of the study. It consists of comparison of multiphase flow model, comparison between various turbulence models, Grid independence study, flow along stepped spillways, flow on the step, velocity profile, turbulence intensity, energy dissipation, pressure on the step, and the proposed coefficients for turbulence model. The details of each topic are as follows;

5.1   Comparison of multiphase flow models

The results of comparison of multiphase flow model illustrate the better multiphase flow models between a Volume of Fluid model, VOF, and a mixure multiphase flow model, MMF, for simulation of flow over spillway. The better multiphase flow model and its results are discussed in terms of flow initiation at the inlet, velocity profiles, and flow recirculation of skimming flow.

5.1.1   Flow initiation at the inlet

At first duration of simulation, the 10 m long tank was filled with water flow from water inlet as shown in Figure 5.1. After 8 seconds of simulation, the difference of flow patterns in the tank from VOF and MMF are shown. The duration of 8 seconds was chosen to show the results because it is the first time that the difference between VOF and MMF can be observed easily. In VOF, the bottom of the tank was filled with water, with the volume fraction of water of 1.0, and the upper part of the tank was the air zone, with the non-volume fraction of water. The interface between air and water can be clearly seen from the thin layer of the volume fraction of water between 0.05 to 0.95. The result from using VOF is better simulated because the tracking of interface in the domain cells with the geometric reconstruction scheme was used. Differently, the mixture properties were calculated without the interpolation of phase volume fractions, therefore the interface cannot be clearly seen in MMF. There was the air zone in the upper part of the tank but no full-water zone at the bottom of the tank. Also, the thick layer of mixture was found which was different from the result from experiments or even VOF. However, with more equation for the tracking of the interface for VOF, more times were needed for better simulation.

After discretisation, the conservation equations for variables at all cells were calculated. The important term called the residual value was computed for each iteration. The residual is the imbalance of variable summed over all the computational cells. The low residual value in each iteration means the difference value of variables between the previous and the present iterations is small. For both VOF and MMF, after 8 seconds as shown in Figure 5.2, the residuals for velocities in both horizontal and vertical directions are fluctuated and quite high. The residuals from VOF as shown in Figure 5.2 (a) are still going up which are different from the residuals from MMF as shown in Figure 5.2 (b). The residuals for velocities from MMF are going down constantly after many iterations. For continuity residual from VOF, it is still fluctuated with the higher residual after many iterations. The continuity residual from MMF is slightly increased and become almost constant after 600 iterations or 4.8 seconds. The lower continuity

residual in MMF caused the faster computation because the difference in each iteration was very low.
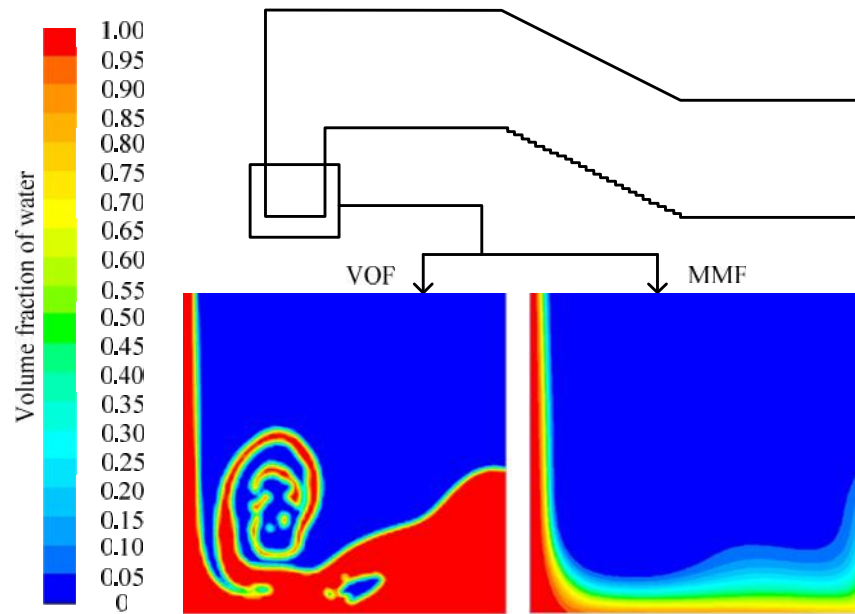
Figure 5.1 Flow initiation at $t = 8$ s
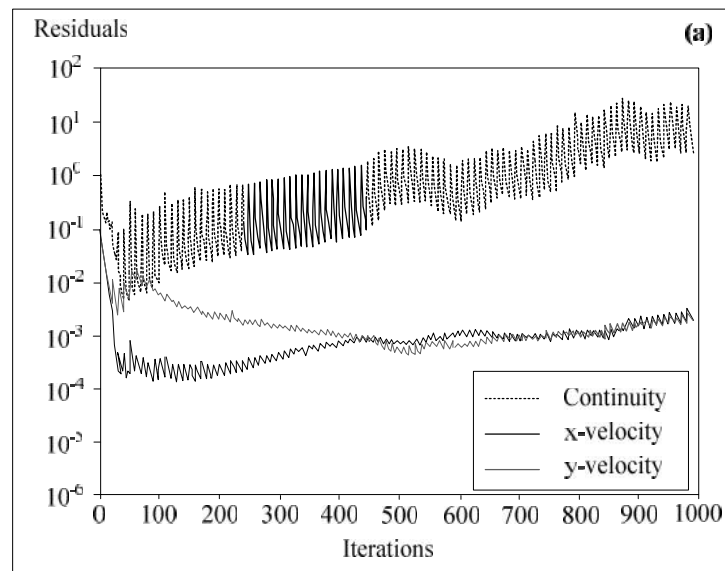
(a) VOF

Figure 5.2 Development of residuals for conservation equations at $t = 8$ s

(b) MMF
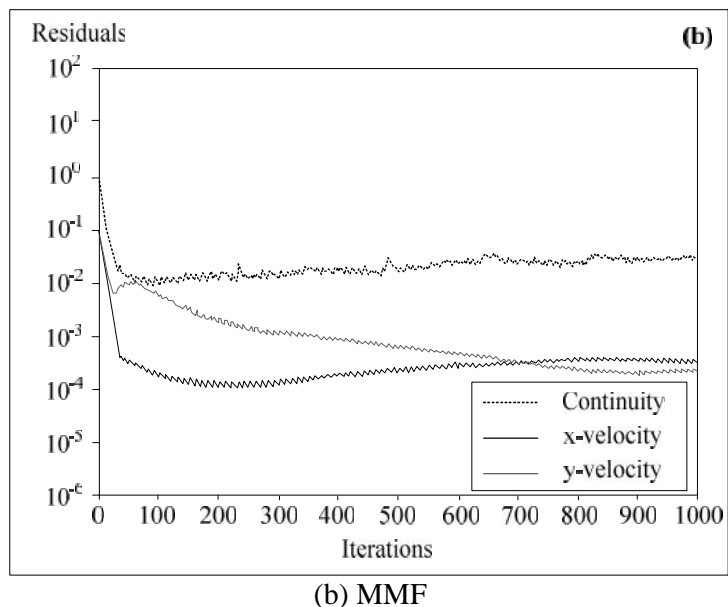
Figure 5.2 (Cont.) Development of residuals for conservation equations at $t = 8$ s

5.1.2 Velocity profiles

The velocity profiles begin with velocity gradually increasing from the bed until the maximum velocity gradient is reached. At some point in the upper region of the depth, an immediate change was observed where the velocity abruptly increases or decreases. The results of velocity from the physical model and numerical model in various grid sizes are shown in appendix B.

For both nappe flow and skimming flow, the VOF shows better agreement with measured data, compared with the MMF. A comparison of the velocity results shows the maximum error in their values mainly amount to 18% and 50% for VOF and MMF, respectively. The results from both VOF and MMF are in the same trend as the experiments; however, the error from MMF is getting higher rapidly.

For a skimming flow regime, the VOF shows the better results than the MMF. The quite-high-error was from the centre of the lowest control volume, or at the depth of 0.025 m above the step floor. The results in this zone were therefore interpolated from the boundary of the cell. With this reason, the error from the bottom domain cells was quite high. For the results mentioned above, it can be seen that the VOF is better used to simulate the complexity of flow over stepped spillway for both nappe flow and skimming flow.

To compare with the previous studies, the studies by Chanson and Toombes (2002) and Pfister and Hager (2011) are used. They are shown in forms of upper and lower bounds in Figure 5.3, where V and y are the velocity and depth, respectively, V_{90} and y_{90} are the characteristics velocity and depth at the point of the air concentration is 90%. All results

from VOF in the present study are plotted. It was found that most of the results are in the same trend of previous studies and also in between the upper and lower bounds. However, for low value of relative depth, y/y_{90}, the relative velocity V/V_{90} is out of bound. They were underestimated because the velocity at $y/y_{90} = 0$ should be zero but in the experiments, there might be some effect from the step floor which affects the measurement. This is therefore the advantage of using the numerical model for simulation near the step or in the zone that is difficult to collect the data. To compare with the 1/6 power law, which is the solid line in Figure 5.3, the results from present study is similar. The equations from present study for the velocity profiles of skimming flow are suggested in equation (5.1) with the R^2 of 0.98.
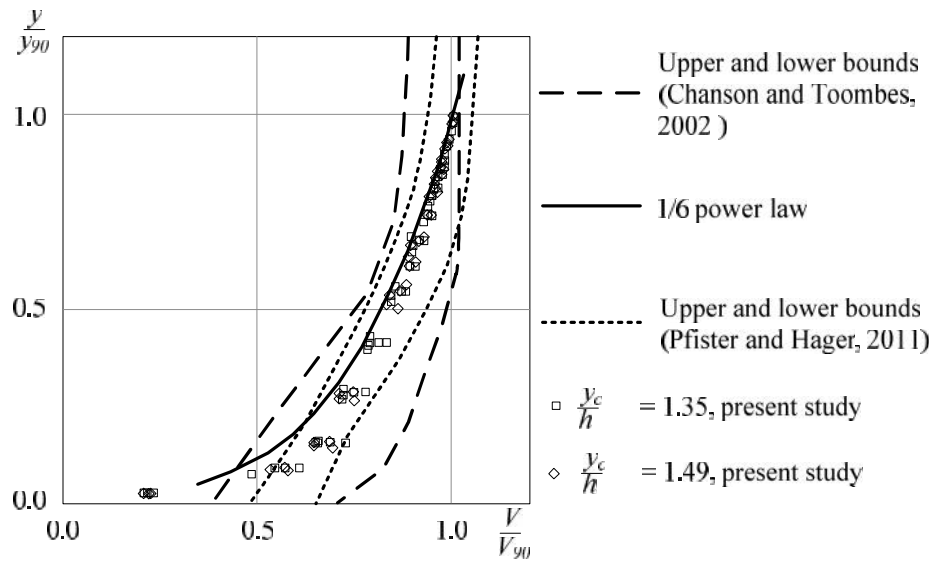
Figure 5.3 Dimensionless air–water velocity distributions

$$\frac{y}{y_{90}} = 0.01e^{4.65\left(\frac{V}{V_{90}}\right)}$$
(5.1)

5.1.3 Flow recirculation of skimming flow

The flow profiles on the step number 16 for the skimming flow case of $y_c/h = 1.35$ from the VOF and MMF are shown in Figure 5.4. The scale ratio of water in the model is shown as the colour bar on the left-hand side on the same figure. The full-of-water zone is shown by the red colour while the air zone is shown by the blue one. Even the recirculation can be seen on both models, it was clearly seen that VOF can give the better result of water surface profile than MMF. With the VOF, beneath the pseudo-bottom, there are both water and air mixing together as a recirculation. The water is obviously covering the vortex of air in this zone. Above the pseudo-bottom is the main flow, there are water zone and then the mixture zone with high ratio of air and then become to the air zone. With the MMF, beneath the pseudo-bottom, the mixture with the water ratio of 0.65 is shown as the recirculation. Above the pseudo-bottom, the water ratio becomes 0.50 and then 0.30 without any full-of-water zone or air zone.
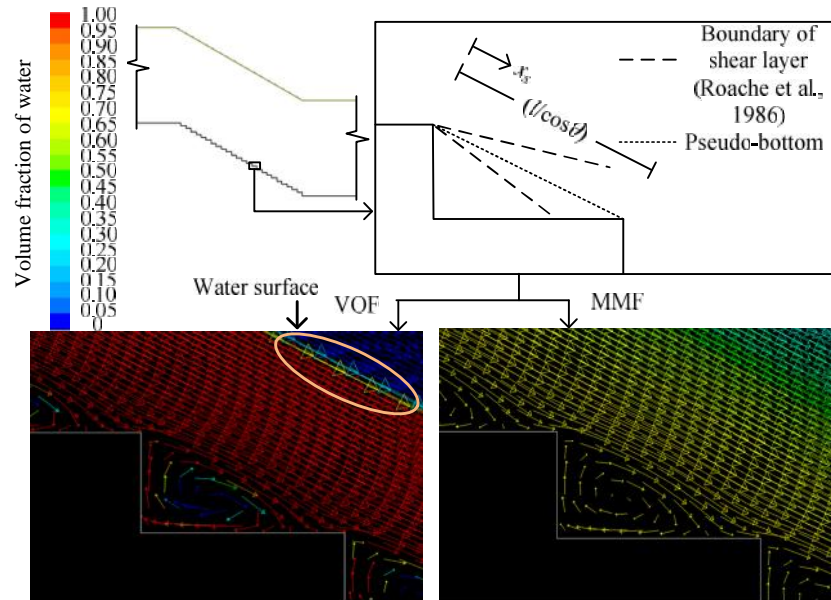
Figure 5.4 Flow profiles at the step number 16 for the skimming flow

In the calculation for VOF, the assumptions are based on the fact that the phases are not interpenetrating and the interface of each fluid is the point of focus while the equations used for MMF are solved in every cell for the mixture. Therefore, the result from each domain cell is the mixture and then cannot be separated to each phase. It is different from the equation of the VOF because the interface between two phases can be simplified while the different continuity equations for the full-of-air and full-of-water zones are solved separately.

Felder and Chanson (2011), with the 26.6°-stepped spillway, found the similar trend of air fraction for a step cavity on a slope of 50° shown by Boes (2000b) at $y/h \geq 0.3$. A bit difference of some features in the developing shear layer and cavity region, $y/h < 0.3$, was found. The momentum from the main flow in the upper region is transferred to the lower region beneath the pseudo-bottom and then the recirculation is generated. The energy from water flowing down from upper to lower step is dissipated by transferring of the momentum in the recirculation. Therefore, the mechanism of air trapping in the recirculation can cause the high air concentration near the pseudo-bottom. Considering only in the present study from VOF in Figure 5.3, the maximum air concentration along the pseudo-bottom line is located at $(x_s \cos_{"})/l \approx 0.50 - 0.60$. Felder and Chanson (2011) also suggested the air concentration in the shear layer increased with increasing distance x_s from the step edge. The maximum air concentration is in the shear layer zone at $(x_s \cos_{"})/l \approx 0.50 - 0.65$. It can be seen that VOF in the present study shows the same location of maximum air concentration along the pseudo-bottom as Felder and Chanson (2011). Beneath and perpendicular to the pseudo-bottom and shear layer zone, the air concentration becomes 1.0 at the core of the flow recirculation due to the mechanism of air trapping. With the influence of turbulence in recirculation, the flow direction above and next to the pseudo-bottom is

curved. The flow velocity near the pseudo-bottom is also less than the velocity in the main flow as can be seen from the model and the velocity profile.

5.2   Comparison between various turbulence models

Figure 5.5 shows a comparison example between the laboratory measurements and the model predictions with the five different turbulence algorithms. Overall, it is found that all turbulence models predict the velocity profiles rather well. The differences between the different models seem slightly accentuated near the free surface where air entrainment becomes significant.
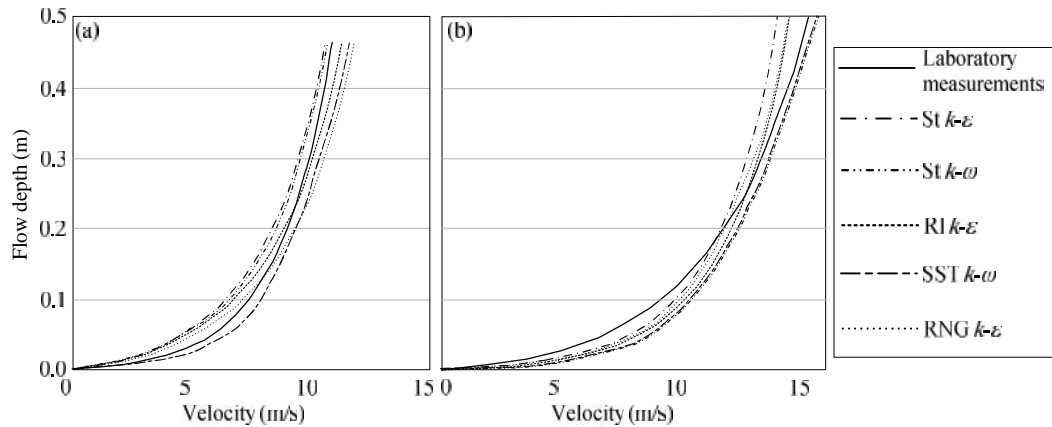
(a) location of $il/L\cos_n = 0.31$ (b) location of $il/L\cos_n = 0.79$

Figure 5.5 Comparison of velocity profiles on the flow of $y_c/h = 1.35$

The RMSE is a measure of the accuracy of a prediction in comparison to the measurements. The RMSE is used to compare the results from physical and numerical velocity profiles. It is the square root of the average squared difference of the simulation results and the physical measurements as can be calculated using equation (5.2)

$$RMSE = \sqrt{\frac{1}{m}\sum_{1}^{m}\left(Velocity_{physical} - Velocity_{numerical}\right)^2}$$ (5.2)

where m is the number of velocity measurements. The value of the RMSE is highly sensitive to large errors and low RMSE values reflect a high accuracy in the numerical prediction of the velocity profiles. The results at all locations show a good agreement with the physical data.

Considering the entire data set, the lowest value of RMSE of 0.96 is found from using the Rl k-ν model. The highest value of RMSE of 1.07 is found from using the St k-ν model. The differences in RMSE values are not very significant but mean that the results from the St k-ν model are slightly less accurate than those of the Rl k-ν model.

The location of maximum error is found at location of $il/L\cos_n = 0.63$, and location of $il/L\cos_n = 0.79$, which are located in the lower half of the stepped spillway. At location

of $il/L\cos_n$ = 0.63 the flow changed from the non-aerated zone to the aerated zone. Therefore, the changes in aerated conditions may largely affect the calculations and cause significant errors. In comparison with all five turbulence models, it was found that the Rl k-ν model is slightly better with an RMSE ranging from 0.19–1.82 m/s, which is very close to the RMSE from the RNG k-ν, St k-Š and SST k-Š models.

The turbulence model that gives the highest RMSE is the St k-Š model, which is developed from an empirical model. At all locations, most of the high RMSEs were observed at 0.10 m above the pseudo-bottom. Further development of the St k-Š model resulted in the SST k-Š model, which resulted in slightly more accurate results in the near-wall region. The Rl k-ν model was developed for flows with a high Reynolds number. In the present study with Reynolds numbers between $1.68 \times 10^6 \leq \mathrm{Re} \leq 7.21 \times 10^6$, the results of the Rl k-ν model were slightly better than those of the St k-ν model in the upper region. Due to the similar equations for both k and ν, the results from the RNG k-ν model are also similar to the St k-ν and the Rl k-ν models. However, with the additional term in the ν equation related to the main strain and turbulence quantities, the RNG k-ν model can be viewed as being slightly better.

Both k-Š models can also provide satisfactory results for near-wall treatments where the mesh is fine enough. In addition, it is more reliable for flows that have adverse pressure gradients. The results from using the SST k-Š model in the near-wall region in the present study show satisfactory agreement for fine mesh sizes. Thus, the point of interest is important in the selection of a turbulence model; e.g. the k-Š models are slightly preferable in the near-wall zone in the lower region, whilst the Rl k-ν model is preferable in the upper part of the velocity profile. The turbulence models suggested by the previous studies by Chen et al. (2002), Cheng et al. (2006), and Qian et al. (2009), are St k-ν, RNG k-ν, and Rl k-ν models, respectively. It can be seen that the newer-developed turbulence model can be better used with the flow with higher flow rate. Moreover, Tongkratoke et al. (2009) also found that Rl k-ν is the closest to the physical data compared with the other linear models. Most of flow rate in the cases simulated by Tongkratoke et al. (2009) are close to or higher than the flow rate simulated by Qian et al. (2009).

The velocity profiles from all turbulence models tended to have the same shape, beginning with velocity gradually increasing from the pseudo-bottom until the maximum velocity was reached. The results of spillway overflow with the flow rate of 2.83 m3/s are shown in Figure 5.6 (a). The velocity at the free surface gradually increases in the downstream direction. The lowest velocity at the free surface among all these measured locations is found at the upstream end. The velocity increases in the downstream direction and becomes relatively constant in the aerated zone. The numerical model with the Rl k-ε turbulence model can simulate velocity profiles at all locations and it can easily be used to find the starting point of uniform flow. The results of spillway overflow near the downstream end with all flow discharges are shown in Figure 5.6 (b). Considering different discharges, a higher discharge causes a higher flow depth but the flow velocity at the downstream end remains the same. Thus, the

roughness of stepped spillways can be used to control the downstream velocity even when the inlet discharge is varied.

(a) At a discharge of 2.83 m³/s

(b) At the downstream end for different discharges
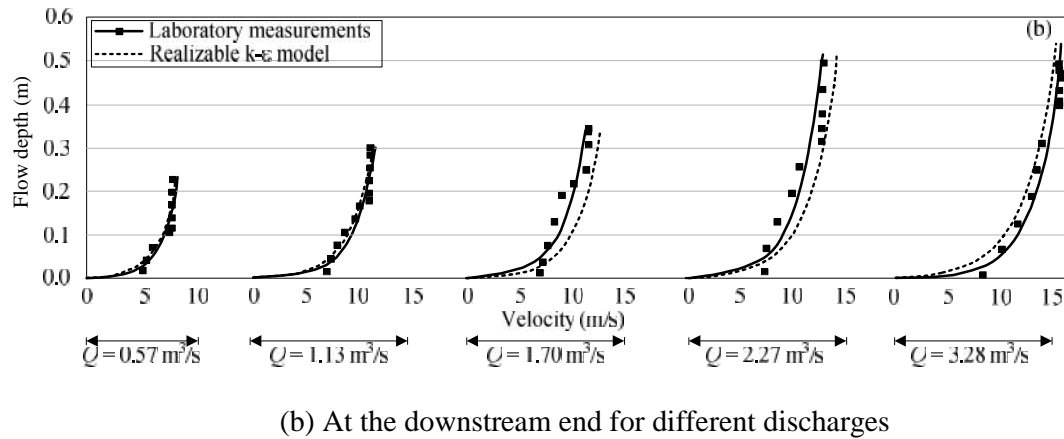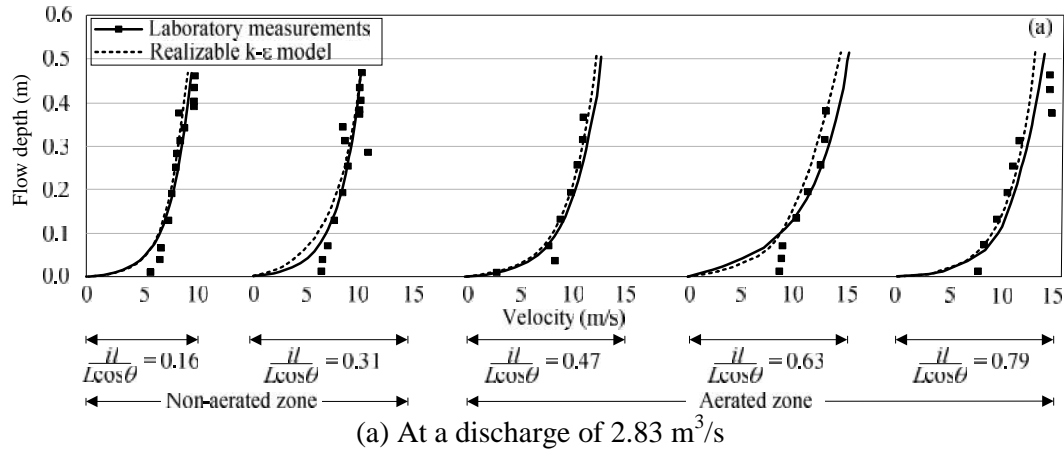
Figure 5.6 Flow velocity profiles along the stepped spillway

5.3 Grid independence study

In order to perform a grid convergence study, GCI was used to provide a consistent manner in reporting the results of grid convergence studies and estimate a discretisation error on the grid convergence of the solution. The subscripts 1, 2, and 3 mean finest (0.035x0.035 m²), fine (0.050x0.050 m²), and coarse (0.100x0.100 m²) grids, respectively. The velocity is, therefore, represented by f_1, f_2, and f_3, respectively. The ratios, r_{21} and r_{32}, are 1.913 and 1.556 which are greater than the recommended minimum value of 1.3. Some results for GCI at five locations on spillway are shown in Figure 5.7. The study shows GCI_{21} and GCI_{32} of less than 5 and 20%, respectively. From the comparison of numerical results at all locations, GCI_{21} cannot be noticeably seen whereas GCI_{32} can be clearly seen or much higher than GCI_{21}. The approximate relative error which is not shown here, e_a^{21} is lower than e_a^{32}. It means that the difference between numerical value of finest and fine grids is lower than that of in between fine and coarse grids. The extrapolated relative error, e_{ext}^{21}, is also very low. It can be defined the results from grid size of less than 0.100×0.100 m² is independent on grid size effect. However, Roy (2003) mentioned the true errors would be quite different

if 5% difference is found. Then, for the better results in present study, the grid size of 0.050×0.050 m^2 was suggested as a representative grid size.
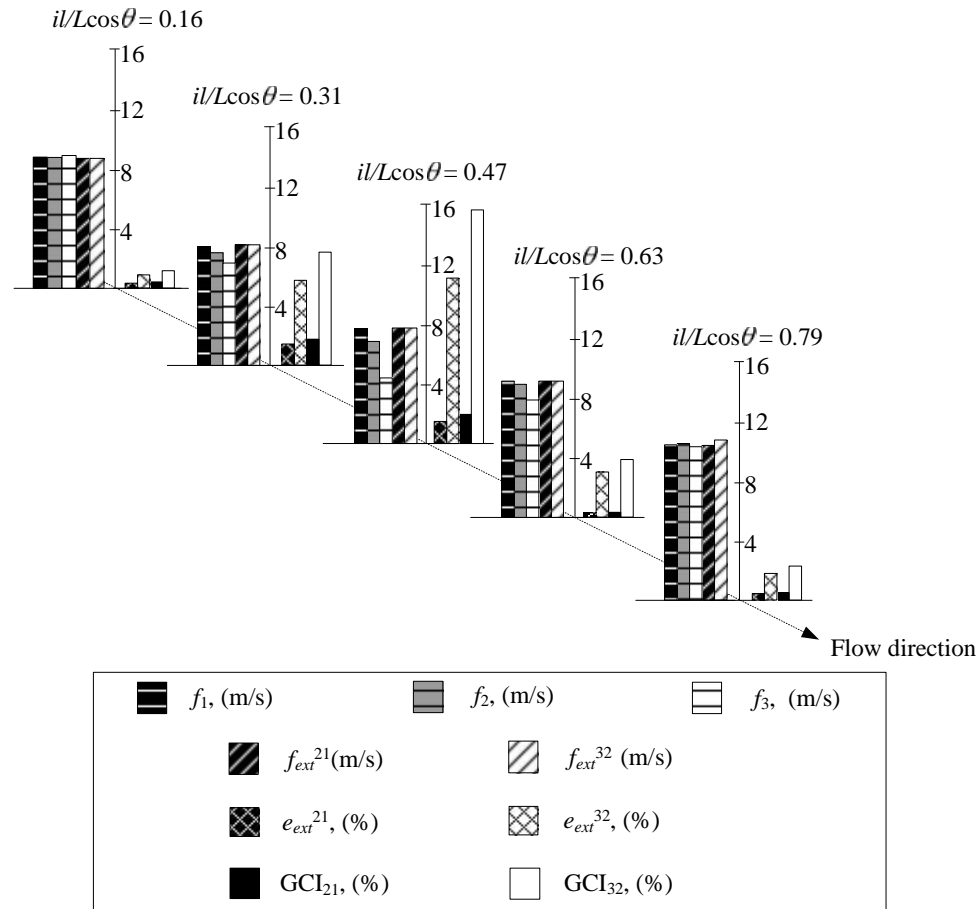
Figure 5.7 Results of grid convergence study

For the 50-step spillway, the values of $e_a{}^{32}$ ranged from 10 to 20% whereas $e_a{}^{21}$ is less than 5%. In the present study, the fine grid is suggested to be an appropriate size because it shows noticeably better results than the coarse grid, while it shows a few differences with the finest grid. The maximum percentage differences between the experimental data and the coarse, fine, and finest grids are 61%, 26% and 19%, respectively. The time and resources required for the simulation from the fine grid were less than for the finest grid, but it shows similar results.

However, one more grid size was simulated to compare the results without using GCI. The grid size of 0.020×0.020 m^2 was analysed. Then, the ratio of grid size over step height was used to compare. The ratios of 0.03, 0.06, 0.08, 0.11, and 0.16 were found. The relationship between velocity from the numerical model and physical model from all data is shown in Figure 5.8. The perfect correlation line, the dotted line in the figure, is the line shows that the results from the numerical model are equal to the results from physical model. It is shown that the ratio of 0.07 should be the best ratio for simulation of flow through a stepped spillway. This chart can be used as a tool for the improvement

of the results from different grid size. If the designers have less time to simulate the flow over stepped spillway, a large grid can be used to spend less time. Then, this chart can be used to improve the results of velocity from the numerical model.
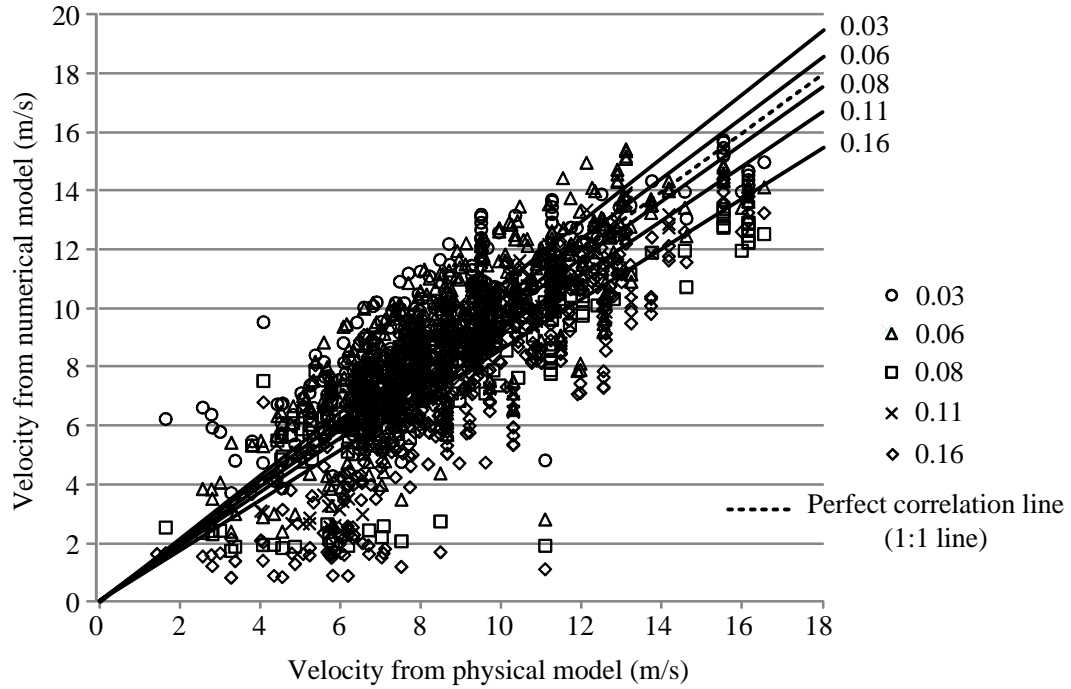
Figure 5.8 Comparison of velocity on the different grid size

5.4 Flow along stepped spillways
5.4.1 Flow regimes

Chinnarasri and Wongwises (2004) proposed the minimum critical flow depth required for the onset of skimming flow and the maximum critical flow depth for the nappe flow regime. The minimum discharge required for the onset of skimming flow on horizontal and inclined steps for $0.10 \leq \dfrac{h}{l} \leq 1.73$ is

$$\frac{y_c}{h} = \left(0.844 + 0.003_n \right)\left(\frac{h}{l}\right)^{-0.153 + 0.004_n} \tag{5.3}$$

While the maximum discharge for the nappe flow regime is

$$\frac{y_c}{h} = 0.927 - 0.005_n - 0.388\left(\frac{h}{l}\right) \tag{5.4}$$

where $\dfrac{y_c}{h}$ means relative critical flow depth. The nappe flow regime is a succession of free-falling nappe and jet impacts from one step onto the next one when the nappe cavity is fully aerated (Chanson, 2002). For the cases of $T_{0.46}$ and $T_{0.73}$, nappe flow was

observed. With the higher discharge, some air pocket is observed while the falling jet disappears, then the flow becomes a transition flow. The skimming flow regime is observed after the higher discharge approach; in this study, it was observed at $T_{0.96}$. Then the air pocket disappears and the flow recirculation is observed. The flow was turbulent along the spillway with the Reynolds number of $5.56 \times 10^5 \leq \mathrm{Re} \leq 3.68 \times 10^6$, $1.68 \times 10^6 \leq \mathrm{Re} \leq 7.21 \times 10^6$, and $1.19 \times 10^6 \leq \mathrm{Re} \leq 5.55 \times 10^6$ for the smooth, 25-step, and 50-step spillways, respectively. All of the values of Re found in the present study were greater than 10^5, which suggested that the viscous effects in the momentum exchange were minimised.

Similarly to the physical models, two cases of nappe flow were found on the 25-step spillway. The interface between the water surface and air can be seen in the numerical results. The numerical results for nappe flow looked similar to the physical model. The wavy water surface with the air pockets underneath can be seen on the steps. For the flow along the entire spillway, the value of V_{90} can be found. In the nappe flow zone, at low relative critical flow depth, y_c/ih, V_{90} stays constant since s is less than 0.2, where $s = il/L\cos_n$. At high y_c/ih, V_{90} stays constant for $s > 0.4$. In the nappe flow regime, it can be obtained that the location where V_{90} stays constant, depending directly on the relative critical flow depth.

In cases of the same inlet velocity, for example; $T_{0.96}$ and $F_{1.91}$, $T_{1.16}$ and $F_{2.32}$, the value of V_{90} from the 50-step spillway was smaller than from the 25-step spillway at the same location. This shows that at the same y_c/ih, the velocity, V_{90}, can be rapidly varied for different locations. However, V_{90}, can be constant after steps at $s > 0.8$. It can be observed that low y_c/ih can produce constant V_{90} faster than high y_c/ih. The flow profile of low y_c/ih and high y_c/ih were therefore compared to locate the point of interest.

The behaviour of skimming flow can be divided into 2 zones; non-aerated zone and aerated zone. In the non-aerated zone, the irrotational flow without air entrainment is observed. The water surface is quite smooth. After flow through some steps, the aerated zone is found where the free surface is wavy with full of air entrainment. The separated point of non-aerated and aerated zone is called the inception point. Downstream of the inception point can be divided into 2 more zones; gradually varied flow zone and uniform flow zone. In gradually varied flow, flow depth and other properties such as velocity and pressure, change gradually. At the end point of the gradually varied flow zone, the attainment of uniform flow is observed.

5.4.2 Uniform flow attainment

Generally, in skimming flow regimes, non-aerated and aerated zones can be found. To separate these two zones, the inception point is used. Upstream of this point, non-aerated zone has been found while the aerated zone has been found downstream. For the non-aerated zone, Bombardelli et al. (2011) found a good agreement between numerical and experimental data. The TruVOF method was used together with the standard k-v and the RNG k-v. The non-aerated zone was studied by using multi-block grids in a Cartesian coordinate system. For the aerated zone, both non-uniform and uniform flows have been found. In a uniform region, flow conditions; the residual specific energy and

the flow velocity, remain constant (Ohtsu et al., 2004). Three different ways for evaluating the attainment of uniform flow were also suggested by Boes and Hager (2003b). First, the air concentration profiles at the spillway end and at any interesting cross-section are used. These two profiles are compared and considered together with the constant flow depth and velocity. Second, the curves of the equivalent clear water depth, h_w, and characteristic mixture depths, h_{90}, are examined. For quasi-constant values at the spillway end, uniform flow is likely to be attained. For a third criterion, the uniform depth-averaged air concentration is compared with the mean air concentration for uniform flow as proposed by Hager (1991). These two values had to be within an arbitrarily selected 20% that is considered sufficiently exact for highly turbulent air-water flow. The hydraulic conditions for the uniform flow are required for the study of stepped spillway. For flow over long enough stepped spillway, the attainment of uniform flow can cause higher energy dissipation than the non-uniform flow in shorter spillway. The energy dissipation can also be deduced from the chute geometry and from the discharge (Chanson, 1993). Therefore, the locations of inception point and the attainment of uniform flow are important.

Considering on the pressure profile on the skimming flow in Figure 5.9, the inception point can be seen on $il/L\cos_n = 0.37$. The pressure isolines in between $0 \leq il/L\cos_n \leq 0.37$ are different among their own steps and also from the other steps. The maximum and minimum absolute pressure at the upstream of the inception point are 1.23×10^5 and 1.03×10^5 Pa, respectively. From the previous study proposed by Boes (2000b), the length of inception point with slopes ranging from 30° to 50° is;

$$L_I = 3.64(\cos_n)^{0.86} \frac{q^{0.86}}{k_s^{0.29}(\tan_n)^{0.43}} \tag{5.5}$$

where L_I is length of inception point from the first step, k_s is the step roughness height which is $k_s = h\cos_n$, $_n$ is the spillway slope, and q is the discharge per unit width. The length of inception point from equation (5.5) is very close to the one from the present study so the pressure profile from the numerical model can be used to locate the inception point on the stepped spillways.

Downstream of the inception point, the pressure profile on each step seems to be the same. However, from the enlargement of pressure isolines on $il/L\cos_n = 0.47$, the maximum absolute pressure is 1.23×10^5 Pa, which is a bit different from $il/L\cos_n = 0.63$ and $il/L\cos_n = 0.79$, where the maximum absolute pressure is 1.29×10^5 Pa. This is because the flow is the gradually varied right after the inception point while the uniform flow occurred after the gradually varied flow. As mentioned above, in a uniform flow, the residual specific energy and the flow velocity remain constant. Also from the pressure profiles, the enlargement of pressure isolines can be used to separate the gradually varied flow and uniform flow. The pressure isolines for the uniform flow from the numerical model also remain constant in every steps, except for the last step of spillway because the effect of tailwater. The pressure isolines for the gradually varied flow change on each step gradually. To locate the location of the separation between gradually varied flow and uniform flow which means the starting point of uniform flow, the equation as follows can be used;

$$L_{SU} = 3.64(\cos_{,,})^{0.86} \frac{q^{0.86}}{(h\cos_{,,})^{0.29}(\tan_{,,})^{0.43}} + 2.42q^{1.07}\left(\frac{\cos^2_{,,}}{\sin_{,,}} + h\sin_{,,}\right) \qquad (5.6)$$

where L_{SU} is the length of starting point of uniform flow.
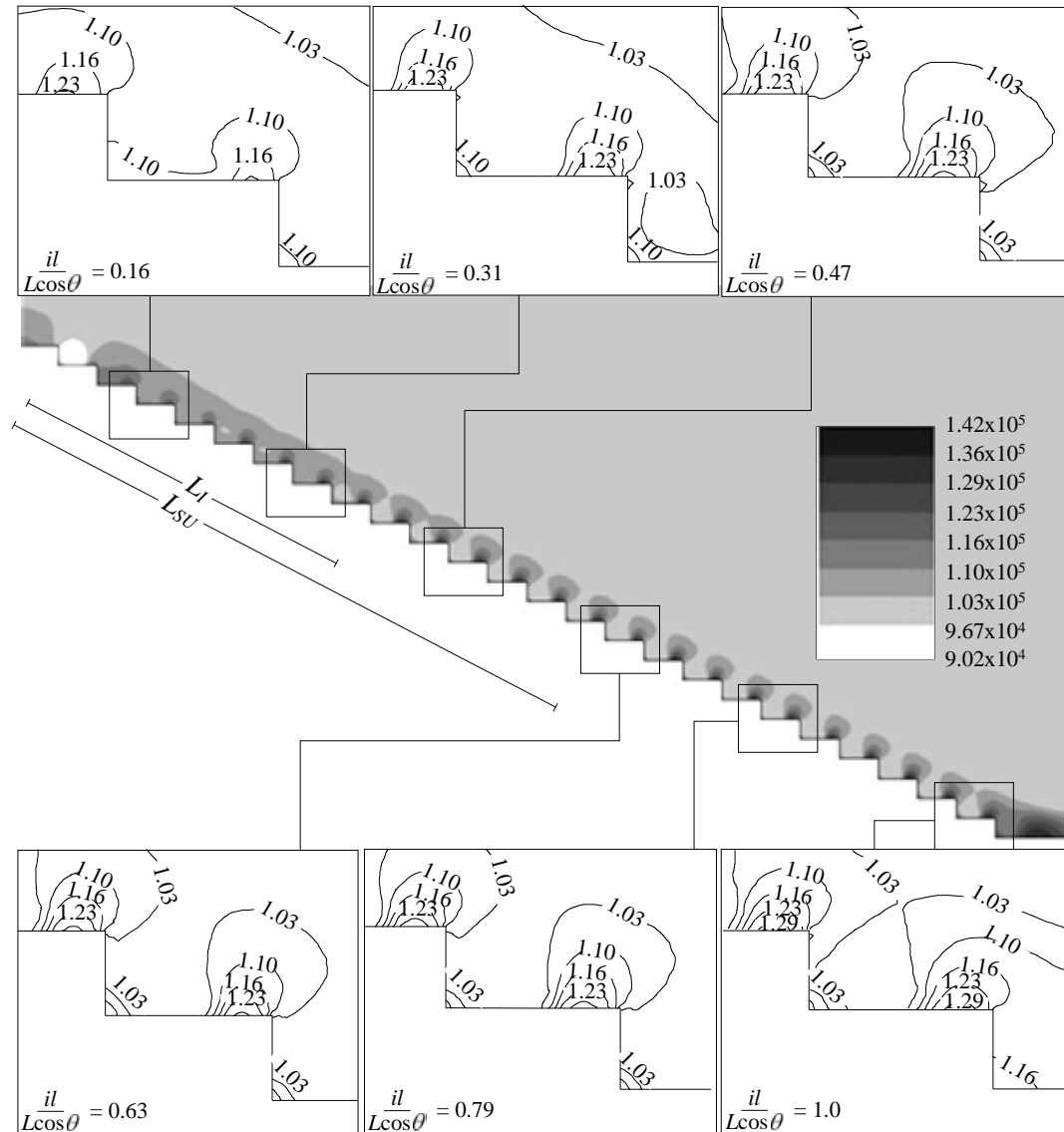
Figure 5.9 Pressure profiles of the skimming flow (unit:Pa) with the enlargement of pressure isolines (unit:$\times 10^5$ Pa)

5.5   Flow on the step

The step which was far away from the inception point and reached a uniform condition was used to observe. The nappe and skimming flow on the steps are shown in Figure 5.10 (a) and (b), respectively. The photos taken from the experiments (Frizell, 2006) with the simulation results of flow direction and volume fraction of water are shown in the same scale. For nappe flow, the flow depth is low and the air pocket is found near

the corner of the tread and riser. The numerical results show good agreement with the photograph, as shown in Figure 5.10 (a). In the air pocket, there was small velocity vectors in different directions which mean some water spilled in and out of the air pocket. Due to the complexity in this zone, it is difficult to measure the velocity or pressure, so it is the advantage of using the numerical model. However, the numerical model should be verified whether it can satisfactorily simulate this kind of flow. The numerical results of the air concentration at the surface or at 90% air concentration are also agreed well with the experimental data.

(a) Nappe flow
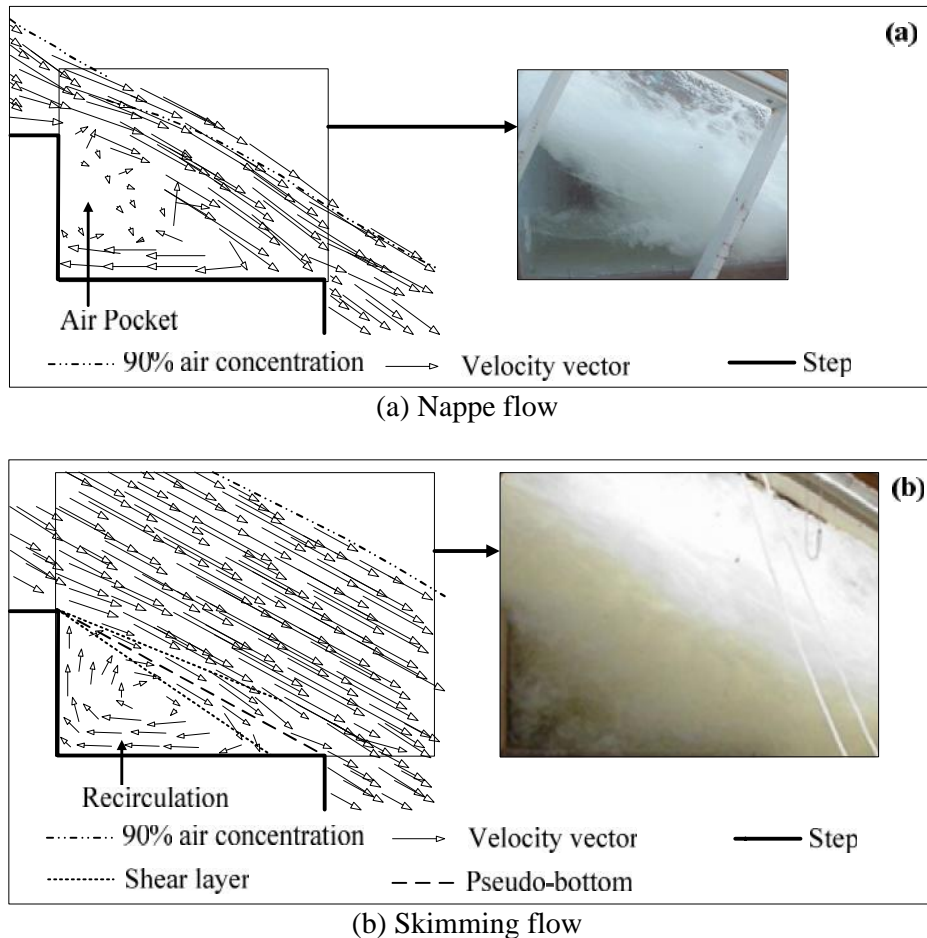
(b) Skimming flow

Figure 5.10 Schematic diagrams of flow on the steps (flow from left to right)

For skimming flow, the flow recirculation was observed in the lower region. The air bubbles in the flow recirculation were distributed with the upper region. High air entrainment was found at the centre of the recirculation flow while the least flow velocity was found there. In the lower region, flow recirculation plays an important role in governing the pressure. The negative gauge pressure could be found in the flow recirculation while the higher pressure could be found in the downstream half of the tread. With the same velocity inlet, the negative pressure in stepped spillway was less than in the smooth spillway whereas the negative pressure in smooth spillway can be found along the entire length wherever the flow depth is higher than the design head at the upstream. Therefore, prevention of damage from cavitation in a stepped spillway is easier than in a smooth spillway. The filling of more air in the recirculation can be one

of the solutions to reduce the negative pressure. The numerical model can be a tool to design the appropriate step size for the reduction of the negative pressure.

The upper region, as shown in Figure 5.10 (b), is the aerated zone. The flow depth in the main flow is higher than the nappe flow and contained a wavy water surface. The numerical results of the air entrainment near the surface are agreed well with the experimental data but they cannot simulate well near the pseudo-bottom. The interaction between lower and upper regions was characterised by a shear layer in the shear layer zone, as shown in Figure 5.10 (b).

5.6   Velocity profile

The velocity profiles tended to have the same shape beginning with velocity gradually increasing from the bed until a maximum velocity was reached. At some point in the upper region of the depth, an immediate change was observed where the velocity abruptly increases. For both smooth and stepped spillways, the numerical results show good agreement of the velocity profiles compared to the experimental data. The velocity profiles along the smooth spillway at five stations with a discharge of 2.27 m^3/s are shown in Figure 5.11. The percentage difference between numerical and experimental data was less than 17%.
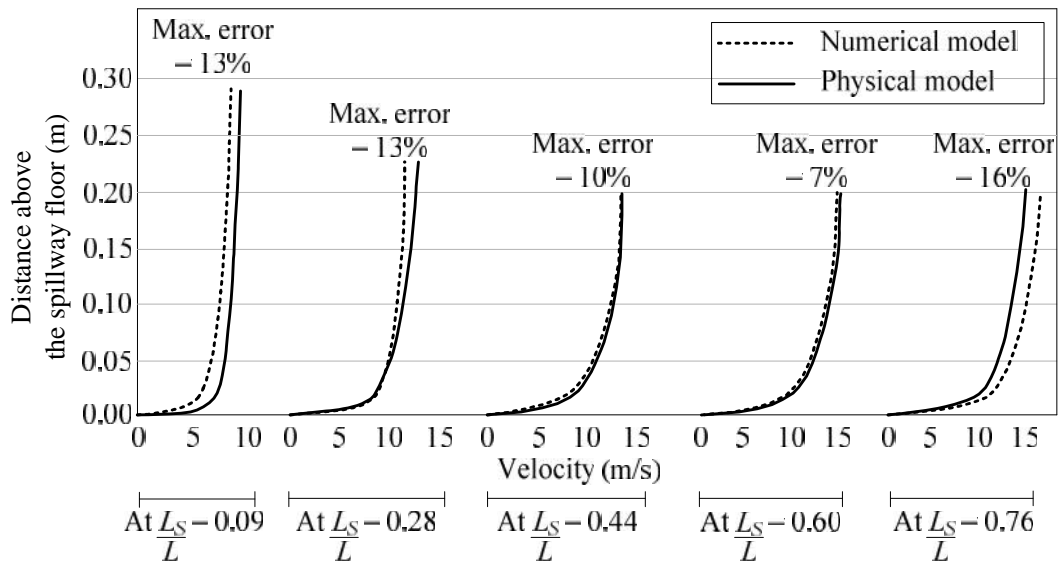
Figure 5.11 Velocity profiles along the smooth spillway with the discharge of 2.27 m^3/s

After flow along some distances through the spillway, the velocity profiles at all stations tended to have the same shape with the same maximum velocity. The maximum velocity at the last station near the outlet in the smooth spillway is high, and can cause more turbulence, compared with the flow along the stepped spillway at the same inlet velocity. On 25-step spillway, velocity profiles at $il/L\cos_n = 0.79$ between the physical and numerical models are shown in Figure 5.12. This location was chosen because it was far from both the inception point and the effect of tail-water. The percentage difference between the numerical and experimental data was less than 15%. It was found that near the water surface, the data from the physical model was quite different

from the velocity profiles trend. This is due to a problem with measurements near the water surface with high turbulence of water and air. In the cases which have the same critical depth at the same location, that maximum velocity from the smooth spillway is higher than in the 25-step spillway. Thus, the stepped spillway is more efficient than the smooth spillway in reducing the flow velocity.
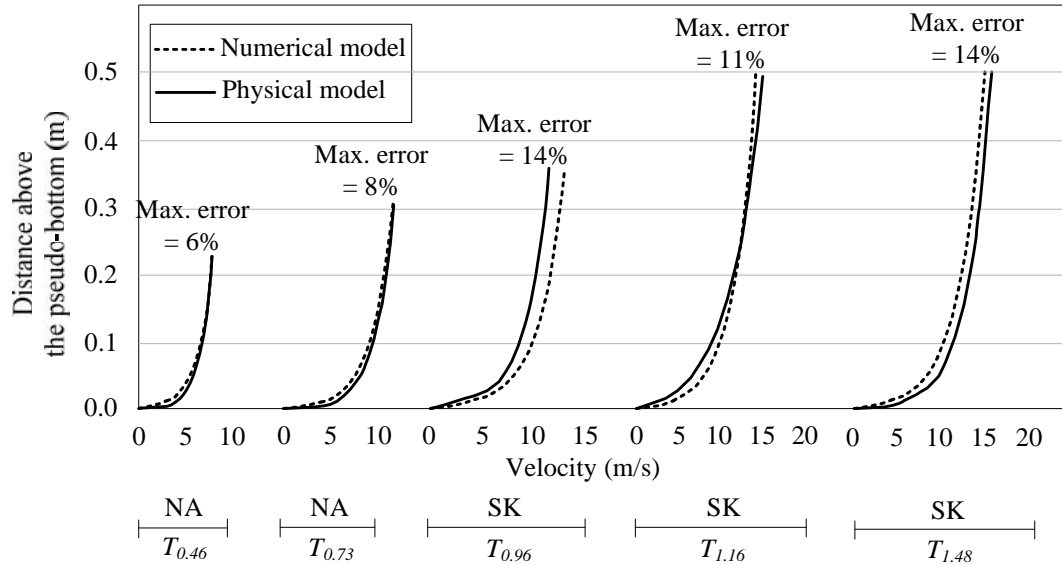
Figure 5.12 Velocity profiles on $il/L\cos_n = 0.79$ of 25-step spillway

For the 50-step spillway, comparison of velocity profiles at $s = 0.79$ in all cases is shown in Figure 5.13. The percentage difference between the numerical and experimental data was less than 12%. Comparison of cases which have the same critical depth at the same location, the maximum velocity from the 25-step spillway is also higher than the 50-step spillway. Considering nappe flow only, Figure 5.14 shows the dimensionless velocity distribution at all five stations. In previous studies on skimming flow, the results followed the power law, as shown in equation (5.7), suggesting different values of n.

$$\frac{V}{V_{90}} = \left(\frac{y}{y_{90}}\right)^{\frac{1}{n}}$$

(5.7)

Different values of n were suggested from smaller-scale experiments; Chanson and Toombes (2001) found $n = 5.1$ and 6 for y_c/h of 1.5 and 1.1, respectively. Matos (2000) obtained $n = 4$, whereas Chanson (1995) suggested $n = 3.5$ and 4 for the earlier works. However, in the present study of skimming flow regimes, $n = 5.09$ is suggested under the limitation of the Reynolds number of $1.68 \times 10^6 \leq Re \leq 7.21 \times 10^6$. This number can be used to design the stepped spillway in various sizes. The designers or engineers can use this empirical formula to initially design the flow or even the flow depth that can be passed the stepped spillway. However, the numerical model, with the turbulence model suggested in the present study, is used to design more details of the stepped spillway.
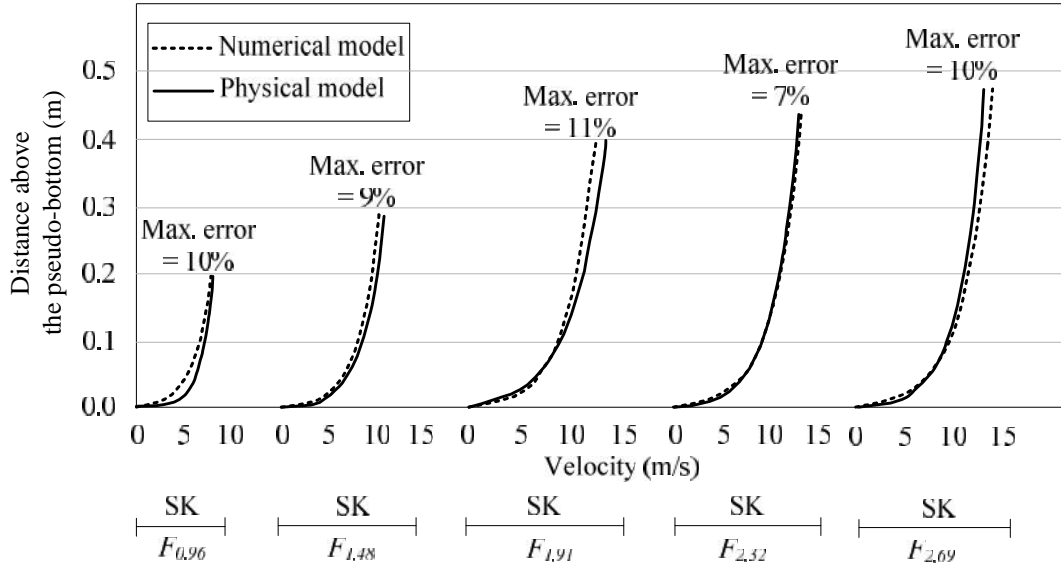
Figure 5.13 Velocity profiles on $il/L\cos_n = 0.79$ of 50-step spillway
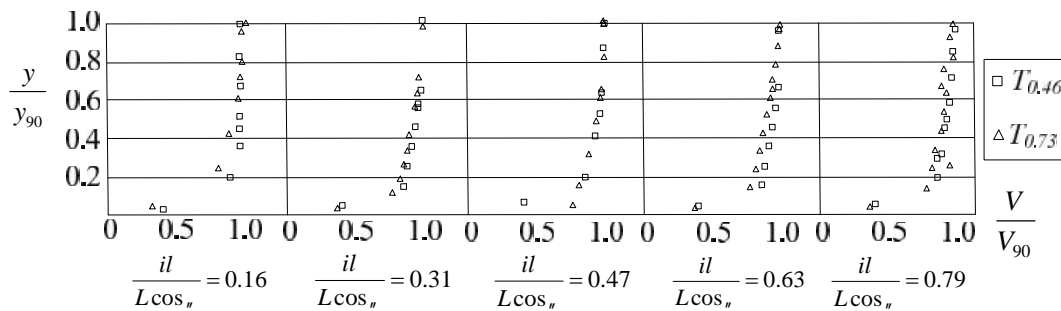
Figure 5.14 Dimensionless velocity distributions on different locations of nappe flow

As concerns in the skimming flow, the numerical results are shown in Figure 5.15. The power law of skimming flow for both the 25-step and 50-step spillways shows the same trend for all five locations. Value of $n = 4.4$ is obtained from the present study, which is quite close to previous studies (Matos, 2000).
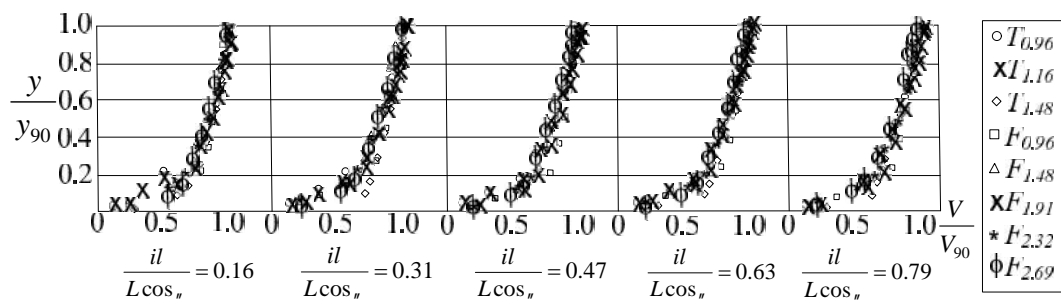
Figure 5.15 Dimensionless velocity distributions of skimming flow

5.7　Turbulence intensity

The turbulence intensity in the flow through the spillway is subjected to the influence of flow patterns of the boundary layers and boundary conditions of different sections. This can be defined as the ratio of root mean square of the longitudinal component of turbulent velocity over velocity at that point. In Figure 5.16, the turbulence intensity distributions from the smooth spillway, with an inlet discharge of 2.27 m^3/s, are shown with the flow direction from left to right. The trends of the turbulence intensity profiles are similar to those on the smooth open-channel flow in previous study (Radhakrishnan and Piomelli, 2008).
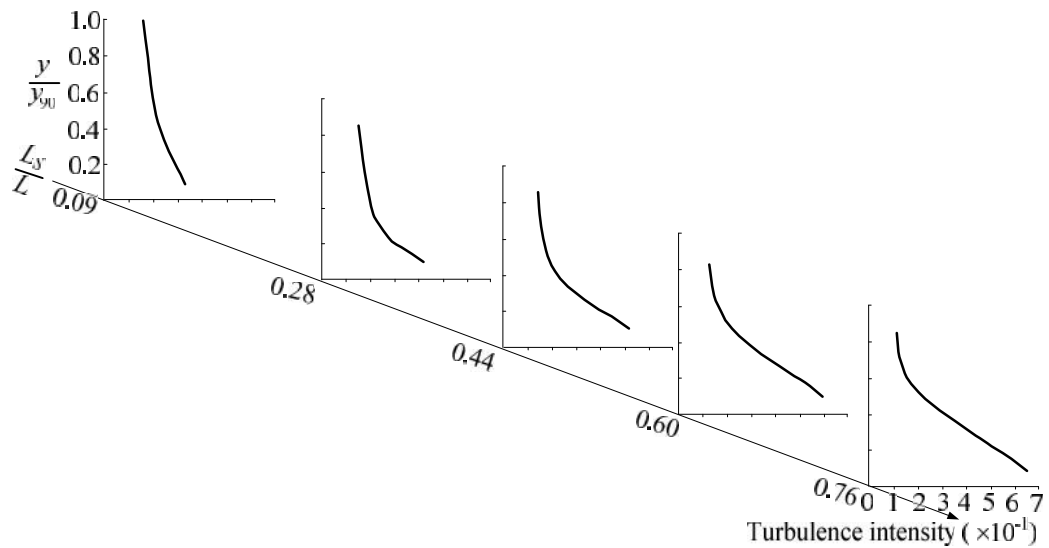
Figure 5.16 Turbulence intensity distributions of flow along smooth spillway with the inlet discharge of 2.27 m^3/s

At each measurement location, the maximum turbulence intensity, I_{max}, occurred close to the spillway floor. Then, with greater water depth, the turbulence intensity decreased to a minimum, I_{min}, near the water surface. For the location upstream, I_{max} is lower than at the stations downstream. It increased gradually along the spillway and reached a maximum near the outlet. As concerns I_{min} near the surface, it slowly decreased from upstream to downstream. On the other hand, it can be observed that both I_{max} and I_{min} for flow along the smooth spillway occur near the spillway outlet. From comparison at the same location with a different critical depth, flow with low critical depth obtained a value of I less than the high critical depth. Critical depth and flow distance have an obvious effect on turbulence intensity.

For the stepped spillway, the turbulence intensity in both nappe and skimming flows showed different trends from some previous studies (Gonzalez and Chanson, 2004; Chanson and Toombes, 2002). This might be because of some of the parameters used to calculate the turbulence intensity. These previous studies used mean or average velocity to calculate the turbulence intensity. However, compared with the studies in which the turbulence intensity was from the friction velocity (Wang et al., 1993; Carollo, 2005),

the results show the same trend. The equation for the distribution of turbulence intensity is used and shown as;

$$\frac{u'}{u_*} = De^{-\lambda(y/H)} \tag{5.8}$$

where H is flow depth normal to the slope, y = depth at point of interest normal to the slope. The turbulence intensity distributions depend directly on the roughness ratio between flow depth and roughness height. The constants in Eq.(5-8) can be divided into 2 groups based on $H/h\cos_n$. However, in the present study, only $H/h\cos_n$ of less than 0.4 was found. Therefore, the results were compared and it was found that all results were under equation (5.8) with $D = 2.14$ and $\lambda = 0.8$. The turbulence intensity distribution was found to decrease in the direction from the water surface to the pseudo-bottom. In the region of y/H of less than 0.2, the turbulence intensity was found to be quite constant with bed distance. It can also found that the roughness of the spillway considerably increases the turbulence intensity

5.8   Energy dissipation

The energy dissipation can be observed and calculated from the energy between the inlet section at the approach channel of spillway, E_0, and any section downstream, E_i, as described in section 2.5 and shown in Figure 2.5. For any section downstream, the energy at the interesting section was calculated. The energy dissipation, E_L/E_0, is one of the dimensionless parameter which is widely used. The energy loss, E_L, is the difference between energy at the inlet section, E_0, and the energy at the point-of-interest section, E_i, $E_L = E_0 - E_i$. The point of interest is superimposed with the datum then the energy E_i consists of flow depth measured in vertical direction and velocity head. The energy E_0 consists of elevation head from datum to the inlet, and the summation of flow depth and velocity head which is equal to $1.5y_c$. The energy dissipation for the smooth spillway rapidly decreases with increasing discharge, while for the stepped spillway it decreases only gradually. For a given height, the energy dissipation increases when the number of steps increases for the case of skimming flow. Because each step acts as a macro roughness, more steps causes more flow resistance and energy dissipation.

To consider on the inlet discharge on stepped and smooth spillways, Figure 5.17 shows the energy dissipation at the last station for both step and smooth spillways. It is shown that for the same spillway, the energy dissipation decreases when the discharge increases. The energy dissipation for the smooth spillway is rapidly decreased with increasing of discharge while the one for stepped spillway is gradually decreased. It can be stated that the stepped spillway is better used for higher design discharge than the smooth one because more energy can be dissipated due to the macro roughness of the steps.

Consideration on the certain discharge, even it is low or high, the results indicate clearly that a great amount of energy dissipation is occurred in a stepped spillway. It is also shown that for a given height, the energy dissipation increases when the number of steps increases. The results can be compared with the study from Rad and Teimouri (2010) and the same trend is found. Because each step acts as a macro roughness, the more

steps can cause the thickness of turbulent boundary layer and more flow resistance and also significantly causes more energy dissipation. However, with high roughness, Chanson (1994) reported the skimming flow will become fully developed and the stepped spillway behaves like a smooth spillway.
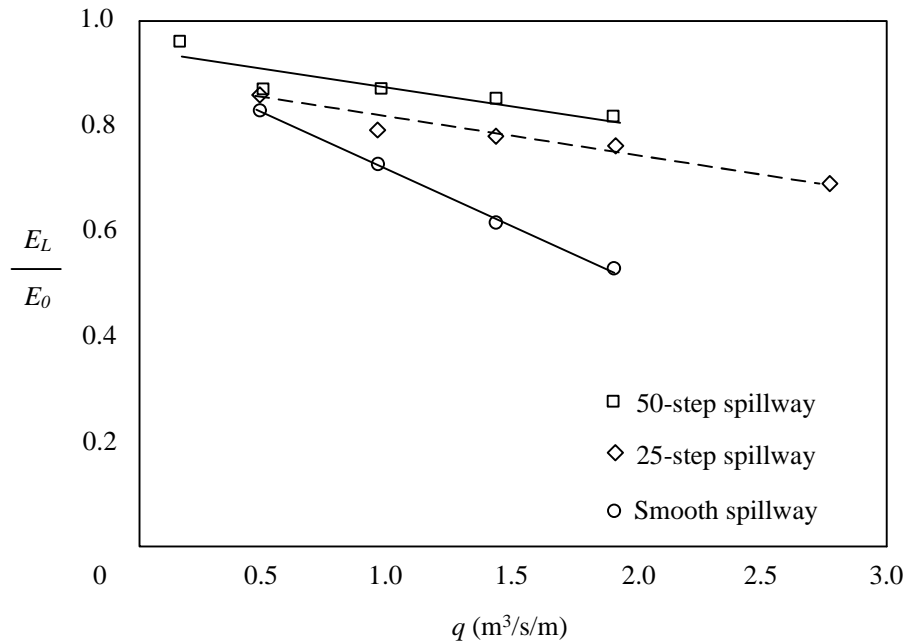
Figure 5.17 The energy dissipation chart on spillways with different step numbers

With the results from simulation, the empirical correlation for the energy dissipation on the critical depth and number of steps, with R^2=0.90 and the limit of 2H:1V stepped spillway, is;

$$\frac{E_L}{E_0} = 0.94e^{-2.84\frac{y_c}{ih}} \tag{5.9}$$

The fitting trend of data in Figure 5.18 is compared with the previous study by Rad and Teimouri (2010), in which the spillway slope was 26.6°, the number of steps was 32, and the Reynolds number was 10^5. The trend of results by Rad and Teimouri (2010) which $0.04 \le \frac{y_c}{Nh} \le 0.13$ fits very well with the results from the present study which $0.02 \le \frac{y_c}{Nh} \le 0.60$. They are also compared with the other large scale studies: Chanson and Toombes (2002) with a spillway slope of 15.9° and $3\times10^5 \le \mathrm{Re} \le 8\times10^5$; Carosi and Chanson (2008) with a spillway slope of 21.8° and $3\times10^4 \le \mathrm{Re} \le 7\times10^5$; and Chanson and Felder (2010) with a spillway slope of 26.6° and $5\times10^4 \le \mathrm{Re} \le 1\times10^6$. The dimensionless residual head, E_i/y_c, is then used for comparison. For the slope of 21.8°, E_i/y_c was 3.1 and it was 4.6 for 15.9° and 26.6° depending on the step height. It is 4.5 from the present study, which is not much different from the previous works and confirmed the results from the other large-scale studies.
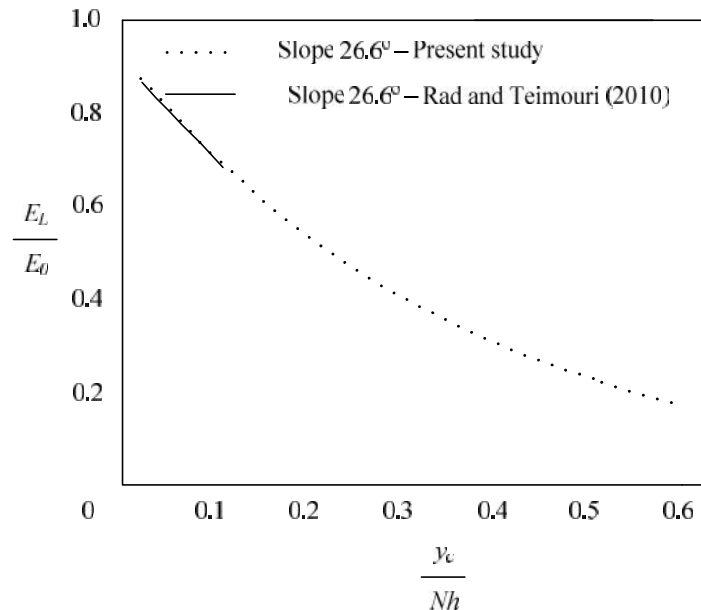
Figure 5.18 Energy dissipation on the correlation of critical depth and number of steps

5.9   Pressure on the step

To consider on the pressure on the step, the absolute pressures on; i) $il/L\cos_n = 0.31$, which is in non-aerated zone, ii) $il/L\cos_n = 0.47$, which is in gradually varied flow, and iii) $il/L\cos_n = 0.79$, which is in uniform flow, were chosen. The measured locations for vertical and horizontal surface were settled on the centre alignment of step. On horizontal face, eight locations were measured; x/l= 0.06, 0.19, 0.31, 0.44, 0.56, 0.69, 0.81, and 0.94, where x means the horizontal distance from the riser of previous step.

The absolute pressure on the horizontal surface of steps in non-aerated zone, gradually varied flow, and uniform flow are shown in Figures 5.19 (a), (b) and (c), respectively. Along the horizontal surface, both nappe and skimming flow regimes, the pressure slightly decreases at the upstream half of the step, or after first 4 stations. It means that air pocket in nappe flow and flow recirculation in skimming flow affect the absolute pressure directly. The minimum pressure was obtained in the zone of $0.30 \le x/l \le 0.45$. The negative pressure was also found in this area. Then, the flow hits the rest of downstream half of the step directly and causes the increased pressure to be the maximum near the tip or in the zone of $0.8 \le x/l \le 0.9$ and a little bit decrease again at the last station. This maximum pressure is caused by the impact of the falling water from the previous step hit directly the next step. To compare with the study from Chinnarasri et al. (2008), a similar trend of pressure on the horizontal step is found even it is the result from the gabion-stepped spillway. The maximum pressure and minimum pressure were found at the location of $0.7 \le x/l \le 0.9$ and $x/l \approx 0.3-0.7$, respectively. Both maximum and minimum pressures from the present study are agreed well with the previous study.

(a) $il/L\cos_n = 0.31$

(b) $il/L\cos_n = 0.47$

(c) $il/L\cos_n = 0.79$
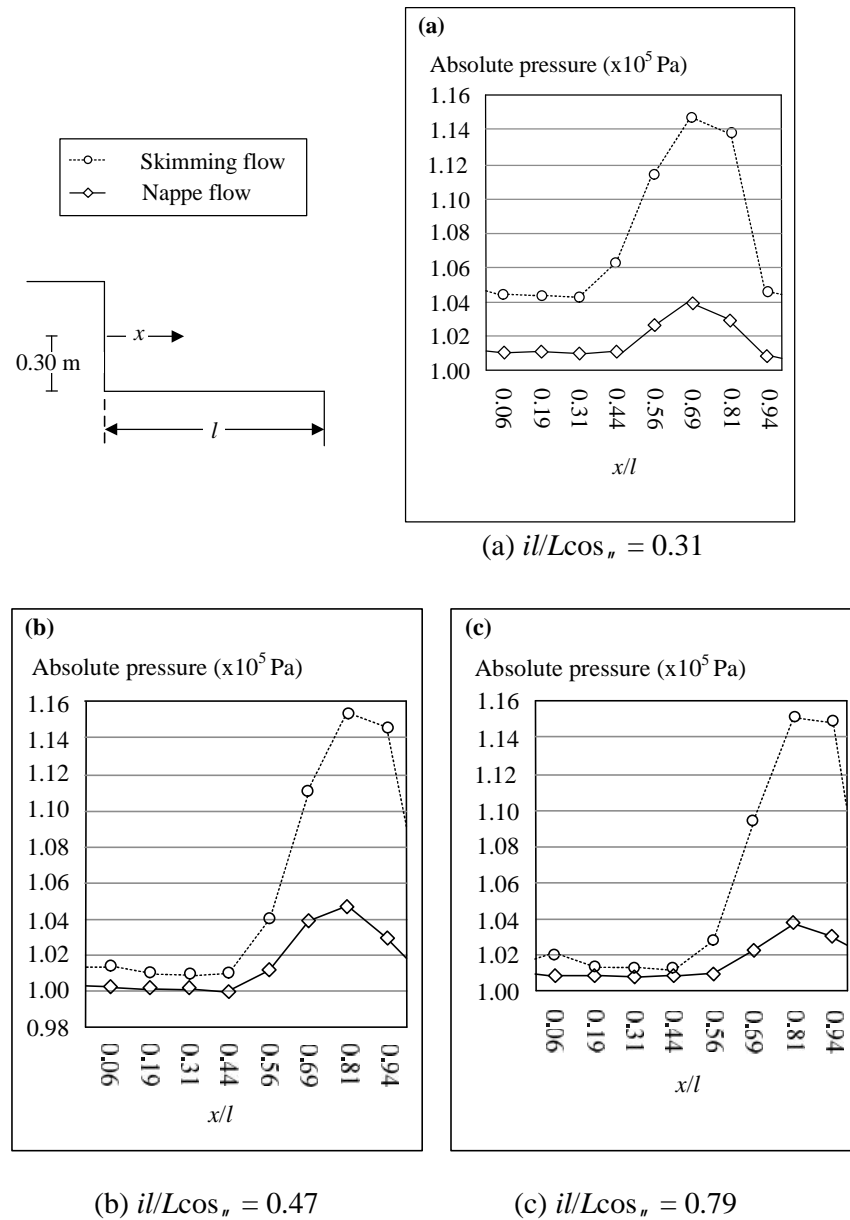
Figure 5.19 Absolute pressure distribution on the horizontal surface

On the vertical surface as shown in Figure 5.20, four locations were measured; $z/h = 0.13, 0.38, 0.63,$ and 0.88 . The absolute pressure on the vertical surface of steps in non-aerated zone, gradually varied flow , and uniform flow are shown in Figures 5.20 (a), (b) and (c), respectively. Both nappe and skimming flow regimes, the pressure decreases at the upper zone of the step, or after first 3 stations. Then, it increases a bit at the last station. The maximum absolute pressure was found at the first station while the minimum one was obtained at $z/h \approx 0.63$. In nappe flow regime, all of the pressure on vertical surface is less than the atmospheric pressure, 101325 Pa, which means the pressure is negative. The results on the vertical steps are different from the previous study because the measured line in the present study located at the middle of the step while the others located at the step edges. However, the pressure near the step floor of skimming flow is negative and clearly be seen. With the effect of negative pressure, the

step face can be damaged easily. Therefore, it is important to know the location of negative pressure and then the experiments are needed. Using the physical model to study, the measurement of negative pressure is quite difficult, so, this numerical model can be used to locate the negative pressure location which is important for the assessment of cavitations potential and cavitations protection.

(a) $il/L\cos_n = 0.31$

(b) $il/L\cos_n = 0.47$ (c) $il/L\cos_n = 0.79$
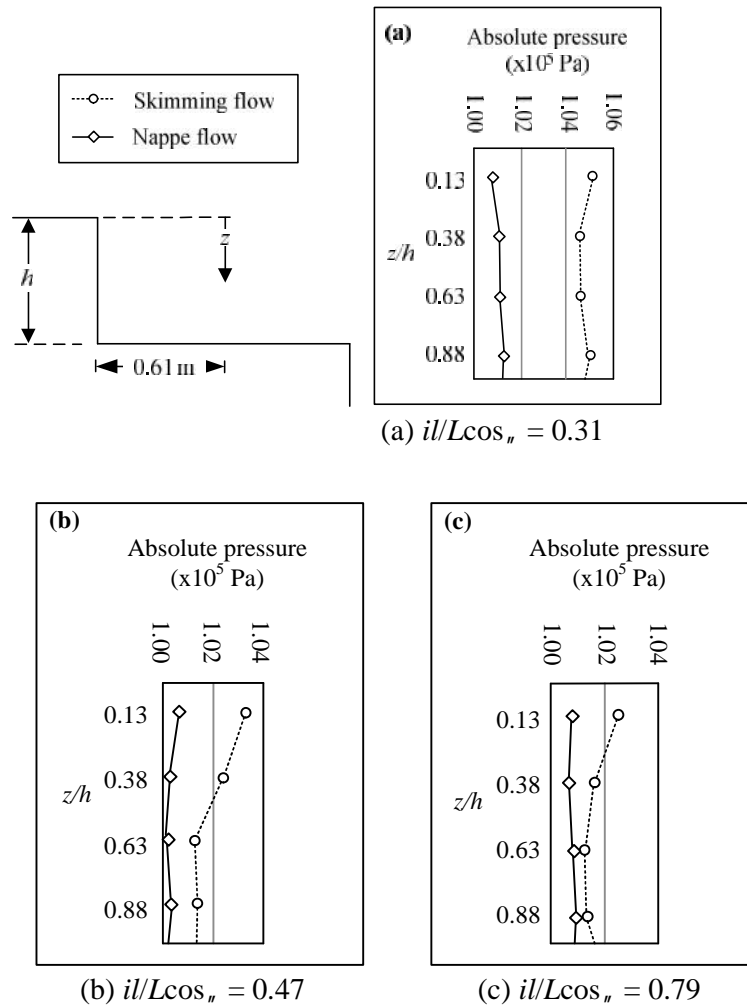
Figure 5.20 Absolute pressure distribution on the vertical surface

5.10   Proposed coefficients for turbulence model

According to the analysis by Shih et al. (1995), the equations for k and v in the Rl k-v model are already shown in equations (3.28) and (3.30), respectively.

$$\frac{\partial}{\partial t}(...k)+\frac{\partial}{\partial x_j}(...ku_j)=\frac{\partial}{\partial x_j}\left[\left(\sim+\frac{\sim_t}{\dagger_k}\right)\frac{\partial k}{\partial x_j}\right]+G_k+G_b-...v-Y_M+S_k \qquad (3.28)$$

$$\frac{\partial}{\partial t}\left(...\nu\right)+\frac{\partial}{\partial x_j}\left(...\nu u_j\right)$$

$$=\frac{\partial}{\partial x_j}\left[\left(\sim+\frac{\sim_t}{\dagger_\nu}\right)\frac{\partial \nu}{\partial x_j}\right]+...C_1 S_\nu -...C_2\frac{\nu^2}{k+\sqrt{\ \nu}}+C_{1\nu}\frac{\nu}{k}C_{3\nu}G_b+S_\nu \qquad (3.30)$$

Shih et al. (1995) developed the flow at large Reynolds number and firstly obtained a modelled dissipation rate equation as follows;

$$\nu+\nu u_j=\left(\overline{\nu u_j}\right)+C_1 S_\nu -C_2\frac{\nu^2}{k+\sqrt{\ \nu}} \qquad (5.10)$$

The coefficients, C_1 and C_2, are expected to be independent of the Reynolds number as the Reynolds number becomes large. They are affected by solid body rotation imposed on turbulence through the reduction of fluctuation vortex stretching, however, it is rather weak compared to the other mechanisms (Shih et al., 1995). For decaying grid turbulence, only the last term on the right hand side of equation (5.10) is non-zero and must be negative, hence C_2 must be positive. For the case of homogeneous shear flow, both the turbulent kinetic energy and its dissipation rate increase with time so that the "source" term in equation (5.10) must be positive, hence C_1 must be positive. In fact, the flow through stepped spillway depends on C_2 more than C_1. The decay of dissipation rate of the turbulent kinetic energy equation is observed along the downstream direction (Jinnah, 2012). Shih et al. (1995) mentioned the decay exponent n_d varies from 1.08 to 1.30. In their study, n_d of 1.11 was chosen and then, C_2 was 1.9 according to equation (5.11).

$$C_2=\frac{n_d+1}{n_d} \qquad (5.11)$$

After that, C_1 was determined due to the use of the experimental data of homogeneous shear flow and boundary layer flow. It is found to be the function of $C_1=$ max [0.43, $y/(y+5)$], $y=Sk/\nu$, $S\equiv(2S_{ij}S_{ij})^{0.5}$, $S_{ij}=(\partial u_i/\partial x_j)+(\partial u_j/\partial x_i)$. However, in the present study, the decaying grid turbulence plays more important role than the homogeneous shear flow and boundary layer flow. Hence, the C_2 should be more important than the case used by Shih et al. (1995). The C_2 of 1.80 shows the better simulation results than C_2 of 1.90 which is proposed in the previous study. The results for velocity at different values of coefficient C_2 are shown in appendix C. The n_d is found to be 1.25 and it is in the range of 1.08 to 1.30 suggested in the previous study. Then, the more appropriate value of C_2 is proposed to be 1.80 for the flow over stepped spillway.

CHAPTER 6 CONCLUSIONS AND RECOMMENDATIONS

Based on the results from both numerical and physical models, the conclusions and recommendations can be drawn as follow:

6.1   Conclusions

The numerical model was used to study the flow behaviour through smooth and stepped spillways. The stepped spillway consists of 25 steps and 50 steps. The numerical results are verified by comparison with the large-scale physical model. First, the physical model, tested by Ward in 2002, was located at Colorado State University. The concrete spillway was 34.09 m long, 1.22 m wide, and 2.13 m deep on a 2H:1V slope with a total height of 15.24 m. Velocity and air concentration instrumentation was installed on a carriage system. The manually operated carriage system allowed for two degrees of freedom, with movement along the spillway, and lateral movement within the width of the spillway. The remotely operated, motorised point gage allowed for vertical movement normal to the pseudo-bottom. All profiles were taken along the centreline of the spillway. A back flushing Pitot-static tube was used to measure the velocity, due to its ability to work in non-homogeneous fluid. The output signal was scanned at 120 Hz for a duration of 20-seconds. The air probe was used to determine the air concentration. Its output signal was scanned at 15 kHz for 5 seconds per probe tip. The error on the vertical position of the probe was less than 0.025 mm. The accuracy on the longitudinal probe position was estimated as $\Delta x < \pm 0.5$ cm.

The numerical model with the Finite Volume Method (FVM) was used with the uniform-sized, structured grids. The meshed domain represents as a 2D grid. The inlet section is at the upstream of the spillway which consists of the inlet of water at bottom and the inlet of air at top. The inlet water velocity was the initial condition and was set uniformly at the water inlet and flow through the spillway which was initially full of air. The air boundaries were defined as an inlet pressure with the atmospheric pressure. The outlet of the spillways at the downstream was defined as an outlet pressure so the water can flow out freely. The calculation domain was discretised into structured grid with various sizes of 0.020×0.020, 0.035×0.035, 0.050×0.050 and 0.100×0.100 m^2 quadrilateral cells. The control volume technique is used to convert the governing equations to algebraic equations that can be solved numerically. The integration governing equations on the control volumes are solved iteratively using implicit form. In the implicit scheme, the unknown value of each variable is computed from the relationship among the neighboring meshes.

The pressure-based segregated solver was used because it is multiphase flow with 2 materials, water and air, flow with different velocities. To start the initial calculation, the uniform velocity of water and the atmospheric pressure are specified at the water inlet and free surface zone, respectively. The momentum equation is then used to calculate. The VOF and MMF models are used in this step to compare the results. Then, the values of parameters will transfer to solve the continuity equation. After that, the values of pressure and velocity are updated and put into the turbulence models. The converged criteria are checked at the difference of 0.0001 in order to assure that the results from the simulation are very close to the data from physical model.

The flow regime on a stepped spillway is classified into three types: nappe flow, transition flow and skimming flow. In nappe flow, usually found on large steps or at low discharges, a free-falling jet impacts from step to step with a fully aerated nappe cavity. Skimming flows occur on small steps or at high discharges. The behaviour of skimming flow can be divided into 2 zones; non-aerated and aerated. In the non-aerated zone, the irrotational flow without air entrainment is observed. The water surface is quite smooth. After flow through some steps, the aerated zone is found where the free surface is wavy with full of air entrainment. The separated point of non-aerated and aerated zone is called the inception point. Downstream of the inception point can be divided into 2 more zones; gradually varied flow and uniform flow. In gradually varied flow, flow depth and other properties such as velocity and pressure, change gradually.

6.1.1   It can be concluded, from the numerical results, that the numerical model can be used to model the complex flow pattern of two-phase turbulence flow in spillways. The Finite Volume Method, FVM, is also found to be the numerical method that can be used to simulate the complex flow. The Volume of Fluid, VOF, and the Realisable k-$\vee$ models are chosen as the multiphase flow model and turbulence model, respectively, that can simulate the flow from the physical model better than the other models. The flow initiation at the inlet is one of the locations that VOF shows the better simulation than MMF. Considering the entire data set, the lowest value of RMSE of 0.96 is found from using the Rl k-$\vee$ model. The highest value of RMSE of 1.07 is found from using the St k-$\vee$ model. The Rl k-$\vee$ model is slightly better than other turbulence models with an RMSE ranging from 0.19–1.82 m/s.

6.1.2   The appropriate grid size for the simulation is suggested based on Grid Convergence Index (GCI). Three sizes of grid sizes which are 0.035x0.035 m^2, 0.050x0.050 m^2, and 0.100x0.100 m^2 were compared by GCI. The grid size of 0.035x0.035 m^2 shows the best results among those grid sizes. For the GCI between the grid size of 0.050x0.050 m^2 and 0.100x0.100 m^2, the values of GCI are less than 20%. For the GCI between the grid size of 0.035x0.035 m^2 and 0.050x0.050 m^2, the values of GCI are less than 5%. It means that the results from grid size of 0.035x0.035 m^2 and 0.050x0.050 m^2 are not noticeably seen. Also, the time and resources required for the simulation from the coarse grid are less than for the fine grid, but it shows similar results. Then, the present study, the grid size of 0.050×0.050 m^2 was suggested as a representative grid size because they can show the good results in appropriate sources and time. Later, the grid size of 0.020x0.020 m^2 was analysed. Then, the ratio of grid size over step height was used for comparison. The ratio of 0.03, 0.06, 0.08, 0.11, and 0.16 were found. It is shown that the ratio of 0.07 should be the best ratio for simulation of flow through a stepped spillway.

6.1.3   It is shown that for the same spillway, the energy dissipation decreases when the discharge increases. The energy dissipation for the smooth spillway is rapidly decreased with increasing of discharge while the one for stepped spillway is gradually decreased. It can be stated that the stepped spillway is better used for higher design discharge than the smooth one because more energy can be dissipated due to the macro roughness of the steps.

6.1.4   It is found that the simulation results from numerical models can be used to simulate the large scale physical models. The flow regimes that can be found on the numerical model are the same as the ones found in the physical model. The inception point and the point of uniform flow attainment can be found from the pressure profiles of numerical model. It is also important to know the location of negative pressure and then the experiments are needed. Using the physical model to study, the measurement of negative pressure is quite difficult, so, this numerical model can be used to locate the negative pressure location which is important for the assessment of cavitations potential and cavitations protection.

6.1.5   The numerical model can be used to develop the equations and charts for the preliminary design of spillways for any cases of possible discharges. The example of preliminary design by these equations and charts are shown in appendix D.

- The velocity profiles from the numerical simulation also show the similar trend as the 1/6 power law from previous studies. The equations from present study for the velocity profiles of skimming flow are suggested in equation (5.1).

$$\frac{y}{y_{90}} = 0.01e^{4.65\left(\frac{V}{V_{90}}\right)} \tag{5.1}$$

- The inception point and the point of uniform flow attainment can be found from the pressure profiles of numerical model. To locate the location of the separation between gradually varied flow and uniform flow which means the starting point of uniform flow, equation (5.6) can be used.

$$L_{SU} = 3.64(\cos_{\theta})^{0.86} \frac{q^{0.86}}{(h\cos_{\theta})^{0.29}(\tan_{\theta})^{0.43}} + 2.42q^{1.07}\left(\frac{\cos^2_{\theta}}{\sin_{\theta}} + h\sin_{\theta}\right) \tag{5.6}$$

where L_{SU} is the length of starting point of uniform flow.

- The results followed the power law, as shown in equation (5.7), suggesting different values of n. In the present study of skimming flow regimes, $n = 5.09$ is suggested under the limitation of the Reynolds number of $1.68 \times 10^6 \leq \text{Re} \leq 7.21 \times 10^6$.

$$\frac{V}{V_{90}} = \left(\frac{y}{y_{90}}\right)^{\frac{1}{n}} \tag{5.7}$$

- The equation for the distribution of turbulence intensity is shown in equation (5.8) with $D = 2.14$ and $\lambda = 0.8$.

$$\frac{u'}{u_*} = De^{-\}(y/H)} \tag{5.8}$$

- The Figure 5.8 can be used as a tool for the improvement of the results from different grid size. If the designers have less time to simulate the flow over stepped spillway, a large grid can be used to spend less time. Then, this chart can be used to improve the results of velocity from the numerical model.
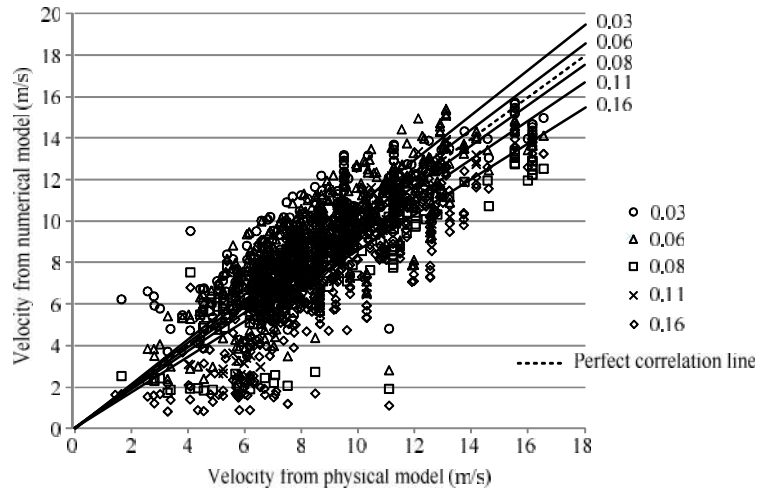
Figure 5.8 Comparison of velocity on the different grid size

- The fitting trend of equation (5.9) and Figure 5.18 can be used as a tool for the energy dissipation on the correlation of critical depth and number of steps.

$$\frac{E_L}{E_0} = 0.94e^{-2.84\frac{y_c}{ih}} \tag{5.9}$$
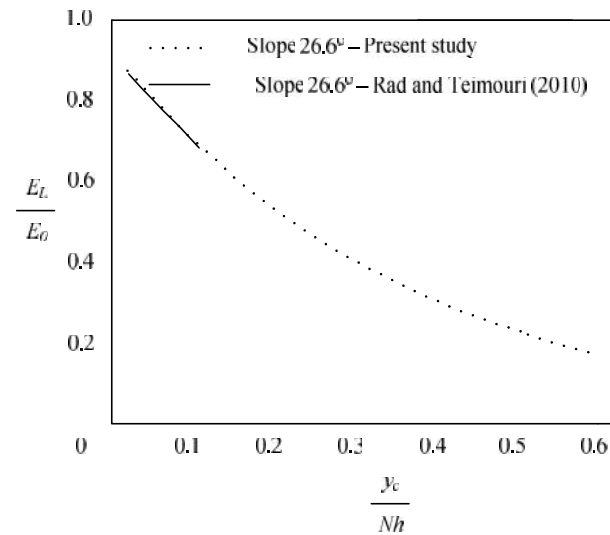
Figure 5.18 Energy dissipation on the correlation of critical depth and number of steps

6.2 Recommendations

Based on the results from this study, the following recommendations are offered for future investigation:

6.2.1 This study attempted to simulate only 25 and 50-step spillways compared with the physical model. It might be better to simulate more number of steps. However, the researcher might have to test the physical model for more number of steps because there is still no physical data of large scale model for stepped spillways.

6.2.2 More kinds of turbulence models should be used because in the present study, only linear equations were used. However, it might take more time to simulate and the results may be almost the same as using the linear equations. It depends on sources and time that the researchers will spend.

6.2.3 More parameters need further studies to understand physical process of flow behaviour through the spillway. They are, for example, friction factor, bed shear stress, etc. The other types of flow regimes; transition flow and nappe flow, are also needed to be studied more. However, the results from the large-scale physical model are needed.

REFERENCES

Amador, A., 2006, "Characterization of the Nonaerated Flow Region in a Stepped Spillway by PIV", **Journal of Fluid Engineering**, Vol. 128, No. 6, pp. 1266-1273.

Amador, A., Sanchez-Juny, M. and Dolz, J., 2009, "Developing Flow Region and Pressure Fluctuations on Steeply Sloping Stepped Spillways", **Journal of Hydraulic Engineering**, Vol. 135, No. 12, pp. 1092-1100.

Amador, A., Sanchez-Juny, M., Dolz, J., Sanchez-Tembleque, F. and Puertas, J., 2004, "Velocity and Pressure Field in Skimming Flow in Stepped Spillways", **Proceedings of the International Conference on Hydraulics of Dams and River Structures**, 26-28 April, Tehran, Iran, pp.279-285.

Andre, S., Boillat, E. and Schleiss, A., 2001, "High Velocity Two-phase Turbulent Flow over Macro-roughness Stepped Chutes: Focus on Dynamic Pressures", **The 3rd International Symposium on Environmental Hydraulics**, 5-7 December, Tempe, Arizona, USA.

Andre, S., 2004, **High Velocity Aerated Flows over Stepped Chutes with Macro-Roughness Elements**, Doctor of Philosophy dissertation, Ecole Polytechnique, Federale de Lausanne, Lausanne, Switzerland.

Andre, S., Boillat, E., Schleiss, A. and Matos, J., 2004, "Energy Dissipation and Hydrodynamic Forces of Aerated Flow over Macro-roughness Lininings for Overtopped Embankment Dams", **Proceedings of the International Conference on Hydraulics of Dams and River Structures**, 26-28 April, Tehran, Iran, pp. 189-196.

Benmamar, S., Kettab, A. and Thirriot, C., 2003, "Numerical Simulation of Turbulent Flow Upstream of the Inception Point in a Stepped Channel", **Proceedings of the 30th IAHR congress**, 24-19 August, Thessaloniki, Greece.

Boes, R. M., 1999, "Physical Model Study on Two-phase Cascade Flow", **Proceedings of the 28th IAHR Congress**, 22-27 August, Graz, Austria.

Boes, R.M., 2000a, "Scale Effects in Modelling Two-phase Stepped Spillway Flow" **Proceedings of the International Workshop on Hydraulics of Stepped Spillways**, 22-24 March, Zürich, Switzerland.

Boes R.M., 2000b, **Two phase flow and energy dissipation on cascades**, Doctor of Philosophy dissertation, VAW-ETH, Zurich. Switzerland, Switzerland.

Boes, R.M. and Hager, W.H., 2003a, "Hydraulic Design of Stepped Spillways", **Journal of Hydraulic Engineering**, Vol. 129, No. 9, pp. 671-679.

Boes, R.M. and Hager, W.H., 2003b, "Two-phase Flow Characteristics of Stepped Spillways", **Journal of Hydraulic Engineering**, Vol. 129, No. 9, pp. 661-670.

Bombardelli, F.A., Meireles, I. and Matos, J., 2011, "Laboratory Measurements and Multi-block Numerical Simulations of the Mean Flow and Turbulence in the Non-

aerated Skimming Flow Region of Steep Stepped Spillways", **Environmental Fluid Mechanics**, Vol. 11, No. 3, pp. 263-288.

Carvalho, R. and Amador, A., 2008, "Physical and Numerical Investigation of the Skimming Flow over a Stepped Spillway", **Proceedings of the 16th IAHR-APD Congress and the 3rd Symposium of IAHR-ISHS**, 20-23 October, Nanjing, China.

Carollo, F.G., Ferro, V. and Termini, D., 2005, "Analyzing Turbulence Intensity in Gravel Bed Channels", **Journal of Hydraulic Engineering**, Vol. 131, No.12, pp. 1050-1061.

Carosi, G. and Chanson, H., 2008, "Turbulence Characteristics in Skimming Flows on Stepped Spillways", **Canadian Journal of Civil Engineering**, Vol. 35, No. 9, pp. 865-880.

Celik, I.B., Ghia, U., Roache, P.J., Freitas, C.J., Coleman, H. and Raad, P.E., 2008, "Procedure for Estimation and Reporting of Uncertainty due to Discretization in CFD Applications", **Journal of Fluid Engineering**, Vol. 130, No.078001, pp. 1-4.

Center of Excellence for Hydro Power Plant project, 2006, **IEA Hydropower Implementing Agreement Annex VIII - Hydropower Good Practices: Environmental Mitigation Measures and Benefits Case Study 12-01: Benefits due to Dam Function – Bhumibol Dam, Thailand**, New Energy Foundation, Japan.

Chamani, M.R. and Rajaratnam, N., 1994, "Jet Flow on Stepped Spillways", **Journal of Hydraulic Engineering**, Vol. 120, No. 2, pp. 254-259.

Chamani, M.R. and Rajaratnam, N., 1999a, "Onset of Skimming Flow on Stepped Spillways", **Journal of Hydraulic Engineering**, Vol. 125, No. 9, pp. 969-971.

Chamani, M.R. and Rajaratnam, A., 1999b, "Characteristics of Skimming Flow over Stepped Spillways", **Journal of Hydraulic Engineering**, Vol. 125, No. 4, pp. 361-368.

Chanel, P.G., 2008, **An Evaluation of Computational Fluid Dynamics for Spillway Modeling**, Master of Science Thesis, Civil Engineering, Faculty of Engineering, University of Manitoba, Canada.

Chanson, H., 1993, "Stepped spillway flows and air entrainment", **Canadian Journal of Civil Engineering**, Vol. 20, No. 3, pp. 422-435.

Chanson, H., 1994, "Hydraulics of Nappe flow regime above Stepped chutes and Spillways", **Australia Civil Engineering Transactions**, Vol. CE 36, No. 1, pp.69-76.

Chanson, H., 1994a, "Hydraulics of Skimming Flows over Stepped Channels and Spillways", **Journal of Hydraulic Research**, Vol. 34, No. 3, pp. 445-460.

Chanson, H., 1994b, "Comparison of Energy Dissipation between Nappe and Skimming Flow Regimes on Stepped Chutes", **Journal of Hydraulic Research**, Vol. 34, No. 2, pp. 213-218.

Chanson, H., 1995. **Hydraulic Design of Stepped Cascades, Channels, Weirs and Spillways**, Pergamon, Oxford, UK.

Chanson, H., 1996, "Prediction of the Transition Nappe/Skimming Flow on a Atepped Channel", **Journal of Hydraulic Research**, Vol. 34, No. 3, pp. 421-429.

Chanson, H., 2000, "Hydraulics of Stepped Spillways: Current Status", **Journal of Hydraulic Engineering**, Vol. 126, No. 9, pp. 636-637.

Chanson, H., 2001, "A Transition Flow Regime on Stepped Spillways: The Fact", **Proceedings of the 29th IAHR Congress**, 16-21 September, Beijing, China.

Chanson, H., 2002, **The Hydraulics of Stepped Chutes and Spillways**, Balkema, Lisse, Netherlands.

Chanson, H. and Felder, S., 2010, "Energy Dissipation on Embankment Dam Stepped Spillways, Overflow Stepped Weirs and Masonry Stepped Spillways. **Proceedings of the 17th Congress of IAHR Asia and Pacific Division**, 21-24 February, Auckland, New Zealand, pp. 1-10.

Chanson, H. and Gonzalez, C. A., 2004, "Stepped Spillways for Embankment Dams: Review, Progress and Developments in Overflow Hydraulics", **Proceedings of the International Conference on Hydraulics of Dams and River Structures**, 26-28 April, Tehran, Iran, pp.287-294.

Chanson, H. and Gonzalez, C.A., 2005, "Physical Modelling and Scale Effects of Air-water Flows on Stepped Spillways", **Journal of Zhejiang University Science**, Vol. 6A, No. 3, pp. 243–250.

Chanson, H. and Toombes, L., 2001, **Experimental Investigations of Air Entrainment in Transition and Skimming Flows down a Stepped Chute: Application to Embankment Overflow Stepped Spillways**. Department of Civil Engineering, University of Queensland.

Chanson, H. and Toombes, L., 2002, "Air–water Flows down Stepped Chutes: Turbulence and Flow Structure Observations", **International Journal of Multiphase Flow**, Vol. 28, No. 11, pp. 1737-1761.

Chanson, H. and Toombes, L., 2002b, "Experimental Investigations of Air Entrainment in Transition and Skimming Flows down a Stepped Chute", **Canadian Journal of Civil Engineering**, Vol. 29, No. 1, pp. 145-156.

Chanson, H. and Toombes, L., 2004. "Hydraulics of Stepped Chutes: The Transition Flow", **Journal of Hydraulic Research**, Vol. 42, No. 1, pp. 43–54.

Chanson, H., Yasuda, Y. and Ohtsu, I., 2002, "Flow Resistance in Skimming Flows in Stepped Spillways and its Modelling", **Canadian Journal of Civil Engineering**, Vol. 29, No. 6, pp. 809-819.

Chatila, J.G and Jurdi, B.R., 2004, "Stepped Spillway as an Energy Dissipater", **Canadian Water Resources Journal**, Vol. 29, No. 3, pp. 147-158.

Chen, Q., Dai, G.Q. and Liu, H.W., 2002, "Volume of Fluid Model for Turbulence Numerical Simulation of Stepped Spillway Overflow", **Journal of Hydraulic Engineering**, Vol. 128, No. 7, pp. 683-688.

Cheng, X.J., Chen, Y.C. and Luo, L., 2006, "Numerical Simulation of Air-water Two-phase Flow over Stepped Spillways", **Science in China Series E: Technological Sciences**, Vol. 49, No. 6, pp. 674-684.

Chiangrai directory, **Mae Suay reservoir** [Online], Available: http://www.chiangraidirectory.com/blog/2011/11/26/13568/%E0%B8%AD%E0%B9%88%E0%B8%B2%E0%B8%87%E0%B9%80%E0%B8%81%E0%B9%87%E0%B8%9A%E0%B8%99%E0%B9%89%E0%B8%B3%E0%B9%81%E0%B8%A1%E0%B9%88%E0%B8%AA%E0%B8%A3%E0%B8%A7%E0%B8%A2-2/ [Accessed on 2013, January 4].

Chinnarasri, C., 2002, "Assessing the Flow Resistance of Skimming Flow on the Step Faces of Stepped Spillways", **Dam Engineering**, Vol. 12, No. 4, pp. 303-321.

Chinnarasri, C. and Wongwises, S., 2004, "Flow Regimes and Energy Loss on Chutes with Upward Inclined Steps", **Canadian Journal of Civil Engineering**, Vol. 31, No. 5, pp.870–879.

Chinnarasri, C. and Wongwises, S., 2006, "Flow Patterns and Energy Dissipation over Various Stepped Chutes"**, Journal of Irrigation and Drainage Engineering**, Vol. 132, No. 1, pp. 70-76.

Chinnarasri, C., Donjadee, S. and Israngkura U., 2008, "Hydraulic Characteristics of Gabion-stepped Weirs" **Journal of Hydraulic Engineering**, Vol. 134, No. 8, pp. 1147-1152.

Christodoulou, G.C., 1993, "Energy Dissipation on Stepped Spillways", **Journal of Hydraulic Engineering**, Vol. 119, No. 5, pp. 644-655.

Chu, T. W. and Shirmohammadi, A., 2004, "Evaluation of the SWAT Model's Hydrology Component in the Piedmont Physiographic Region of Maryland", **Transactions of the American Society of Agricultural Engineers**, Vol. 47, No. 4, pp. 1057-1073.

Craft, T.J., Launder, B.E. and Suga, K., 1996, "Development and Application of a Cubic Eddy-viscosity Model of Turbulence", **International Journal of Heat and Fluid Flow**, Vol. 17, No. 2, pp. 108-115.

Dargahi, B., 2006, "Experimental Study and 3D Numerical Simulations for a Free-Overflow Spillway", **Journal of Hydraulic Engineering**, Vol. 132, No. 9, pp. 899-907.

Dastgheib, A., Niksokhan, M.H. and Nowroozpour, A. R., 2012, "Comparing of Flow Pattern and Energy Dissipation over different forms of Stepped Spillway", **World Environmental and Water Resources Congress**, 20-24 May, New Mexico, USA.

De Marinis, G., Fratino, U. and Piccinni, A.F., 2001, "Flow Regimes on Stepped Spillways", **Proceedings of the 29th IAHR Congress**, 16-21 September, Beijing, China.

Dong, Z.Y. and Lee, J.H., 2006, "Numerical Simulation of Skimming Flow over Mild Stepped Channel", **Journal of Hydrodynamics Serie B**, Vol. 18, No. 3, pp. 367-371.

Dubler, J.R. and Grigg, N.S., 1996, "Dam Safety Policy for Spillway Design Floods", **Journal of Professional Issues in Engineering Education and Practice**, Vol. 122, No. 4. pp. 163-169.

Dunstan, M.R.H., 1994, "The State-of-the-Art of RCC Dams". **International Journal on Hydropower and Dams**, Vol. 1, No. 2.

Shotittayanggoon, C. and Hiruntiyakul, C., 2009, **The prediction of Probable Maximum Flood (PMF): A case study of Bhumibhol Dam**, Report No. 50-2115-005-JOB NO.565-SUT,

Essery, I.T.S. and Horner, M.N., 1978, **The Hydraulic Design of Stepped Spillways**, Ciria Report No.33, London, UK, 45 pages.

Felder, S. and Chanson, H., 2009, "Energy Dissipation, Flow Resistance and Gas-liquid Interfacial Area in Skimming Flows on Moderate-slope Stepped Spillways", **Environmental Fluid Mechanics**, Vol. 9, No. 4, pp. 427-441.

Felder, S. and Chanson, H., 2011, "Energy Dissipation down a Stepped Spillway with Non-Uniform Step Heights", **Journal of Hydraulic Engineering**, Vol. 137, No. 11, pp. 1543-1548.

Fluent Inc., 2005, **Fluent 6.2 Getting Started Guide**, Fluent Inc., Lebanon.

Franz, D.D. and Melching, C.S., 1997, **Full Equations (FEQ) Model for the Solution of the Full, Dynamic Equations of Motion for One-Dimensional Unsteady Flow in Open Channels and through Control Structures**, U.S. Geological survey, Water Resources Investigations Report 96–4240.

Fratino, U., 2004, "Nappe and Transition Flows over Stepped Chutes", In **Fluvial, Environmental and Coastal Developments in Hydraulic Engineering**, Mossa, M., Yasuda, Y. and Chanson, H. (Eds.), A.A.Balkema, Rotterdam, Netherlands, pp. 99-113.

Fratino, U., Amador, A., Valenzano, B., Renna, F.M., Sanchez-Juny, M. and Dolz, J., 2003, "Air Inception and Pressure Fields over a Stepped Spillway in Transition Flow Regime", **Proceedings of the 30th IAHR Congress**, 24-29 August, Thessaloniki, Greece, pp. 711-718.

Frizell, K.H., 1992, "Hydraulics of Stepped Spillways for RCC Dams and Dam Rehabilitations", **Proceedings of 3rd Specialty Conference on Roller Compacted Concret**e, 2-5 February, San Diego, CA, USA, pp. 423-439.

Frizell, K.H., 2006, **Research State-of-the-art and Needs for Hydraulic Design of Stepped Spillways**, U.S. Department of the Interior Bureau of Reclamation, HL-2005-06.

Fu, X., Politano, M.S. and Weber, L., 2008, "Free Surface Simulations for a Removable Spillway Weir", World Environmental and Water Resources Congress, 12-16 May, Honolulu, Hawaii, USA.

Georgia Association, **Towaliga Soil&Water Conservation District** [Online], Available: http://www.ofig.org/nrcs/tow_rt.php [Accessed on 2012, November 10].

Gaston, M., 1995, **Air Entrainment and Energy Dissipation on a Stepped Block Spillway**, Master of Engineering Thesis, Civil Engineering, Faculty of Engineering, Colorado State University, USA.

Gonzalez, C., 2005, **An Experimental Study of Free-surface Aeration on Embankment Stepped Chutes**, Doctor of Engineering dissertation, Civil Engineering, Faculty of Engineering, University of Queensland, Brisbane, Australia.

Gonzalez, A.C. and Chanson, H., 2004, "Scale Effects in Moderate Slope Stepped Spillways Experimental Studies in Air-water Flows", **Proceedings of the 8th National Conference on Hydraulics in Water Engineering**, 13-16 July, Gold Coast, Australia.

Gonzalez, A.C. and Chanson, H., 2004b, "Interactions between Cavity Flow and Main Stream Skimming Flows: an Experimental Study", **Canadian Journal of Civil Engineering**, Vol. 31, No. 1, pp. 33-44.

Gonzalez, C., and Chanson, H., 2007, "Hydraulic Design of Stepped Spillways and Downstream Energy Dissipators for Embankment Dams", **Dam Engineering**, Vol. 17, No. 4, pp. 223–244.

Gonzalez, A.C. and Chanson, H., 2008, "Turbulence and Cavity Recirculation in Air–water Skimming Flows on a Stepped Spillway", **Journal of Hydraulic Research**, Vol. 46, No. 1, pp. 65–72.

Hager, W.H., 1991, "Uniform Aerated Chute Flow", **Journal of Hydraulic Engineering**, Vol. 117, No. 4, pp. 528–533.

Hirt, C.W. and Nichols, B.D., 1981, "Volume of Fluid (VOF) Method for the Dynamics of Free Boundaries", **Journal of Computational Physics**, Vol. 39, No. 1, pp. 201-225.

Hollingworth, F., and Druyts, F.H.W.M., 1986, "Rollcrete: Some Applications to Dams in South Africa", **Water Power and Dam Construction**, Vol. 38, No. 1, pp. 13-16.

Hunt, S.L. and Kadavy, K.C., 2010, "Energy Dissipation on Flat-sloped Stepped Spillways: Part2. Downstream of the Inception Point", **American Society of Agricultural and Biological Engineers**, Vol. 53, No. 1, pp. 111-118.

Hunt, S., Reep, D. and Kadavy, K.C., 2008, "RCC Stepped Spillways for Renwick Dam - A Partnership in Research and Design", **Dam Safety Journal**, Vol. 6, No. 2, pp. 32-40.
Israngkura, U. and Chinnarasri, C., 1994, "Flow Depth and Energy Losses through Stepped Chutes", **Proceedings of the 9th Congress of Asian and Pacific Division of the International Association for Hydraulic Research**, 24-26 August, Singapore, pp. 156–163.

James S.F., **Blog Archive: December 2004** [Online], Available: http://www.politics1.com/blog-1204.htm [Accessed on 2012, November 10].

Jinnah, M.A., 2012, "Numerical Simulation of the Decay of Grid-generated Turbulence in a Shock tube", **Asian Journal of Engineering**, Vol. 2, No. 2, pp. 59-64.

Johansen, S.T., Anderson, N.M. and De Silva, S.R., 1990, "A Two-phase Model for Particle Local Equilibrium Applied to Air Classification of Powers", **Power Technology**, Vol. 63, pp. 121-132.

Khan, L.A., Wicklein, E.A., Rashid, M., Ebner, L.L. and Richards, N.A., 2008, "Case Study of an Application of a Computational Fluid Dynamics Model to the Forebay of the Dalles Dam, Oregon", **Journal of Hydraulic Engineering**, Vol. 134, No. 5, pp. 509-519.

Khatsuria, R.M., 2005, **Hydraulics of Spillways and Energy Dissipators**, Marcel Dekker, New York, USA.

Kim, S.D., Lee, H.J. and An, S.D., 2010, "Improvement of Hydraulic Stability for Spillway using CFD Model", **International Journal of Physical Sciences**, Vol. 5, No. 6, pp. 774-780.

Launder, B.E. and Spalding, D.B., 1974, "The Numerical Computation of Turbulent Flows", **Computer Methods in Applied Mechanics and Engineering**, Vol. 3, No. 2, pp. 269-289.

Li, S., Cain, S., Wosnik, M., Kocahan, H. and Wyckoff, R., 2011, "Numerical Modeling of Probable Maximum Flood Flowing through a System of Spillways", **Journal of Hydraulic Engineering**, Vol. 137, No. 1, pp,. 66-74.

Logie, C.V., 1985, "Economic Considerations in Selection of a Roller Compacted Concrete Dam", **Proceedings of the Symposium on Roller Compacted Concrete**, 1-2 May, Denver, Colorado, USA.

Matos, J., 2000, "Hydraulic Design of Stepped Spillways over RCC Dams", **Proceedings of the International Workshop on Hydraulics of Stepped Spillway**, 22-24 March, Zurich, Switzerland, pp. 187–194.

Matos, J. and Quintela, A., 1995, "Discussion of Jet Flow on Stepped Spillways by Chamani, M.R. and Rajaratnam, N.", **Journal of Hydraulic Research**, Vol. 120, No. 2, pp. 443-444.

Matos, J., Sanchez, M., Quintela, A. and Dolz, J., 1999, "Characteristic Depth and Pressure Profiles in Skimming Flow over Stepped Spillways", **Proceedings of the 28th IAHR Congress**, 22-27 August, Graz, Austria.

McCabe, T., **Concrete chute spillway in dam built as part of a watershed** [Online], Available: http://luirig.altervista.org/naturaitaliana/viewpics.php?title=Concrete+chute+spillway+in+dam+built+as+part+of+a+watershed+p... [Accessed on 2012, November 10].

Meireles, I. and Matos, J., 2009, "Skimming Flow in the Nonaerated Region of Stepped Spillways over Embankment Dams", **Journal of Hydraulic Engineering**, Vol. 135, No. 8, pp. 685-689.

Meireles, I., Renna, F., Matos, J. and Bombardelli, F., 2012, "Skimming, Nonaerated Flow on Stepped Spillways over Roller Compacted Concrete Dams", **Journal of Hydraulic Engineering**, Vol. 138, No. 10, pp. 879-877.

Menter, F.R., 1993, "Zonal Two Equation k- Turbulence Models for Aerodynamic Flows. **Proceedings of 24th Fluid Dynamics Conference**, 6-9 July, Florida, USA, paper no. AIAA 93-2906.

Mondardo, J.M. and Fabiani, A.L., 1995, "Comparison of Energy dissipation between Nappe and Skimming Flow Regimes on Stepped Chutes", **Journal of Hydraulic Research**, Vol. 33, No. 1, pp. 119-122.

Nikseresht, A.H., Alishahi, M.M. and Emdad, A., 2008, "Complete Flow Field Computation around an ACV (Air Cushion Vehicle) using 3-D VOF with Lagrangian Propagation in Computational Domain", **Computers and Structures**, Vol. 86, No. 7-8, pp. 627-641.

Ohtsu, I. and Yasuda, Y., 1997, "Characteristics of Flow Conditions on Stepped Channels", **Proceedings of 27th IAHR Congress**, 10-15 August, San Francisco, USA.

Ohtsu, I., Yasuda, Y. and Takahashi, M., 2000, "Discussion of Characteristics of Skimming Flow over Stepped Spillways", **Journal of Hydraulic Engineering**, Vol. 126, No.11, pp.869-871.

Ohtsu, I., Yasuda, Y. and Takahashi, M., 2001, "Discussion on Onset of Skimming Flow of Stepped Spillways", **Journal of Hydraulic Engineering**, Vol. **127**, No. 6, pp. 522-524.

Ohtsu, I., Yasuda, Y. and Takahashi, M., 2004., "Flow Characteristics of Skimming Flow in Stepped Channels". **Journal of Hydraulic Engineering**, Vol. 130, No. 9, pp. 860-869.

Parker, J.W., 1992, "Economic Factors in Roller Compacted Concrete Dam Construction". **Proceedings of the Roller Compacted Concrete III**, 2-5 February, San Diego, California, pp. 227–241.

Pegram, G.G.S., Officer, A.K. and Mottram, S.R., 1999, "Hydraulics of Skimming Flow on Modeled Stepped Spillways", **Journal of Hydraulic Engineering**, Vol. 125, No. 5, pp. 500-510.

Peyras, L., Royet, P. and Degoutte, G., 1992, "Flow and Energy Dissipation over Stepped Gabion Weirs", **Journal of Hydraulic Engineering**, Vol. 118, No. 5, pp. 707-717.

Pfister M. and Hager W.H., 2011, "Self-entrainment of Air on Stepped Spillways", **International Journal of Multiphase Flow**, Vol. 37, No. 2, pp. 99-107.

Pfister, M., Hager, W. H. and Minor, H.E., 2006, "Bottom Aeration of Stepped Spillways" **Journal of Hydraulic Engineering**, Vol. 132, No. 8, pp. 850-853.

Pinheiro, A.N. and Fael, C.S., 2000, "Nappe Flow in Stepped Channels-Occurrence and Energy Dissipation", **Proceedings of the International Workshop on Hydraulics of Stepped Spillway**, 22-24 March, Zurich, Switzerland, pp. 119–126.

Qian, Z., Hu, X., Huai, W. and Amador, A., 2009, "Numerical Simulation and Analysis of Water Flow over Stepped Spillways", **Science in China Series E: Technological Sciences**, Vol. 52, No. 7, pp. 1958-1965.

Rad, I.N. and Teimouri, M., 2010, "An Investigation of Flow Energy Dissipation in Simple Stepped Spillways by Numerical Model", **European Journal of Scientific Research**, Vol. 47, No. 4, pp. 544-553.

Radhakrishnan, S. and Piomelli, U., 2008, "Large-eddy Simulation of Oscillating Boundary Layers: Model Comparison and Validation", **Journal of Geophysical Research**, Vol. 113, No. C02022, pp. 1-14.

Rajaratnam, N., 1990, "Skimming Flow in Stepped Spillways", **Journal of Hydraulic Engineering**, Vol. 116, No. 4, pp. 587-591.

Rice, C.E. and Kadavy, K.C., 1996, "Model Study of a Roller Compacted Concrete Stepped Spillway", **Journal of Hydraulic Engineering**, Vol. 122, No. 6, pp. 292-297.

Roache, P.J., 1997, "Quantification of Uncertainty in Computational Fluid Dynamics", **Annual Review of Fluid Mechanics**, Vol. 29, No.1, pp. 123-160.

Roache, P.J., 1998, **Verification and validation in computational science and engineering**, Hermosa Publishers, New Mexico, USA,.

Roache, P.J., Ghia, K. and White, F., 1986, "Editorial Policy Statement on the Control of Numerical Accuracy", **Journal of Fluid Engineering**, Vol. 108, No. 1, p. 2.

Roshan, R., Azamathulla, H.M., Marosi, M., Sarkardeh, H., Pahlavan, H. and Ghani, A. A., 2010, "Hydraulics of Stepped Spillways with Different Numbers of Steps", **Dams and Reservoirs**, Vol. 20, No. 3, pp. 131-136.

Ross, M., **Invergarry Power Station** [Online], Available: http://www.corestore.org/GarryDam.htm [Accessed on 2012, November 10].

Roy, C.J., 2003, "Grid Convergence Error Analysis for Mixed-order Numerical Schemes", **AIAA Journal**, Vol. 41, No. 4, pp. 595-604.

Ru, S.X., Tang, C.Y., Pan, R.W. and He, X.M., 1994, "Stepped Dissipator on Spillway Face", **Proceedings of the 9th Congress of the Asian and Pacific Division of the International Association for Hydraulic Research**, 24-26 August, Singapore, pp. 193-200.

Sanchez-Juny, M. and Dolz, J., 2003, "Characterization of the Pressure Field over a Stepped Spillway in Roller Compacted Concrete Dams", **Proceedings of the 4th International Symposium on Roller Compacted Concrete Dams**, 17-19 November, Madrid, Spain, pp. 697-700.

Sanchez-Juny, M. and Dolz, J., 2005, "Experimental Study of Transition and Skimming Flows on Stepped Spillways in RCC Dams: Qualitative Analysis and Pressure Measurements", **Journal of Hydraulic Research**, Vol. 43, No. 5, pp. 540–548.

Sanchez-Juny, M., Pomares, J. and Dolz, J., 2000, "Pressure Field in Skimming Flow over a Stepped Spillway", **Proceedings of the International Workshop on Hydraulics of Stepped Spillway**, 22-24 March, Zurich, Switzerland.

Sartaj, M., Beirami, M. and Fooladgar, A., 2006., "Analysis of Two-Dimensional Flow over Standard Ogee Spillway Using RNG Turbulence Model", **The 7th International Congress on Civil Engineering**, 7-9 May, Tehran, Iran.

Schwer, L.E., 2008, "Is Your Mesh Refined Enough? Estimating Discretization Error Using GCI", **LS-DYNA Forum**, 30 September-1 October, Bamberg, Germany.

Shih, T.H., Liou, W.W., Shabbir, A., Yang, Z. and Zhu, J., 1995, "A New k-v Eddy Viscosity Model for High Reynolds Number Turbulent Flows", **Computers and Fluids**, Vol. 24, No. 3, pp. 227-238.

Shvainshtein, A.M., 1999, "Stepped Spillway and Energy Dissipation", **Hydrotechnical Construction**, Vol. 33, No. 5, pp. 275-282.

Singh, J., Knapp, H.V. and Demissie, M., 2004, "Hydrologic Modeling of the Iroquois River Watershed using HSPF and SWAT" Illinois State Water Survey, Champaign, Illinois, USA, 24 p.

Sorensen, R. M., 1985, "Stepped Spillway Hydraulic Model Investigation", **Journal of Hydraulic Engineering**, Vol. 111, No. 12, pp. 1461–1472.

Stephenson, D., 1991, "Energy Dissipation Down Stepped Spillways", **International Water Power and Dam Construction**, Vol.43, No. 9, pp. 27–30.

Tadayon, R. and Ramamurthy, A.S., 2009, "Turbulence Modeling of Flows over Circular Spillways"**, Journal of Irrigation and Drainage Engineering**, Vol. 135, No. 4, pp. 493-498.

Tabbara, M., Chatila, J. and Awwad, R., 2005, "Computational Simulation of Flow over Stepped Spillways", **Computers and Structures**, Vol. 83, No. 27, pp. 2215–2224.

Takahashi, M., Gonzalez, C.A. and Chanson, H., 2006, "Self-aeration and Turbulence in a Stepped Channel: Influence of Cavity Surface Roughness", **International Journal of Multiphase Flow**, Vol. 32, No. 12, pp. 1370-1385.

Takasu, S. and Yamaguchi, J. 1988, "Principle for Selecting Type of Spillway for Flood Control Dams in Japan", **Proceedings of 16th Congress of the International Commission on Large Dams**, 13-16 June, San Francisco, USA.

Thailandg.com, **Bhumibol dam** [Online], Available:
http://www.thailandg.com/812/Tak/Travel-and-Transport/Bhumibol-Dam.html
[Accessed on 2013, January 4].

Tongkratoke, A., Chinnarasri, C., Pornprommin, A., Dechaumphai, P. and Juntasaro, V., 2009, "Non-linear Turbulence Models for Multiphase Recirculating Free-surface Flow over Stepped Spillways", **International Journal of Computational Fluid Dynamics**, Vol. 23, No. 5, pp. 401-409.

Turan, C., McDaniel, B., Politano, M.S., Carrica, P.M. and Weber, L., 2006, "A Study of the Free Surface Flow on Brownlee Dam", **World Environmental and Water Resource Congress**, 21-25 May, Nebraska, USA.

Unami, K., Kawachi T., Munir Babar M. and Itagaki, H., 1999, "Two-Dimensional Numerical Model of Spillway Flow", **Journal of Hydraulic Research**, Vol. 125, No. 4, pp. 369-375.

Vazquez-Amábile, G.G. and Engel, B.A., 2005, "Use of SWAT to Compute Groundwater Table Depth and Streamflow in the Muscatatuck River watershed", **Transactions of the American Society of Agricultural Engineers**, Vol. 48, No. 3, pp. 991-1003.

Vischer, D.L. and Hager, W.H. eds., 1995, **Energy dissipaters**, A.A.Balkema, Rotterdam, Netherlands.

Walsh Construction, **Lake Brazos Dam Replacement** [Online], Available:
http://www.walshgroup.com/portfolio/heavy+civil/dams/lake-brazos-dam-replacement.html [Accessed on 2012, November 10].

Wang, J., Dong, Z., Chen, C. and Xia, Z., 1993, "The Effects of Bed Roughness on the Distribution of Turbulent Intensities in Open Channel Flow", **Journal of Hydraulic Research**, Vol. 31, No.1, pp. 89-98.

Ward, J.P., 2002, **Hydraulic Design of Stepped Spillways**, Doctor of Philosophy dissertation, Civil Engineering, Faculty of Engineering, Colorado State University, USA.

Water Affairs, **About the Hartbeespoort Dam** [Online], Available: http://196.3.165.92/aboutdam.aspx [Accessed on 2012, November 10].

Wilcox, D.C., 1988, "Re-assessment of the Scale-determining Equation for Advanced Turbulence Models", **AIAA Journal**, Vol. 26, No. 11, pp. 1299-1310.

Xun, S.R., Yang, C.T., Wan, R.P. and Min, X.H., 1994, "Stepped Dissipator on Spillway Face", **Proceedings of the 9th Congress of Asian and Pacific Division of the International Association for Hydraulic Research**, 24-26 August, Singapore.

Yakhot, V. and Orszag, S.A., 1986, "Renormalization Group Analysis of Turbulence: I. Basic Theory", **Journal of Scientific Computing**, Vol. 1, No. 1, pp. 1–51.

Yasuda, Y. and Ohtsu, I., 1999, "Flow Resistance of Skimming Flows in Stepped Channels. **Proceedings of the 28th IAHR Congress**, 22-27 August, Graz, Austria.

Yasuda, Y., Takahashi, M. and Ohtsu, I., 2001, "Energy Dissipation of Skimming Flows on Stepped-channel Chutes", **Proceedings of the 29th IAHR Congress**, 16-21 September, Beijing, China.

Young, M.F., 1982. "Feasibility Study of a Stepped Spillway." **Proceedings of the ASCE Hydraulics Division Specialty Conference**, 17-20 August, Jackson, Mississippi, USA, pp. 96-106.

APPENDIX A

Measurement locations on the physical model

Table A.1 Measurement locations on the smooth spillway

Discharge (m³/s)	Velocity (m/s)	$\dfrac{L_S}{L}$	Reynolds number	Depth normal to the pseudo-bottom (m)	Position	
					x	y
0.57	0.12	0.09	116245.11	0.02	-27.61	13.83
			245929.53	0.04	-27.60	13.85
			348318.37	0.05	-27.60	13.86
			452187.62	0.07	-27.59	13.87
			555520.31	0.09	-27.58	13.89
			555520.31	0.09	-27.58	13.89
			597370.20	0.09	-27.58	13.89
		0.28	191276.39	0.02	-22.04	11.05
			368903.01	0.04	-22.04	11.07
			528175.73	0.05	-22.03	11.08
			687202.87	0.07	-22.02	11.09
			813607.06	0.08	-22.02	11.10
			845532.02	0.09	-22.02	11.11
			877607.04	0.09	-22.01	11.11
		0.44	180765.18	0.02	-17.20	8.62
			430811.94	0.04	-17.19	8.64
			621170.21	0.05	-17.18	8.65
			819943.39	0.07	-17.17	8.66
			976433.81	0.08	-17.17	8.67
			1016199.54	0.09	-17.17	8.68
			1214702.68	0.10	-17.16	8.69
			1214702.68	0.10	-17.16	8.69
			1328103.82	0.11	-17.16	8.70
		0.60	216938.11	0.02	-12.31	6.18
			488389.57	0.04	-12.31	6.20
			703274.18	0.05	-12.30	6.21
			927139.42	0.07	-12.29	6.22
			1061416.01	0.08	-12.29	6.23
			1152528.05	0.09	-12.28	6.24
			1336370.00	0.10	-12.28	6.25
			1380042.66	0.10	-12.28	6.25
		0.76	259260.44	0.02	-7.43	3.74
			542892.39	0.04	-7.42	3.76
			778717.67	0.05	-7.41	3.77
			1019648.66	0.07	-7.41	3.78
			1260138.30	0.09	-7.40	3.80
			1500321.00	0.10	-7.39	3.81
			1500321.00	0.10	-7.39	3.81
			1735483.65	0.12	-7.39	3.82
			1735483.65	0.12	-7.39	3.82
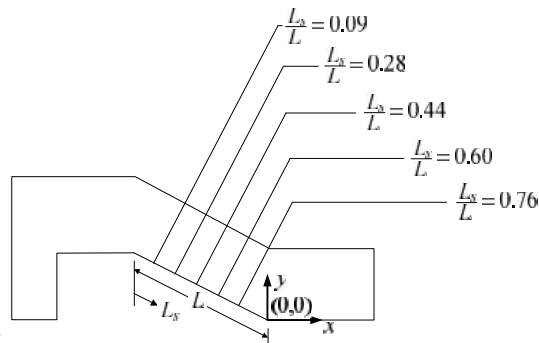
Remarks:

Table A.1 (Cont.) Measurement locations on the smooth spillway

Discharge (m³/s)	Velocity (m/s)	$\dfrac{L_S}{L}$	Reynolds number	Depth normal to the pseudo-bottom (m)	Position	
					x	y
1.13	0.24	0.09	127042.59	0.02	-27.61	13.83
			260446.97	0.04	-27.60	13.85
			370826.87	0.05	-27.59	13.86
			482997.63	0.07	-27.59	13.87
			595254.77	0.09	-27.58	13.89
			707927.29	0.10	-27.57	13.90
			819868.29	0.12	-27.57	13.91
			931964.65	0.13	-27.56	13.93
			1043492.80	0.15	-27.55	13.94
			1155231.84	0.16	-27.55	13.95
			1155231.84	0.16	-27.55	13.95
			1199744.16	0.17	-27.54	13.96
		0.28	198709.61	0.02	-22.04	11.05
			383032.13	0.04	-22.04	11.07
			548011.26	0.05	-22.03	11.08
			713252.12	0.07	-22.02	11.09
			878309.24	0.09	-22.02	11.11
			1041828.96	0.10	-22.01	11.12
			1203527.18	0.12	-22.00	11.13
			1300616.96	0.12	-22.00	11.14
			1364677.69	0.13	-22.00	11.15
		0.44	186874.59	0.02	-17.20	8.62
			444993.37	0.04	-17.19	8.64
			640208.02	0.05	-17.18	8.65
			843379.16	0.07	-17.17	8.66
			1043321.87	0.09	-17.17	8.68
			1245752.96	0.10	-17.16	8.69
			1441232.78	0.12	-17.15	8.70
			1598894.24	0.13	-17.15	8.71
			1637395.66	0.13	-17.15	8.72
			1714472.57	0.14	-17.14	8.72
		0.60	221874.16	0.02	-12.31	6.18
			499496.18	0.04	-12.31	6.20
			719261.55	0.05	-12.30	6.21
			948170.62	0.07	-12.29	6.22
			1178575.04	0.09	-12.28	6.24
			1411897.61	0.10	-12.28	6.25
			1547779.28	0.11	-12.27	6.26
			1639129.67	0.12	-12.27	6.26
			1866862.51	0.13	-12.26	6.28
		0.76	261055.10	0.02	-7.43	3.74
			547635.38	0.04	-7.42	3.76
			787896.42	0.05	-7.41	3.77
			1037314.87	0.07	-7.41	3.78
			1291826.52	0.09	-7.40	3.80
			1549959.21	0.10	-7.39	3.81
			1807039.72	0.12	-7.39	3.82
			2063694.42	0.13	-7.38	3.84
			2213912.36	0.14	-7.38	3.85
			2314456.13	0.15	-7.37	3.85
			2564543.31	0.16	-7.37	3.86

Table A.1 (Cont.) Measurement locations on the smooth spillway

Discharge (m³/s)	Velocity (m/s)	$\dfrac{L_S}{L}$	Reynolds number	Depth normal to the pseudo-bottom (m)	Position	
					x	y
1.70	0.36	0.09	129013.06	0.02	-27.61	13.83
			265303.68	0.04	-27.60	13.85
			379588.65	0.05	-27.59	13.86
			615837.18	0.09	-27.58	13.89
			857826.13	0.12	-27.57	13.91
			980217.17	0.13	-27.56	13.93
			1102671.30	0.15	-27.55	13.94
			1226020.42	0.16	-27.55	13.95
			1349199.58	0.18	-27.54	13.97
			1473115.96	0.19	-27.53	13.98
			1597035.44	0.21	-27.53	14.00
			1696814.04	0.22	-27.52	14.01
		0.28	202514.73	0.02	-22.04	11.05
			390544.84	0.04	-22.04	11.07
			559097.08	0.05	-22.03	11.08
			900865.66	0.09	-22.02	11.11
			1242420.88	0.12	-22.00	11.13
			1412804.39	0.13	-22.00	11.15
			1582862.98	0.15	-21.99	11.16
			1753220.88	0.16	-21.98	11.17
			1754997.86	0.16	-21.98	11.17
			202514.73	0.17	-21.98	11.18
		0.44	189589.99	0.02	-17.20	8.62
			451598.69	0.04	-17.19	8.64
			650242.64	0.05	-17.18	8.65
			1064325.02	0.09	-17.17	8.68
			1478447.03	0.12	-17.15	8.70
			1683923.38	0.13	-17.15	8.72
			1885536.69	0.15	-17.14	8.73
			2007097.94	0.16	-17.14	8.74
			2088004.66	0.16	-17.13	8.74
			189589.99	0.17	-17.13	8.75
		0.60	224930.94	0.02	-12.31	6.18
			506378.87	0.04	-12.31	6.20
			729175.48	0.05	-12.30	6.21
			1197888.38	0.09	-12.28	6.24
			1674166.43	0.12	-12.27	6.26
			1911332.52	0.13	-12.26	6.28
			2142095.39	0.15	-12.26	6.29
			2142095.39	0.15	-12.26	6.29
			2373404.45	0.16	-12.25	6.30
			2418942.79	0.16	-12.25	6.31
		0.76	264734.65	0.02	-7.43	3.74
			555322.44	0.04	-7.42	3.76
			798863.73	0.05	-7.41	3.77
			1051861.45	0.07	-7.41	3.78
			1310286.43	0.09	-7.40	3.80
			1573656.80	0.10	-7.39	3.81
			1837929.98	0.12	-7.39	3.82
			2102764.60	0.13	-7.38	3.84
			2362721.82	0.15	-7.37	3.85
			2622069.13	0.16	-7.37	3.86
			2774175.00	0.17	-7.36	3.87
			2875763.01	0.18	-7.36	3.88

Table A.1 (Cont.) Measurement locations on the smooth spillway

Discharge (m³/s)	Velocity (m/s)	$\dfrac{L_S}{L}$	Reynolds number	Depth normal to the pseudo-bottom (m)	Position	
					x	y
2.27	0.48	0.09	131363.92	0.02	-27.61	13.83
			270779.32	0.04	-27.60	13.85
			388879.32	0.05	-27.59	13.86
			634978.99	0.09	-27.58	13.89
			889106.72	0.12	-27.57	13.91
			1146901.93	0.15	-27.55	13.94
			1406242.47	0.18	-27.54	13.97
			1536505.00	0.19	-27.53	13.98
			1666591.17	0.21	-27.53	14.00
			1797407.34	0.22	-27.52	14.01
			1928179.92	0.24	-27.51	14.02
			2059681.89	0.25	-27.50	14.04
			2349613.28	0.29	-27.49	14.07
		0.28	206206.95	0.02	-22.04	11.05
			397607.03	0.04	-22.04	11.07
			569098.79	0.05	-22.03	11.08
			918233.16	0.09	-22.02	11.11
			1269071.99	0.12	-22.00	11.13
			1619921.78	0.15	-21.99	11.16
			1795706.95	0.16	-21.98	11.17
			1971442.13	0.18	-21.97	11.19
			2147538.81	0.19	-21.97	11.20
			2500010.44	0.22	-21.95	11.23
		0.44	192608.97	0.02	-17.20	8.62
			458699.31	0.04	-17.19	8.64
			660123.65	0.05	-17.18	8.65
			1080250.21	0.09	-17.17	8.68
			1502225.70	0.12	-17.15	8.70
			1918908.63	0.15	-17.14	8.73
			2126549.06	0.16	-17.13	8.74
			2332541.13	0.18	-17.13	8.76
			2539286.97	0.19	-17.12	8.77
			2542608.99	0.19	-17.12	8.77
			2704044.48	0.20	-17.11	8.78
		0.60	227970.41	0.02	-12.31	6.18
			513206.09	0.04	-12.31	6.20
			738963.22	0.05	-12.30	6.21
			1213335.65	0.09	-12.28	6.24
			1696080.33	0.12	-12.27	6.26
			2172687.55	0.15	-12.26	6.29
			2408976.44	0.16	-12.25	6.30
			2641895.45	0.18	-12.24	6.32
			2641895.45	0.18	-12.24	6.32
			2875348.17	0.19	-12.24	6.33
			2968134.78	0.20	-12.23	6.34
		0.76	267821.66	0.02	-7.43	3.74
			561832.66	0.04	-7.42	3.76
			808316.80	0.05	-7.41	3.77
			1064255.83	0.07	-7.41	3.78
			1325486.20	0.09	-7.40	3.80
			1591671.39	0.10	-7.39	3.81
			1858731.97	0.12	-7.39	3.82
			2126801.74	0.13	-7.38	3.84
			2390841.45	0.15	-7.37	3.85
			2654636.40	0.16	-7.37	3.86
			2913258.89	0.18	-7.36	3.88
			3171833.23	0.19	-7.35	3.89
			3325327.16	0.20	-7.35	3.90
			3427773.48	0.21	-7.35	3.91
			3683842.98	0.22	-7.34	3.92

Table A.2 Measurement locations on the 25-step spillway

Discharge (m³/s)	Velocity (m/s)	$\dfrac{il}{L\cos_{''}}$	Reynolds number	Depth normal to the pseudo-bottom (m)	Position	
					x	y
0.57	0.12	0.16	36639.70	0.02	-25.59	13.42
			407936.70	0.08	-25.57	13.48
			791119.68	0.14	-25.54	13.53
			1020654.50	0.17	-25.52	13.56
			1213617.74	0.20	-25.51	13.59
			1640756.23	0.26	-25.49	13.64
			2039038.85	0.32	-25.46	13.70
			2207925.48	0.38	-25.43	13.75
		0.31	43096.13	0.02	-20.72	10.98
			279730.50	0.05	-20.71	11.01
			481638.10	0.08	-20.70	11.04
			696020.86	0.11	-20.68	11.07
			922125.31	0.14	-20.67	11.09
			1155666.57	0.17	-20.66	11.12
			1202414.69	0.17	-20.65	11.13
			1390754.85	0.20	-20.64	11.15
			2165223.00	0.30	-20.59	11.24
		0.47	44248.43	0.02	-15.84	8.54
			328791.69	0.05	-15.83	8.58
			764042.74	0.11	-15.80	8.63
			1021797.38	0.15	-15.79	8.66
			1236081.26	0.17	-15.77	8.69
			1704972.56	0.23	-15.75	8.74
			1974347.46	0.27	-15.73	8.77
			2152204.20	0.30	-15.72	8.79
		0.63	45890.23	0.02	-10.96	6.11
			296805.10	0.05	-10.95	6.14
			509404.62	0.08	-10.94	6.17
			734688.09	0.11	-10.92	6.20
			972096.81	0.14	-10.91	6.22
			972096.81	0.14	-10.91	6.22
			1216883.67	0.17	-10.90	6.25
			1462470.33	0.20	-10.88	6.28
			2194190.31	0.30	-10.84	6.36
		0.79	45665.75	0.02	-6.09	3.67
			296692.17	0.05	-6.08	3.70
			511711.96	0.08	-6.07	3.73
			739061.97	0.11	-6.05	3.76
			809527.52	0.12	-6.05	3.76
			977533.83	0.14	-6.04	3.78
			1222313.53	0.17	-6.03	3.81
			1467130.11	0.20	-6.01	3.84
			1682703.63	0.23	-6.00	3.86
			1706556.15	0.23	-6.00	3.86

$\dfrac{il}{L\cos\theta}=0.16$

$\dfrac{il}{L\cos\theta}=0.31$

$\dfrac{il}{L\cos\theta}=0.47$

$\dfrac{il}{L\cos\theta}=0.63$

$\dfrac{il}{L\cos\theta}=0.79$

y

$(0,0)$

x
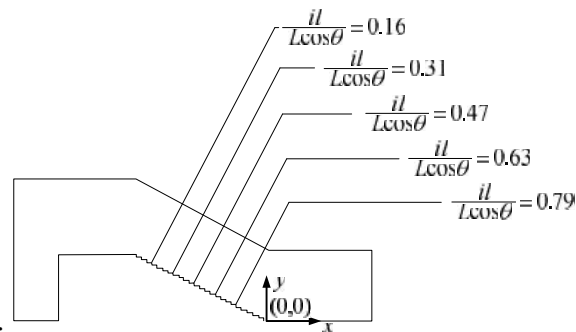
Remarks:

Table A.2 (Cont.) Measurement locations on the 25-step spillway

Discharge (m³/s)	Velocity (m/s)	$\dfrac{il}{L\cos_{''}}$	Reynolds number	Depth normal to the pseudo-bottom (m)	Position x	y
		13.4	36767.72	0.02	-25.59	13.42
			463984.09	0.08	-25.57	13.48
			915891.39	0.14	-25.54	13.53
			1391775.17	0.20	-25.51	13.59
			1689001.50	0.23	-25.50	13.62
			1891037.87	0.26	-25.49	13.64
			2406031.92	0.32	-25.46	13.70
			2431821.99	0.32	-25.46	13.70
		31.3	53400.05	0.02	-20.72	10.98
			345564.56	0.05	-20.71	11.01
			610051.87	0.08	-20.70	11.04
			886941.79	0.11	-20.68	11.07
			1174724.65	0.14	-20.67	11.09
			1470945.45	0.17	-20.66	11.12
			2089301.13	0.23	-20.63	11.17
			2408210.78	0.26	-20.62	11.20
			2730640.56	0.29	-20.60	11.23
			3843615.17	0.40	-20.55	11.33
		49.2	138568.94	0.02	-15.84	8.67
			491014.63	0.05	-15.83	8.70
			1127996.83	0.11	-15.80	8.75
			1806037.84	0.17	-15.77	8.81
			2322437.01	0.22	-15.75	8.85
			2492166.42	0.23	-15.75	8.86
			3112045.49	0.30	-15.72	8.92
			3344840.54	0.36	-15.69	8.97
1.13	0.24		3357113.56	0.36	-15.69	8.98
			3468490.65	0.42	-15.66	9.03
		67.1	60868.71	0.02	-10.96	6.11
			394375.23	0.05	-10.95	6.14
			687595.27	0.08	-10.94	6.17
			998466.13	0.11	-10.92	6.20
			1326098.54	0.14	-10.91	6.22
			1667746.42	0.17	-10.90	6.25
			2021695.73	0.20	-10.88	6.28
			2276526.82	0.22	-10.87	6.30
			2386995.48	0.23	-10.87	6.30
			2756300.30	0.26	-10.86	6.33
			3125684.38	0.29	-10.84	6.36
			3490132.21	0.32	-10.83	6.39
			3525342.40	0.32	-10.83	6.39
		85	60936.84	0.02	-6.09	3.67
			396086.08	0.05	-6.08	3.70
			694204.86	0.08	-6.07	3.73
			1009997.17	0.11	-6.05	3.76
			1342490.53	0.14	-6.04	3.78
			1688922.71	0.17	-6.03	3.81
			1867003.63	0.18	-6.02	3.82
			2047887.19	0.20	-6.01	3.84
			2418176.52	0.23	-6.00	3.86
			2792752.86	0.26	-5.99	3.89
			3167873.27	0.29	-5.97	3.92
			3354171.60	0.30	-5.96	3.93

Table A.2 (Cont.) Measurement locations on the 25-step spillway

Discharge (m³/s)	Velocity (m/s)	$\dfrac{il}{L\cos_{''}}$	Reynolds number	Depth normal to the pseudo-bottom (m)	Position x	y
1.70	0.37	0.16	38899.19	0.02	-25.59	13.42
			460123.79	0.08	-25.57	13.48
			911813.62	0.14	-25.54	13.53
			1405431.58	0.20	-25.51	13.59
			1935856.12	0.26	-25.49	13.64
			2182869.03	0.29	-25.47	13.67
			2489210.31	0.32	-25.46	13.70
			2572803.39	0.33	-25.45	13.70
			3049905.00	0.38	-25.43	13.75
		0.31	53769.62	0.02	-20.72	10.98
			350097.24	0.05	-20.71	11.01
			621034.57	0.08	-20.70	11.04
			1199285.89	0.14	-20.67	11.09
			1826186.95	0.20	-20.64	11.15
			2158283.47	0.23	-20.63	11.17
			2498655.61	0.26	-20.62	11.20
			2845601.67	0.29	-20.60	11.23
			2915579.12	0.30	-20.60	11.23
			3197100.39	0.32	-20.59	11.26
			3549716.04	0.35	-20.57	11.28
			3655804.73	0.36	-20.57	11.29
		0.47	58898.18	0.02	-15.84	8.54
			328566.96	0.04	-15.83	8.57
			671872.16	0.08	-15.82	8.60
			1309378.74	0.14	-15.79	8.65
			2016346.49	0.20	-15.76	8.71
			2781223.80	0.26	-15.74	8.76
			3417728.50	0.31	-15.71	8.81
			3578687.28	0.32	-15.71	8.82
			4383900.30	0.38	-15.68	8.87
			4704765.09	0.41	-15.67	8.89
			5180655.12	0.44	-15.65	8.93
		0.63	62222.79	0.02	-10.96	6.11
			404854.71	0.05	-10.95	6.14
			715518.00	0.08	-10.94	6.17
			1398922.27	0.14	-10.91	6.22
			2154772.93	0.20	-10.88	6.28
			2558125.44	0.23	-10.87	6.30
			2972580.29	0.26	-10.86	6.33
			3353164.54	0.29	-10.84	6.36
			3395670.12	0.29	-10.84	6.36
			3824510.00	0.32	-10.83	6.39
			4253665.36	0.35	-10.81	6.41
			4681613.70	0.38	-10.80	6.44
			4895782.94	0.40	-10.79	6.46
		0.79	66209.72	0.02	-6.09	3.67
			428274.78	0.05	-6.08	3.70
			746622.08	0.08	-6.07	3.73
			1454252.62	0.14	-6.04	3.78
			2239152.24	0.20	-6.01	3.84
			2656789.20	0.23	-6.00	3.86
			3042325.84	0.26	-5.99	3.89
			3085927.79	0.26	-5.99	3.89
			3524292.67	0.29	-5.97	3.92
			3968912.05	0.32	-5.96	3.95
			4414238.57	0.35	-5.94	3.97
			4547951.28	0.36	-5.94	3.98

Table A.2 (Cont.) Measurement locations on the 25-step spillway

Discharge (m³/s)	Velocity (m/s)	$\dfrac{il}{L\cos_{"}}$	Reynolds number	Depth normal to the pseudo-bottom (m)	Position x	y
2.27	0.49	0.16	45929.70	0.02	-25.59	13.42
			295486.53	0.05	-25.58	13.45
			510170.43	0.08	-25.57	13.48
			970754.01	0.14	-25.54	13.53
			1474680.46	0.20	-25.51	13.59
			2018525.96	0.26	-25.49	13.64
			2300200.94	0.29	-25.47	13.67
			2586604.89	0.32	-25.46	13.70
			2875157.83	0.35	-25.44	13.72
			2933448.33	0.36	-25.44	13.73
			3136400.66	0.38	-25.43	13.75
			3165568.98	0.38	-25.43	13.75
		0.31	55415.69	0.02	-20.72	10.98
			359506.88	0.05	-20.71	11.01
			627263.92	0.08	-20.70	11.04
			1210376.65	0.14	-20.67	11.09
			1852523.04	0.20	-20.64	11.15
			2546186.42	0.26	-20.62	11.20
			2905416.08	0.29	-20.60	11.23
			3270392.75	0.32	-20.59	11.26
			3563789.57	0.34	-20.58	11.28
			3637661.51	0.35	-20.57	11.28
			4006786.50	0.38	-20.56	11.31
			4376542.43	0.41	-20.55	11.34
			5116241.74	0.47	-20.52	11.39
		0.47	58722.16	0.02	-15.84	8.54
			329011.15	0.04	-15.83	8.57
			-	0.08	-15.82	8.60
			1340331.63	0.14	-15.79	8.65
			2069264.34	0.20	-15.76	8.71
			2862108.58	0.26	-15.74	8.76
			3694829.80	0.32	-15.71	8.82
			4204074.70	0.36	-15.69	8.85
			4544568.00	0.38	-15.68	8.87
			5356701.50	0.44	-15.66	8.92
			5399204.34	0.44	-15.65	8.93
			6248428.96	0.50	-15.63	8.98
2.27	0.49	0.63	-	0.02	-10.96	6.11
			421423.64	0.05	-10.95	6.14
			740814.88	0.08	-10.94	6.17
			1446077.88	0.14	-10.91	6.22
			2231940.67	0.20	-10.88	6.28
			3089192.20	0.26	-10.86	6.33
			3535932.98	0.29	-10.84	6.36
			3991314.85	0.32	-10.83	6.39
			4128230.71	0.33	-10.82	6.39
			4450692.65	0.35	-10.81	6.41
			4912995.00	0.38	-10.80	6.44
			5376274.24	0.41	-10.79	6.47
			5561754.18	0.42	-10.78	6.48
			5839484.89	0.44	-10.77	6.50
			6300979.52	0.47	-10.76	6.52
			6756529.03	0.50	-10.75	6.55
		0.79	67624.76	0.02	-6.09	3.67
			773871.96	0.08	-6.07	3.73
			1513560.60	0.14	-6.04	3.78
			2339519.83	0.20	-6.01	3.84
			3241583.05	0.26	-5.99	3.89
			4191819.91	0.32	-5.96	3.95
			4675691.44	0.35	-5.94	3.97
			5162359.50	0.38	-5.93	4.00
			6135951.66	0.44	-5.90	4.06
			6135951.66	0.44	-5.90	4.06
			7094742.73	0.50	-5.88	4.11

Table A.2 (Cont.) Measurement locations on the 25-step spillway

Discharge (m³/s)	Velocity (m/s)	$\dfrac{il}{L\cos{}_{\prime\prime}}$	Reynolds number	Depth normal to the pseudo-bottom (m)	Position	
					x	y
3.28	0.71	0.16	40581.99	0.02	-25.59	13.42
			268027.56	0.05	-25.58	13.45
			491476.28	0.08	-25.57	13.48
			991661.31	0.14	-25.54	13.53
			1542401.84	0.20	-25.51	13.59
			2136726.03	0.26	-25.49	13.64
			2445785.91	0.29	-25.47	13.67
			2760168.98	0.32	-25.46	13.70
			3076885.59	0.35	-25.44	13.72
			3394645.23	0.38	-25.43	13.75
			3712882.80	0.41	-25.42	13.78
			3967962.02	0.44	-25.41	13.80
			4031055.29	0.44	-25.40	13.81
			4348106.26	0.47	-25.39	13.83
			4662797.63	0.50	-25.38	13.86
			4757530.30	0.51	-25.37	13.87
		0.31	56348.99	0.02	-20.72	10.98
			365474.25	0.05	-20.71	11.01
			642595.36	0.08	-20.70	11.04
			1249272.48	0.14	-20.67	11.09
			1918806.07	0.20	-20.64	11.15
			2643704.14	0.26	-20.62	11.20
			3019763.33	0.29	-20.60	11.23
			3402217.22	0.32	-20.59	11.26
			3787613.96	0.35	-20.57	11.28
			4175455.20	0.38	-20.56	11.31
			4214504.35	0.38	-20.56	11.31
			4564671.08	0.41	-20.55	11.34
			4954857.76	0.44	-20.53	11.37
			5306007.17	0.47	-20.52	11.39
			5345327.89	0.47	-20.52	11.39
		0.63	65606.98	0.02	-10.96	6.11
			429064.37	0.05	-10.95	6.14
			757955.30	0.08	-10.94	6.17
			1487664.79	0.14	-10.91	6.22
			2302768.57	0.20	-10.88	6.28
			3196477.22	0.26	-10.86	6.33
			4144005.94	0.32	-10.83	6.39
			5121554.40	0.38	-10.80	6.44
			5121554.40	0.38	-10.80	6.44
			5617113.48	0.41	-10.79	6.47
			5667012.29	0.41	-10.79	6.47
			6116019.26	0.44	-10.77	6.50
			6616852.91	0.47	-10.76	6.52
			7116720.34	0.50	-10.75	6.55
			7166834.33	0.51	-10.75	6.55
		0.79	66981.02	0.02	-6.09	3.67
			436716.53	0.05	-6.08	3.70
			765131.82	0.08	-6.07	3.73
			1509336.07	0.14	-6.04	3.78
			2364007.46	0.20	-6.01	3.84
			3315213.59	0.26	-5.99	3.89
			4331613.38	0.32	-5.96	3.95
			5384482.50	0.38	-5.93	4.00
			5812517.41	0.41	-5.92	4.02
			5919304.39	0.41	-5.92	4.03
			6458228.89	0.44	-5.90	4.06
			6999482.06	0.47	-5.89	4.08
			7214813.51	0.48	-5.88	4.09
			7539223.43	0.50	-5.88	4.11
			8079409.80	0.53	-5.86	4.14

Table A.3 Measurement locations on the 50-step spillway

Discharge (m³/s)	Velocity (m/s)	$\dfrac{il}{L\cos_{"}}$	Reynolds number	Depth normal to the pseudo-bottom (m)	Position x	y
0.6	0.13	0.16	35698.94	0.02	-26.20	13.42
			238319.16	0.05	-26.19	13.45
			425626.53	0.08	-26.18	13.48
			623997.99	0.11	-26.16	13.51
			623997.99	0.11	-26.16	13.51
			833338.90	0.14	-26.15	13.53
			1051620.81	0.17	-26.14	13.56
			1276415.84	0.20	-26.12	13.59
			1457708.26	0.22	-26.11	13.61
		0.31	38901.62	0.02	-21.33	10.98
			259523.64	0.05	-21.32	11.01
			467852.00	0.08	-21.31	11.04
			671309.44	0.10	-21.29	11.06
			694752.43	0.11	-21.29	11.07
			937665.54	0.14	-21.28	11.09
			1192451.82	0.17	-21.27	11.12
			1192451.82	0.17	-21.27	11.12
			1454541.57	0.20	-21.25	11.15
		0.47	40837.41	0.02	-16.45	8.54
			273582.08	0.05	-16.44	8.57
			493557.31	0.08	-16.43	8.60
			727690.95	0.11	-16.41	8.63
			975258.35	0.14	-16.40	8.65
			1026151.32	0.14	-16.40	8.66
			1233288.92	0.17	-16.39	8.68
			1498133.91	0.20	-16.37	8.71
			1577175.41	0.21	-16.37	8.72
		0.63	40763.04	0.02	-11.57	6.11
			273525.39	0.05	-11.56	6.14
			493151.16	0.08	-11.55	6.17
			728149.67	0.11	-11.53	6.20
			977245.80	0.14	-11.52	6.22
			1002714.34	0.14	-11.52	6.23
			1236712.13	0.17	-11.51	6.25
			1501630.73	0.20	-11.49	6.28
			1528144.55	0.20	-11.49	6.28
		0.79	41001.24	0.02	-6.70	3.67
			274853.10	0.05	-6.69	3.70
			494182.91	0.08	-6.68	3.73
			728635.07	0.11	-6.66	3.76
			977167.62	0.14	-6.65	3.78
			1002579.74	0.14	-6.65	3.79
			1236170.65	0.17	-6.64	3.81
			1500895.70	0.20	-6.62	3.84
			1553583.43	0.20	-6.62	3.84

$$\frac{il}{L\cos\theta} = 0.16$$

$$\frac{il}{L\cos\theta} = 0.31$$

$$\frac{il}{L\cos\theta} = 0.47$$

$$\frac{il}{L\cos\theta} = 0.63$$

$$\frac{il}{L\cos\theta} = 0.79$$
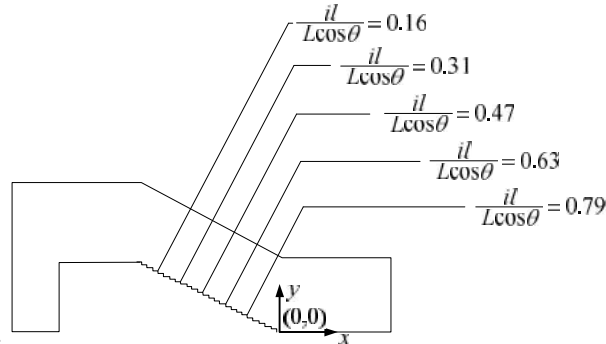
Remarks:

Table A.3 (Cont.) Measurement locations on the 50-step spillway

Discharge (m³/s)	Velocity (m/s)	$\dfrac{il}{L\cos_{\,''}}$	Reynolds number	Depth normal to the pseudo-bottom (m)	Position x	y
1.16	0.25	0.16	36833.40	0.02	-26.20	13.42
			245723.51	0.05	-26.19	13.45
			440047.38	0.08	-26.18	13.48
			878110.66	0.14	-26.15	13.53
			1367307.35	0.20	-26.12	13.59
			1519725.18	0.22	-26.11	13.60
			1882358.69	0.26	-26.10	13.64
			1960661.11	0.27	-26.09	13.65
			2142778.75	0.29	-26.08	13.67
		0.31	41780.46	0.02	-21.33	10.98
			279704.90	0.05	-21.32	11.01
			509749.81	0.08	-21.31	11.04
			764150.97	0.11	-21.29	11.07
			1040575.31	0.14	-21.28	11.09
			1612740.20	0.20	-21.25	11.14
			1644261.28	0.20	-21.25	11.15
			1963555.13	0.23	-21.24	11.17
			2223630.70	0.25	-21.23	11.20
			2289039.16	0.26	-21.23	11.20
		0.47	43860.57	0.02	-16.45	8.54
			295904.87	0.05	-16.44	8.57
			539745.17	0.08	-16.43	8.60
			1107406.52	0.14	-16.40	8.65
			1758473.50	0.20	-16.37	8.71
			2103444.61	0.23	-16.36	8.73
			2349308.42	0.25	-16.35	8.75
			2455008.40	0.26	-16.35	8.76
			2809093.95	0.29	-16.33	8.79
			2879775.18	0.30	-16.33	8.79
		0.63	48095.76	0.02	-11.57	6.11
			318623.14	0.05	-11.56	6.14
			570392.05	0.08	-11.55	6.17
			1152122.05	0.14	-11.52	6.22
			1817400.33	0.20	-11.49	6.28
			2276598.50	0.24	-11.47	6.31
			2525848.64	0.26	-11.47	6.33
			2884949.98	0.29	-11.45	6.36
			3064032.48	0.30	-11.44	6.37
		0.79	50158.35	0.02	-6.70	3.67
			331420.17	0.05	-6.69	3.70
			586696.57	0.08	-6.68	3.73
			1175284.26	0.14	-6.65	3.78
			1847758.26	0.20	-6.62	3.84
			2202787.31	0.23	-6.61	3.86
			2202787.31	0.23	-6.61	3.86
			2563648.42	0.26	-6.60	3.89
			2890132.50	0.29	-6.58	3.92
			2926090.67	0.29	-6.58	3.92

Table A.3 (Cont.) Measurement locations on the 50-step spillway

Discharge (m³/s)	Velocity (m/s)	$\dfrac{il}{L\cos_{''}}$	Reynolds number	Depth normal to the pseudo-bottom (m)	Position	
					x	y
1.70	0.37	0.16	37403.38	0.02	-26.20	13.42
			249053.30	0.05	-26.19	13.45
			447430.40	0.08	-26.18	13.48
			897635.39	0.14	-26.15	13.53
			1405546.49	0.20	-26.12	13.59
			1946566.49	0.26	-26.10	13.64
			2001659.82	0.27	-26.09	13.65
			2501419.84	0.32	-26.07	13.70
		0.31	43750.53	0.02	-21.33	10.98
			292193.78	0.05	-21.32	11.01
			529723.35	0.08	-21.31	11.04
			1081697.25	0.14	-21.28	11.09
			1716612.72	0.20	-21.25	11.15
			2401373.66	0.26	-21.23	11.20
			2577628.68	0.27	-21.22	11.22
			3109278.21	0.32	-21.20	11.26
			3466628.78	0.35	-21.18	11.28
		0.47	46897.59	0.02	-16.45	8.54
			315663.68	0.05	-16.44	8.57
			573242.69	0.08	-16.43	8.60
			1175380.28	0.14	-16.40	8.65
			1875368.26	0.20	-16.37	8.71
			2637874.84	0.26	-16.35	8.76
			3392194.79	0.32	-16.32	8.81
			3431756.92	0.32	-16.32	8.82
			3833461.98	0.35	-16.30	8.84
			4114028.86	0.37	-16.29	8.86
			4234891.20	0.38	-16.29	8.87
		0.63	52313.89	0.02	-11.57	6.11
			348069.10	0.05	-11.56	6.14
			620905.03	0.08	-11.55	6.17
			1256969.90	0.14	-11.52	6.22
			1994474.04	0.20	-11.49	6.28
			2794747.78	0.26	-11.47	6.33
			3249528.88	0.29	-11.45	6.36
			3627685.40	0.32	-11.44	6.39
			4048120.43	0.35	-11.42	6.41
			4090569.62	0.35	-11.42	6.42
		0.79	53252.37	0.02	-6.70	3.67
			354268.74	0.05	-6.69	3.70
			633625.10	0.08	-6.68	3.73
			1284388.19	0.14	-6.65	3.78
			2038298.18	0.20	-6.62	3.84
			2858015.11	0.26	-6.60	3.89
			3282017.82	0.29	-6.58	3.92
			3712560.01	0.32	-6.57	3.95
			4143987.65	0.35	-6.55	3.97
			4274031.18	0.36	-6.55	3.98
			4574743.20	0.38	-6.54	4.00

Table A.3 (Cont.) Measurement locations on the 50-step spillway

Discharge (m³/s)	Velocity (m/s)	$\dfrac{il}{L\cos_{"}}$	Reynolds number	Depth normal to the pseudo-bottom (m)	Position x	y
2.27	0.49	0.16	39086.64	0.02	-26.20	13.42
			261123.38	0.05	-26.19	13.45
			471510.36	0.08	-26.18	13.48
			936429.72	0.14	-26.15	13.53
			1458918.04	0.20	-26.12	13.59
			2018852.40	0.26	-26.10	13.64
			2596222.09	0.32	-26.07	13.70
			2712169.29	0.33	-26.06	13.71
			3179715.51	0.38	-26.04	13.75
			3355664.27	0.40	-26.03	13.77
			3472348.05	0.41	-26.03	13.78
		0.31	44704.10	0.02	-21.33	10.98
			300906.18	0.05	-21.32	11.01
			547273.73	0.08	-21.31	11.04
			1114606.05	0.14	-21.28	11.09
			1764690.50	0.20	-21.25	11.15
			2467871.72	0.26	-21.23	11.20
			3088475.06	0.31	-21.20	11.25
			3199203.05	0.32	-21.20	11.26
			3570642.08	0.35	-21.18	11.28
			3756720.96	0.37	-21.18	11.30
			3943654.80	0.38	-21.17	11.31
		0.47	47514.21	0.02	-16.45	8.54
			320131.44	0.05	-16.44	8.57
			582753.22	0.08	-16.43	8.60
			1201465.36	0.14	-16.40	8.65
			1924638.72	0.20	-16.37	8.71
			2717852.83	0.26	-16.35	8.76
			3551611.90	0.32	-16.32	8.82
			3977280.34	0.35	-16.30	8.84
			4191060.96	0.37	-16.30	8.86
			4405960.20	0.38	-16.29	8.87
			4837482.32	0.41	-16.28	8.90
			4837482.32	0.41	-16.28	8.90
		0.63	53247.04	0.02	-11.57	6.11
			354600.66	0.05	-11.56	6.14
			637063.24	0.08	-11.55	6.17
			1298168.65	0.14	-11.52	6.22
			2069581.33	0.20	-11.49	6.28
			2915712.23	0.26	-11.47	6.33
			3808315.98	0.32	-11.44	6.39
			4218727.05	0.35	-11.43	6.41
			4218727.05	0.35	-11.43	6.41
			4725428.70	0.38	-11.41	6.44
			5142894.06	0.41	-11.40	6.47
		0.79	53923.69	0.02	-6.70	3.67
			360807.15	0.05	-6.69	3.70
			649416.02	0.08	-6.68	3.73
			1331871.61	0.14	-6.65	3.78
			2132940.11	0.20	-6.62	3.84
			3013955.36	0.26	-6.60	3.89
			3945229.09	0.32	-6.57	3.95
			4325724.34	0.34	-6.56	3.97
			4421774.75	0.35	-6.55	3.97
			4902708.00	0.38	-6.54	4.00
			5338328.77	0.41	-6.53	4.03

Table A.3 (Cont.) Measurement locations on the 50-step spillway

Discharge (m³/s)	Velocity (m/s)	$\dfrac{il}{L\cos{}_{_n}}$	Reynolds number	Depth normal to the pseudo-bottom (m)	Position	
					x	y
		0.16	39915.69	0.02	-26.20	13.42
			266385.29	0.05	-26.19	13.45
			475491.81	0.08	-26.18	13.48
			950132.01	0.14	-26.15	13.53
			1489202.66	0.20	-26.12	13.59
			2069064.70	0.26	-26.10	13.64
			2669037.59	0.32	-26.07	13.70
			3277632.51	0.38	-26.04	13.75
			3339109.45	0.39	-26.04	13.76
			3889871.16	0.44	-26.01	13.81
			4011819.81	0.45	-26.01	13.82
			4195531.77	0.47	-26.00	13.83
		0.31	45681.90	0.02	-21.33	10.98
			305624.94	0.05	-21.32	11.01
			550464.99	0.08	-21.31	11.04
			1122754.73	0.14	-21.28	11.09
			1785867.55	0.20	-21.25	11.15
			2506723.36	0.26	-21.23	11.20
			3258583.27	0.32	-21.20	11.26
			3334414.46	0.33	-21.20	11.26
			4025226.90	0.38	-21.17	11.31
			4411806.26	0.41	-21.16	11.34
			4799773.99	0.44	-21.14	11.37
2.83	0.61	0.47	49084.23	0.02	-16.45	8.54
			329683.72	0.05	-16.44	8.57
			596489.79	0.08	-16.43	8.60
			1225601.41	0.14	-16.40	8.65
			1962507.38	0.20	-16.37	8.71
			2772881.42	0.26	-16.35	8.76
			3627077.33	0.32	-16.32	8.82
			4506391.80	0.38	-16.29	8.87
			4640645.84	0.39	-16.29	8.88
			4952490.98	0.41	-16.28	8.90
			5312397.60	0.44	-16.27	8.92
			5401723.51	0.44	-16.26	8.93
		0.63	53801.62	0.02	-11.57	6.11
			358004.97	0.05	-11.56	6.14
			643966.20	0.08	-11.55	6.17
			1317168.05	0.14	-11.52	6.22
			2107184.51	0.20	-11.49	6.28
			2978228.23	0.26	-11.47	6.33
			3902823.79	0.32	-11.44	6.39
			4860378.90	0.38	-11.41	6.44
			4860378.90	0.38	-11.41	6.44
			5104958.04	0.40	-11.40	6.46
			5838512.58	0.44	-11.38	6.50
			6034226.79	0.45	-11.38	6.51
		0.79	55676.75	0.02	-6.70	3.67
			370662.10	0.05	-6.69	3.70
			665933.14	0.08	-6.68	3.73
			1365167.20	0.14	-6.65	3.78
			2190573.22	0.20	-6.62	3.84
			3105073.80	0.26	-6.60	3.89
			4079485.87	0.32	-6.57	3.95
			5091150.60	0.38	-6.54	4.00
			5400969.13	0.40	-6.53	4.02
			5606661.89	0.41	-6.53	4.03
			6125609.80	0.44	-6.51	4.06
			6332513.83	0.45	-6.51	4.07

APPENDIX B

Comparison of velocity from the physical model and
various grid sizes of numerical model

Table B.1 Comparison of velocity from the physical model and various grid sizes of numerical model on the smooth spillway

Discharge (m³/s)	$\dfrac{L_S}{L}$	Depth normal to the pseudo-bottom (m)	Velocity from physical model (m/s)	Velocity (m/s) from various grid sizes of numerical model (m²)		
				0.035x0.035	0.050x0.050	0.100x0.100
0.57	0.09	0.02	7.02	4.77	6.18	1.75
		0.04	7.37	6.21	6.43	2.85
		0.05	7.48	6.35	6.51	3.96
		0.07	6.15	6.45	6.56	5.06
		0.09	7.07	6.51	6.58	6.16
		0.09	7.14	6.51	6.58	6.16
		0.09	-	6.53	6.59	6.46
	0.28	0.02	7.97	7.84	9.11	2.94
		0.04	8.56	9.31	9.61	4.59
		0.05	7.22	9.63	9.87	6.25
		0.07	5.28	9.80	9.95	7.91
		0.08	8.89	9.89	9.97	9.23
		0.09	10.73	9.91	9.98	9.56
		0.09	-	9.93	9.98	9.72
	0.44	0.02	8.40	7.41	10.45	2.82
		0.04	9.55	10.87	11.14	4.79
		0.05	10.95	11.32	11.58	6.78
		0.07	11.94	11.70	11.89	8.76
		0.08	13.64	11.86	12.04	10.35
		0.09	13.96	11.91	12.06	10.74
		0.10	8.74	12.08	12.13	11.41
		0.10	5.17	12.08	12.13	11.41
		0.11	-	12.10	12.15	11.18
	0.6	0.02	8.49	8.90	11.85	3.37
		0.04	9.48	12.33	12.58	5.59
		0.05	10.28	12.82	13.05	7.83
		0.07	12.18	13.23	13.39	10.06
		0.08	12.12	13.39	13.56	11.40
		0.09	12.06	13.50	13.65	12.28
		0.10	9.63	13.70	13.82	12.91
		0.10	8.37	13.72	13.85	12.84
	0.76	0.02	8.74	10.63	13.12	3.94
		0.04	9.34	13.70	13.86	6.35
		0.05	10.43	14.19	14.34	8.77
		0.07	11.03	14.54	14.70	11.19
		0.09	10.44	14.77	14.99	13.61
		0.10	9.64	14.92	15.23	13.92
		0.10	9.61	14.92	15.23	13.92
		0.12	6.70	14.98	15.40	13.57
		0.12	-	14.98	15.40	13.57

$\frac{L_x}{L}=0.09$

$\frac{L_x}{L}=0.28$

$\frac{L_x}{L}=0.44$

$\frac{L_x}{L}=0.60$

$\frac{L_x}{L}=0.76$

L_S L y $(0,0)$ x
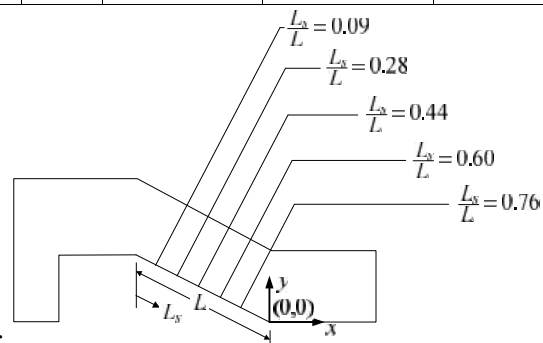
Remarks:

Table B.1 (Cont.) Comparison of velocity from the physical model and various grid
sizes of numerical model on the smooth spillway

Discharge (m³/s)	$\frac{L_S}{L}$	Depth normal to the pseudo-bottom (m)	Velocity from physical model (m/s)	Velocity (m/s) from various grid sizes of numerical model (m²)		
				0.035x0.035	0.050x0.050	0.100x0.100
1.13	0.09	0.02	7.31	5.21	6.52	1.93
		0.04	7.88	6.57	6.76	3.10
		0.05	7.98	6.76	6.89	4.27
		0.07	8.19	6.89	6.98	5.45
		0.09	8.17	6.97	7.04	6.62
		0.10	8.20	7.04	7.08	6.92
		0.12	8.20	7.08	7.11	6.98
		0.13	7.74	7.11	7.14	7.05
		0.15	-	7.13	7.17	7.11
		0.16	8.27	7.15	7.19	7.18
		0.16	8.57	7.15	7.19	7.18
		0.17	-	7.16	7.20	7.20
	0.28	0.02	8.94	8.15	9.27	3.06
		0.04	9.86	9.67	9.76	4.78
		0.05	10.49	9.99	10.01	6.52
		0.07	10.82	10.17	10.11	8.25
		0.09	10.77	10.29	10.16	9.97
		0.10	12.87	10.36	10.20	10.19
		0.12	12.43	10.39	10.24	10.25
		0.12	11.91	10.41	10.26	10.29
		0.13	10.96	10.41	10.27	10.32
	0.44	0.02	9.31	7.66	10.71	2.93
		0.04	10.43	11.23	11.41	4.98
		0.05	11.09	11.67	11.85	7.05
		0.07	11.52	12.03	12.16	9.11
		0.09	11.77	12.22	12.35	11.16
		0.10	11.72	12.39	12.45	12.12
		0.12	11.35	12.44	12.50	12.20
		0.13	13.99	12.49	12.53	12.27
		0.13	15.25	12.49	12.53	12.28
		0.14	-	12.50	12.54	12.31
	0.6	0.02	10.27	9.10	12.16	3.52
		0.04	11.31	12.61	12.90	5.84
		0.05	11.67	13.11	13.37	8.18
		0.07	12.12	13.53	13.73	10.51
		0.09	12.42	13.81	13.98	12.84
		0.10	13.04	14.04	14.17	13.74
		0.11	15.05	14.11	14.24	13.79
		0.12	16.36	14.15	14.28	13.83
		0.13	-	14.24	14.33	13.93
	0.76	0.02	9.85	10.71	13.40	4.17
		0.04	11.27	13.82	14.15	6.72
		0.05	11.80	14.36	14.64	9.29
		0.07	12.22	14.80	15.02	11.85
		0.09	12.78	15.14	15.31	14.41
		0.10	12.82	15.41	15.54	15.11
		0.12	12.82	15.60	15.73	15.22
		0.13	14.85	15.75	15.85	15.33
		0.14	14.13	15.79	15.90	15.40
		0.15	13.37	15.82	15.92	15.44
		0.16	14.64	15.88	15.96	15.55

Table B.1 (Cont.) Comparison of velocity from the physical model and various grid sizes of numerical model on the smooth spillway

Discharge (m³/s)	$\dfrac{L_S}{L}$	Depth normal to the pseudo-bottom (m)	Velocity from physical model (m/s)	Velocity (m/s) from various grid sizes of numerical model (m²)		
				0.035x0.035	0.050x0.050	0.100x0.100
1.70	0.09	0.02	7.79	5.29	6.90	2.02
		0.04	7.96	6.70	7.14	3.23
		0.05	8.10	6.92	7.29	4.46
		0.09	8.39	7.22	7.50	6.90
		0.12	8.52	7.41	7.63	7.32
		0.13	8.42	7.48	7.67	7.40
		0.15	8.48	7.54	7.71	7.49
		0.16	8.42	7.59	7.74	7.58
		0.18	-	7.63	7.76	7.67
		0.19	-	7.67	7.78	7.71
	0.28	0.02	8.84	8.31	-	3.15
		0.04	9.72	9.86	10.31	4.92
		0.05	10.31	10.19	10.58	6.70
		0.09	11.09	10.56	10.78	10.26
		0.12	11.46	10.73	10.86	10.57
		0.13	11.54	10.78	10.89	10.64
		0.15	10.49	10.82	10.91	10.71
		0.16	11.34	10.85	10.93	10.79
		0.16	11.38	10.86	10.93	10.79
		0.17	-	-	-	10.82
	0.44	0.02	9.57	7.78	11.04	2.99
		0.04	10.61	11.40	11.76	5.09
		0.05	11.38	11.85	12.14	7.20
		0.09	12.84	12.47	12.73	11.40
		0.12	13.09	12.76	12.90	12.48
		0.13	12.93	12.85	12.94	12.58
		0.15	12.41	12.89	12.96	12.67
		0.16	12.98	12.91	12.98	12.73
		0.16	13.36	12.93	12.98	12.76
		0.17	-	-	12.99	12.80
	0.6	0.02	10.60	9.22	12.39	3.58
		0.04	12.06	12.78	13.15	5.94
		0.05	12.67	13.29	13.63	8.31
		0.09	13.16	14.04	14.26	13.05
		0.12	12.66	14.45	14.60	14.09
		0.13	12.23	14.58	14.68	14.21
		0.15	13.34	14.64	14.72	14.33
		0.15	13.46	14.64	14.74	14.33
		0.16	12.11	14.69	14.75	14.45
		0.16	-	14.70	14.75	14.48
	0.76	0.02	10.82	10.86	13.62	4.22
		0.04	11.73	14.01	14.37	6.81
		0.05	12.27	14.56	14.87	9.41
		0.07	12.84	15.00	15.25	12.01
		0.09	13.26	15.35	15.54	14.60
		0.10	13.60	15.65	15.78	15.34
		0.12	13.85	15.87	15.98	15.48
		0.13	14.10	16.04	16.12	15.63
		0.15	14.29	16.15	16.22	15.78
		0.16	14.40	16.23	16.27	15.93
		0.17	15.94	16.25	16.29	16.02
		0.18	16.82	16.27	16.30	16.08
		0.19	-	16.29	16.31	16.11

Table B.1 (Cont.) Comparison of velocity from the physical model and various grid sizes of numerical model on the smooth spillway

Discharge (m³/s)	$\dfrac{L_S}{L}$	Depth normal to the pseudo-bottom (m)	Velocity from physical model (m/s)	Velocity (m/s) from various grid sizes of numerical model (m²)		
				0.035x0.035	0.050x0.050	0.100x0.100
2.27	0.09	0.02	7.28	5.39	6.78	2.08
		0.04	8.28	6.83	7.05	3.33
		0.05	8.08	7.09	7.28	4.59
		0.09	8.54	7.44	7.65	7.10
		0.12	8.63	7.68	7.89	7.56
		0.15	8.68	7.84	8.02	7.77
		0.18	8.78	7.95	8.12	7.99
		0.19	8.74	8.00	8.16	8.04
		0.21	8.70	8.04	8.20	8.08
		0.22	8.20	8.08	8.23	8.13
		0.24	6.77	8.11	8.26	8.17
		0.25	4.19	8.14	8.29	8.22
		0.29	-	8.20	8.35	8.28
	0.28	0.02	8.67	8.46	9.90	3.21
		0.04	9.91	10.03	10.38	5.02
		0.05	10.26	10.37	10.65	6.84
		0.09	11.23	10.76	10.91	10.47
		0.12	11.44	10.96	11.05	10.80
		0.15	11.72	11.07	11.15	10.97
		0.16	11.49	11.12	11.20	11.05
		0.18	12.62	11.15	11.23	11.13
		0.19	12.90	11.18	11.26	11.17
		0.22	12.52	11.24	11.32	11.23
	0.44	0.02	9.51	7.90	11.15	3.04
		0.04	10.70	11.58	11.87	5.17
		0.05	11.59	12.03	12.32	7.32
		0.09	12.96	12.66	12.83	11.59
		0.12	13.24	12.97	13.04	12.70
		0.15	13.09	13.12	13.15	12.90
		0.16	12.02	13.16	13.19	13.00
		0.18	10.72	13.19	13.22	13.10
		0.19	10.19	13.22	13.25	13.16
		0.19	10.17	13.24	13.25	13.16
		0.20	-	13.24	13.28	13.18
	0.6	0.02	10.44	9.35	12.44	3.63
		0.04	12.13	12.95	13.19	6.02
		0.05	12.98	13.47	13.67	8.43
		0.09	14.12	14.22	14.29	13.23
		0.12	14.15	14.64	14.64	14.29
		0.15	12.98	14.85	14.80	14.54
		0.16	12.53	14.91	14.85	14.67
		0.18	11.35	14.94	14.90	14.80
		0.18	11.33	14.94	14.90	14.80
		0.19	7.68	14.97	14.93	14.85
		0.20	-	14.98	14.95	14.87
	0.76	0.02	10.70	10.98	13.53	4.27
		0.04	12.03	14.18	14.28	6.89
		0.05	13.26	14.73	14.77	9.52
		0.07	13.72	15.18	15.15	12.14
		0.09	14.01	15.53	15.44	14.76
		0.10	14.79	15.82	15.68	15.51
		0.12	14.90	16.05	15.87	15.67
		0.13	14.90	16.23	16.03	15.82
		0.15	14.81	16.34	16.15	15.98
		0.16	14.54	16.43	16.23	16.13
		0.18	14.03	16.48	16.30	16.29
		0.19	14.72	16.52	16.36	16.35
		0.20	14.30	16.53	16.39	16.37
		0.21	13.82	16.54	16.41	16.39
		0.22	-	16.56	16.46	16.44

Table B.2 Comparison of velocity from the physical model and various grid sizes of numerical model on the 25-step spillway

Discharge (m³/s)	$\dfrac{iL}{L\cos_n}$	Depth normal to the pseudo-bottom (m)	Velocity from physical model (m/s)	Velocity (m/s) from various grid sizes of numerical model (m²)			
				0.020x0.020	0.035x0.035	0.050x0.050	0.100x0.100
0.57	0.16	0.02	3.26	3.73	2.40	1.75	0.84
		0.08	3.79	5.49	5.35	5.34	3.69
		0.14	4.52	6.12	5.77	5.64	5.74
		0.17	6.69	6.40	5.98	5.78	6.12
		0.20	6.69	6.58	6.13	5.88	6.25
		0.26	6.69	6.82	6.33	6.03	6.44
		0.32	6.69	6.74	6.37	6.06	6.42
		0.38	6.69	5.32	5.80	5.81	6.13
	0.31	0.02	11.08	4.84	2.83	1.93	1.13
		0.05	4.54	6.78	6.12	4.97	3.16
		0.08	5.01	7.13	6.32	5.90	4.90
		0.11	5.23	7.39	6.52	6.05	6.28
		0.14	6.60	7.62	6.72	6.19	6.54
		0.17	6.11	7.81	6.89	6.32	6.78
		0.17	6.43	7.85	6.92	6.34	6.82
		0.20	6.43	7.97	7.02	6.42	6.99
		0.30	6.43	7.06	7.10	6.55	7.20
	0.47	0.02	4.06	4.75	2.90	1.96	1.43
		0.05	4.42	6.75	6.35	5.51	4.38
		0.11	5.69	7.71	6.77	6.18	6.68
		0.15	7.23	8.14	6.98	6.33	7.04
		0.17	7.23	8.41	7.11	6.45	7.26
		0.23	7.23	8.64	7.26	6.61	7.50
		0.27	7.23	8.51	7.28	6.65	7.51
		0.30	-	8.02	7.28	6.66	7.49
	0.63	0.02	3.36	4.83	3.01	1.90	1.41
		0.05	4.51	6.74	6.49	4.87	3.88
		0.08	5.22	7.14	6.69	5.79	5.90
		0.11	5.56	7.55	6.89	5.95	6.61
		0.14	6.73	7.91	7.09	6.09	6.90
		0.14	6.73	7.91	7.09	6.09	6.90
		0.17	6.73	8.16	7.26	6.21	7.16
		0.20	6.73	8.29	7.38	6.31	7.29
		0.30	6.73	8.16	7.42	6.45	7.40
	0.79	0.02	4.86	5.39	3.00	1.90	1.31
		0.05	5.28	7.44	6.49	4.88	3.63
		0.08	5.59	7.69	6.72	5.79	5.57
		0.11	7.15	7.92	6.93	5.94	6.45
		0.12	7.46	7.98	6.99	5.98	6.54
		0.14	7.46	8.12	7.13	6.07	6.74
		0.17	7.46	8.28	7.29	6.20	6.99
		0.20	7.46	8.38	7.41	6.29	7.14
		0.23	7.46	8.39	7.46	6.36	7.21
		0.23	-	8.39	7.47	6.37	7.22

$$\frac{il}{L\cos\theta} = 0.16$$
$$\frac{il}{L\cos\theta} = 0.31$$
$$\frac{il}{L\cos\theta} = 0.47$$
$$\frac{il}{L\cos\theta} = 0.63$$
$$\frac{il}{L\cos\theta} = 0.79$$

Remarks:

Table B.2 (Cont.) Comparison of velocity from the physical model and various grid sizes of numerical model on the 25-step spillway

Discharge (m³/s)	$\dfrac{iL}{L\cos_n}$	Depth normal to the pseudo-bottom (m)	Velocity from physical model (m/s)	Velocity (m/s) from various grid sizes of numerical model (m²)			
				0.020x0.020	0.035x0.035	0.050x0.050	0.100x0.100
1.13	0.16	0.02	4.54	3.89	2.41	1.86	0.86
		0.08	4.75	5.68	6.09	5.70	3.82
		0.14	4.81	6.39	6.68	6.10	6.00
		0.20	5.06	6.95	7.02	6.51	6.71
		0.23	5.75	7.20	7.20	6.74	6.98
		0.26	5.75	7.34	7.30	6.87	7.13
		0.32	5.75	7.59	7.52	7.15	7.42
		0.32	5.75	7.60	7.53	7.17	7.43
	0.31	0.02	7.50	4.78	3.50	2.08	1.21
		0.05	5.32	6.63	7.56	5.36	3.40
		0.08	5.65	7.07	8.01	6.43	5.29
		0.11	6.26	7.50	8.31	6.69	6.82
		0.14	6.31	7.91	8.56	6.96	7.28
		0.17	6.66	8.31	8.77	7.21	7.72
		0.23	7.95	8.99	9.14	7.72	8.47
		0.26	7.95	9.27	9.30	7.94	8.74
		0.29	7.95	9.49	9.43	8.14	8.99
		0.40	7.95	9.94	9.70	8.62	9.44
	0.47	0.02	7.95	8.90	9.09	6.95	7.50
		0.05	6.14	9.39	9.48	7.36	8.14
		0.11	6.57	10.05	10.00	7.99	9.11
		0.17	7.92	10.50	10.40	8.47	9.78
		0.22	9.84	10.71	10.58	8.76	10.08
		0.23	9.84	10.75	10.62	8.83	10.14
		0.30	9.84	10.45	10.53	9.02	10.24
		0.36	9.84	8.87	9.38	9.08	10.05
		0.36	9.84	8.74	9.26	9.07	9.99
		0.42		7.71	8.31	8.79	9.14
	0.63	0.02	5.71	5.83	3.99	2.19	1.62
		0.05	6.19	8.35	8.63	5.65	4.46
		0.08	6.78	8.92	9.02	6.78	6.81
		0.11	7.22	9.37	9.36	7.06	7.76
		0.14	7.46	9.80	9.67	7.35	8.26
		0.17	7.57	10.20	9.95	7.63	8.74
		0.20	9.79	10.56	10.20	7.91	9.15
		0.22	9.26	10.78	10.37	8.09	9.40
		0.23	9.26	10.87	10.44	8.17	9.51
		0.26	9.26	11.12	10.64	8.39	9.82
		0.29	9.26	11.32	10.79	8.60	10.02
		0.32	9.26	11.46	10.91	8.76	10.19
		0.32	9.26	11.47	10.91	8.78	10.21
	0.79	0.02	7.01	5.27	4.00	2.23	1.53
		0.05	7.36	7.37	8.66	5.74	4.25
		0.08	8.02	7.99	9.11	6.86	6.55
		0.11	8.75	8.66	9.47	7.12	7.70
		0.14	9.94	9.31	9.79	7.39	8.21
		0.17	10.41	9.89	10.07	7.66	8.70
		0.18	11.22	10.16	10.21	7.79	8.92
		0.20	11.22	10.40	10.34	7.92	9.12
		0.23	11.22	10.84	10.58	8.17	9.46
		0.26	11.22	11.19	10.78	8.39	9.78
		0.29	11.22	11.46	10.94	8.58	9.99
		0.30	11.22	11.56	11.00	8.67	10.07

Table B.2 (Cont.) Comparison of velocity from the physical model and various grid sizes of numerical model on the 25-step spillway

Discharge (m³/s)	$\dfrac{iL}{L\cos_n}$	Depth normal to the pseudo-bottom (m)	Velocity from physical model (m/s)	Velocity (m/s) from various grid sizes of numerical model (m²)			
				0.020x0.020	0.035x0.035	0.050x0.050	0.100x0.100
1.70	0.16	0.02	6.18	4.04	2.55	1.93	0.90
		0.08	6.30	5.87	6.04	5.91	3.99
		0.14	6.80	6.58	6.65	6.35	6.26
		0.20	6.44	7.19	7.09	6.79	6.99
		0.26	6.44	7.65	7.47	7.19	7.42
		0.29	6.44	7.81	7.62	7.35	7.60
		0.32	6.44	7.96	7.78	7.52	7.74
		0.33	6.44	8.00	7.82	7.56	7.78
		0.38	-	8.17	8.01	7.78	-
	0.31	0.02	2.80	5.95	3.53	2.32	1.23
		0.05	6.07	8.17	7.66	5.98	3.46
		0.08	6.54	8.44	8.15	7.15	5.40
		0.14	6.61	9.00	8.74	7.69	7.45
		0.20	7.58	9.58	9.22	8.23	8.39
		0.23	7.81	9.83	9.44	8.49	8.77
		0.26	8.32	10.04	9.64	8.73	9.10
		0.29	8.29	10.22	9.83	8.96	9.42
		0.30	8.63	10.25	9.86	9.00	9.48
		0.32	8.63	10.37	9.99	9.16	9.71
		0.35	8.63	10.49	10.13	9.35	9.90
		0.36	8.63	10.53	10.16	9.40	9.95
	0.47	0.02	2.56	6.64	3.86	2.36	1.57
		0.04	6.95	9.10	8.29	5.44	3.81
		0.08	6.39	9.54	8.82	7.33	6.63
		0.14	6.89	10.22	9.55	8.01	8.03
		0.20	7.46	10.93	10.18	8.70	9.10
		0.26	8.71	11.51	10.74	9.33	10.03
		0.31	12.01	11.85	11.10	9.76	10.66
		0.32	12.01	11.92	11.18	9.86	10.82
		0.38	12.01	12.21	11.51	10.29	11.39
		0.41	12.01	12.29	11.61	10.43	11.58
		0.44	-	12.38	11.72	10.61	11.76
	0.63	0.02	2.99	5.81	4.08	2.44	1.68
		0.05	5.57	8.19	8.86	6.30	4.63
		0.08	6.06	8.83	9.39	7.58	7.07
		0.14	6.80	10.09	10.20	8.27	8.63
		0.20	7.67	11.20	10.88	8.96	9.69
		0.23	8.46	11.67	11.19	9.29	10.17
		0.26	9.64	12.07	11.47	9.59	10.63
		0.29	9.49	12.38	11.70	9.85	10.99
		0.29	9.49	12.41	11.73	9.88	11.03
		0.32	9.49	12.70	11.95	10.13	11.40
		0.35	9.49	12.94	12.14	10.37	11.73
		0.38	9.49	13.13	12.29	10.57	11.97
		0.40	9.49	13.21	12.36	10.67	12.09
	0.79	0.02	6.70	6.80	4.34	2.46	1.65
		0.05	7.00	9.56	9.37	6.34	4.58
		0.08	7.35	10.20	9.80	7.62	7.06
		0.14	7.98	11.27	10.60	8.31	8.91
		0.20	8.69	12.21	11.30	9.01	10.01
		0.23	9.93	12.60	11.62	9.35	10.48
		0.26	11.25	12.91	11.88	9.63	10.89
		0.26	11.25	12.94	11.91	9.66	10.93
		0.29	11.25	13.23	12.17	9.95	11.31
		0.32	11.25	13.47	12.40	10.21	11.65
		0.35	11.25	13.66	12.59	10.45	11.97
		0.36	11.25	13.71	12.65	10.52	12.04

Table B.2 (Cont.) Comparison of velocity from the physical model and various grid sizes of numerical model on the 25-step spillway

Discharge (m³/s)	$\dfrac{iL}{L\cos_{_{"}}}$	Depth normal to the pseudo-bottom (m)	Velocity from physical model (m/s)	Velocity (m/s) from various grid sizes of numerical model (m²)			
				0.020x0.020	0.035x0.035	0.050x0.050	0.100x0.100
2.27	0.16	0.02	4.33	4.15	3.01	1.96	0.91
		0.05	6.29	5.71	6.46	5.05	2.56
		0.08	6.74	6.06	6.70	6.03	4.00
		0.14	7.21	6.81	7.08	6.48	6.29
		0.20	7.19	7.47	7.44	6.94	7.07
		0.26	7.50	7.96	7.79	7.37	7.55
		0.29	6.77	8.14	7.94	7.56	7.78
		0.32	7.28	8.30	8.08	7.74	7.94
		0.35	5.36	8.42	8.20	7.89	8.08
	0.31	0.02	-	5.02	3.64	2.30	1.24
		0.05	6.50	6.84	7.86	5.93	3.49
		0.08	6.80	7.25	8.23	7.11	5.43
		0.14	7.65	8.20	8.82	7.70	7.48
		0.20	8.31	9.09	9.35	8.31	8.41
		0.26	9.10	9.79	9.83	8.88	9.17
		0.29	9.57	10.07	10.03	9.14	9.52
		0.32	10.59	10.31	10.22	9.38	9.83
	0.47	0.02	2.77	6.40	3.85	2.43	1.61
		0.04	7.71	8.91	8.30	5.61	3.92
		0.08	4.07	9.55	-	7.54	6.82
		0.14	8.03	10.35	9.77	8.25	8.18
		0.20	8.71	11.07	10.44	8.97	9.22
		0.26	9.51	11.66	11.05	9.64	10.14
		0.32	11.06	12.11	11.54	10.23	10.94
	0.63	0.02	1.63	6.25	-	2.55	1.68
		0.05	7.73	8.72	9.22	6.57	4.64
		0.08	8.73	9.28	9.72	7.90	7.09
		0.14	9.55	10.46	10.54	8.64	8.66
		0.20	10.13	11.54	11.27	9.40	9.74
		0.26	12.38	12.42	11.92	10.11	10.73
		0.29	11.72	12.77	12.21	10.44	11.16
		0.32	14.60	13.07	12.47	10.74	11.59
		0.33	-	13.15	12.54	10.74	11.71
		0.35	-	13.33	12.70	10.83	11.97
		0.38	-	13.55	12.90	11.02	12.31
		0.41	-	13.74	13.07	11.27	12.62
		0.42	-	13.80	13.13	11.50	12.74
		0.44	-	13.89	13.21	11.58	12.88
		0.47	-	14.02	13.34	11.70	13.11
		0.50	-	14.12	13.43	11.88	13.32
	0.79	0.02	7.06	6.82	4.44	2.59	1.67
		0.08	7.28	9.92	10.16	8.05	7.17
		0.14	8.20	11.11	11.04	8.82	9.05
		0.20	9.55	12.24	11.81	9.60	10.19
		0.26	10.34	13.18	12.51	10.33	11.21
		0.32	12.48	13.90	13.10	10.98	12.07
		0.35	-	14.19	13.34	11.26	12.48
		0.38	-	14.43	13.55	11.52	12.80
		0.44	-	14.82	13.88	11.96	13.37
		0.44	-	14.82	13.88	11.96	13.37
		0.50	-	15.07	14.11	12.30	13.75

Table B.2 (Cont.) Comparison of velocity from the physical model and various grid sizes of numerical model on the 25-step spillway

Discharge (m³/s)	$\dfrac{iL}{L\cos_{\theta}}$	Depth normal to the pseudo-bottom (m)	Velocity from physical model (m/s)	Velocity (m/s) from various grid sizes of numerical model (m²)			
				0.020x0.020	0.035x0.035	0.050x0.050	0.100x0.100
3.28	0.16	0.02	5.79	4.30	2.66	2.00	0.92
		0.05	6.17	5.95	5.86	5.14	2.59
		0.08	6.52	6.33	6.45	6.14	4.06
		0.14	7.24	7.15	7.23	6.62	6.39
		0.20	7.61	7.86	7.79	7.13	7.22
		0.26	7.83	8.40	8.25	7.60	7.75
		0.29	8.06	8.62	8.45	7.81	8.00
		0.32	8.07	8.79	8.62	8.01	8.18
		0.35	8.65	8.94	8.78	8.20	8.34
		0.38	8.09	9.07	8.91	8.36	8.49
		0.41	9.52	9.17	9.02	8.51	8.63
		0.44	9.45	9.24	9.10	8.61	8.73
		0.44	9.45	9.26	9.12	8.64	8.75
		0.47	9.45	9.33	9.20	8.76	8.81
		0.50	9.45	9.39	9.27	8.86	8.87
		0.51	9.45	9.40	9.29	8.89	8.89
	0.31	0.02	-	5.76	3.70	-	-
		0.05	6.87	7.83	7.99	6.05	3.52
		0.08	7.06	8.22	8.43	7.26	5.48
		0.14	8.06	9.10	9.11	7.90	7.55
		0.20	8.72	9.86	9.69	8.56	8.48
		0.26	9.47	10.45	10.20	9.17	9.24
		0.29	9.32	10.69	10.43	9.44	9.60
		0.32	9.60	10.88	10.63	9.70	9.92
		0.35	10.25	11.05	10.81	9.93	10.17
		0.38	11.25	11.20	10.96	10.14	10.41
		0.38	11.43	11.21	10.97	10.16	10.43
		0.41	11.43	11.33	11.09	10.33	10.63
		0.44	11.43	11.44	11.21	10.50	10.79
		0.47	11.43	11.52	11.30	10.64	10.91
		0.47	-	11.53	11.31	10.66	10.92
	0.63	0.02	5.66	6.34	4.30	2.66	1.71
		0.05	8.95	8.86	9.38	6.86	4.74
		0.08	9.05	9.44	9.95	8.27	7.24
		0.14	10.77	10.69	10.85	9.09	8.84
		0.20	11.32	11.83	11.62	9.91	9.95
		0.26	11.87	12.75	12.34	10.69	10.96
		0.32	12.93	13.46	12.95	11.38	11.85
		0.38	14.55	13.99	13.44	11.98	12.62
		0.38	15.97	13.99	13.44	11.98	12.62
		0.41	16.14	14.20	13.65	12.25	12.97
		0.41	16.14	14.22	13.67	12.28	13.00
		0.44	16.14	14.39	13.84	12.49	13.27
		0.47	16.14	14.55	14.01	12.72	13.55
		0.50	16.14	14.69	14.15	12.92	13.82
		0.51	16.14	14.70	14.16	12.94	13.85
	0.79	0.02	8.47	6.40	4.40	2.76	1.71
		0.05	9.60	9.01	9.55	7.12	4.76
		0.08	10.12	9.75	10.04	8.58	7.34
		0.14	11.70	11.15	11.00	9.44	9.25
		0.20	12.78	12.44	11.93	10.34	10.43
		0.26	13.20	13.52	12.80	11.17	11.49
		0.32	13.74	14.35	13.53	11.91	12.43
		0.38	16.53	14.99	14.13	12.54	13.26
		0.41	15.52	15.21	14.34	12.77	13.56
		0.41	15.52	15.25	14.39	12.82	13.63
		0.44	15.52	15.48	14.61	13.08	13.98
		0.47	15.52	15.68	14.82	13.31	14.29
		0.48	15.52	15.75	14.89	13.39	14.41
		0.50	-	15.84	14.99	13.52	14.59
		0.53	-	15.99	15.15	13.71	14.88

Table B.3 Comparison of velocity from the physical model and various grid sizes of numerical model on the 50-step spillway

Discharge (m³/s)	$\dfrac{iL}{L\cos_{\theta}}$	Depth normal to the pseudo-bottom (m)	Velocity from physical model (m/s)	Velocity (m/s) from various grid sizes of numerical model (m²)		
				0.020x0.020	0.035x0.035	0.050x0.050
0.6	0.16	0.02	5.76	3.29	2.34	1.52
		0.05	6.16	4.74	5.21	3.92
		0.08	6.57	5.23	5.59	4.77
		0.11	8.64	5.71	5.85	5.07
		0.11	8.64	5.71	5.85	5.07
		0.14	8.64	6.12	6.08	5.34
		0.17	8.64	6.44	6.27	5.59
		0.20	8.64	6.68	6.44	5.80
		0.22	8.64	6.82	6.55	5.96
	0.31	0.02	6.08	3.73	2.55	1.61
		0.05	6.52	5.41	5.68	4.16
		0.08	7.54	6.02	6.14	5.06
		0.10	10.29	6.55	6.48	5.35
		0.11	10.29	6.61	6.51	5.39
		0.14	10.29	7.12	6.84	5.68
		0.17	10.29	7.52	7.11	5.96
		0.17	10.29	7.52	7.11	5.96
		0.20	0.00	7.83	7.34	6.19
	0.47	0.02	5.22	4.38	2.68	1.60
		0.05	6.22	6.26	5.98	4.13
		0.08	7.78	6.76	6.48	5.03
		0.11	6.74	7.24	6.82	5.35
		0.14	8.35	7.67	7.11	5.66
		0.14	8.47	7.75	7.16	5.71
		0.17	8.47	8.02	7.36	5.94
		0.20	8.47	8.28	7.56	6.17
		0.21	8.47	8.34	7.61	6.24
	0.63	0.02	5.06	4.79	2.67	1.65
		0.05	5.97	6.84	5.98	4.25
		0.08	6.45	7.34	6.47	5.17
		0.11	7.46	7.81	6.83	5.47
		0.14	9.13	8.22	7.12	5.75
		0.14	9.20	8.26	7.15	5.78
		0.17	9.20	8.54	7.38	6.01
		0.20	9.20	8.76	7.58	7.33
		0.20	9.20	8.78	7.60	6.25
	0.79	0.02	4.78	5.11	2.69	1.67
		0.05	6.41	7.24	6.01	4.29
		0.08	6.91	7.74	6.49	5.21
		0.11	6.70	8.17	6.83	5.51
		0.14	7.84	8.54	7.12	5.78
		0.14	7.95	8.57	7.15	5.81
		0.17	7.95	8.83	7.37	6.03
		0.20	7.95	9.02	7.58	6.25
		0.20	7.95	9.04	7.61	6.29

$$\frac{il}{L\cos\theta}=0.16$$
$$\frac{il}{L\cos\theta}=0.31$$
$$\frac{il}{L\cos\theta}=0.47$$
$$\frac{il}{L\cos\theta}=0.63$$
$$\frac{il}{L\cos\theta}=0.79$$

y

$(0,0)$

x

Remarks:

Table B.3 (Cont.) Comparison of velocity from the physical model and various grid sizes of numerical model on the 50-step spillway

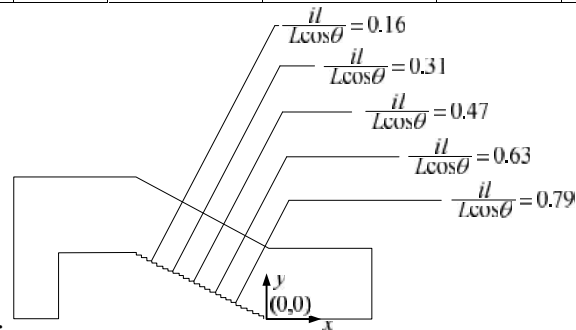| Discharge (m³/s)	$\dfrac{iL}{L\cos_{\theta}}$	Depth normal to the pseudo-bottom (m)	Velocity from physical model (m/s)	Velocity (m/s) from various grid sizes of numerical model (m²)		
				0.020x0.020	0.035x0.035	0.050x0.050
1.16	0.16	0.02	5.77	3.87	2.42	1.63
		0.05	4.39	5.67	5.37	4.19
		0.08	7.26	6.08	5.77	5.12
		0.14	7.39	6.72	6.40	5.78
		0.20	8.42	7.21	6.90	6.36
		0.22	9.70	7.32	7.02	6.51
		0.26	9.70	7.54	7.27	6.80
		0.27	9.70	7.57	7.31	6.86
		0.29	-	7.65	7.40	6.98
	0.31	0.02	7.10	4.80	2.74	1.82
		0.05	8.17	7.00	6.12	4.70
		0.08	8.20	7.58	6.69	5.77
		0.11	8.60	8.07	7.16	6.20
		0.14	9.10	8.52	7.59	6.60
		0.20	12.53	9.20	8.27	7.30
		0.20	12.53	9.23	8.30	7.34
		0.23	12.53	9.48	8.59	7.66
		0.25	12.53	9.65	8.79	7.87
		0.26	0.00	9.69	8.84	7.92
	0.47	0.02	5.22	5.23	2.88	1.86
		0.05	7.02	7.72	6.47	4.79
		0.08	7.30	8.41	7.08	5.90
		0.14	7.83	9.50	8.07	6.82
		0.20	8.81	10.33	8.88	7.62
		0.23	8.75	10.63	9.20	7.96
		0.25	10.75	10.80	9.40	8.16
		0.26	10.75	10.87	9.48	8.24
		0.29	10.75	11.05	9.70	8.49
		0.30	10.75	11.08	9.74	8.53
	0.63	0.02	5.96	6.05	3.16	1.99
		0.05	7.05	8.61	6.97	5.13
		0.08	7.70	9.17	7.49	6.27
		0.14	8.37	10.19	8.40	7.10
		0.20	8.95	11.00	9.17	7.83
		0.24	10.86	11.38	9.58	8.23
		0.26	10.86	11.53	9.75	8.41
		0.29	10.86	11.70	9.96	8.64
		0.30	10.86	11.77	10.05	8.74
	0.79	0.02	5.68	6.22	3.29	1.99
		0.05	7.00	8.72	7.25	5.13
		0.08	7.59	9.36	7.70	6.28
		0.14	8.13	10.48	8.57	7.10
		0.20	8.07	11.34	9.33	7.83
		0.23	10.99	11.64	9.64	8.15
		0.23	10.99	11.64	9.64	8.15
		0.26	10.99	11.88	9.90	8.41
		0.29	10.99	12.03	10.09	8.63
		0.29	-	12.05	10.11	8.65

Table B.3 (Cont.) Comparison of velocity from the physical model and various grid sizes of numerical model on the 50-step spillway

Discharge (m³/s)	$\dfrac{iL}{L\cos_{_\#}}$	Depth normal to the pseudo-bottom (m)	Velocity from physical model (m/s)	Velocity (m/s) from various grid sizes of numerical model (m²)		
				0.020x0.020	0.035x0.035	0.050x0.050
1.70	0.16	0.02	6.00	3.92	2.45	1.69
		0.05	6.49	5.79	5.45	4.34
		0.08	7.33	6.26	5.87	5.30
		0.14	8.23	6.97	6.54	6.00
		0.20	8.48	7.51	7.09	6.61
		0.26	11.89	7.89	7.51	7.09
		0.27	11.96	7.92	7.55	7.13
		0.32	11.96	8.13	7.82	7.45
	0.31	0.02	6.68	4.78	2.87	1.94
		0.05	7.69	7.13	6.39	4.99
		0.08	8.17	7.79	6.95	6.11
		0.14	8.69	8.79	7.89	6.98
		0.20	8.99	9.55	8.66	7.77
		0.26	10.60	10.06	9.27	8.43
		0.27	12.59	10.16	9.40	8.57
		0.32	12.59	10.40	9.72	8.94
		0.35	12.59	10.53	9.89	9.15
	0.47	0.02	4.07	5.32	3.08	2.05
		0.05	7.07	7.89	6.90	5.28
		0.08	7.75	8.64	7.52	6.48
		0.14	8.07	9.84	8.57	7.43
		0.20	8.58	10.77	9.47	8.31
		0.26	8.96	11.41	10.18	9.04
		0.32	11.68	11.85	10.70	9.59
		0.32	11.68	11.86	10.72	9.62
		0.35	11.68	12.03	10.94	9.86
		0.37	11.68	12.13	11.06	10.00
		0.38	-	12.17	11.12	10.06
	0.63	0.02	6.05	6.12	3.43	2.16
		0.05	6.99	8.78	7.61	5.59
		0.08	7.55	9.46	8.15	6.86
		0.14	8.35	10.68	9.16	7.81
		0.20	8.93	11.67	10.07	8.68
		0.26	10.63	12.38	10.79	9.40
		0.29	12.52	12.67	11.11	9.74
		0.32	12.52	12.87	11.34	9.98
		0.35	12.52	13.05	11.55	10.22
		0.35	12.52	13.06	11.57	10.24
	0.79	0.02	6.30	6.46	3.49	2.19
		0.05	7.08	9.14	7.75	5.66
		0.08	7.89	9.88	8.32	6.94
		0.14	8.53	11.18	9.36	7.90
		0.20	9.11	12.23	10.29	8.78
		0.26	10.39	12.99	11.03	9.51
		0.29	13.72	13.27	11.33	9.83
		0.32	13.72	13.50	11.60	10.10
		0.35	13.72	13.69	11.82	10.34
		0.36	13.72	13.74	11.88	10.41
		0.38	-	13.83	12.01	10.55

Table B.3 (Cont.) Comparison of velocity from the physical model and various grid sizes of numerical model on the 50-step spillway

Discharge (m³/s)	$\dfrac{iL}{L\cos_{\shortmid\shortmid}}$	Depth normal to the pseudo-bottom (m)	Velocity from physical model (m/s)	Velocity (m/s) from various grid sizes of numerical model (m²)		
				0.020x0.020	0.035x0.035	0.050x0.050
2.27	0.16	0.02	5.73	-	2.56	1.70
		0.05	6.10	-	5.71	4.37
		0.08	7.68	-	6.19	5.35
		0.14	8.08	7.06	6.83	6.07
		0.20	8.29	7.67	7.36	6.71
		0.26	8.61	8.11	7.79	7.23
		0.32	9.34	8.41	8.11	7.63
		0.33	9.39	8.46	8.16	7.70
		0.38	9.39	8.61	8.35	7.93
		0.40	9.39	8.66	8.40	8.01
		0.41	-	8.68	8.44	8.06
	0.31	0.02	-	5.01	2.93	1.95
		0.05	-	7.25	6.58	5.04
		0.08	8.03	7.87	7.18	6.19
		0.14	9.27	8.92	8.13	7.09
		0.20	9.70	9.72	8.91	7.92
		0.26	9.77	10.27	9.53	8.61
		0.31	10.35	10.60	9.93	9.08
		0.32	10.35	10.65	10.00	9.15
		0.35	10.35	10.79	10.19	9.38
		0.37	10.35	10.86	10.27	9.49
		0.38	-	10.91	10.35	9.59
	0.47	0.02	4.01	5.51	3.12	2.11
		0.05	7.30	8.02	7.00	5.44
		0.08	7.57	8.76	7.65	6.69
		0.14	8.47	9.98	8.76	7.70
		0.20	9.30	10.95	9.71	8.63
		0.26	10.09	11.64	10.49	9.41
		0.32	10.64	12.14	11.10	10.04
		0.35	10.54	12.34	11.35	10.31
		0.37	12.70	12.43	11.46	10.43
		0.38	12.70	12.51	11.56	10.55
		0.41	12.70	12.65	11.76	10.77
		0.41	12.70	12.65	11.76	10.77
	0.63	0.02	5.94	6.09	3.49	2.27
		0.05	6.79	8.91	7.76	5.85
		0.08	7.09	9.63	8.36	7.18
		0.14	8.46	10.92	9.46	8.20
		0.20	8.89	11.97	10.45	9.16
		0.26	9.94	12.74	11.25	9.97
		0.32	11.94	13.31	11.90	10.64
		0.35	12.98	13.52	12.14	10.90
		0.35	12.98	13.52	12.14	11.18
		0.38	12.98	13.73	12.40	11.18
		0.41	-	13.87	12.59	11.38
	0.79	0.02	6.32	6.72	3.54	2.30
		0.05	6.83	9.43	7.89	5.95
		0.08	7.82	10.14	8.52	7.31
		0.14	9.10	11.51	9.71	8.38
		0.20	9.94	12.64	10.77	9.36
		0.26	10.45	13.49	11.63	10.21
		0.32	12.25	14.12	12.33	10.90
		0.34	12.88	14.32	12.56	11.15
		0.35	12.88	14.37	12.61	11.20
		0.38	12.88	14.58	12.87	11.46
		0.41	12.88	14.74	13.07	11.68

Table B.3 (Cont.) Comparison of velocity from the physical model and various grid sizes of numerical model on the 50-step spillway

Discharge (m³/s)	$\dfrac{iL}{L\cos_{\#}}$	Depth normal to the pseudo-bottom (m)	Velocity from physical model (m/s)	Velocity (m/s) from various grid sizes of numerical model (m²)		
				0.020x0.020	0.035x0.035	0.050x0.050
0.60	0.16	0.02	5.85	4.20	2.62	1.73
		0.05	6.22	6.11	5.83	4.46
		0.08	7.09	6.56	6.24	5.45
		0.14	7.96	7.31	6.93	6.20
		0.20	8.65	7.92	7.52	6.87
		0.26	9.31	8.37	7.99	7.42
		0.32	9.65	8.69	8.34	7.86
		0.38	10.98	8.92	8.60	8.19
		0.39	11.47	8.93	8.63	8.22
		0.44	11.47	9.07	8.80	8.46
		0.45	11.47	9.09	8.83	8.51
		0.47	-	9.12	8.88	8.57
	0.31	0.02	6.54	5.06	3.00	2.02
		0.05	7.37	7.40	6.68	5.20
		0.08	7.95	8.05	7.22	6.37
		0.14	9.05	9.10	8.19	7.31
		0.20	9.98	9.92	9.01	8.16
		0.26	10.41	10.49	9.68	8.87
		0.32	12.57	10.89	10.18	9.45
		0.33	13.22	10.92	10.22	9.50
		0.38	13.22	11.17	10.56	9.91
		0.41	-	11.28	10.72	10.10
		0.44	-	11.36	10.86	10.28
	0.47	0.02	3.27	5.44	3.22	2.16
		0.05	7.00	8.11	7.21	5.58
		0.08	7.53	8.90	7.83	6.85
		0.14	8.74	10.15	8.94	7.91
		0.20	9.41	11.14	9.91	8.88
		0.26	10.09	11.84	10.70	9.71
		0.32	10.33	12.36	11.33	10.39
		0.38	11.54	12.75	11.83	10.94
		0.39	12.30	12.79	11.89	11.02
		0.41	12.30	12.90	12.04	11.18
		0.44	12.30	13.00	12.19	11.35
		0.44	0.00	13.02	12.22	11.40
	0.63	0.02	6.19	6.30	3.53	2.31
		0.05	6.65	9.12	7.83	5.96
		0.08	7.31	9.81	8.45	7.35
		0.14	8.86	11.09	9.60	8.46
		0.20	9.51	12.15	10.64	9.47
		0.26	10.19	12.95	11.50	10.33
		0.32	11.17	13.55	12.19	11.05
		0.38	12.32	14.01	12.76	11.65
		0.38	14.16	14.01	12.76	11.65
		0.40	14.16	14.10	12.88	11.78
		0.44	14.16	14.34	13.21	12.14
		0.45	-	14.40	13.29	12.23
	0.79	0.02	5.57	6.68	3.65	2.36
		0.05	7.64	9.48	8.11	6.12
		0.08	8.46	10.26	8.74	7.55
		0.14	9.51	11.69	9.95	8.71
		0.20	10.24	12.87	11.06	9.76
		0.26	11.71	13.76	11.99	10.67
		0.32	11.52	14.45	12.75	11.42
		0.38	12.11	14.97	13.36	12.05
		0.40	13.09	15.10	13.53	12.22
		0.41	13.09	15.18	13.63	12.32
		0.44	13.09	15.37	13.86	12.57
		0.45	13.09	15.43	13.94	12.66

APPENDIX C

Velocity at different values of coefficient C_2 in the Realisable k-v model

Table C.1 Velocity at values of coefficient C_2 between 1.70-1.76 in the Realisable k-v model

Discharge (m³/s)	$\dfrac{iL}{L\cos_{\prime\prime}}$	Depth normal to the pseudo-bottom (m)	Velocity (m/s) at various values of coefficient C_2						
			C_2=1.70	C_2=1.71	C_2=1.72	C_2=1.73	C_2=1.74	C_2=1.75	C_2=1.76
0.57	0.16	0.02	1.70	1.80	1.63	1.73	1.72	1.71	1.73
		0.08	5.19	5.48	5.11	5.30	5.28	5.26	5.37
		0.14	5.54	5.74	5.66	5.63	5.63	5.63	5.83
		0.17	5.71	5.87	5.87	5.79	5.80	5.80	6.01
		0.20	5.84	5.96	5.99	5.90	5.91	5.91	6.12
		0.26	6.03	6.10	6.19	6.07	6.07	6.07	6.28
		0.32	6.11	6.13	6.25	6.09	6.11	6.11	6.26
		0.38	5.91	5.84	5.85	5.80	5.89	5.88	5.78
	0.31	0.02	2.08	1.94	2.15	1.90	1.82	1.82	1.86
		0.05	5.30	4.98	5.50	4.88	4.70	4.70	4.75
		0.08	6.37	5.93	6.59	5.83	5.61	5.62	5.66
		0.11	6.66	6.12	6.84	6.02	5.81	5.82	5.85
		0.14	6.84	6.27	7.02	6.18	5.98	6.00	6.03
		0.17	6.98	6.40	7.16	6.33	6.13	6.16	6.20
		0.17	7.01	6.42	7.18	6.35	6.16	6.19	6.23
		0.20	7.07	6.50	7.25	6.45	6.25	6.28	6.35
		0.30	7.07	6.61	7.27	6.61	6.43	6.47	6.59
	0.47	0.02	1.92	1.90	2.13	1.96	1.86	1.83	2.16
		0.05	5.40	5.36	6.00	5.52	5.24	5.17	6.07
		0.11	6.13	6.03	6.93	6.21	5.95	5.88	6.75
		0.15	6.33	6.20	7.12	6.35	6.12	6.06	6.86
		0.17	6.48	6.33	7.24	6.46	6.25	6.20	6.94
		0.23	6.71	6.54	7.37	6.61	6.44	6.40	7.04
		0.27	6.77	6.59	7.39	6.65	6.48	6.45	7.06
		0.30	6.81	6.62	7.33	6.66	6.50	6.47	7.06
	0.63	0.02	2.14	1.91	2.21	2.11	1.89	1.83	2.00
		0.05	5.50	4.91	5.67	5.40	4.87	4.71	5.15
		0.08	6.56	5.85	6.78	6.45	5.79	5.62	6.14
		0.11	6.76	6.03	7.02	6.66	5.96	5.82	6.33
		0.14	6.91	6.19	7.19	6.81	6.11	5.99	6.50
		0.14	6.91	6.19	7.19	6.81	6.11	5.99	6.50
		0.17	7.02	6.33	7.33	6.93	6.25	6.15	6.65
		0.20	7.10	6.45	7.43	7.01	6.36	6.27	6.77
		0.30	7.17	6.62	7.54	7.09	6.52	6.46	6.93
	0.79	0.02	2.01	1.90	2.16	1.95	1.99	1.83	2.11
		0.05	5.14	4.88	5.55	4.98	5.10	4.71	5.42
		0.08	6.16	5.81	6.65	5.97	6.09	5.63	6.43
		0.11	6.41	5.98	6.90	6.22	6.29	5.83	6.60
		0.12	6.48	6.03	6.97	6.29	6.35	5.88	6.65
		0.14	6.61	6.13	7.08	6.42	6.45	6.00	6.72
		0.17	6.78	6.27	7.23	6.58	6.58	6.16	6.82
		0.20	6.90	6.38	7.32	6.71	6.68	6.28	6.89
		0.23	6.98	6.46	7.37	6.80	6.75	6.37	6.92
		0.23	6.99	6.47	7.38	6.81	6.76	6.38	6.93

Remarks: C_2 is the values of coefficient turbulence in the Realisable k-v model

Table C.1 (Cont.) Velocity at values of coefficient C_2 between 1.70-1.76 in the Realisable k-ν model

Discharge (m³/s)	$\dfrac{iL}{L\cos_n}$	Depth normal to the pseudo-bottom (m)	Velocity (m/s) at various values of coefficient C_2						
			C_2=1.70	C_2=1.71	C_2=1.72	C_2=1.73	C_2=1.74	C_2=1.75	C_2=1.76
1.13	0.16	0.02	1.83	1.99	1.83	1.85	1.80	1.82	1.84
		0.08	5.67	6.07	5.63	5.71	5.59	5.62	5.68
		0.14	6.21	6.45	6.14	6.20	6.13	6.15	6.20
		0.20	6.62	6.76	6.54	6.58	6.57	6.57	6.61
		0.23	6.80	6.90	6.71	6.75	6.75	6.75	6.79
		0.26	6.95	7.03	6.87	6.90	6.91	6.91	6.94
		0.31	7.19	7.24	7.11	7.14	7.17	7.17	7.19
		0.32	7.22	7.26	7.14	7.17	7.20	7.19	7.21
		0.38	7.42	7.43	7.35	7.37	7.41	7.41	7.42
	0.31	0.02	2.41	2.32	2.31	2.30	2.40	2.30	2.37
		0.05	6.15	5.95	5.94	5.92	6.13	5.91	6.07
		0.08	7.34	7.15	7.15	7.16	7.38	7.16	7.31
		0.11	7.61	7.46	7.47	7.53	7.73	7.53	7.66
		0.14	7.85	7.72	7.74	7.80	7.98	7.81	7.92
		0.17	8.06	7.96	7.98	8.04	8.20	8.06	8.16
		0.23	8.45	8.39	8.41	8.44	8.55	8.46	8.54
		0.26	8.61	8.57	8.58	8.61	8.70	8.63	8.70
		0.29	8.76	8.73	8.74	8.76	8.84	8.78	8.84
		0.40	9.09	9.09	9.10	9.10	9.15	9.11	9.17
	0.47	0.02	8.15	7.91	8.10	8.06	8.01	8.12	8.10
		0.05	8.51	8.30	8.47	8.44	8.44	8.50	8.46
		0.11	9.00	8.83	8.96	8.95	8.99	9.00	8.96
		0.17	9.38	9.24	9.33	9.35	9.39	9.38	9.35
		0.22	9.59	9.47	9.54	9.57	9.61	9.60	9.56
		0.23	9.64	9.53	9.59	9.63	9.66	9.65	9.62
		0.30	9.76	9.67	9.71	9.75	9.75	9.77	9.74
		0.36	9.58	9.51	9.49	9.55	9.48	9.58	9.53
		0.36	9.54	9.48	9.45	9.50	9.44	9.54	9.49
	0.63	0.02	2.63	2.63	2.58	2.56	2.67	2.64	2.59
		0.05	6.73	6.73	6.64	6.57	6.82	6.77	6.67
		0.08	8.08	8.05	8.01	7.91	8.15	8.10	8.03
		0.11	8.44	8.35	8.38	8.28	8.47	8.40	8.38
		0.14	8.72	8.61	8.67	8.58	8.73	8.68	8.66
		0.17	8.97	8.85	8.92	8.85	8.98	8.92	8.91
		0.20	9.20	9.08	9.14	9.08	9.20	9.14	9.13
		0.22	9.34	9.23	9.29	9.23	9.34	9.29	9.27
		0.23	9.40	9.29	9.34	9.29	9.40	9.35	9.33
		0.26	9.57	9.46	9.51	9.47	9.57	9.52	9.50
		0.29	9.72	9.61	9.66	9.63	9.72	9.67	9.65
		0.32	9.84	9.73	9.78	9.76	9.85	9.78	9.77
		0.32	9.85	9.74	9.80	9.77	9.86	9.80	9.78
	0.79	0.02	2.63	2.64	2.64	2.60	2.67	2.55	2.61
		0.05	6.75	6.76	6.76	6.69	6.85	6.54	6.69
		0.08	8.12	8.08	8.09	8.09	8.21	7.92	8.01
		0.11	8.47	8.38	8.40	8.49	8.53	8.34	8.32
		0.14	8.76	8.65	8.68	8.79	8.80	8.67	8.60
		0.17	9.02	8.90	8.93	9.04	9.04	8.96	8.87
		0.18	9.14	9.02	9.05	9.16	9.15	9.08	9.00
		0.20	9.25	9.13	9.16	9.27	9.26	9.20	9.12
		0.23	9.46	9.35	9.38	9.47	9.46	9.42	9.36
		0.26	9.63	9.53	9.56	9.64	9.63	9.61	9.55
		0.29	9.79	9.69	9.72	9.79	9.78	9.77	9.72
		0.30	9.85	9.75	9.79	9.85	9.84	9.84	9.79

Table C.1 (Cont.) Velocity at values of coefficient C_2 between 1.70-1.76 in the Realisable k-v model

Discharge (m³/s)	$\dfrac{iL}{L\cos{}_{\textit{n}}}$	Depth normal to the pseudo-bottom (m)	Velocity (m/s) at various values of coefficient C_2						
			C_2=1.70	C_2=1.71	C_2=1.72	C_2=1.73	C_2=1.74	C_2=1.75	C_2=1.76
1.70	0.16	0.02	2.01	1.91	1.90	1.88	1.88	2.00	1.89
		0.05	5.13	4.88	4.89	4.83	4.86	5.13	4.85
		0.08	6.15	5.82	5.91	5.87	6.01	6.17	5.87
		0.14	6.62	6.27	6.46	6.46	6.73	6.65	6.42
		0.20	7.00	6.73	6.88	6.89	7.15	7.02	6.85
		0.26	7.33	7.15	7.24	7.24	7.46	7.33	7.22
		0.27	7.39	7.22	7.31	7.31	7.52	7.39	7.28
		0.32	7.61	7.49	7.55	7.55	7.73	7.61	7.53
		0.38	7.84	7.77	7.80	7.80	7.94	7.84	7.79
		0.40	7.89	7.83	7.85	7.86	7.99	7.89	7.85
	0.31	0.02	2.44	2.46	2.44	2.47	2.51	2.46	2.45
		0.05	6.27	6.29	6.25	6.35	6.47	6.29	6.29
		0.08	7.56	7.54	7.49	7.62	7.78	7.55	7.56
		0.14	8.21	8.13	8.07	8.20	8.39	8.16	8.17
		0.20	8.73	8.61	8.58	8.68	8.86	8.67	8.67
		0.23	8.96	8.84	8.82	8.90	9.07	8.90	8.90
		0.26	9.17	9.05	9.04	9.10	9.26	9.11	9.10
		0.29	9.37	9.24	9.24	9.29	9.44	9.31	9.30
		0.30	9.41	9.28	9.28	9.33	9.48	9.34	9.34
		0.32	9.55	9.42	9.43	9.47	9.61	9.49	9.48
		0.35	9.71	9.59	9.60	9.63	9.76	9.65	9.64
		0.36	9.75	9.63	9.64	9.67	9.80	9.69	9.68
	0.47	0.02	2.64	2.62	2.67	2.62	2.70	2.66	2.66
		0.04	6.07	6.02	6.12	6.03	6.20	6.10	6.10
		0.08	8.13	8.12	8.21	8.14	8.29	8.18	8.19
		0.14	8.80	8.82	8.88	8.89	8.94	8.85	8.86
		0.20	9.40	9.42	9.46	9.49	9.52	9.44	9.44
		0.26	9.92	9.93	9.97	9.99	10.03	9.96	9.95
		0.31	10.29	10.29	10.32	10.34	10.39	10.32	10.31
		0.32	10.38	10.37	10.41	10.42	10.47	10.40	10.39
		0.38	10.73	10.72	10.75	10.77	10.83	10.76	10.74
		0.41	10.85	10.83	10.87	10.88	10.94	10.87	10.86
		0.44	10.99	10.98	11.01	11.02	11.08	11.01	11.00
	0.63	0.02	2.75	2.75	2.75	2.82	2.79	2.77	2.72
		0.05	7.04	7.08	7.08	7.24	7.17	7.12	7.02
		0.08	8.46	8.53	8.51	8.65	8.60	8.55	8.47
		0.14	9.19	9.27	9.21	9.30	9.31	9.24	9.22
		0.20	9.82	9.89	9.83	9.89	9.92	9.85	9.85
		0.23	10.12	10.17	10.12	10.17	10.20	10.14	10.14
		0.26	10.38	10.43	10.38	10.42	10.46	10.40	10.40
		0.29	10.61	10.64	10.60	10.64	10.68	10.62	10.62
		0.29	10.64	10.67	10.62	10.66	10.70	10.64	10.64
		0.32	10.86	10.89	10.85	10.88	10.92	10.86	10.86
		0.35	11.07	11.08	11.05	11.08	11.12	11.06	11.06
		0.38	11.24	11.25	11.22	11.24	11.28	11.22	11.23
		0.40	11.32	11.32	11.30	11.32	11.36	11.30	11.30
	0.79	0.02	2.83	2.88	2.82	2.83	2.79	2.83	2.82
		0.05	7.27	7.37	7.26	7.25	7.18	7.24	7.23
		0.08	8.75	8.81	8.73	8.70	8.66	8.70	8.70
		0.14	9.48	9.48	9.46	9.42	9.43	9.43	9.44
		0.20	10.10	10.08	10.09	10.06	10.07	10.06	10.07
		0.23	10.39	10.37	10.37	10.35	10.37	10.35	10.36
		0.26	10.63	10.60	10.61	10.60	10.61	10.59	10.60
		0.26	10.66	10.63	10.64	10.62	10.64	10.62	10.62
		0.29	10.90	10.87	10.88	10.88	10.90	10.86	10.87
		0.32	11.13	11.10	11.11	11.10	11.13	11.09	11.09
		0.35	11.33	11.30	11.31	11.31	11.33	11.29	11.29
		0.36	11.38	11.35	11.36	11.36	11.38	11.34	11.35

Table C.1 (Cont.) Velocity at values of coefficient C_2 between 1.70-1.76 in the Realisable k-ν model

Discharge (m³/s)	$\dfrac{iL}{L\cos_{\,n}}$	Depth normal to the pseudo-bottom (m)	Velocity (m/s) at various values of coefficient C_2						
			C_2=1.70	C_2=1.71	C_2=1.72	C_2=1.73	C_2=1.74	C_2=1.75	C_2=1.76
2.27	0.16	0.02	2.00	2.00	1.99	2.11	1.95	1.96	2.02
		0.05	5.12	5.12	5.12	5.42	5.00	5.02	5.19
		0.08	6.16	6.15	6.18	6.48	6.05	6.08	6.30
		0.14	6.70	6.65	6.74	6.90	6.63	6.68	6.93
		0.20	7.16	7.08	7.20	7.26	7.07	7.15	7.35
		0.26	7.56	7.46	7.59	7.59	7.45	7.55	7.68
		0.29	7.74	7.64	7.76	7.74	7.63	7.73	7.83
		0.32	7.90	7.80	7.92	7.88	7.79	7.89	7.97
		0.35	8.05	7.95	8.07	8.01	7.94	8.04	8.10
		0.36	8.08	7.98	8.09	8.04	7.96	8.07	8.13
		0.38	8.17	8.07	8.18	8.12	8.06	8.15	8.20
		0.38	8.18	8.09	8.19	8.13	8.07	8.17	8.22
	0.31	0.02	2.58	2.46	2.52	2.49	2.54	2.52	2.57
		0.05	6.59	6.31	6.47	6.39	6.53	6.49	6.60
		0.08	7.90	7.60	7.75	7.67	7.84	7.80	7.92
		0.14	8.50	8.25	8.37	8.30	8.45	8.42	8.54
		0.20	9.01	8.80	8.91	8.85	8.96	8.94	9.06
		0.26	9.46	9.29	9.37	9.34	9.41	9.39	9.52
		0.29	9.67	9.51	9.59	9.55	9.62	9.60	9.73
		0.32	9.86	9.71	9.78	9.76	9.81	9.80	9.92
		0.34	10.00	9.86	9.93	9.91	9.95	9.95	10.06
		0.35	10.03	9.90	9.96	9.94	9.98	9.98	10.09
		0.38	10.19	10.06	10.12	10.10	10.14	10.14	10.24
		0.41	10.19	10.06	10.12	10.10	10.14	10.14	10.24
		0.47	10.55	10.46	10.51	10.49	10.50	10.51	10.59
	0.47	0.02	2.74	2.73	2.73	2.72	2.71	2.76	2.76
		0.04	6.29	6.27	6.26	6.26	6.24	6.35	6.33
		0.08	8.48	8.43	8.42	8.43	8.39	8.52	8.50
		0.14	9.24	9.15	9.19	9.17	9.13	9.21	9.21
		0.20	9.87	9.77	9.82	9.80	9.77	9.82	9.83
		0.26	10.42	10.33	10.39	10.36	10.34	10.38	10.39
		0.32	10.90	10.82	10.88	10.86	10.84	10.87	10.89
		0.36	11.16	11.08	11.14	11.12	11.10	11.13	11.15
		0.38	11.31	11.23	11.29	11.27	11.26	11.28	11.31
		0.44	11.62	11.55	11.61	11.58	11.57	11.60	11.62
		0.44	11.63	11.56	11.62	11.60	11.59	11.61	11.64
		0.50	11.88	11.81	11.87	11.84	11.84	11.86	11.88
	0.63	0.02	2.89	2.90	2.86	2.85	2.93	2.89	2.91
		0.05	7.44	7.45	7.32	7.34	7.49	7.40	7.47
		0.08	8.94	8.96	8.82	8.83	8.99	8.91	8.96
		0.14	9.69	9.70	9.65	9.60	9.76	9.71	9.70
		0.20	10.37	10.36	10.35	10.29	10.43	10.40	10.38
		0.26	10.99	10.97	10.98	10.91	11.03	11.01	10.99
		0.29	11.27	11.24	11.26	11.20	11.31	11.28	11.27
		0.32	11.53	11.50	11.52	11.46	11.56	11.54	11.53
		0.32	11.53	11.50	11.52	11.46	11.56	11.54	11.53
		0.33	11.61	11.58	11.60	11.54	11.64	11.62	11.60
		0.35	11.77	11.74	11.76	11.71	11.80	11.78	11.77
		0.38	11.98	11.95	11.98	11.92	12.01	11.99	11.98
		0.41	12.17	12.13	12.17	12.12	12.19	12.17	12.17
		0.42	12.24	12.20	12.23	12.18	12.26	12.24	12.23
		0.44	12.34	12.30	12.33	12.28	12.36	12.34	12.33
		0.47	12.48	12.44	12.47	12.43	12.50	12.48	12.47
	0.79	0.02	2.97	2.99	3.00	2.96	3.03	2.98	2.92
		0.05	7.62	7.68	7.70	7.61	7.76	7.66	7.49
		0.08	9.18	9.23	9.25	9.16	9.30	9.21	9.04
		0.14	10.02	10.01	10.02	9.95	10.06	10.01	9.91
		0.20	10.74	10.71	10.72	10.66	10.76	10.72	10.65
		0.26	11.38	11.34	11.35	11.31	11.39	11.36	11.31
		0.29	11.67	11.63	11.64	11.60	11.67	11.65	11.60
		0.32	11.94	11.90	11.91	11.87	11.94	11.92	11.88
		0.32	11.97	11.93	11.94	11.90	11.97	11.94	11.91
		0.35	12.19	12.15	12.16	12.13	12.19	12.17	12.13
		0.38	12.41	12.37	12.38	12.35	12.40	12.38	12.35
		0.41	12.60	12.56	12.57	12.54	12.59	12.58	12.55
		0.42	12.65	12.61	12.63	12.60	12.64	12.63	12.60
		0.44	12.77	12.73	12.74	12.72	12.76	12.75	12.72
		0.47	12.92	12.87	12.89	12.86	12.90	12.89	12.87

Table C.1 (Cont.) Velocity at values of coefficient C_2 between 1.70-1.76 in the Realisable k-v model

Discharge (m³/s)	$\dfrac{iL}{L\cos_\eta}$	Depth normal to the pseudo-bottom (m)	Velocity (m/s) at various values of coefficient C_2						
			C_2=1.70	C_2=1.71	C_2=1.72	C_2=1.73	C_2=1.74	C_2=1.75	C_2=1.76
2.83	0.16	0.02	1.97	1.99	2.00	2.03	2.03	1.99	2.09
		0.05	5.08	5.11	5.12	5.20	5.21	5.12	5.37
		0.08	6.13	6.19	6.19	6.28	6.32	6.21	6.43
		0.14	6.69	6.81	6.79	6.88	6.95	6.84	6.91
		0.20	7.18	7.32	7.28	7.36	7.43	7.34	7.33
		0.26	7.62	7.76	7.70	7.78	7.84	7.77	7.71
		0.29	7.82	7.95	7.89	7.97	8.02	7.96	7.88
		0.32	8.01	8.13	8.07	8.14	8.18	8.14	8.05
		0.35	8.18	8.30	8.23	8.30	8.33	8.30	8.20
		0.38	8.33	8.44	8.38	8.44	8.46	8.44	8.33
		0.40	8.42	8.53	8.47	8.53	8.55	8.53	8.42
		0.41	8.46	8.56	8.50	8.56	8.58	8.56	8.46
		0.44	8.58	8.68	8.62	8.67	8.68	8.67	8.57
		0.47	8.67	8.76	8.71	8.76	8.76	8.76	8.65
	0.31	0.02	2.54	2.55	2.57	2.64	2.61	2.56	2.54
		0.05	6.51	6.55	6.59	6.76	6.68	6.57	6.51
		0.08	7.80	7.86	7.90	8.09	7.97	7.89	7.82
		0.14	8.43	8.49	8.51	8.68	8.56	8.52	8.44
		0.20	8.98	9.05	9.05	9.20	9.09	9.05	8.99
		0.26	9.48	9.55	9.55	9.66	9.57	9.54	9.49
		0.29	9.71	9.77	9.77	9.88	9.79	9.76	9.72
		0.32	9.93	9.98	9.98	10.08	10.00	9.97	9.93
		0.35	10.13	10.18	10.18	10.26	10.19	10.16	10.13
		0.38	10.29	10.33	10.33	10.41	10.35	10.32	10.29
		0.38	10.30	10.35	10.35	10.43	10.36	10.34	10.30
		0.41	10.46	10.50	10.50	10.58	10.52	10.49	10.46
		0.44	10.61	10.65	10.64	10.71	10.66	10.63	10.61
		0.47	10.73	10.77	10.77	10.82	10.78	10.75	10.73
	0.47	0.02	2.76	2.76	2.81	2.78	2.78	2.71	2.78
		0.04	6.34	6.35	6.45	6.38	6.40	6.25	6.39
		0.08	8.53	8.57	8.63	8.57	8.62	8.44	8.56
		0.14	9.27	9.32	9.33	9.33	9.38	9.23	9.27
		0.20	9.94	9.98	9.97	9.99	10.02	9.92	9.92
		0.26	10.54	10.58	10.56	10.60	10.61	10.54	10.52
		0.32	11.07	11.11	11.09	11.14	11.13	11.08	11.05
		0.38	11.53	11.56	11.55	11.59	11.58	11.54	11.50
		0.40	11.63	11.66	11.65	11.69	11.68	11.65	11.61
		0.44	11.90	11.93	11.92	11.96	11.94	11.92	11.88
		0.49	12.15	12.18	12.17	12.21	12.19	12.17	12.13
		0.50	12.19	12.22	12.21	12.25	12.23	12.21	12.18
		0.56	12.43	12.46	12.44	12.48	12.46	12.44	12.41
	0.63	0.02	2.93	2.97	2.99	2.96	2.96	2.98	2.95
		0.05	7.54	7.61	7.65	7.61	7.59	7.65	7.56
		0.08	9.07	9.16	9.19	9.17	9.12	9.18	9.08
		0.14	9.88	9.97	9.97	9.98	9.93	9.96	9.87
		0.20	10.61	10.68	10.67	10.69	10.64	10.66	10.58
		0.26	11.26	11.33	11.32	11.33	11.29	11.30	11.23
		0.32	11.85	11.91	11.90	11.91	11.88	11.88	11.82
		0.35	12.12	12.17	12.16	12.17	12.14	12.15	12.09
		0.37	12.24	12.29	12.28	12.29	12.26	12.27	12.21
		0.38	12.36	12.40	12.40	12.40	12.38	12.38	12.32
		0.41	12.57	12.62	12.61	12.62	12.60	12.60	12.54
		0.44	12.77	12.81	12.80	12.81	12.79	12.79	12.74
		0.47	12.94	12.98	12.97	12.98	12.96	12.96	12.91
		0.48	12.97	13.01	13.00	13.02	13.00	12.99	12.95
		0.50	13.09	13.13	13.13	13.14	13.12	13.12	13.07
	0.79	0.02	3.11	3.06	3.07	3.09	3.05	3.13	3.00
		0.05	7.96	7.85	7.89	7.95	7.84	8.03	7.73
		0.08	9.55	9.44	9.49	9.57	9.45	9.61	9.36
		0.14	10.36	10.31	10.33	10.41	10.31	10.35	10.27
		0.20	11.10	11.08	11.08	11.16	11.07	11.08	11.06
		0.26	11.79	11.78	11.77	11.83	11.76	11.76	11.76
		0.32	12.40	12.41	12.39	12.45	12.38	12.38	12.39
		0.35	12.68	12.69	12.67	12.72	12.66	12.66	12.67
		0.37	12.81	12.81	12.79	12.85	12.79	12.78	12.80
		0.38	12.93	12.94	12.92	12.97	12.91	12.91	12.92
		0.41	13.15	13.17	13.15	13.19	13.14	13.14	13.15
		0.44	13.36	13.37	13.36	13.40	13.35	13.34	13.36
		0.46	13.45	13.47	13.45	13.49	13.44	13.44	13.45
		0.47	13.54	13.55	13.54	13.58	13.53	13.52	13.54

Table C.1 (Cont.) Velocity at values of coefficient C_2 between 1.70-1.76 in the Realisable k-v model

Discharge (m³/s)	$\frac{iL}{L\cos_n}$	Depth normal to the pseudo-bottom (m)	Velocity (m/s) at various values of coefficient C_2						
			C_2=1.70	C_2=1.71	C_2=1.72	C_2=1.73	C_2=1.74	C_2=1.75	C_2=1.76
3.28	0.16	0.02	2.06	2.14	1.97	1.97	2.04	2.00	2.08
		0.05	5.28	5.47	5.04	5.07	5.22	5.13	5.35
		0.08	6.30	6.57	6.10	6.16	6.31	6.24	6.44
		0.14	6.82	7.09	6.73	6.80	6.91	6.92	6.98
		0.20	7.33	7.52	7.24	7.30	7.40	7.46	7.43
		0.26	7.79	7.91	7.70	7.75	7.84	7.92	7.84
		0.29	8.00	8.09	7.91	7.95	8.04	8.13	8.03
		0.32	8.19	8.26	8.10	8.15	8.22	8.32	8.21
		0.35	8.36	8.41	8.28	8.32	8.40	8.49	8.37
		0.38	8.50	8.55	8.45	8.48	8.55	8.64	8.52
		0.41	8.64	8.68	8.60	8.63	8.69	8.78	8.65
		0.44	8.74	8.78	8.71	8.74	8.79	8.87	8.75
		0.44	8.76	8.80	8.73	8.76	8.82	8.90	8.78
		0.47	8.87	8.90	8.85	8.88	8.92	9.00	8.88
		0.50	8.96	8.99	8.95	8.98	9.02	9.09	8.98
		0.51	8.99	9.02	8.98	9.01	9.05	9.11	9.00
	0.31	0.02	2.61	2.57	2.57	2.57	2.55	2.64	2.59
		0.05	6.68	6.61	6.60	6.60	6.56	6.76	6.64
		0.08	7.98	7.95	7.92	7.93	7.89	8.07	7.98
		0.14	8.57	8.61	8.55	8.57	8.56	8.64	8.62
		0.20	9.11	9.17	9.11	9.13	9.13	9.18	9.17
		0.26	9.61	9.68	9.62	9.64	9.65	9.67	9.67
		0.29	9.84	9.91	9.85	9.88	9.88	9.91	9.91
		0.32	10.06	10.13	10.07	10.10	10.10	10.12	10.12
		0.35	10.26	10.33	10.28	10.30	10.31	10.32	10.32
		0.38	10.44	10.51	10.46	10.48	10.49	10.50	10.50
		0.38	10.46	10.53	10.48	10.50	10.51	10.52	10.52
		0.41	10.60	10.67	10.62	10.65	10.65	10.66	10.66
		0.44	10.75	10.82	10.77	10.80	10.80	10.81	10.81
		0.47	10.87	10.94	10.89	10.91	10.92	10.93	10.92
		0.47	10.89	10.95	10.91	10.93	10.93	10.94	10.94
	0.63	0.02	3.00	3.04	2.96	3.00	2.99	2.97	3.01
		0.05	7.69	7.78	7.61	7.71	7.69	7.63	7.71
		0.08	9.24	9.33	9.15	9.25	9.25	9.20	9.25
		0.14	10.03	10.09	9.96	10.03	10.07	10.04	10.04
		0.20	10.77	10.81	10.71	10.76	10.80	10.79	10.77
		0.26	11.45	11.48	11.40	11.44	11.48	11.47	11.45
		0.32	12.06	12.08	12.03	12.05	12.09	12.08	12.07
		0.38	12.59	12.61	12.57	12.58	12.61	12.61	12.60
		0.38	12.59	12.61	12.57	12.58	12.61	12.61	12.60
		0.41	12.82	12.84	12.80	12.82	12.84	12.84	12.83
		0.41	12.85	12.86	12.82	12.84	12.86	12.86	12.85
		0.44	13.03	13.05	13.01	13.03	13.05	13.05	13.04
		0.47	13.22	13.23	13.21	13.22	13.24	13.24	13.23
		0.50	13.39	13.40	13.38	13.39	13.41	13.41	13.40
		0.51	13.41	13.42	13.39	13.40	13.42	13.43	13.42
	0.79	0.02	3.07	3.15	3.10	3.15	3.11	3.20	3.08
		0.05	7.91	8.05	7.96	8.07	8.01	8.17	7.91
		0.08	9.54	9.67	9.59	9.68	9.66	9.78	9.54
		0.14	10.43	10.52	10.47	10.51	10.52	10.58	10.44
		0.20	11.23	11.30	11.26	11.29	11.30	11.33	11.25
		0.26	11.96	12.02	11.99	12.02	12.02	12.04	11.99
		0.32	12.63	12.67	12.65	12.67	12.68	12.68	12.65
		0.38	13.20	13.24	13.22	13.23	13.24	13.25	13.23
		0.41	13.41	13.44	13.43	13.44	13.44	13.45	13.43
		0.41	13.45	13.49	13.47	13.48	13.49	13.49	13.48
		0.44	13.68	13.72	13.70	13.71	13.71	13.72	13.70
		0.47	13.89	13.92	13.90	13.91	13.92	13.92	13.91
		0.48	13.96	13.99	13.98	13.98	13.99	14.00	13.98
		0.50	14.07	14.10	14.09	14.09	14.10	14.10	14.09
		0.53	14.24	14.26	14.25	14.25	14.26	14.26	14.25

Table C.2 Velocity at values of coefficient C_2 between 1.77-1.83 in the Realisable k-ν model

Discharge (m³/s)	$\dfrac{iL}{L\cos_n}$	Depth normal to the pseudo-bottom (m)	Velocity (m/s) at various values of coefficient C_2						
			C_2=1.77	C_2=1.78	C_2=1.79	C_2=1.80	C_2=1.81	C_2=1.82	C_2=1.83
0.57	0.16	0.02	1.73	1.71	1.73	1.67	1.76	1.76	1.74
		0.08	5.32	5.23	5.29	5.18	5.40	5.35	5.32
		0.14	5.65	5.57	5.63	5.64	5.81	5.65	5.63
		0.17	5.81	5.73	5.79	5.82	5.97	5.79	5.78
		0.20	5.92	5.85	5.90	5.94	6.08	5.90	5.89
		0.26	6.08	6.02	6.05	6.12	6.25	6.06	6.06
		0.32	6.13	6.08	6.09	6.18	6.29	6.10	6.11
		0.38	5.88	5.83	5.84	5.82	5.85	5.84	5.89
	0.31	0.02	2.00	1.94	1.86	2.08	2.01	1.95	1.84
		0.05	5.16	5.00	4.79	5.31	5.17	4.98	4.75
		0.08	6.12	5.95	5.71	6.36	6.12	5.96	5.66
		0.11	6.29	6.12	5.89	6.63	6.25	6.19	5.83
		0.14	6.42	6.27	6.05	6.82	6.36	6.37	5.99
		0.17	6.53	6.39	6.20	6.98	6.46	6.52	6.14
		0.17	6.55	6.42	6.22	7.01	6.48	6.55	6.16
		0.20	6.61	6.49	6.31	7.09	6.53	6.63	6.25
		0.30	6.67	6.63	6.46	7.17	6.64	6.73	6.42
	0.47	0.02	1.89	1.91	1.85	2.17	1.97	1.97	1.83
		0.05	5.33	5.38	5.22	6.09	5.53	5.54	5.16
		0.11	5.98	6.23	5.89	6.96	6.17	6.29	5.83
		0.15	6.14	6.45	6.06	7.13	6.31	6.49	6.00
		0.17	6.25	6.59	6.19	7.24	6.42	6.63	6.13
		0.23	6.40	6.80	6.37	7.35	6.58	6.85	6.32
		0.27	6.44	6.85	6.42	7.39	6.61	6.90	6.37
		0.30	6.47	6.83	6.44	7.35	6.62	6.94	6.39
	0.63	0.02	2.03	2.03	2.03	2.18	1.88	2.00	1.80
		0.05	5.23	5.20	5.22	5.61	4.84	5.14	4.63
		0.08	6.22	6.24	6.18	6.75	5.76	6.11	5.52
		0.11	6.38	6.48	6.32	7.04	5.94	6.27	5.72
		0.14	6.51	6.67	6.43	7.22	6.12	6.41	5.90
		0.14	6.51	6.67	6.43	7.22	6.12	6.41	5.90
		0.17	6.62	6.84	6.52	7.36	6.28	6.53	6.06
		0.20	6.70	6.95	6.59	7.45	6.41	6.62	6.19
		0.30	6.80	7.07	6.67	7.54	6.63	6.75	6.39
	0.79	0.02	1.93	2.04	1.98	2.17	1.89	1.95	2.02
		0.05	4.95	5.24	5.09	5.56	4.86	5.01	5.19
		0.08	5.92	6.20	6.05	6.68	5.77	5.93	6.17
		0.11	6.14	6.35	6.22	6.97	5.93	6.07	6.34
		0.12	6.20	6.39	6.27	7.04	5.97	6.12	6.38
		0.14	6.31	6.46	6.38	7.16	6.07	6.20	6.48
		0.17	6.45	6.56	6.51	7.31	6.19	6.31	6.60
		0.20	6.56	6.63	6.61	7.41	6.29	6.39	6.70
		0.23	6.64	6.68	6.69	7.47	6.36	6.45	6.77
		0.23	6.64	6.68	6.69	7.47	6.36	6.46	6.77

Table C.2 (Cont.) Velocity at values of coefficient C_2 between 1.77-1.83 in the Realisable k-v model

Discharge (m³/s)	$\dfrac{iL}{L\cos_n}$	Depth normal to the pseudo-bottom (m)	Velocity (m/s) at various values of coefficient C_2						
			C_2=1.77	C_2=1.78	C_2=1.79	C_2=1.80	C_2=1.81	C_2=1.82	C_2=1.83
1.13	0.16	0.02	1.82	1.82	1.82	1.86	1.82	1.75	1.85
		0.08	5.62	5.65	5.64	5.76	5.63	5.44	5.70
		0.14	6.16	6.16	6.18	6.25	6.16	6.03	6.18
		0.20	6.59	6.55	6.59	6.61	6.58	6.49	6.56
		0.23	6.77	6.72	6.77	6.77	6.76	6.68	6.72
		0.26	6.92	6.87	6.93	6.92	6.92	6.85	6.87
		0.31	7.17	7.12	7.18	7.15	7.17	7.12	7.12
		0.32	7.20	7.14	7.20	7.17	7.19	7.15	7.14
		0.38	7.41	7.35	7.41	7.38	7.41	7.37	7.35
	0.31	0.02	2.42	2.32	2.44	2.42	2.37	2.36	2.42
		0.05	6.19	5.95	6.23	6.19	6.07	6.06	6.20
		0.08	7.42	7.18	7.46	7.40	7.30	7.30	7.41
		0.11	7.72	7.52	7.77	7.69	7.63	7.65	7.69
		0.14	7.96	7.79	8.01	7.93	7.88	7.91	7.92
		0.17	8.18	8.03	8.21	8.14	8.10	8.14	8.13
		0.23	8.55	8.43	8.57	8.50	8.47	8.52	8.50
		0.26	8.70	8.60	8.71	8.65	8.63	8.67	8.66
		0.29	8.84	8.75	8.85	8.79	8.78	8.81	8.80
		0.40	9.17	9.09	9.15	9.10	9.11	9.13	9.11
	0.47	0.02	8.06	7.92	8.07	8.03	8.06	8.18	8.01
		0.05	8.45	8.32	8.46	8.42	8.44	8.56	8.40
		0.11	8.96	8.84	8.97	8.94	8.95	9.05	8.92
		0.17	9.35	9.25	9.36	9.33	9.35	9.42	9.32
		0.22	9.57	9.47	9.58	9.55	9.57	9.62	9.55
		0.23	9.62	9.53	9.63	9.60	9.62	9.67	9.61
		0.30	9.75	9.66	9.76	9.71	9.75	9.77	9.74
		0.36	9.54	9.49	9.54	9.50	9.55	9.54	9.54
		0.36	9.49	9.45	9.50	9.46	9.50	9.50	9.50
	0.63	0.02	2.56	2.56	2.69	2.51	2.66	2.61	2.52
		0.05	6.57	6.57	6.91	6.43	6.80	6.69	6.45
		0.08	7.89	7.92	8.23	7.76	8.12	8.03	7.78
		0.11	8.22	8.29	8.50	8.16	8.42	8.37	8.16
		0.14	8.51	8.58	8.74	8.48	8.69	8.65	8.47
		0.17	8.78	8.84	8.97	8.76	8.93	8.90	8.75
		0.20	9.02	9.08	9.18	9.01	9.16	9.13	8.99
		0.22	9.18	9.23	9.32	9.17	9.31	9.28	9.15
		0.23	9.24	9.29	9.38	9.23	9.36	9.34	9.21
		0.26	9.43	9.47	9.54	9.42	9.54	9.52	9.40
		0.29	9.59	9.62	9.69	9.59	9.69	9.67	9.57
		0.32	9.73	9.75	9.81	9.72	9.81	9.79	9.71
		0.32	9.74	9.76	9.82	9.74	9.83	9.80	9.72
	0.79	0.02	2.62	2.61	2.58	2.63	2.73	2.51	2.68
		0.05	6.69	6.71	6.64	6.73	6.97	6.41	6.86
		0.08	8.02	8.05	8.02	8.10	8.27	7.77	8.23
		0.11	8.35	8.38	8.40	8.46	8.52	8.20	8.58
		0.14	8.63	8.66	8.70	8.75	8.76	8.55	8.85
		0.17	8.88	8.91	8.97	9.01	8.98	8.85	9.09
		0.18	9.00	9.03	9.09	9.12	9.09	8.98	9.20
		0.20	9.12	9.14	9.20	9.23	9.19	9.11	9.30
		0.23	9.33	9.36	9.41	9.43	9.39	9.34	9.49
		0.26	9.51	9.54	9.59	9.60	9.56	9.53	9.66
		0.29	9.67	9.69	9.74	9.75	9.70	9.70	9.80
		0.30	9.73	9.76	9.81	9.81	9.76	9.77	9.86

Table C.2 (Cont.) Velocity at values of coefficient C_2 between 1.77-1.83 in the Realisable k-ν model

Discharge (m³/s)	$\dfrac{iL}{L\cos_n}$	Depth normal to the pseudo-bottom (m)	Velocity (m/s) at various values of coefficient C_2						
			C_2=1.77	C_2=1.78	C_2=1.79	C_2=1.80	C_2=1.81	C_2=1.82	C_2=1.83
1.70	0.16	0.02	1.97	1.94	1.95	1.88	1.84	1.89	1.89
		0.05	5.03	4.97	4.99	4.81	4.74	4.84	4.84
		0.08	6.02	5.99	6.00	5.82	5.79	5.85	5.80
		0.14	6.49	6.52	6.51	6.40	6.44	6.44	6.27
		0.20	6.89	6.95	6.91	6.84	6.91	6.90	6.73
		0.26	7.24	7.31	7.25	7.21	7.29	7.28	7.14
		0.27	7.31	7.38	7.32	7.28	7.36	7.35	7.22
		0.32	7.55	7.62	7.55	7.52	7.61	7.60	7.48
		0.38	7.80	7.86	7.80	7.78	7.86	7.85	7.75
		0.40	7.86	7.92	7.85	7.83	7.91	7.90	7.81
	0.31	0.02	2.47	2.51	2.53	2.49	2.52	2.54	2.45
		0.05	6.32	6.44	6.50	6.40	6.46	6.51	6.29
		0.08	7.57	7.71	7.80	7.68	7.74	7.78	7.54
		0.14	8.16	8.29	8.39	8.25	8.30	8.32	8.11
		0.20	8.66	8.76	8.85	8.73	8.77	8.78	8.60
		0.23	8.89	8.97	9.06	8.94	8.98	8.99	8.83
		0.26	9.10	9.17	9.25	9.14	9.18	9.19	9.03
		0.29	9.29	9.36	9.43	9.33	9.36	9.38	9.23
		0.30	9.33	9.39	9.46	9.36	9.40	9.41	9.27
		0.32	9.47	9.53	9.59	9.50	9.53	9.55	9.41
		0.35	9.63	9.69	9.74	9.66	9.69	9.70	9.57
		0.36	9.68	9.73	9.78	9.70	9.73	9.74	9.62
	0.47	0.02	2.63	2.70	2.68	2.65	2.71	2.55	2.65
		0.04	6.03	6.20	6.14	6.08	6.23	5.88	6.09
		0.08	8.11	8.34	8.25	8.21	8.36	7.97	8.19
		0.14	8.82	9.06	8.96	8.93	9.05	8.75	8.88
		0.20	9.42	9.62	9.54	9.51	9.60	9.39	9.46
		0.26	9.94	10.11	10.04	10.02	10.08	9.94	9.97
		0.31	10.31	10.45	10.40	10.37	10.42	10.31	10.32
		0.32	10.39	10.52	10.48	10.45	10.50	10.40	10.40
		0.38	10.75	10.85	10.83	10.79	10.83	10.76	10.74
		0.41	10.87	10.96	10.94	10.90	10.94	10.87	10.85
		0.44	11.01	11.09	11.08	11.03	11.08	11.02	10.99
	0.63	0.02	2.83	2.79	2.80	2.81	2.74	2.78	2.74
		0.05	7.27	7.16	7.20	7.21	7.05	7.11	7.05
		0.08	8.70	8.59	8.65	8.65	8.50	8.53	8.49
		0.14	9.34	9.30	9.34	9.31	9.25	9.23	9.20
		0.20	9.92	9.90	9.94	9.91	9.90	9.86	9.82
		0.23	10.19	10.18	10.22	10.19	10.19	10.15	10.10
		0.26	10.44	10.44	10.47	10.44	10.45	10.41	10.36
		0.29	10.66	10.66	10.69	10.66	10.68	10.63	10.58
		0.29	10.68	10.69	10.71	10.68	10.70	10.65	10.60
		0.32	10.90	10.91	10.93	10.90	10.92	10.87	10.82
		0.35	11.09	11.11	11.12	11.09	11.12	11.07	11.02
		0.38	11.26	11.28	11.28	11.26	11.29	11.24	11.19
		0.40	11.33	11.36	11.36	11.33	11.37	11.32	11.27
	0.79	0.02	2.89	2.89	2.82	2.89	2.84	2.89	2.79
		0.05	7.39	7.40	7.25	7.40	7.29	7.38	7.18
		0.08	8.83	8.86	8.72	8.85	8.75	8.83	8.63
		0.14	9.51	9.57	9.46	9.52	9.48	9.50	9.36
		0.20	10.13	10.17	10.10	10.13	10.11	10.10	10.00
		0.23	10.41	10.46	10.40	10.41	10.41	10.39	10.30
		0.26	10.65	10.69	10.64	10.64	10.65	10.62	10.54
		0.26	10.67	10.71	10.66	10.67	10.67	10.65	10.57
		0.29	10.92	10.96	10.91	10.91	10.92	10.89	10.82
		0.32	11.14	11.18	11.14	11.13	11.15	11.11	11.05
		0.35	11.34	11.37	11.34	11.32	11.35	11.31	11.25
		0.36	11.39	11.42	11.39	11.37	11.40	11.36	11.30

Table C.2 (Cont.) Velocity at values of coefficient C_2 between 1.77-1.83 in the
Realisable k-v model

Discharge (m³/s)	$\dfrac{iL}{L\cos_n}$	Depth normal to the pseudo-bottom (m)	Velocity (m/s) at various values of coefficient C_2						
			C_2=1.77	C_2=1.78	C_2=1.79	C_2=1.80	C_2=1.81	C_2=1.82	C_2=1.83
2.27	0.16	0.02	2.00	2.03	1.94	2.02	1.97	2.07	1.94
		0.05	5.12	5.21	4.98	5.19	5.06	5.29	5.00
		0.08	6.09	6.30	6.07	6.28	6.12	6.34	6.05
		0.14	6.52	6.85	6.73	6.86	6.70	6.82	6.63
		0.20	6.98	7.28	7.21	7.30	7.16	7.21	7.08
		0.26	7.41	7.64	7.59	7.66	7.56	7.56	7.47
		0.29	7.60	7.81	7.76	7.82	7.73	7.71	7.64
		0.32	7.77	7.96	7.92	7.97	7.89	7.86	7.80
		0.35	7.92	8.09	8.06	8.10	8.04	8.00	7.95
		0.36	7.95	8.12	8.09	8.12	8.07	8.02	7.98
		0.38	8.04	8.20	8.17	8.21	8.15	8.11	8.07
		0.38	8.06	8.21	8.18	8.22	8.17	8.12	8.08
	0.31	0.02	2.45	2.50	2.55	2.48	2.49	2.59	2.51
		0.05	6.31	6.41	6.54	6.39	6.39	6.61	6.44
		0.08	7.59	7.69	7.92	7.70	7.66	7.87	7.72
		0.14	8.22	8.32	8.64	8.36	8.29	8.41	8.34
		0.20	8.76	8.85	9.15	8.91	8.83	8.90	8.86
		0.26	9.24	9.34	9.57	9.39	9.31	9.36	9.33
		0.29	9.46	9.55	9.76	9.61	9.54	9.57	9.55
		0.32	9.66	9.76	9.94	9.81	9.74	9.77	9.75
		0.34	9.81	9.91	10.07	9.96	9.89	9.91	9.90
		0.35	9.85	9.94	10.10	9.99	9.93	9.95	9.93
		0.38	10.01	10.11	10.24	10.15	10.09	10.10	10.09
		0.41	10.01	10.11	10.24	10.15	10.09	10.10	10.09
		0.47	10.41	10.49	10.58	10.52	10.48	10.48	10.47
	0.47	0.02	2.69	2.71	2.71	2.76	2.68	2.75	2.69
		0.04	6.16	6.24	6.22	6.33	6.18	6.31	6.20
		0.08	8.27	8.38	8.42	8.50	8.34	8.44	8.37
		0.14	8.99	9.10	9.22	9.19	9.09	9.12	9.13
		0.20	9.63	9.74	9.87	9.80	9.74	9.74	9.77
		0.26	10.21	10.32	10.43	10.36	10.32	10.31	10.33
		0.32	10.72	10.82	10.92	10.85	10.82	10.80	10.83
		0.36	10.98	11.09	11.18	11.11	11.09	11.07	11.09
		0.38	11.14	11.24	11.34	11.26	11.24	11.22	11.24
		0.44	11.47	11.56	11.65	11.58	11.56	11.54	11.56
		0.44	11.48	11.58	11.66	11.59	11.58	11.55	11.57
		0.50	11.74	11.83	11.91	11.84	11.83	11.80	11.82
	0.63	0.02	2.89	2.88	2.88	2.92	2.86	2.86	2.80
		0.05	7.44	7.37	7.39	7.51	7.36	7.35	7.20
		0.08	8.92	8.86	8.89	9.01	8.87	8.84	8.70
		0.14	9.65	9.64	9.67	9.72	9.65	9.59	9.54
		0.20	10.30	10.32	10.35	10.37	10.33	10.27	10.26
		0.26	10.91	10.93	10.97	10.97	10.94	10.89	10.90
		0.29	11.18	11.21	11.26	11.25	11.22	11.17	11.18
		0.32	11.44	11.48	11.52	11.50	11.48	11.44	11.45
		0.32	11.44	11.48	11.52	11.50	11.48	11.44	11.45
		0.33	11.52	11.55	11.60	11.58	11.55	11.52	11.52
		0.35	11.68	11.72	11.76	11.74	11.72	11.68	11.69
		0.38	11.89	11.93	11.98	11.95	11.93	11.90	11.90
		0.41	12.08	12.12	12.17	12.14	12.12	12.09	12.09
		0.42	12.15	12.19	12.24	12.21	12.19	12.16	12.16
		0.44	12.25	12.29	12.34	12.31	12.29	12.26	12.26
		0.47	12.39	12.43	12.48	12.45	12.43	12.40	12.41
	0.79	0.02	2.98	2.95	2.98	3.01	3.03	3.02	3.01
		0.05	7.65	7.59	7.64	7.71	7.75	7.73	7.70
		0.08	9.19	9.14	9.20	9.23	9.28	9.23	9.23
		0.14	9.96	9.94	10.00	9.97	10.02	9.96	9.98
		0.20	10.65	10.66	10.71	10.66	10.70	10.64	10.67
		0.26	11.29	11.30	11.35	11.29	11.33	11.27	11.30
		0.29	11.58	11.59	11.64	11.59	11.62	11.57	11.59
		0.32	11.85	11.87	11.91	11.86	11.89	11.84	11.86
		0.32	11.87	11.89	11.93	11.88	11.91	11.86	11.89
		0.35	12.10	12.11	12.16	12.11	12.14	12.09	12.11
		0.38	12.31	12.33	12.38	12.33	12.35	12.31	12.33
		0.41	12.51	12.53	12.57	12.52	12.55	12.50	12.52
		0.42	12.56	12.58	12.62	12.58	12.60	12.56	12.58
		0.44	12.68	12.70	12.74	12.70	12.72	12.68	12.70
		0.47	12.82	12.85	12.89	12.84	12.86	12.83	12.84

Table C.2 (Cont.) Velocity at values of coefficient C_2 between 1.77-1.83 in the Realisable k-v model

Discharge (m³/s)	$\dfrac{iL}{L\cos{}_{\textit{n}}}$	Depth normal to the pseudo-bottom (m)	Velocity (m/s) at various values of coefficient C_2						
			C_2=1.77	C_2=1.78	C_2=1.79	C_2=1.80	C_2=1.81	C_2=1.82	C_2=1.83
2.83	0.16	0.02	1.95	1.99	2.09	2.15	2.01	2.00	1.94
		0.05	5.01	5.10	5.34	5.49	5.16	5.13	4.99
		0.08	6.07	6.15	6.42	6.55	6.23	6.19	6.09
		0.14	6.66	6.73	6.99	7.01	6.82	6.79	6.79
		0.20	7.14	7.19	7.44	7.40	7.32	7.29	7.31
		0.26	7.57	7.59	7.83	7.76	7.74	7.73	7.75
		0.29	7.77	7.78	8.00	7.92	7.94	7.92	7.94
		0.32	7.96	7.96	8.16	8.08	8.11	8.10	8.12
		0.35	8.12	8.12	8.31	8.23	8.27	8.27	8.28
		0.38	8.27	8.27	8.44	8.35	8.41	8.41	8.42
		0.40	8.37	8.37	8.53	8.44	8.51	8.50	8.51
		0.41	8.41	8.41	8.56	8.47	8.54	8.54	8.55
		0.44	8.53	8.53	8.67	8.58	8.65	8.65	8.66
		0.47	8.63	8.62	8.75	8.66	8.74	8.74	8.74
	0.31	0.02	2.56	2.63	2.58	2.52	2.52	2.61	2.59
		0.05	6.56	6.73	6.63	6.48	6.48	6.66	6.65
		0.08	7.87	8.03	8.01	7.79	7.81	7.95	7.96
		0.14	8.48	8.59	8.70	8.45	8.50	8.53	8.57
		0.20	9.01	9.11	9.24	9.01	9.06	9.06	9.09
		0.26	9.50	9.58	9.70	9.52	9.56	9.55	9.57
		0.29	9.72	9.80	9.91	9.75	9.78	9.77	9.79
		0.32	9.94	10.00	10.11	9.96	9.99	9.98	10.00
		0.35	10.13	10.19	10.29	10.16	10.18	10.18	10.19
		0.38	10.29	10.34	10.43	10.31	10.33	10.33	10.34
		0.38	10.30	10.35	10.45	10.33	10.35	10.35	10.35
		0.41	10.46	10.50	10.60	10.49	10.50	10.50	10.51
		0.44	10.60	10.64	10.73	10.63	10.64	10.64	10.65
		0.47	10.73	10.76	10.84	10.75	10.76	10.76	10.77
	0.47	0.02	2.79	2.82	2.74	2.77	2.71	2.78	2.80
		0.04	6.41	6.48	6.30	6.35	6.24	6.40	6.44
		0.08	8.61	8.68	8.50	8.52	8.43	8.58	8.63
		0.14	9.31	9.37	9.29	9.24	9.24	9.29	9.33
		0.20	9.95	10.01	9.97	9.90	9.93	9.94	9.97
		0.26	10.54	10.59	10.58	10.50	10.54	10.54	10.55
		0.32	11.07	11.12	11.12	11.04	11.08	11.06	11.08
		0.38	11.52	11.56	11.57	11.50	11.54	11.51	11.53
		0.40	11.62	11.66	11.68	11.61	11.64	11.62	11.63
		0.44	11.89	11.93	11.94	11.88	11.91	11.89	11.90
		0.49	12.14	12.18	12.20	12.13	12.16	12.14	12.15
		0.50	12.19	12.22	12.24	12.18	12.21	12.18	12.20
		0.56	12.42	12.45	12.47	12.41	12.44	12.42	12.43
	0.63	0.02	2.93	2.96	3.00	2.89	2.99	2.97	2.93
		0.05	7.54	7.59	7.69	7.44	7.67	7.60	7.55
		0.08	9.08	9.12	9.21	8.98	9.20	9.10	9.10
		0.14	9.87	9.90	9.97	9.81	9.96	9.87	9.90
		0.20	10.58	10.62	10.67	10.55	10.65	10.58	10.62
		0.26	11.24	11.28	11.32	11.22	11.29	11.24	11.27
		0.32	11.83	11.87	11.91	11.82	11.87	11.83	11.86
		0.35	12.09	12.14	12.17	12.09	12.14	12.10	12.12
		0.37	12.21	12.26	12.29	12.21	12.26	12.22	12.24
		0.38	12.33	12.38	12.41	12.33	12.37	12.34	12.36
		0.41	12.55	12.60	12.62	12.55	12.59	12.56	12.58
		0.44	12.74	12.79	12.82	12.75	12.78	12.76	12.77
		0.47	12.92	12.96	12.99	12.92	12.95	12.93	12.94
		0.48	12.95	13.00	13.02	12.96	12.98	12.96	12.97
		0.50	13.07	13.12	13.14	13.08	13.11	13.09	13.10
	0.79	0.02	3.06	3.04	3.11	3.07	3.07	3.04	3.16
		0.05	7.86	7.82	7.98	7.90	7.90	7.80	8.08
		0.08	9.46	9.43	9.58	9.49	9.50	9.40	9.65
		0.14	10.30	10.28	10.40	10.30	10.33	10.27	10.39
		0.20	11.06	11.04	11.13	11.05	11.07	11.03	11.10
		0.26	11.75	11.75	11.81	11.74	11.75	11.73	11.77
		0.32	12.37	12.38	12.42	12.36	12.37	12.36	12.38
		0.35	12.64	12.66	12.70	12.63	12.65	12.64	12.65
		0.37	12.77	12.79	12.82	12.76	12.78	12.77	12.78
		0.38	12.89	12.91	12.95	12.88	12.90	12.90	12.90
		0.41	13.12	13.14	13.17	13.11	13.13	13.12	13.13
		0.44	13.33	13.35	13.38	13.32	13.33	13.33	13.33
		0.46	13.43	13.45	13.47	13.42	13.43	13.43	13.43
		0.47	13.51	13.54	13.56	13.50	13.51	13.51	13.51

Table C.2 (Cont.) Velocity at values of coefficient C_2 between 1.77-1.83 in the
Realisable k-ν model

Discharge (m³/s)	$\dfrac{iL}{L\cos_n}$	Depth normal to the pseudo-bottom (m)	Velocity (m/s) at various values of coefficient C_2						
			C_2=1.77	C_2=1.78	C_2=1.79	C_2=1.80	C_2=1.81	C_2=1.82	C_2=1.83
3.28	0.16	0.02	2.11	2.09	2.02	2.12	2.06	2.06	2.08
		0.05	5.40	5.36	5.18	5.44	5.29	5.26	5.34
		0.08	6.50	6.46	6.25	6.54	6.37	6.30	6.46
		0.14	7.08	7.06	6.83	7.10	6.95	6.82	7.06
		0.20	7.56	7.55	7.31	7.57	7.46	7.28	7.55
		0.26	7.98	7.98	7.75	7.98	7.90	7.70	7.98
		0.29	8.16	8.17	7.95	8.17	8.09	7.90	8.17
		0.32	8.33	8.34	8.14	8.35	8.28	8.09	8.34
		0.35	8.49	8.50	8.31	8.50	8.44	8.27	8.50
		0.38	8.63	8.64	8.47	8.64	8.59	8.42	8.64
		0.41	8.76	8.77	8.61	8.77	8.73	8.57	8.77
		0.44	8.85	8.86	8.72	8.86	8.82	8.67	8.86
		0.44	8.88	8.88	8.74	8.88	8.85	8.70	8.88
		0.47	8.97	8.98	8.85	8.98	8.95	8.82	8.97
		0.50	9.06	9.07	8.95	9.06	9.04	8.92	9.06
		0.51	9.09	9.09	8.98	9.09	9.07	8.95	9.08
	0.31	0.02	2.60	2.62	2.55	2.60	2.61	2.64	2.59
		0.05	6.68	6.72	6.55	6.67	6.68	6.75	6.63
		0.08	8.00	8.05	7.88	7.98	8.01	8.05	7.97
		0.14	8.61	8.67	8.55	8.59	8.63	8.62	8.62
		0.20	9.16	9.21	9.12	9.15	9.18	9.14	9.17
		0.26	9.67	9.70	9.63	9.67	9.68	9.62	9.68
		0.29	9.90	9.93	9.87	9.90	9.91	9.85	9.91
		0.32	10.12	10.14	10.09	10.12	10.13	10.06	10.13
		0.35	10.33	10.34	10.29	10.32	10.32	10.26	10.33
		0.38	10.51	10.51	10.47	10.50	10.50	10.44	10.50
		0.38	10.52	10.53	10.49	10.52	10.52	10.45	10.52
		0.41	10.67	10.67	10.63	10.66	10.66	10.60	10.67
		0.44	10.82	10.82	10.78	10.81	10.81	10.75	10.81
		0.47	10.94	10.94	10.90	10.93	10.92	10.86	10.93
		0.47	10.95	10.95	10.91	10.94	10.94	10.88	10.94
	0.63	0.02	3.01	3.00	3.01	2.99	3.05	3.02	2.93
		0.05	7.71	7.70	7.73	7.68	7.80	7.72	7.53
		0.08	9.25	9.25	9.28	9.26	9.34	9.26	9.10
		0.14	10.03	10.04	10.06	10.07	10.10	10.03	9.98
		0.20	10.76	10.77	10.79	10.81	10.81	10.75	10.74
		0.26	11.43	11.45	11.46	11.48	11.48	11.43	11.42
		0.32	12.04	12.07	12.06	12.08	12.08	12.04	12.04
		0.38	12.57	12.60	12.59	12.61	12.60	12.57	12.57
		0.38	12.57	12.60	12.59	12.61	12.60	12.57	12.57
		0.41	12.81	12.83	12.82	12.84	12.83	12.80	12.80
		0.41	12.83	12.86	12.84	12.86	12.86	12.82	12.83
		0.44	13.02	13.05	13.03	13.05	13.04	13.01	13.02
		0.47	13.21	13.23	13.21	13.23	13.23	13.20	13.21
		0.50	13.39	13.41	13.38	13.40	13.40	13.37	13.38
		0.51	13.40	13.42	13.40	13.42	13.42	13.39	13.40
	0.79	0.02	3.13	3.15	3.08	3.13	3.10	3.12	3.16
		0.05	8.04	8.06	7.92	8.05	7.97	8.00	8.12
		0.08	9.67	9.70	9.55	9.68	9.61	9.61	9.72
		0.14	10.52	10.57	10.45	10.54	10.49	10.44	10.52
		0.20	11.29	11.35	11.26	11.32	11.27	11.22	11.28
		0.26	12.01	12.06	11.99	12.03	12.00	11.95	12.00
		0.32	12.67	12.71	12.65	12.68	12.65	12.60	12.65
		0.38	13.23	13.27	13.22	13.24	13.22	13.17	13.21
		0.41	13.43	13.47	13.42	13.44	13.43	13.37	13.41
		0.41	13.48	13.52	13.47	13.48	13.47	13.42	13.46
		0.44	13.71	13.74	13.70	13.71	13.70	13.64	13.69
		0.47	13.91	13.94	13.90	13.91	13.90	13.85	13.89
		0.48	13.98	14.02	13.97	13.98	13.98	13.92	13.96
		0.50	14.09	14.12	14.08	14.09	14.09	14.04	14.07
		0.53	14.25	14.28	14.25	14.25	14.25	14.20	14.23

Table C.3 Velocity at values of coefficient C_2 between 1.84-1.91 in the Realisable k-ᴠ model

Discharge (m³/s)	$\dfrac{iL}{L\cos{_{\textit{u}}}}$	Depth normal to the pseudo-bottom (m)	Velocity (m/s) at various values of coefficient C_2						
			C_2=1.84	C_2=1.85	C_2=1.86	C_2=1.87	C_2=1.88	C_2=1.89	C_2=1.91
0.57	0.16	0.02	1.74	1.67	1.69	1.72	1.70	1.70	1.71
		0.08	5.30	5.17	5.24	5.29	5.26	5.23	5.25
		0.14	5.61	5.60	5.71	5.63	5.69	5.58	5.64
		0.17	5.77	5.78	5.89	5.78	5.86	5.74	5.81
		0.20	5.88	5.89	6.00	5.89	5.97	5.86	5.93
		0.26	6.05	6.07	6.18	6.04	6.15	6.02	6.11
		0.32	6.10	6.14	6.24	6.08	6.20	6.06	6.16
		0.38	5.86	5.86	5.90	5.85	5.84	5.83	5.82
	0.31	0.02	2.06	2.01	2.11	1.84	2.01	1.81	1.96
		0.05	5.28	5.16	5.41	4.73	5.18	4.65	5.03
		0.08	6.28	6.14	6.44	5.62	6.28	5.55	5.99
		0.11	6.46	6.33	6.64	5.79	6.61	5.73	6.17
		0.14	6.59	6.48	6.80	5.95	6.82	5.90	6.34
		0.17	6.69	6.61	6.92	6.09	6.99	6.06	6.49
		0.17	6.71	6.63	6.94	6.11	7.02	6.08	6.52
		0.20	6.76	6.71	7.00	6.20	7.10	6.18	6.62
		0.30	6.80	6.80	7.08	6.37	7.16	6.36	6.79
	0.47	0.02	2.07	2.09	1.95	1.80	2.17	1.82	2.20
		0.05	5.82	5.87	5.46	5.09	6.07	5.11	6.17
		0.11	6.56	6.64	6.30	5.77	6.90	5.76	6.80
		0.15	6.72	6.81	6.51	5.95	7.06	5.93	6.89
		0.17	6.82	6.93	6.65	6.08	7.17	6.06	6.94
		0.23	6.96	7.09	6.85	6.28	7.31	6.26	7.00
		0.27	6.98	7.12	6.91	6.33	7.35	6.31	7.00
		0.30	6.97	7.10	6.91	6.35	7.33	6.33	6.97
	0.63	0.02	2.07	2.07	2.04	1.80	2.12	1.91	1.93
		0.05	5.30	5.30	5.23	4.64	5.43	4.90	4.96
		0.08	6.33	6.33	6.25	5.54	6.48	5.81	5.89
		0.11	6.58	6.54	6.48	5.72	6.73	5.96	6.05
		0.14	6.76	6.70	6.65	5.89	6.91	6.10	6.19
		0.14	6.76	6.70	6.65	5.89	6.91	6.10	6.19
		0.17	6.92	6.82	6.79	6.04	7.06	6.22	6.32
		0.20	7.02	6.90	6.89	6.15	7.16	6.32	6.41
		0.30	7.14	7.00	6.99	6.32	7.27	6.45	6.56
	0.79	0.02	2.20	2.05	1.94	1.81	2.12	1.87	1.92
		0.05	5.66	5.23	4.98	4.65	5.43	4.82	4.93
		0.08	6.75	6.22	5.92	5.54	6.51	5.73	5.85
		0.11	6.95	6.41	6.09	5.72	6.76	5.90	6.01
		0.12	7.00	6.46	6.14	5.77	6.83	5.95	6.06
		0.14	7.09	6.56	6.24	5.88	6.94	6.05	6.15
		0.17	7.19	6.70	6.38	6.03	7.09	6.18	6.28
		0.20	7.24	6.80	6.50	6.14	7.19	6.29	6.39
		0.23	7.27	6.87	6.59	6.23	7.26	6.37	6.46
		0.23	7.27	6.87	6.59	6.24	7.27	6.38	6.47

Table C.3 (Cont.) Velocity at values of coefficient C_2 between 1.84-1.91 in the Realisable k-v model

Discharge (m³/s)	$\dfrac{iL}{L\cos_n}$	Depth normal to the pseudo-bottom (m)	Velocity (m/s) at various values of coefficient C_2						
			C_2=1.84	C_2=1.85	C_2=1.86	C_2=1.87	C_2=1.88	C_2=1.89	C_2=1.91
1.13	0.16	0.02	1.84	2.04	1.84	1.88	1.77	1.77	1.83
		0.08	5.66	6.31	5.67	5.73	5.52	5.55	5.60
		0.14	6.17	6.73	6.18	6.19	6.10	6.13	6.10
		0.20	6.58	6.97	6.59	6.56	6.55	6.56	6.51
		0.23	6.76	7.07	6.76	6.72	6.73	6.74	6.69
		0.26	6.91	7.17	6.92	6.87	6.89	6.90	6.84
		0.31	7.16	7.33	7.16	7.11	7.15	7.16	7.10
		0.32	7.19	7.35	7.19	7.13	7.18	7.18	7.12
		0.38	7.40	7.48	7.40	7.34	7.39	7.39	7.33
	0.31	0.02	2.33	2.40	2.38	2.38	2.35	2.36	2.37
		0.05	5.99	6.15	6.09	6.10	6.03	6.06	6.07
		0.08	7.23	7.34	7.27	7.31	7.25	7.30	7.27
		0.11	7.57	7.62	7.54	7.60	7.57	7.63	7.55
		0.14	7.83	7.86	7.78	7.84	7.83	7.89	7.80
		0.17	8.07	8.08	8.00	8.06	8.06	8.11	8.01
		0.23	8.45	8.47	8.40	8.44	8.45	8.48	8.40
		0.26	8.62	8.64	8.57	8.60	8.61	8.63	8.56
		0.29	8.77	8.79	8.72	8.74	8.76	8.77	8.71
		0.40	9.10	9.13	9.07	9.07	9.10	9.10	9.05
	0.47	0.02	8.07	8.00	8.00	8.08	8.08	7.87	8.07
		0.05	8.44	8.37	8.39	8.45	8.46	8.27	8.44
		0.11	8.94	8.88	8.91	8.94	8.96	8.81	8.94
		0.17	9.32	9.26	9.30	9.32	9.34	9.23	9.31
		0.22	9.54	9.48	9.51	9.53	9.56	9.46	9.52
		0.23	9.59	9.53	9.57	9.58	9.61	9.52	9.57
		0.30	9.72	9.66	9.69	9.70	9.74	9.66	9.69
		0.36	9.52	9.47	9.49	9.48	9.50	9.47	9.47
		0.36	9.48	9.42	9.45	9.44	9.46	9.43	9.43
	0.63	0.02	2.63	2.65	2.54	2.60	2.50	2.58	2.53
		0.05	6.74	6.77	6.54	6.65	6.40	6.62	6.49
		0.08	8.08	8.07	7.87	7.95	7.73	7.95	7.83
		0.11	8.41	8.35	8.23	8.26	8.12	8.30	8.19
		0.14	8.69	8.60	8.53	8.54	8.44	8.58	8.49
		0.17	8.93	8.83	8.80	8.79	8.72	8.83	8.75
		0.20	9.14	9.05	9.04	9.03	8.97	9.05	8.99
		0.22	9.28	9.20	9.19	9.18	9.14	9.19	9.14
		0.23	9.34	9.25	9.25	9.24	9.20	9.25	9.20
		0.26	9.51	9.43	9.43	9.42	9.39	9.42	9.38
		0.29	9.66	9.59	9.60	9.58	9.56	9.58	9.54
		0.32	9.78	9.71	9.73	9.71	9.69	9.70	9.67
		0.32	9.79	9.73	9.74	9.72	9.70	9.71	9.68
	0.79	0.02	2.65	2.61	2.74	2.64	2.66	2.59	2.58
		0.05	6.80	6.68	7.02	6.79	6.82	6.66	6.61
		0.08	8.14	7.99	8.36	8.15	8.17	8.05	7.95
		0.11	8.45	8.31	8.64	8.48	8.49	8.44	8.31
		0.14	8.72	8.59	8.88	8.75	8.75	8.73	8.61
		0.17	8.96	8.84	9.11	8.98	8.99	8.98	8.88
		0.18	9.08	8.96	9.21	9.09	9.10	9.09	9.00
		0.20	9.18	9.07	9.31	9.20	9.20	9.19	9.12
		0.23	9.39	9.28	9.50	9.39	9.40	9.39	9.34
		0.26	9.55	9.46	9.65	9.56	9.56	9.55	9.52
		0.29	9.70	9.62	9.79	9.70	9.71	9.70	9.68
		0.30	9.76	9.69	9.84	9.77	9.77	9.76	9.75

Table C.3 (Cont.) Velocity at values of coefficient C_2 between 1.84-1.91 in the
Realisable k-v model

Discharge (m³/s)	$\dfrac{iL}{L\cos{_n}}$	Depth normal to the pseudo-bottom (m)	Velocity (m/s) at various values of coefficient C_2						
			C_2=1.84	C_2=1.85	C_2=1.86	C_2=1.87	C_2=1.88	C_2=1.89	C_2=1.91
1.70	0.16	0.02	2.01	1.91	2.03	1.93	1.98	1.90	1.90
		0.05	5.15	4.89	5.22	4.95	5.07	4.87	4.87
		0.08	6.18	5.91	6.24	5.97	6.07	5.89	5.88
		0.14	6.67	6.47	6.67	6.52	6.56	6.43	6.44
		0.20	7.06	6.92	7.02	6.95	6.96	6.86	6.87
		0.26	7.39	7.29	7.33	7.31	7.31	7.22	7.22
		0.27	7.45	7.36	7.39	7.37	7.37	7.29	7.28
		0.32	7.67	7.60	7.60	7.61	7.60	7.53	7.51
		0.38	7.90	7.85	7.83	7.85	7.84	7.78	7.75
		0.40	7.95	7.91	7.88	7.90	7.89	7.84	7.81
	0.31	0.02	2.51	2.47	2.43	2.49	2.44	2.49	2.47
		0.05	6.42	6.32	6.25	6.36	6.27	6.39	6.34
		0.08	7.67	7.59	7.52	7.61	7.57	7.65	7.64
		0.14	8.22	8.21	8.13	8.20	8.23	8.20	8.27
		0.20	8.70	8.71	8.64	8.70	8.73	8.67	8.76
		0.23	8.92	8.93	8.87	8.93	8.95	8.89	8.98
		0.26	9.13	9.14	9.08	9.13	9.15	9.09	9.17
		0.29	9.32	9.33	9.28	9.33	9.34	9.28	9.36
		0.30	9.36	9.37	9.32	9.37	9.37	9.32	9.40
		0.32	9.50	9.51	9.46	9.51	9.51	9.46	9.53
		0.35	9.66	9.67	9.63	9.67	9.67	9.62	9.68
		0.36	9.70	9.71	9.67	9.71	9.71	9.66	9.72
	0.47	0.02	2.64	2.64	2.67	2.67	2.66	2.64	2.70
		0.04	6.06	6.05	6.13	6.11	6.10	6.07	6.20
		0.08	8.13	8.12	8.23	8.20	8.20	8.15	8.28
		0.14	8.81	8.83	8.88	8.89	8.90	8.83	8.90
		0.20	9.40	9.43	9.45	9.48	9.48	9.42	9.48
		0.26	9.92	9.96	9.95	9.99	9.99	9.93	9.99
		0.31	10.28	10.32	10.31	10.35	10.35	10.29	10.34
		0.32	10.37	10.40	10.39	10.43	10.43	10.37	10.42
		0.38	10.73	10.76	10.74	10.78	10.78	10.73	10.77
		0.41	10.84	10.87	10.85	10.90	10.90	10.84	10.88
		0.44	10.99	11.01	10.99	11.04	11.03	10.98	11.02
	0.63	0.02	2.76	2.79	2.81	2.77	2.76	2.74	2.79
		0.05	7.08	7.14	7.19	7.12	7.11	7.02	7.17
		0.08	8.50	8.56	8.61	8.56	8.56	8.46	8.60
		0.14	9.19	9.25	9.29	9.26	9.31	9.20	9.28
		0.20	9.81	9.86	9.89	9.88	9.93	9.82	9.88
		0.23	10.10	10.14	10.17	10.16	10.21	10.11	10.16
		0.26	10.36	10.40	10.42	10.42	10.46	10.37	10.42
		0.29	10.58	10.62	10.63	10.65	10.68	10.59	10.63
		0.29	10.61	10.64	10.65	10.67	10.70	10.61	10.65
		0.32	10.83	10.87	10.87	10.89	10.92	10.83	10.87
		0.35	11.03	11.07	11.06	11.09	11.12	11.03	11.07
		0.38	11.20	11.23	11.23	11.26	11.28	11.19	11.23
		0.40	11.28	11.31	11.30	11.34	11.36	11.27	11.31
	0.79	0.02	2.82	2.79	2.85	2.84	2.86	2.81	2.83
		0.05	7.21	7.15	7.34	7.29	7.36	7.20	7.27
		0.08	8.67	8.62	8.82	8.76	8.85	8.68	8.73
		0.14	9.41	9.40	9.51	9.49	9.57	9.43	9.44
		0.20	10.04	10.06	10.11	10.10	10.17	10.05	10.06
		0.23	10.33	10.35	10.38	10.38	10.44	10.34	10.34
		0.26	10.57	10.59	10.61	10.61	10.67	10.57	10.58
		0.26	10.60	10.62	10.64	10.64	10.69	10.60	10.60
		0.29	10.85	10.86	10.87	10.88	10.93	10.84	10.85
		0.32	11.07	11.09	11.09	11.10	11.15	11.07	11.07
		0.35	11.27	11.29	11.29	11.30	11.34	11.27	11.27
		0.36	11.32	11.34	11.34	11.35	11.39	11.32	11.32

Table C.3 (Cont.) Velocity at values of coefficient C_2 between 1.84-1.91 in the Realisable k-v model

Discharge (m³/s)	$\dfrac{iL}{L\cos_n}$	Depth normal to the pseudo-bottom (m)	Velocity (m/s) at various values of coefficient C_2						
			C_2=1.84	C_2=1.85	C_2=1.86	C_2=1.87	C_2=1.88	C_2=1.89	C_2=1.91
2.27	0.16	1.96	2.10	1.96	1.97	1.96	2.03	1.97	1.96
		5.02	5.37	5.01	5.06	5.02	5.20	5.05	5.02
		6.09	6.41	6.05	6.11	6.07	6.27	6.10	6.09
		6.68	6.87	6.62	6.66	6.64	6.83	6.69	6.68
		7.14	7.27	7.09	7.12	7.09	7.26	7.14	7.14
		7.54	7.62	7.49	7.51	7.47	7.61	7.53	7.54
		7.71	7.78	7.67	7.69	7.65	7.77	7.70	7.71
		7.87	7.92	7.83	7.85	7.81	7.92	7.86	7.87
		8.02	8.06	7.98	8.00	7.95	8.05	8.01	8.02
		8.04	8.08	8.01	8.02	7.98	8.07	8.03	8.04
		8.13	8.16	8.10	8.11	8.07	8.15	8.12	8.13
		8.15	8.17	8.11	8.12	8.08	8.16	8.13	8.15
	0.31	2.55	2.53	2.50	2.48	2.49	2.51	2.48	2.55
		6.54	6.50	6.43	6.38	6.42	6.45	6.38	6.54
		7.82	7.80	7.74	7.66	7.72	7.76	7.67	7.82
		8.39	8.41	8.37	8.28	8.35	8.38	8.29	8.39
		8.90	8.93	8.90	8.81	8.87	8.91	8.83	8.90
		9.36	9.39	9.37	9.29	9.34	9.38	9.31	9.36
		9.57	9.60	9.58	9.51	9.55	9.59	9.52	9.57
		9.77	9.80	9.77	9.71	9.74	9.79	9.73	9.77
		9.92	9.95	9.92	9.86	9.89	9.94	9.88	9.92
		9.95	9.98	9.95	9.90	9.92	9.97	9.91	9.95
		10.11	10.14	10.11	10.06	10.08	10.13	10.07	10.11
		10.11	10.14	10.11	10.06	10.08	10.13	10.07	10.11
		10.49	10.51	10.48	10.45	10.46	10.50	10.46	10.49
	0.47	2.72	2.73	2.70	2.75	2.73	2.67	2.76	2.72
		6.26	6.29	6.20	6.30	6.25	6.14	6.34	6.26
		8.41	8.46	8.36	8.44	8.38	8.30	8.47	8.41
		9.13	9.18	9.12	9.11	9.08	9.09	9.12	9.13
		9.76	9.80	9.76	9.72	9.73	9.74	9.72	9.76
		10.33	10.35	10.32	10.28	10.30	10.31	10.29	10.33
		10.83	10.85	10.82	10.77	10.80	10.82	10.78	10.83
		11.09	11.11	11.09	11.04	11.06	11.08	11.05	11.09
		11.24	11.26	11.24	11.20	11.22	11.24	11.20	11.24
		11.56	11.57	11.56	11.52	11.53	11.55	11.52	11.56
		11.57	11.59	11.57	11.53	11.55	11.57	11.54	11.57
		11.82	11.83	11.82	11.79	11.80	11.82	11.79	11.82
	0.63	2.84	2.87	2.94	2.88	2.92	2.82	2.93	2.84
		7.31	7.36	7.51	7.41	7.48	7.24	7.50	7.31
		8.82	8.85	8.95	8.91	8.96	8.72	8.98	8.82
		9.62	9.62	9.63	9.65	9.67	9.53	9.68	9.62
		10.31	10.31	10.28	10.31	10.33	10.24	10.33	10.31
		10.93	10.93	10.89	10.91	10.93	10.87	10.93	10.93
		11.21	11.22	11.17	11.19	11.21	11.16	11.20	11.21
		11.47	11.48	11.43	11.44	11.46	11.43	11.46	11.47
		11.47	11.48	11.43	11.44	11.46	11.43	11.46	11.47
		11.55	11.56	11.50	11.52	11.54	11.50	11.54	11.55
		11.72	11.72	11.67	11.68	11.70	11.67	11.70	11.72
		11.93	11.94	11.88	11.89	11.91	11.89	11.91	11.93
		12.12	12.13	12.08	12.08	12.10	12.08	12.10	12.12
		12.19	12.20	12.15	12.15	12.17	12.15	12.17	12.19
		12.29	12.30	12.25	12.25	12.27	12.25	12.27	12.29
		12.43	12.44	12.39	12.39	12.41	12.40	12.41	12.43
	0.79	2.98	2.94	2.99	2.93	2.97	2.97	2.92	2.98
		7.65	7.55	7.69	7.54	7.62	7.64	7.51	7.65
		9.19	9.09	9.23	9.08	9.16	9.18	9.04	9.19
		9.97	9.89	9.98	9.90	9.95	9.96	9.86	9.97
		10.68	10.60	10.66	10.62	10.65	10.66	10.58	10.68
		11.31	11.25	11.29	11.26	11.29	11.30	11.24	11.31
		11.60	11.55	11.58	11.56	11.59	11.60	11.53	11.60
		11.87	11.83	11.85	11.83	11.86	11.87	11.81	11.87
		11.90	11.85	11.87	11.86	11.89	11.89	11.84	11.90
		12.12	12.08	12.09	12.08	12.11	12.12	12.06	12.12
		12.34	12.30	12.31	12.30	12.33	12.33	12.29	12.34
		12.53	12.50	12.50	12.50	12.52	12.53	12.49	12.53
		12.59	12.55	12.56	12.56	12.58	12.58	12.54	12.59
		12.70	12.67	12.68	12.68	12.69	12.70	12.66	12.70
		12.85	12.82	12.82	12.82	12.84	12.84	12.81	12.85

Table C.3 (Cont.) Velocity at values of coefficient C_2 between 1.84-1.91 in the Realisable k-ν model

Discharge (m³/s)	$\dfrac{iL}{L\cos_n}$	Depth normal to the pseudo-bottom (m)	Velocity (m/s) at various values of coefficient C_2						
			C_2=1.84	C_2=1.85	C_2=1.86	C_2=1.87	C_2=1.88	C_2=1.89	C_2=1.91
2.83	0.16	0.02	2.13	2.00	2.05	2.07	2.09	1.95	2.09
		0.05	5.45	5.14	5.27	5.31	5.36	5.01	5.33
		0.08	6.51	6.21	6.38	6.38	6.45	6.11	6.42
		0.14	6.95	6.81	6.97	6.90	7.00	6.79	6.98
		0.20	7.34	7.30	7.43	7.34	7.44	7.29	7.44
		0.26	7.70	7.73	7.83	7.73	7.82	7.72	7.82
		0.29	7.86	7.92	8.00	7.90	8.00	7.91	7.99
		0.32	8.02	8.09	8.16	8.06	8.16	8.08	8.15
		0.35	8.17	8.25	8.31	8.21	8.30	8.24	8.30
		0.38	8.30	8.39	8.44	8.34	8.43	8.38	8.42
		0.40	8.39	8.49	8.53	8.43	8.52	8.48	8.51
		0.41	8.42	8.52	8.56	8.46	8.55	8.51	8.54
		0.44	8.53	8.63	8.66	8.57	8.65	8.62	8.64
		0.47	8.61	8.72	8.74	8.65	8.73	8.71	8.72
	0.31	0.02	2.58	2.55	2.56	2.49	2.55	2.59	2.58
		0.05	6.62	6.53	6.59	6.41	6.55	6.63	6.62
		0.08	7.91	7.83	7.91	7.73	7.84	7.93	7.93
		0.14	8.51	8.47	8.52	8.41	8.45	8.52	8.53
		0.20	9.04	9.02	9.06	8.98	9.01	9.04	9.06
		0.26	9.52	9.51	9.55	9.49	9.50	9.52	9.54
		0.29	9.75	9.73	9.77	9.72	9.73	9.74	9.76
		0.32	9.96	9.94	9.98	9.94	9.94	9.95	9.97
		0.35	10.15	10.14	10.17	10.13	10.14	10.14	10.16
		0.38	10.30	10.29	10.33	10.29	10.29	10.29	10.32
		0.38	10.32	10.31	10.35	10.31	10.31	10.31	10.33
		0.41	10.48	10.47	10.50	10.47	10.47	10.46	10.49
		0.44	10.62	10.61	10.64	10.61	10.61	10.60	10.63
		0.47	10.74	10.73	10.76	10.73	10.74	10.73	10.75
	0.47	0.02	2.78	2.79	2.78	2.74	2.76	2.77	2.78
		0.04	6.38	6.42	6.39	6.30	6.36	6.37	6.38
		0.08	8.56	8.60	8.59	8.51	8.55	8.57	8.56
		0.14	9.29	9.30	9.29	9.29	9.29	9.31	9.28
		0.20	9.94	9.94	9.94	9.95	9.94	9.95	9.93
		0.26	10.54	10.54	10.53	10.55	10.53	10.54	10.52
		0.32	11.07	11.07	11.06	11.08	11.06	11.07	11.06
		0.38	11.52	11.52	11.52	11.53	11.52	11.52	11.51
		0.40	11.63	11.63	11.62	11.63	11.62	11.62	11.62
		0.44	11.89	11.89	11.89	11.90	11.89	11.89	11.89
		0.49	12.15	12.14	12.14	12.15	12.14	12.14	12.14
		0.50	12.19	12.19	12.18	12.19	12.18	12.18	12.18
		0.56	12.42	12.42	12.42	12.42	12.42	12.41	12.42
	0.63	0.02	2.89	2.90	2.90	2.93	3.00	2.95	2.96
		0.05	7.42	7.46	7.45	7.54	7.68	7.55	7.58
		0.08	8.96	8.98	8.98	9.07	9.19	9.06	9.08
		0.14	9.82	9.79	9.81	9.87	9.91	9.83	9.85
		0.20	10.57	10.52	10.55	10.58	10.60	10.55	10.57
		0.26	11.24	11.19	11.21	11.24	11.25	11.21	11.22
		0.32	11.83	11.79	11.80	11.83	11.83	11.81	11.81
		0.35	12.10	12.06	12.06	12.10	12.10	12.07	12.08
		0.37	12.22	12.18	12.18	12.22	12.22	12.19	12.20
		0.38	12.34	12.30	12.30	12.34	12.33	12.31	12.31
		0.41	12.55	12.52	12.52	12.55	12.55	12.53	12.53
		0.44	12.75	12.72	12.72	12.75	12.75	12.73	12.73
		0.47	12.93	12.90	12.90	12.92	12.92	12.90	12.90
		0.48	12.96	12.93	12.93	12.96	12.95	12.94	12.93
		0.50	13.08	13.06	13.06	13.08	13.08	13.06	13.06
	0.79	0.02	3.08	3.03	3.03	3.08	3.10	3.11	3.09
		0.05	7.91	7.76	7.80	7.91	7.96	7.97	7.94
		0.08	9.50	9.35	9.39	9.49	9.55	9.56	9.52
		0.14	10.29	10.22	10.25	10.28	10.33	10.35	10.31
		0.20	11.03	11.00	11.01	11.01	11.06	11.07	11.04
		0.26	11.72	11.70	11.70	11.70	11.74	11.75	11.73
		0.32	12.34	12.34	12.33	12.32	12.35	12.36	12.34
		0.35	12.62	12.62	12.61	12.60	12.63	12.63	12.62
		0.37	12.75	12.75	12.74	12.73	12.76	12.76	12.75
		0.38	12.87	12.87	12.87	12.85	12.88	12.88	12.87
		0.41	13.10	13.10	13.10	13.08	13.11	13.11	13.10
		0.44	13.31	13.31	13.31	13.29	13.31	13.31	13.31
		0.46	13.41	13.41	13.40	13.39	13.41	13.41	13.40
		0.47	13.49	13.50	13.49	13.47	13.49	13.49	13.49

Table C.3 (Cont.) Velocity at values of coefficient C_2 between 1.84-1.91 in the Realisable k-v model

Discharge (m³/s)	$\dfrac{iL}{L\cos_n}$	Depth normal to the pseudo-bottom (m)	Velocity (m/s) at various values of coefficient C_2						
			C_2=1.84	C_2=1.85	C_2=1.86	C_2=1.87	C_2=1.88	C_2=1.89	C_2=1.91
3.28	0.16	0.02	1.97	2.08	2.03	1.99	2.06	2.00	1.97
		0.05	5.07	5.32	5.22	5.12	5.30	5.16	5.06
		0.08	6.16	6.40	6.30	6.21	6.44	6.28	6.17
		0.14	6.78	6.98	6.89	6.84	7.08	6.96	6.87
		0.20	7.28	7.47	7.39	7.36	7.57	7.49	7.42
		0.26	7.72	7.90	7.83	7.81	7.98	7.92	7.87
		0.29	7.92	8.10	8.03	8.01	8.17	8.12	8.07
		0.32	8.11	8.28	8.22	8.20	8.33	8.29	8.25
		0.35	8.29	8.44	8.39	8.37	8.49	8.45	8.42
		0.38	8.45	8.59	8.54	8.52	8.63	8.59	8.57
		0.41	8.59	8.73	8.68	8.66	8.75	8.72	8.71
		0.44	8.69	8.82	8.77	8.76	8.84	8.81	8.80
		0.44	8.72	8.84	8.80	8.78	8.86	8.84	8.83
		0.47	8.83	8.95	8.90	8.89	8.95	8.93	8.93
		0.50	8.94	9.04	9.00	8.99	9.04	9.02	9.02
		0.51	8.96	9.06	9.03	9.01	9.06	9.05	9.05
	0.31	0.02	2.54	2.60	2.54	2.56	2.60	2.57	2.56
		0.05	6.54	6.67	6.52	6.59	6.67	6.60	6.60
		0.08	7.87	7.99	7.83	7.92	7.98	7.92	7.95
		0.14	8.55	8.60	8.51	8.59	8.60	8.55	8.61
		0.20	9.11	9.15	9.09	9.15	9.15	9.12	9.17
		0.26	9.62	9.66	9.62	9.65	9.65	9.63	9.67
		0.29	9.85	9.89	9.86	9.88	9.89	9.86	9.90
		0.32	10.07	10.10	10.08	10.09	10.10	10.08	10.12
		0.35	10.27	10.30	10.29	10.29	10.31	10.28	10.31
		0.38	10.45	10.48	10.47	10.47	10.49	10.46	10.49
		0.38	10.47	10.50	10.49	10.49	10.51	10.48	10.51
		0.41	10.62	10.64	10.63	10.63	10.65	10.63	10.65
		0.44	10.77	10.79	10.78	10.78	10.80	10.78	10.79
		0.47	10.89	10.90	10.90	10.90	10.92	10.90	10.91
		0.47	10.90	10.92	10.92	10.91	10.93	10.91	10.92
	0.63	0.02	3.01	3.01	2.99	2.99	2.92	2.97	2.97
		0.05	7.73	7.71	7.69	7.68	7.51	7.63	7.61
		0.08	9.27	9.25	9.24	9.25	9.06	9.16	9.15
		0.14	10.04	10.06	10.02	10.04	9.92	9.95	9.97
		0.20	10.75	10.79	10.74	10.76	10.69	10.68	10.71
		0.26	11.43	11.46	11.41	11.43	11.39	11.37	11.40
		0.32	12.04	12.07	12.03	12.04	12.02	11.98	12.01
		0.38	12.57	12.59	12.56	12.57	12.55	12.52	12.54
		0.38	12.57	12.59	12.56	12.57	12.55	12.52	12.54
		0.41	12.80	12.82	12.79	12.80	12.79	12.75	12.78
		0.41	12.82	12.84	12.82	12.82	12.81	12.77	12.80
		0.44	13.01	13.03	13.01	13.01	13.00	12.97	12.99
		0.47	13.20	13.22	13.20	13.20	13.20	13.16	13.18
		0.50	13.37	13.39	13.37	13.37	13.37	13.34	13.35
		0.51	13.39	13.40	13.39	13.38	13.39	13.35	13.37
	0.79	0.02	3.13	3.09	3.13	3.14	3.18	3.16	3.13
		0.05	8.04	7.93	8.04	8.07	8.14	8.10	8.03
		0.08	9.66	9.57	9.66	9.67	9.74	9.71	9.64
		0.14	10.49	10.47	10.50	10.47	10.54	10.50	10.46
		0.20	11.26	11.27	11.27	11.23	11.28	11.26	11.23
		0.26	11.98	12.00	11.98	11.95	11.98	11.97	11.95
		0.32	12.63	12.66	12.64	12.61	12.62	12.62	12.61
		0.38	13.19	13.23	13.20	13.18	13.19	13.18	13.18
		0.41	13.39	13.43	13.40	13.39	13.39	13.38	13.38
		0.41	13.44	13.48	13.45	13.43	13.43	13.42	13.43
		0.44	13.66	13.71	13.68	13.66	13.66	13.65	13.66
		0.47	13.87	13.91	13.88	13.87	13.86	13.85	13.86
		0.48	13.94	13.98	13.95	13.94	13.94	13.93	13.94
		0.50	14.05	14.09	14.06	14.05	14.05	14.04	14.05
		0.53	14.21	14.25	14.22	14.21	14.21	14.20	14.21

APPENDIX D

Sample cases of preliminary design by the proposed equations and charts

This appendix presents two sample cases of preliminary design by the proposed equations and charts. The first case is the existing stepped spillway in Thailand which is located at Mae Suay Reservoir, Chiang Rai. The second case is the first and highest concrete arch dam in Thailand, Bhumibol dam, which is capable of storing as much as 13,462 million cubic meters of heavy runoff to prevent downstream flooding and provide the needed irrigation water supply in the Central Plains and for other purposes all year (Center of Excellence for Hydro Power Plant project, 2006). The details are as follows:

D.1 Mae Suay Reservoir

Stepped spillway at Mae Suay Reservoir, as shown in Figure D.1, located in Mae Suay District, Chiang Rai since 2002. It is the first Roller compacted concrete reservoir in Thailand. The schematic designed plan of stepped spillway at Mae Suay reservoir is shown in Figure D.2. The height of reservoir is 59 m. The reservoir crest is 400 m long. The ungated overflow weir, Creager Type, is 145 m long. The spillway width is 140.8 m. The storage capacity is 73 million cubic meters. The step height is 0.5 m and the step length is 0.4 m. The possible discharges of flow through a spillway depend on the total head on the spillway crest which is at the elevation of 507.00 m MSL. The spilled discharge at the spillway can be shown in Table D.1.

Figure D.1 Stepped spillway at Mae Suay reservoir
(Source: Chiangrai directory, 2013)

From the result of numerical model, it was shown that 88 steps of spillway can dissipate only 46% of energy dissipation. However, the equations and charts for preliminary design were used as a tool to re-design for the higher energy dissipation.

The fitting trend of equation (5.9) and Figure 5.18 was used to figure out the energy dissipation on the correlation of critical depth and number of steps, as shown in Figure D.3. It can be concluded that if the slope of stepped spillway is re-designed to be 2H:1V with the step height of 0.25 m and the step length of 0.5 m, the minimum energy dissipation will be about 78% at the highest water level in the reservoir.
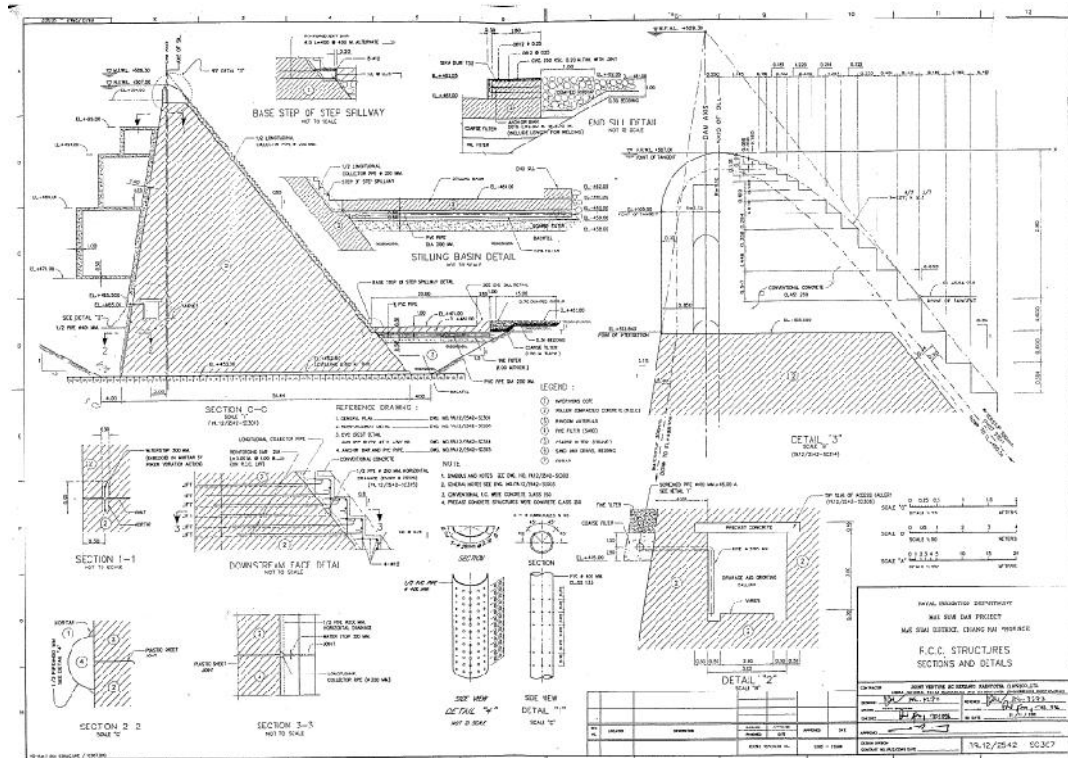
Figure D.2 Schematic designed plan of stepped spillway at Mae Suay reservoir

Table D.1 The spilled discharge at the spillway of Mae Suay Reservoir

Elevation (m MSL)	Discharge (m³/s)	Elevation (m MSL)	Discharge (m³/s)	Elevation (m MSL)	Discharge (m³/s)	Elevation (m MSL)	Discharge (m³/s)
+507.000	0.000	+508.500	543.199	+510.000	1536.398	+511.500	2957.778
+507.500	104.539	+509.000	836.309	+510.500	1936.083	+512.000	3688.303
+508.000	295.680	+509.500	1168.778	+511.000	2365.440	+512.500	4516.568
						+513.000	5427.464

The calculation for the spillway width can be shown as follows;
- From $y_c = (q^2/g)^{1/3}$, the critical depth, $y_c = 3.64$
- The relative critical depth, $(y_c/Nh) = 0.08$
- The dam height, $Nh = 44$ m
- The unit discharge, $q = 21.71$ m³/s/m
- From $Q/B = q$, the spillway width, $B = 250$ m

The inception point and the point of uniform flow attainment can be found from the pressure profiles of numerical model. To locate the location of the separation between gradually varied flow and uniform flow which means the starting point of uniform flow, equation (5.6) can be used.

$$L_{SU} = 3.64(\cos{}_{"})^{0.86} \frac{q^{0.86}}{(h\cos{}_{"})^{0.29}(\tan{}_{"})^{0.43}} + 2.42q^{1.07}\left(\frac{\cos^2{}_{"}}{\sin{}_{"}} + h\sin{}_{"}\right) \qquad (5.6)$$

where L_{SU} is the length of starting point of uniform flow.

Then, equation (5.6) was calculated to check the length of uniform flow. From the dam height, $Nh = 44$ m. Let the number of step, $N = 176$ steps, step height, $h = 0.25$ m. The length of starting point of uniform flow, $L_{SU} = 94$ m which is shorter than the spillway length, 98 m. It means the flow will be in uniform flow and can dissipate as much energy as design. The appropriate grid size for numerical simulation is (Grid size / h) = 0.07, thus, the grid size = 0.07× 0.5 = 0.018 m

However, this is only the preliminary design. More details, for example; slope stability data, should be more considered.
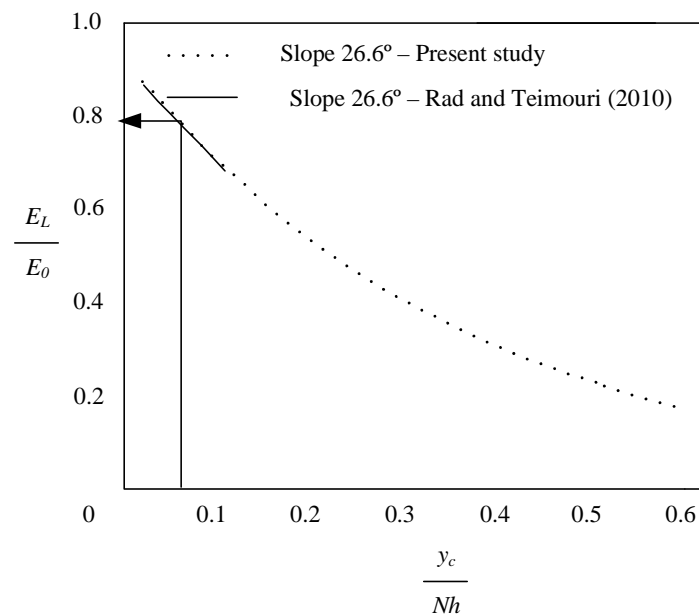
Figure D.3 Energy dissipation at Mae Suay Reservoir stepped spillway

D.2   Bhumibol dam

The Bhumibol dam, as shown in Figure D.4, is a concrete dam with 154 m tall and 486 m long. The storage capacity is 13,462 million cubic meters. It has been operated since 1964 with the designed extreme flood of 6,000 m^3/s. Physical condition of the catchment area is different from the condition at the time of design period. Then, the design extreme flood has been revised based on standard concept of Probable Maximum Precipitation (PMP) and Probable Maximum Flood (PMF) (Shotittayanggoon and Hiruntiyakul, 2009). This reason confirmed that there should be a revision of spillway design to decrease the efficiency of spillway and transfer higher flow. Shotittayanggoon

and Hiruntiyakul (2009) presented the PMF of Bhumibol Dam of 6,311 m^3/s and the PMP of Bhumibol Dam of 6,784 m^3/s under the effect of La Nina.

Figure D.4 Bhumibol Dam
(Source: thailandg.com, 2013)

The fitting trend of equation (5.9) and Figure 5.18 was used to figure out the energy dissipation on the correlation of critical depth and number of steps, as shown in Figure D.5. If the slope of stepped spillway is designed to be 2H:1V with the step height of 0.5 m and the step length of 1.0 m, the energy dissipation will be about 80% at the discharges of both PMF and PMP. The spillway has 308 steps with the critical depth of 7.7m. However, this is only the preliminary design. More details, for example; slope stability data, should be more considered.

The calculation for the spillway width can be shown as follows;
- From $y_c = (q^2/g)^{1/3}$, the critical depth, $y_c = 7.77$
- The relative critical depth, $(y_c/Nh) = 0.05$
- The dam height, $Nh = 154$ m
- The unit discharge, $q = 66.92$ m^3/s/m
- From $Q/B = q$, the spillway width, $B = 100$ m

The inception point and the point of uniform flow attainment can be found from the pressure profiles of numerical model. To locate the location of the separation between gradually varied flow and uniform flow which means the starting point of uniform flow, equation (5.6) can be used.

$$L_{SU} = 3.64(\cos_{\, ''})^{0.86} \frac{q^{0.86}}{(h\cos_{\, ''})^{0.29}(\tan_{\, ''})^{0.43}} + 2.42q^{1.07}\left(\frac{\cos^2_{\, ''}}{\sin_{\, ''}} + h\sin_{\, ''}\right) \qquad (5.6)$$

where L_{SU} is the length of starting point of uniform flow.

Then, equation (5.6) was calculated to check the length of uniform flow. From the dam height, $Nh = 154$ m. Let the number of step, $N = 308$ steps, step height, $h = 0.5$ m. The

length of starting point of uniform flow, L_{SU} = 286 m which is shorter than the spillway length, 344 m. It means the flow will be in uniform flow and can dissipate as much energy as design. The appropriate grid size for numerical simulation is (Grid size / h) = 0.07, thus, the grid size = 0.07× 0.5 = 0.035 m

However, this is only the preliminary design. More details, for example; slope stability data, should be more considered.
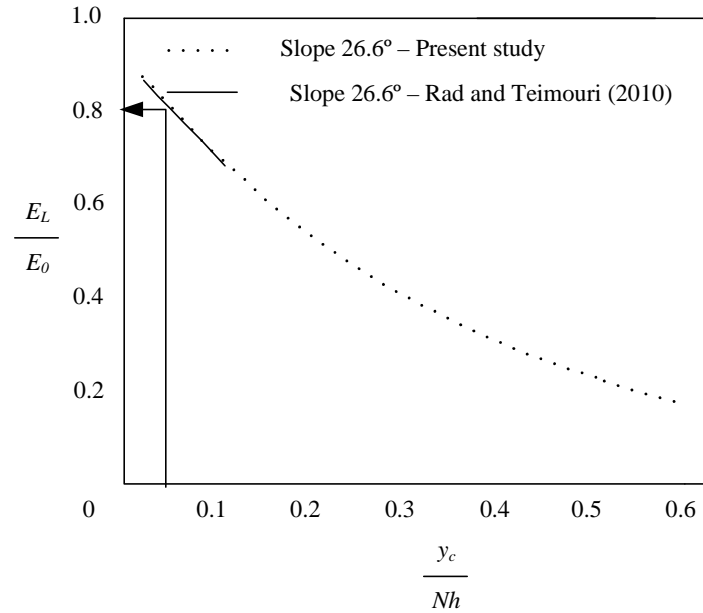

Figure D.5 Energy dissipation at Bhumibol Dam stepped spillway

CURRICULUM VITAE

NAME	Duangrudee Kositgittiwong
DATE OF BIRTH	August 06, 1982

EDUCATION RECORD

HIGH SCHOOL	Suksanari, 2001
BACHELOR'S DEGREE	Bachelor of Engineering in Civil Engineering (1st Class Honors) King Mongkut's University of Technology Thonburi, 2005
DOCTOR'S DEGREE	Doctor of Philosophy (Civil Engineering) King Mongkut's University of Technology Thonburi, 2012

SCHOLARSHIP/ RESEARCH GRANT	Thailand Research Fund (TRF) under the Royal Golden Jubilee Ph.D. Program, 2007-2010
EMPLOYMENT RECORD	Water Resources Engineering and Management Research Center (WAREE)

PUBLICATIONS

International Journal

Duangrudee Kositgittiwong, Chaiyuth Chinnarasri, and Pierre Y. Julien, 2013, "Numerical simulation of flow velocity profiles along a stepped spillway.", **Proceedings of the Institution of Mechanical Engineers Part E: Journal of Process Mechanical Engineering**. (Accepted for publication).

Chaiyuth Chinnarasri, Duangrudee Kositgittiwong, and Pierre Y. Julien, 2013, "Modelling of flow behavior through spillways using CFD.", **Water Management**. (Accepted for publication).

Duangrudee Kositgittiwong, Chaiyuth Chinnarasri, and Pierre Y. Julien, 2012, "Two-phase flow over stepped and smooth spillways: Numerical and physical models.", **Ovidius University Annals Series: Civil Engineering**, Issue 14, pp. 147-154.

Chaiyuth Chinnarasri, Duangrudee Kositgittiwong, 2008, "Laboratory study of maximum scour depth downstream of sills.", **Water Management**, Vol. 161, No. 5, pp. 267-275.

National Journal

Duangrudee Kositgittiwong, and Chaiyuth Chinnarasri, 2006, "Experimental investigation of local scour downstream of bed sills.", **Journal of Research in Engineering and Technology – Kasetsart University**, Vol. 3, No. 2, pp. 131-143.

Chaiyuth Chinnarasri, Surakrai Baanchuen, and Duangrudee Kositgittiwong, 2010, "Potential of run-of-river type hydropower in the central watershed of Thailand.", **Research and Development Journal of EIT**, Vol. 21, No. 2, pp. 23-34. (in Thai)

International Conference   Chaiyuth Chinnarasri, and Duangrudee Kositgittiwong, "Comparison of physical and numerical models on smooth and stepped spillway overflow.", **Proceedings of the 1st EIT International Conference on Water Resources Engineering**, Petchaburi, Thailand, 18-19 August, 2011, pp. 90-96.

Chaiyuth Chinnarasri, and Duangrudee Kositgittiwong, "Local scour phenomenon downstream of grade-control structures.", **The CBNU-BK21 and KMUTT International Symposium on the Sustainable Resources Recycling Technology Development in Environmental and Urban Engineering**, Bangkok, Thailand, 11 February, 2008, pp. 1.44-1.51

National Conference   Duangrudee Kositgittiwong, and Chaiyuth Chinnarasri, "Experimental investigation of local scour downstream of bed sills.", **Proceedings of the 11th National Convention on Civil Engineering**, Phuket, Thailand, 20-22 April, 2006.

Duangrudee Kositgittiwong, and Chaiyuth Chinnarasri, "Numerical simulation of flow over stepped spillways.", **RGJ – Ph.D. Congress XI**, Chonburi, Thailand, 1-3 April, 2010.